Entwicklung und Evaluation additiv gefertigter Systeme für die Zellkulturtechnik und Biosensorik

Von der Naturwissenschaftlichen Fakultät der

Gottfried Wilhelm Leibniz Universität Hannover

zur Erlangung des Grades

Doktorin der Naturwissenschaften (Dr. rer. nat.)

genehmigte Dissertation

von

Ina Gerhild Siller, M. Sc.

[2021]

„Wer immer tut, was er schon kann,

bleibt immer das, was er schon ist"

Henry Ford (1863-1947)

Kurzfassung

Die additive Fertigung, auch bekannt unter der Bezeichnung „3D-Druck", hat sich längst in etlichen Herstellungsbereichen als vielfältig einsetzbares, nützliches Werkzeug bewährt. Die schnelle Fertigung selbst komplexer Systeme bei gleichzeitig hoher Auflösung birgt ein enormes Potential als disruptive Technologie klassische Fertigungsverfahren zu ersetzen. Der Einsatz der additiven Fertigung in biologischen und medizinischen Anwendungen ist jedoch noch verhältnismäßig beschränkt. Vor allem die Auswahl an charakterisierten und für eine biologische Anwendung geeigneten Materialien begrenzen den Einsatz. In der vorliegenden Doktorarbeit wurden Materialien der additiven Fertigung eingehend auf eine Eignung für biotechnologische Zwecke evaluiert und die Anwendung in spezifisch-entwickelten Systemen demonstriert.

Im ersten Teil dieser Arbeit wurde der Einfluss verschiedener Desinfektions- bzw. Sterilisationsverfahren auf die biologische Verträglichkeit (Biokompatibilität) additiv gefertigter Elemente untersucht. Zudem wurde ein Vergleich dreier Verfahren zur Analyse der Biokompatibilität angestellt, bei dem sich eine bildbasierte Echtzeitanalyse als überlegen erwies. Insgesamt konnte die Eignung des untersuchten 3D-Druckmaterials für biologische Anwendungen festgestellt werden.

Im zweiten Teil dieser Arbeit wurde ein Zellkultursystem für die Kultivierung adhärent wachsender Zellen entwickelt und 3D-gedruckt. Nach eingehender Charakterisierung des 3D-Druckmaterials hinsichtlich der Oberflächeneigenschaften konnte die biologische Verträglichkeit in Studien zur Zellproliferation, -viabilität, -morphologie und Apoptose/Nekrose-Verteilungen sichergestellt werden.

Der dritte Teil dieser Arbeit zeigt das große Potential der additiven Fertigung zur individuellen Herstellung maßgeschneiderter, autarker Versuchssysteme auf. Es wurde unter anderem ein Ko-Kultivierungssystem zur Analyse der Angiogenese entwickelt, das die separate Kultivierung zweier Zelllinien in einem gemeinsamen Kultivierungsmedium ermöglicht. In einer Anwendung konnte gezeigt werden, dass das angiogene Potential von kokultivierten mesenchymalen Stammzellen zur Ausbildung gefäßähnlicher Strukturen bei Endothelzellen führt.

Im vierten Teil dieser Arbeit werden additiv gefertigte, statische und dynamische Durchflusszellen vorgestellt, die als Apparatur für elektrochemische Messungen in der (Bio)Sensorik dienen. Mithilfe des statischen Systems konnte eine aptamerbasierte impedimetrische Detektion eines *Escherichia coli* Crooks Stammes realisiert werden.

Schlagwörter: 3D-Druck, additive Fertigung, Tierzellkultivierung, Materialuntersuchung, Biokompatibilität, Zellkulturtechnik, Polymere, elektrochemische Biosensoren

Abstract

Additive manufacturing, also known as "3D printing", has proven to be a versatile and useful tool in numerous manufacturing sectors, enabling an efficient production of complex devices in high resolution. Already called a disruptive technology, it has an enormous potential to replace conventional manufacturing methods. However, the use in biological and biomedical applications is still limited. Especially the variety of characterized materials that are suitable for biological applications limits the possible use. In the present doctoral thesis, various 3D printing materials were evaluated with regard to their suitability for biotechnological applications and their use was demonstrated with specially developed 3D-printed systems.

In the first part of this work, the influence of different disinfection and sterilization procedures on biological compatibility (biocompatibility) of 3D-printed parts was investigated. In addition, a comparison of three methods for the analysis of biocompatibility was conducted, in which an image-based real-time analysis proved to be advantageous. Overall, the suitability of the examined 3D printing material for biological applications could be determined.

In the second part of this work, a cell culture system for the cultivation of adherent growing cells was developed and 3D-printed. After detailed characterization of the 3D printed material with respect to surface properties, biological compatibility was ensured in studies on cell proliferation, viability, morphology and apoptosis/necrosis distributions.

The third part of this thesis demonstrates the great potential of additive manufacturing for the individual production of tailor-made systems. A co-cultivation system for the study of angiogenesis was developed, which allows the separate cultivation of two cell types in a single, shared cultivation medium. It could be shown that the angiogenic potential of co-cultivated mesenchymal stem cells leads to the formation of tubular-like structures in endothelial cells.

In the fourth part of this thesis, additive manufactured static and dynamic flow cells are presented, which serve as a device for electrochemical measurements in (bio)sensor technology. By means of the static system an aptamer-based impedimetric detection of an *Escherichia coli* Crook's strain could be realized in biosensor experiments.

Keywords: 3D printing, additive manufacturing, mammalian cell culture, material testing, biocompatibility, cell culture technology, polymers, electrochemical biosensing

Inhaltsverzeichnis

Abbildungsverzeichnis

Abkürzungsverzeichnis

2PP	Zwei-Photonen-Polymerisation (engl.: *Two-photon polymerization*)
3D	Dreidimensional (engl.: *Three-dimensional*)
ABS	Acrylnitril-Butadien-Styrol (engl.: *Acrylonitrile butadiene styrene*)
AD-MSC	Humane, adipogene, mesenchymale Stammzellen (engl.: *human, adipogenic mesenchymal stem cells*)
AM	Additive Fertigung (engl.: *Additive Manufacturing*)
bspw.	beispielsweise
bzw.	beziehungsweise
CAD	Computergestütztes Konstruktionsprogramm/Design (engl.: *Computer-aided design*)
CFD	Numerische Strömungsmechanik (engl.: *Computational Fluid Dynamics*)
CHO	Zelllinie aus Ovarien des Chinesischen Zwerghamsters (engl.: *Chinese Hamster Ovary*)
CTB	CellTiterBlue®
d. h.	das heißt
E. coli	*Escherichia coli*
EHDP	Elektrohydrodynamische Tintenstrahldruck (engl.: *Electrodynamic jet printing*)
engl.:	englisch
FDM	Schmelzschichtung (engl.: *Fused Deposition Modeling*)
GFP	Grün fluoreszierendes Protein (engl.: *Green fluorescent protein*)
HUVEC	Endothelzellen aus humanen Nabelschnurvenen (engl.: *Human umbilical vein endothelial cells*)

LDH	Laktatdehydrogenase
LoC	Mikrofluidisches Chipsystem (engl.: *Lab-on-a-chip*)
mind.	mindestens
MSL	Mikro-Stereolithographie (engl.: *Microstereolithography*)
NAD	Nicotinamid-Adenin-Dinukleotid (engl.: *Nicotinamide adenine dinucleotide*)
PDMS	Polydimethylsiloxan (engl.: *Polydimethylsiloxane)*
PET	Polyethylenterephthalat (engl.: *Polyethylene terephthalate*)
PLA	Polylactide (engl.: *Polylactic acid*)
POCT	Patientennahe Labordiagnostik (engl.: *Point-of-care-testing*)
SLA	Stereolithographie (engl.: *Stereolitography apparatus*)
SPE	Mittels Siebdruckverfahrens aufgebrachte Elektrode (engl.: *Screen-printed electrode*)
STL	Dateiformat, Abkürzung von Stereolithographie (engl.: *file format, abbreviation of stereolithography*)
USB	System zur Verbindung mit externen Geräten (engl.: *Universal Serial Bus*)
UV	Ultraviolett (engl.: *Ultraviolet*)
z. B.	zum Beispiel

1 Einleitung

"Game-changing, groundbreaking, enabling and disruptive".

Dies sind nur einige der vielen Umschreibungen, die im Zusammenhang mit der additiven Fertigung, auch bekannt als „3D-Druck", genannt werden. Dabei ist die revolutionäre Idee der Technologie auf ein einfaches Prinzip zurück zu führen: das gewünschte Objekt wird durch Auftragen neuen Materials, additiv, Schicht-für-Schicht aufgebaut. Die additive Fertigung erwirkt damit ein Umdenken – wo sich bisweilen die Komplexität eines Bauteils nach den Möglichkeiten der Herstellungsverfahren richtete, kann nun die gewünschte Funktion und das Design im Vordergrund stehen. Mittels additiver Fertigung lassen sich selbst komplexe Geometrien herstellen, die mit konventionellen Verfahren nicht oder nur unter hohem Aufwand realisiert werden können. In der Natur des Verfahrens liegen die Vermeidung von Abfällen und die Einsparung von Materialressourcen. Die potentielle Verkürzung globaler Herstellungsketten durch eine Produktion vor Ort reduziert darüber hinaus deutlich den Transport- und Logistikaufwand. Nachhaltigkeit und Umweltschutz als globale Herausforderungen sind somit als zentrale Grundsätze in der Technologie verankert [1].

All diese Vorteile lassen es wenig überraschend erscheinen, dass der weltweite Markt additiv gefertigter Produkte 2020 auf 16 Milliarden US-Dollar geschätzt wird und sich dieser bis 2024 voraussichtlich auf mehr als 40 Milliarden US-Dollar verdoppeln wird [2]. Limitierungen und Restriktionen betreffen gegenwärtig in erster Linie die verfügbaren Materialien, welche für eine additive Fertigung genutzt werden können. Die Auswahl an kommerziell erhältlichen Materialien ist begrenzt und die physikalischen Eigenschaften der verarbeiteten Materialien lassen häufig nicht gleichwertige Ergebnisse erzielen, wie durch konventionelle Fertigungsverfahren erreicht werden können. Aus der Flexibilität im Design bei gleichzeitig hoher Auflösung ergibt sich ein enormes Potential der additiven Fertigung im biotechnologischen und medizinischen Sektor, um beispielsweise maßgefertigte Versuchssysteme, experiment-spezifisches Equipment oder perfekt auf den Patienten zugeschnittene Prothesen zu fertigen. Den auf dem Markt verfügbaren Materialien mangelt es jedoch häufig an umfassenden Charakterisierungen hinsichtlich einer Eignung für biologische Applikationen oder sie können für diese direkt ausgeschlossen werden. Das Risiko für die biologische Umgebung muss allerdings zwingend evaluiert und minimiert sein, um die Sicherheit für Produkt und, im Falle von Implantaten und Prothesen, letztendlich den Patienten zu gewährleisten.

2 Zielsetzung

Ziel dieser Arbeit ist die Charakterisierung und Evaluation polymerbasierter 3D-Druckmaterialien hinsichtlich einer Eignung für biologische Anwendungen und die Integration dieser in maßgeschneiderten Systemen für die biotechnologische/biomedizinische Forschung.

Dazu soll zunächst der Einfluss verschiedener Desinfektions- bzw. Sterilisationsverfahren auf die biologische Verträglichkeit (Biokompatibilität) additiv gefertigter Bauteile untersucht werden – denn für eine biologische Verwendung eines Materials ist eine Desinfektion bzw. Sterilisation zwingend erforderlich. Zudem sollen verschiedene *In-Vitro*-Testverfahren zur Analyse der Biokompatibilität miteinander und hinsichtlich einer Eignung für Hochdurchsatz-*Screenings* verglichen werden. Mithilfe der *In-Vitro*-Testverfahren, die eine Analyse der Zellproliferation, -viabilität, -morphologie und der Apoptose/Nekrose-Verteilungen in Kontakt mit dem Material umfassen, sollen Rückschlüsse auf die biologische Verträglichkeit von polymerbasierten 3D-Druckmaterialien gezogen werden. Insbesondere die Verwendung der Materialien in der (adhärenten) Zellkulturtechnik setzt weitere Materialuntersuchungen voraus. Dazu sollen die durch den additiven Fertigungsprozess bedingten Oberflächenstrukturen bezüglich Rauheit und Topographie umfassend analysiert werden. Das Proliferations- und Adhäsionsverhalten von adhärent wachsenden Zellen wird von der Benetzbarkeit der Materialoberfläche beeinflusst, sodass diese in weiteren Studien untersucht werden soll. Die optischen Materialeigenschaften sollen zudem in mikroskopischen Anwendungen beleuchtet werden.

Nach eingehender Charakterisierung der polymerbasierten 3D-Druckmaterialien soll das Potential der additiven Fertigungstechnologie in biotechnologischen/biomedizinischen Anwendungen aufgezeigt werden. Dazu sollen Objekte für die adhärente Zellkultivierung additiv gefertigt werden, die beispielsweise als Kultivierungsgefäße eingesetzt werden könnten. Daneben sollen Versuchssysteme entwickelt werden, mit wessen Hilfe die Wechselwirkungen unterschiedlicher Zelltypen und der Prozess der Angiogenese *in vitro* näher untersucht werden kann. Für die Durchführung elektrochemischer Messungen in der (Bio)Sensorik sollen des Weiteren Durchflusszellen entwickelt und additiv gefertigt werden, die den experimentellen Ablauf erleichtern. Die Vorteile von mikrofluidischen Systemen und einer Automatisierung sollen dabei in einer dynamischen Durchflusszelle verdeutlicht werden.

3 Theoretische Grundlagen

3.1 Additive Fertigung

Kostensenkungen, Effizienzsteigerungen, Förderung von Innovation – viele Menschen sind begeistert von den Vorteilen und positiven Einflüssen, die der 3D-Druck auf die Fertigung hat. Das Konzept moderner additiver Herstellungsverfahren geht dabei bereits auf die frühen 1980er Jahre zurück. Der japanische Wissenschaftler Hideo Kodama war 1981 der Erste, der die Ansätze einer schichtweisen Fertigung publizierte [3]. Er entwickelte eine Methode, bei der Photopolymere mittels UV-Licht polymerisiert werden und beschrieb damit einen Vorläufer der Stereolithographie (SLA). Eine Patentanmeldung für die Technologie scheiterte jedoch. Wissenschaftler aus Frankreich verfolgten wenig später ebenso Ansätze zur dreidimensionalen Fertigung – als Erfinder der additiven Fertigung gilt allgemein allerdings der aus Amerika stammende Ingenieur Charles Hull, dem 1986 ein Patent zum Verfahren der Stereolithographie bewilligt wurde [4]. Im selben Jahr gründete er das Unternehmen 3D Systems, das auch heute noch zu den führenden Firmen im Bereich der additiven Fertigung zählt. Hull legte wesentliche Grundsteine des modernen 3D-Drucks: er entwarf das STL-Dateiformat (STL als Abkürzung für „Stereolithographie"), das sich mittlerweile als anerkanntes Datenübertragungsformat in der additiven Fertigung etabliert hat. In diesem Zusammenhang entwickelte er auch erste Ansätze des digitalen *Slicing,* das zur Umwandlung eines 3D-Objekts im STL-Format in spezifische Druckerbefehle dient [5].

In den letzten Jahrzehnten wurden eine Vielzahl von additiven Fertigungsverfahren und -technologien entwickelt, die dennoch allesamt auf das gleiche Grundprinzip zurückzuführen sind: das gewünschte Produkt wird Schicht-für-Schicht, additiv, aus Material aufgebaut. Die 3D-Drucktechnologie unterscheidet sich somit fundamental von traditionellen Fertigungsverfahren, bei denen entweder subtraktiv Material abgetragen wird (Schleifen, Fräsen, Bohren) oder Objekte durch Formen des Materials hergestellt werden (Gießen, Biegen, Pressen) [6]. Mithilfe der additiven Fertigung können geometrisch komplexe Formen gefertigt werden, die mit den konventionellen Fertigungsverfahren nicht oder nur schwierig realisiert werden können. So ist zur Herstellung von verzweigten, dreidimensionalen Hohlräumen, wie beispielsweise Kanalstrukturen, eine Kombination mehrerer traditioneller Verfahren notwendig, während die 3D-Drucktechnologie eine Fertigung in einem einzigen Schritt erlaubt. Damit entfallen Arbeitsschritte, wie umfangreiche Vor- und Nachbereitungen, wodurch der Arbeitsaufwand erheblich reduziert wird. Zusätzlich werden Materialressourcen eingespart und Abfälle vermieden, da generell das gesamte

zuvor einberechnete Rohmaterial zu dem gewünschten Objekt verarbeitet wird [7]. Zu einer nachhaltigen, umweltfreundlichen Produktion tragen auch die Möglichkeit der Produktherstellung nur auf Nachfrage und die *just-in-time* Fertigung direkt am Verbrauchsort bei [7,8]. Ferner können Änderungen am Modell im Vergleich zu konventionellen Herstellungsverfahren sehr viel schneller umgesetzt werden. Bezüglich des Zeitaufwandes ist die additive Fertigung vor allem bei der Herstellung von Einzelstücken den traditionellen Verfahren überlegen. Je nach 3D-Druckverfahren und Produkt können Objekte innerhalb weniger Stunden gefertigt werden.

Dennoch gibt es Einschränkungen und Nachteile des 3D-Drucks, die nicht außer Acht gelassen werden dürfen. Obwohl die 3D-Druckbranche in den letzten Jahren wirtschaftlich stark gewachsen ist, weist sie eine vergleichsweise geringe Materialvielfalt auf [7,9]. Weiter verschärft wird diese Problematik dadurch, dass der Verbraucher durch die Wahl eines 3D-Drucksystems häufig auf die vom Hersteller angebotene Materialauswahl beschränkt ist [5]. Eine Trendwende scheint sich jedoch bemerkbar zu machen: immer mehr Unternehmen beteiligen sich aktiv an der Entwicklung und Produktion neuer Materialien und reagieren damit auf die hohe Nachfrage [10,11]. Ferner werden zwar Herstellungskosten durch reduzierten Transport-, Lager- und Arbeitsaufwand eingespart, die Preise für Rohmaterialien zur additiven Fertigung sind allgemein jedoch sehr hoch. Die hohen Materialkosten und die gleichzeitig begrenzte Auswahl an Materialien bilden somit die entscheidendsten Engpässe der Technologie [10]. Weitere Limitierungen ergeben sich bei der Druckauflösung und -qualität, insbesondere der mechanischen Eigenschaften. Gegenwärtig können mittels 3D-Druck nicht immer gleichwertige Ergebnisse erzielt werden, die durch traditionelle Fertigungsverfahren erreicht werden. Häufig lässt sich dies jedoch durch Nachbearbeitungsschritte der additiv gefertigten Produkte kompensieren.

Von der Idee bis zum fertigen Produkt sind es bei der additiven Fertigung nur wenige Schritte. Das gewünschte Objekt wird zunächst mittels computergestützter Konstruktionsprogramme (*computer-aided design*, CAD) geplant und gezeichnet. CAD-Programme werden in der Fertigungstechnik vielseitig eingesetzt, um beispielsweise Simulationen und Berechnungen durchzuführen. Sie ermöglichen es somit noch vor der eigentlichen Herstellung einen ersten Eindruck vom Objekt zu gewinnen. CAD-Dateien konstruierter Objekte können auf online Plattformen der Allgemeinheit zugänglich gemacht werden. Damit wird die Grundlage für eine hohe Transparenz und wissenschaftlichen Austausch geschaffen [4]. In der vorliegenden Arbeit wurde das CAD-Programm SolidWorks von Dassault Systèmes verwendet, das neben Autodesk Inventor (Autodesk Corporation) zu den meist verwendeten Konstruktionsprogrammen zählt [12]. Das im CAD-Programm er-

stellte 3D-Objekt wird in das STL-Dateiformat konvertiert und abgespeichert. Die Modelloberfläche wird dabei über Dreiecke angenähert und beschrieben (Polygondaten) [13]. Dabei gilt: je komplexer die Form, desto mehr Dreiecke sind nötig, um die Oberfläche abzubilden [13]. Um nun aus der STL-Datei das gewünschte Produkt zu fertigen, ist noch ein weiteres Bindeglied notwendig. Mithilfe eines sogenannten *Slicer* wird die STL-Datei in Schichten unterteilt und diese in einen für den 3D-Drucker verständlichen Code übersetzt [14]. Die *Slicer*-Software ist häufig Druckermodell-spezifisch und erlaubt dem Anwender, weitere Einstellungen vorzunehmen. So können an dieser Stelle beispielsweise Parameter wie Drucktemperatur und -geschwindigkeit festgelegt werden. Die einzustellenden Parameter können dabei je nach additiver Fertigungstechnologie und Druckermodell variieren [14,15]. Ferner werden in der *Slicer*-Software der Materialverbrauch und die Druckdauer berechnet. Die Dauer eines Drucks wird neben dem Druckermodell und der zugrunde liegenden 3D-Drucktechnologie auch von den Qualitätseinstellungen beeinflusst. Nach Festlegen aller Parameter im *Slicer* kann die Code-Datei an den Drucker übermittelt werden, wo sie übersetzt und das gewünschte Modell 3D-gedruckt wird. Nach Beenden des Drucks können je nach verwendeter Drucktechnologie, Material und Objektgeometrie zusätzliche Nachbearbeitungsschritte (*Post-Processing*) notwendig sein, bevor das gefertigte Objekt gebrauchsfertig ist [14].

Getrieben durch das Auslaufen früherer Patente, verzeichnete der Markt der additiven Fertigung ab 2006 ein großes Wachstum [9]. Die Technologie wurde zugänglicher und Herstellern wurde ermöglicht neue 3D-Druckverfahren zu entwickeln und zu optimieren. Laut einer Studie existierten im Jahr 2018 weltweit über 24000 Patente im Bereich der additiven Fertigung während es 2007 lediglich 2355 Patente waren – damit hat sich die Anzahl der Patente innerhalb nur eines Jahrzehnts verzehnfacht [16]. Schon heute wird die additive Fertigung mit ihrer hohen Tragweite auf etliche Herstellungsbereiche als disruptive Technologie bezeichnet und damit dem Einfluss des Automobils und des mobilen Internets gleichgestellt [17,18]. Die 3D-Drucktechnologie findet Einsatz in weiten Feldern der Produktion und Fertigung und bringt darüber hinaus neue Möglichkeiten für Herstellungsbereiche hervor (siehe **Abbildung 3-1**). Einfache 3D-Drucker sind kostengünstig und für jedermann kommerziell erhältlich, CAD-Programme sind im Internet frei verfügbar. Diese Umstände eröffneten mit einer individuellen Fertigung zu Hause einen gänzlich neuen Anwendungsbereich [19]. Das individuelle Designen und Drucken von Alltagsgegenständen revolutioniert die häusliche Werkstatt und hat sich geradezu zu einem Hobby entwickelt [19].
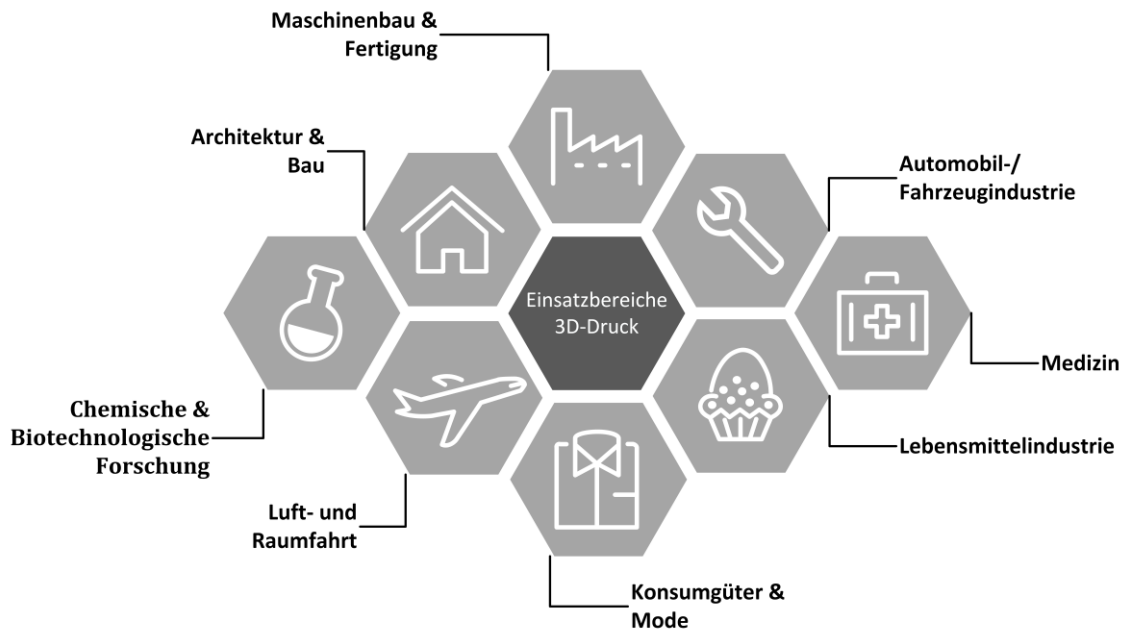
Abbildung 3-1 Aktuelle Einsatzbereiche additiver Fertigungsverfahren. (Verändert nach [20])

Auch findet die additive Fertigung Einzug im Bereich der Konsumgüter und Mode. Beispielsweise kann eine Schuhsohle ergonomisch und individuell auf den Verbraucher angepasst oder Spikes bei Sportschuhen optimal platziert werden [19]. In der Lebensmittelindustrie wird das additive Herstellungsverfahren zur Entwicklung neuer Texturen und Kreieren komplexer Strukturen im Süßwarenbereich verwendet [21]. Ganz andere Dimensionen nimmt der 3D-Druck in der Baubranche ein [9]. Im Jahr 2014 wurde in Amsterdam im Rahmen eines Kunstprojektes das erste Haus additiv gefertigt und noch im gleichen Jahr fertigte die Firma WinSun in Shanghai mehrere Häuser serienmäßig mittels 3D-Druck in unter 24 Stunden [9,22].

Der hohe Grad der Individualisierbarkeit bei gleichzeitig rascher Herstellung machen den 3D-Druck zu einem idealen Werkzeug für die Fertigung von Prototypen, die bis dato in zeitaufwändigen und kostenintensiven Arbeitsschritten hergestellt wurden [4]. Anpassungen des Prototyps können innerhalb kürzester Zeit umgesetzt und selbst komplexe Geometrien realisiert werden. Vom sogenannten *Rapid Prototyping* profitiert daher besonders die Produktentwicklung, aber auch allgemein ist das Anwendungsspektrum von Prototypen in der industriellen Fertigung immens [4]. Doch die additive Fertigung eignet sich längst nicht mehr nur zur schnellen Anfertigung von Prototypen, besonders die Flug- und Fahrzeugindustrie setzt auf die serienmäßige Fertigung von Komponenten aus dem 3D-Drucker. Bei Bauteilen, die komplex aufgebaut sind und/oder Gewichtsbegrenzungen eingehalten werden müssen, wird gerne auf eine additive Fertigung zurückgegriffen [9]. So

wird geschätzt, dass 2030 bis zu 5 % aller Elemente für Fahr- und Flugzeuge additiv gefertigt werden [23].

Bereits in den frühen 2000er Jahren fand der 3D-Druck erste Anwendungen im Bereich der Medizin [5,24,25]. Daten aus bildgebenden Verfahren, die beispielsweise Knochen des Patienten abbilden, können in ein 3D-Modell umgewandelt und 3D-gedruckt werden, sodass patienten-spezifische Produkte erzielt werden [26,27]. Auf diesem Wege werden maßgeschneiderte Prothesen und Implantate hergestellt, die nicht nur für den Patienten, sondern auch für die Ärzte von großem Nutzen sind. Maßgefertigte Prothesen, medizinische Vorrichtungen und chirurgische Instrumente können positive Auswirkungen sowohl auf die Operationszeit, die Genesungszeit als auch den allgemeinen Erfolg des medizinischen Eingriffs haben [26]. Des Weiteren helfen 3D-gedruckte anatomische Modelle den Ärzten bei Planungen von Operationen [27,28]. Besonders mit der Entwicklung des *Bioprinting*, der das 3D-Drucken von biologischen Systemen wie beispielsweise Zellen ermöglicht, ist das öffentliche Interesse für den Einsatz von 3D-Druck im bio-medizinischen Sektor geweckt worden [26,29]. Große Hoffnung wird darauf gesetzt, dass zukünftig das 3D-Drucken von Gewebestrukturen und Organen möglich sein könnte. Jedoch wirft dieses Ziel bislang noch große Herausforderungen auf, wie beispielsweise eine gleichmäßige Sauerstoffversorgung der Zellen oder das *Bioprinting* verschiedener Materialien [9,29,30]. In der chemischen und biotechnologischen Forschung werden die Vorzüge des 3D-Drucks beispielsweise zur Herstellung von individuellen, experiment-spezifischen Laborequipment sowie Versuchssystemen genutzt [31,32]. Einen wesentlichen Einfluss hat die 3D-Drucktechnologie dabei auf das Gebiet der Mikrofluidik, indem sie sowohl die Fertigungsdauer von mikrofluidischen Systemen bedeutend verkürzt als auch die Herstellung komplexer Geometrien ermöglicht [5,33]. In Kapitel 3.3 wird der Einfluss der additiven Fertigung auf die Biotechnologie und Biomedizin weiter ausgeführt.

3.2 Übersicht über additive Fertigungsverfahren

Vorangetrieben durch die Ambition beispielsweise neue Materialien einzubinden, in höheren Auflösungen zu drucken, Druckfehler zu reduzieren oder größere Objekte zu fertigen, wurden in den vergangenen Jahren eine Vielzahl von additiven Fertigungs-verfahren entwickelt [9]. Allen Verfahren ist das aufbauende (additive) Grundprinzip gemein: Schicht für Schicht wird das gewünschte Objekt gebildet. Mit dem Ziel die verschiedenen 3D-Druckverfahren und -technologien einzuordnen und zu klassifizieren, wurde 2015 die Norm DIN EN ISO/ASTM 52900 eingeführt. Sie definiert sieben Prozesskategorien von additiven Fertigungsverfahren, denen jeweils teils mehrere 3D-Drucktechnologien zugeordnet werden [34].

Folgende sieben Prozesskategorien werden beschrieben [34]:

1. Freistrahl-Bindemittelauftrag (engl.: *binder jetting*)

   · Fertigungsverfahren, bei dem ein flüssiger Bindestoff selektiv an ausgewählten Bereichen eines Pulverbettes aufgetragen wird, um Pulverpartikel miteinander zu verbinden.

2. Materialauftrag mit gerichteter Energieeinbringung (engl.: *directed energy deposition*)

   · Fertigungsverfahren, bei dem fokussierte thermische Energie genutzt wird, um Materialien durch Schmelzen miteinander zu verbinden.

3. Materialextrusion (engl.: *material extrusion*)

   · Fertigungsverfahren, bei dem Material durch eine beheizte Düse zum Schmelzen gebracht und selektiv ausgegeben wird.

4. Freistrahl-Materialauftrag (engl.: *material jetting*)

   · Fertigungsverfahren, bei dem Materialtröpfchen selektiv gesetzt und ausgehärtet werden.

5. Pulverbettbasiertes Schmelzen (engl.: *powder bed fusion*)

   · Fertigungsverfahren, bei dem thermische Energie zum selektiven Schmelzen von Pulverpartikeln innerhalb eines Behälters dient.

6. Schichtlaminierung (engl.: *sheet lamination*)

   · Fertigungsverfahren, bei dem Materialschichten zu einem Objekt zusammengefügt werden.

7. Badbasierte Photopolymerisation (engl.: *vat photopolymerization*)

   · Fertigungsverfahren, bei dem flüssige Photopolymere in einem Behälter durch eine Lichtquelle selektiv ausgehärtet werden.

Die Anzahl an entwickelten Technologien ist immens, sodass in den folgenden Abschnitten nur auf einige ausgewählte Beispiele eingegangen wird. Eine ausführliche Beschreibung gegenwärtiger additiver Fertigungsverfahren und -technologien lässt sich in den Ausführungen von Gibsen *et al.* finden [14].

Die durch Charles Hull patentierte, erste 3D-Drucktechnologie namens Stereolithographie (SLA) wird der badbasierten Photopolymerisation zugeordnet. Bei dieser Technologie wird ein Laserstrahl über mehrere Spiegel selektiv an ausgewählte Bereiche eines Behälters gelenkt, der mit flüssigem Photopolymer-Gemisch gefüllt ist. Die aktivierten Polymere bzw. Monomere/Oligomere polymerisieren und bilden die erste Festkörperschicht [5,35]. Nach Beenden des Drucks wird das neu gefertigte Objekt aus dem Flüssigkeitsbehälter entfernt und optional nachbearbeitet. Beispielsweise kann eine zusätzliche Aushärtung mittels UV-Licht die mechanischen Materialeigenschaften weiter

verändern [9]. Mittels SLA können Objekte mit einer hohen Auflösung gefertigt werden (Schichtdicke von bis zu 10 µm), die Druckgeschwindigkeit ist jedoch im Vergleich zu anderen Fertigungstechnologien relativ langsam und die Auswahl an möglichen Materialien begrenzt [9]. Außerdem limitieren die Maße des Flüssigkeitstanks die mögliche Größe des Objektes und der notwendige Füllstand des Behälters führt zu erhöhten Abfallmengen von flüssigem Ausgangsmaterial [5].

Die verbreitetste 3D-Drucktechnologie ist das *Fused Deposition Modeling* (FDM), die der Prozesskategorie „Materialextrusion" zugehört [5]. Bei dieser Methode wird ein Filament aus festem, thermoplastischem Material an einer beheizten Düse geschmolzen und gemäß der gewünschten Objektgeometrie auf eine Plattform extrudiert [5,36]. Nach Aushärten der ersten Schicht wird die nächste aufgetragen, bis das Objekt fertiggestellt ist. Einfache FDM-Drucker sind handelsüblich verfügbar, verhältnismäßig günstig und eignen sich daher für eine Anschaffung zu privaten Zwecken für Zuhause [9,35]. Neben den vergleichsweise niedrigen Kosten ist die schnelle Druckgeschwindigkeit einer der Hauptvorteile dieses Fertigungsverfahrens [9,36]. Dagegen sprechen schwache mechanische Eigenschaften, eine schlechte Oberflächenqualität, die Erkennung der einzelnen Schichten des schichtweisen Prozesses und die nur limitierte Anzahl an thermoplastischen Materialien [36].

Alle im experimentellen Teil dieser Arbeit beschriebenen 3D-gedruckten Objekte wurden mittels *Polymer Inkjet Printing* gefertigt. *Polymer Inkjet Printing* bezeichnet eine 3D-Drucktechnologie, bei der kleine Tröpfchen eines lichtsensitiven Photopolymerharzes auf eine Plattform abgegeben und dort mittels UV-Licht selektiv ausgehärtet werden (siehe **Abbildung 3-2**) [14,37]. Entsprechend wird diese Technologie der Prozesskategorie „Freistrahl-Materialauftrag (engl.: *material jetting*)" zugeordnet.

Ein Hauptvorteil dieser Fertigungstechnologie besteht darin, verschiedene Materialien im selben Druckprozess zu verwenden. Diese Option wird vor allem genutzt, um unterstützendes Stützmaterial (Supportmaterial) direkt im Druckprozess an entsprechende Objektstellen zu platzieren. Stützmaterial dient dazu Modellstrukturen während des Druckvorgangs Halt zu geben. Nach Fertigstellung des Druckvorgangs wird das Stützmaterial mechanisch entfernt oder im Fall von löslichem Stützmaterial thermisch geschmolzen, sodass einzig das Photopolymer als Modellmaterial erhalten bleibt [14,37]. Meist wird das flüssige Support- und Photopolymermaterial durch zahlreiche Druckköpfe bzw. Druckdüsen auf die Druckplattform aufgegeben. Dort werden die Materialtröpfchen mit einer Planierschiene (*leveling blade*) geglättet und anschließend mittels UV-Licht ausgehärtet (siehe **Abbildung 3-2**).
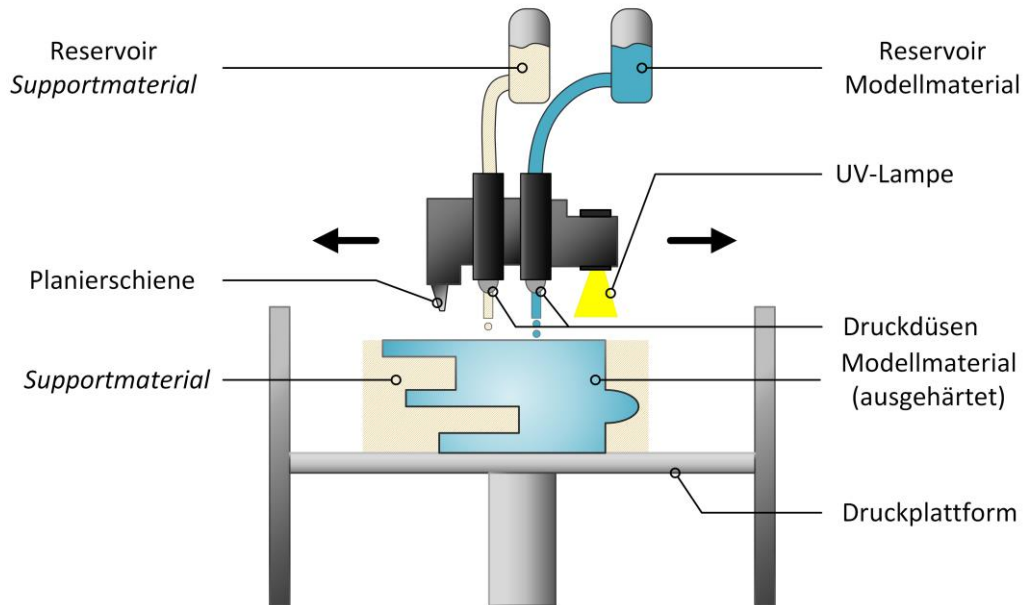
Abbildung 3-2 Darstellung der additiven Fertigungstechnologie *Inkjet Printing*.

Durch diesen Prozessvorgang wird nicht nur eine schnelle Fertigung, sondern auch eine hohe Druckauflösung (Schichtdicke von bis zu 10 µm) und Oberflächenqualität erreicht [14,37]. Jedoch ist auch bei dieser Fertigungstechnologie die Auswahl an möglichen Materialien begrenzt [38]. Verschiedene polymerbasierte Materialien sind kommerziell erhältlich, darunter sind unter anderem transparente Acrylate sowie Silikonmaterialien.

In den vergangenen Jahren ist das Interesse vor allem an hochauflösenden additiven Fertigungstechnologien stark gestiegen [39,40]. Als „hochauflösend" wird dabei die additive Herstellung mit Schichtdicken kleiner als 50 µm bezeichnet [37]. Traditionelle Verfahren zur Fertigung von Modellen im Mikro- oder Nanomaßstab weisen neben den geometrischen Einschränkungen, die durch das subtraktive oder formative Prozessverfahren bedingt sind, hohe Fabrikationszeiten und -kosten auf [39]. Diese Verfahrensbeschränkungen könnten zukünftig mit additiven Fertigungstechnologien umgangen werden. Herausforderungen bieten, wie zuvor beschrieben, weiterhin allerdings die begrenzte Materialauswahl und der hohe Nachbearbeitungsaufwand [40]. Beispiele additiver Fertigungstechnologien, die sich zur Herstellung von Objekten im Mikro- und Nanomaßstab eignen, sind die Zwei-Photonen-Polymerisation (2PP), Mikro-Stereolithographie (MSL) und der Elektrohydrodynamische Tintenstrahldruck (EHDP) [39-41].

3.3 Additive Fertigung in der Biotechnologie und Biomedizin

Obwohl die additive Fertigungstechnologie bereits vor mehr als 30 Jahren entwickelt wurde, findet sie in der heutigen biotechnologischen und biomedizinischen Forschung eher beschränkt Anwendung [42]. Dabei bietet die additive Fertigung gerade für die Forschung ein wertvolles Werkzeug zur kreativen Problemlösung und zur Schaffung individueller Experimentierbedingungen. Das folgende Kapitel soll einen Überblick über aktuelle Anwendungsbereiche der additiven Fertigung in der Biotechnologie und Biomedizin geben. Dabei konzentrieren sich die Ausführungen auf polymerbasierte 3D-Druckmaterialien.

Wie bereits in Kapitel 3.1 beschrieben, fand die additive Fertigung anfangs vor allem Anwendung zur schnellen, physischen Umsetzung von Konstruktionsentwürfen bevor ein Produkt mit anderen Fertigungsverfahren in Serie gefertigt wurde [4]. Übertragen auf die Laborumgebung konnte mittels *Rapid Prototyping* beispielsweise eine schnelle Anpassung von Formen oder Formeinsätzen für die konventionelle Fertigung von Laborgeräten realisiert werden [14]. Die Anwendungen der additiven Fertigung sind jedoch längst nicht mehr auf den Bau von Prototypen beschränkt. Mit einem modernen 3D-Drucker können Laborartikel mit den gleichen Materialeigenschaften wie kommerziell erhältliche Produkte gefertigt werden [31,42]. CAD Dateien für entsprechende Laborartikel, wie z. B. Gelkämme oder Pipettenhalter, sind in Online-Datenbanken in unterschiedlichen Variationen zur freien Verwendung bereitgestellt. Das sogenannte *Print-on-demand*, die Fertigung nur nach Bedarf, von benötigten Artikeln und Hilfsmaterialien für die Laborumgebung leistet dabei zugleich einen Beitrag zur Nachhaltigkeit und Reduktion von Kunststoffen [14]. Darüber hinaus können mittels 3D-Druck individuelle, spezialisierte Versuchssysteme und Laborartikel direkt vor Ort gefertigt werden. Es wird ein Umdenken möglich: Wo bisweilen das Experiment an kommerziell erhältliche Versuchssysteme und Equipment angepasst werden musste, können nun Versuchsapparaturen für ein spezifisches Experiment individuell maßgefertigt werden. So wurden beispielsweise Kolbendeckel mit individuellen Anschlüssen eigens für ein Experiment entworfen und additiv gefertigt, sowie eine Probenahme ohne Entfernung des Kolbendeckels ermöglicht [43,44].

Wesentlichen Einfluss hat die additive Fertigung auf das Gebiet der Mikrofluidik, welches die Handhabung und Analyse von Flüssigkeiten im Mikrometermaßstab beschreibt [45-48]. Komplexe Kanalstrukturen und Geometrien konnten bisweilen nur in zeit-, energie- und kostenaufwendigen Fertigungsverfahren hergestellt werden. Mithilfe von hochauflösenden 3D-Drucktechnologien lassen sich gleichwertige Ergebnisse in nur einem Bruchteil der

Zeit erzielen und mittels der Verwendung transparenter Materialien wird eine optische Sichtung ermöglicht [45,48]. Die Fähigkeit, mehrere Prozessschritte auf einem einzigen Chip zu kombinieren, gibt mikrofluidischen Systemen einen bedeutenden Vorteil gegenüber traditionellen Methoden, die in der Laborumgebung verwendet werden [49,50]. Diese Systeme, die allgemein als *Lab-on-Chip* (LoC) bezeichnet werden, ermöglichen die Vereinfachung und Automatisierung komplexer Protokolle und Abläufe, sowie die Parallelisierung von Experimenten. Gleichzeitig reduzieren sie das notwendige Proben- und Reagenzienvolumen [49,51]. Als in LoC-Systeme integrierbare Einheiten sind beispielsweise mikrofluidische Separatoren, passive Mikromischer, funktionale Ventile, Inkubationsschleifen oder Reaktionskammern zu nennen [33,49,52-54]. In Kapitel 4.4 wird eine 3D-gedruckte, dynamische Durchflusszelle vorgestellt, die eine homogene Vermischung von Flüssigkeitsströmen durch Integration von passiven Mikromischer-Einheiten bewirkt. Wie in **Abbildung 3-3** schematisch dargestellt, könnten additiv gefertigte LoC-Systeme beispielsweise direkt an einen Bioprozess gekoppelt werden und eine kontinuierliche Kultivierung ermöglichen.
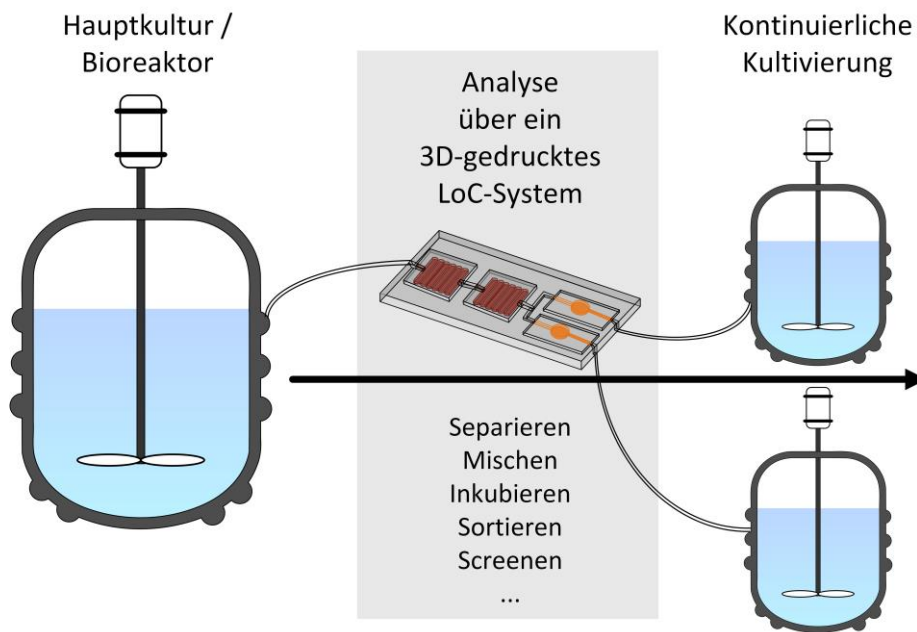
Abbildung 3-3 Schematische Darstellung von möglichen Analysemethoden eines in einen Bioprozess integrierten, additiv gefertigten, mikrofluidischen LoC-Systems.

Der 3D-Druck bietet die Möglichkeit Reaktoren und Reaktionssysteme individuell, maßgefertigt herzustellen. Die Fertigung ist dabei jedoch in der Größe limitiert – abhängig vom verwendeten 3D-Drucker können nur eher kleine Systeme im Mikroreaktormaßstab gefertigt werden. Der kleine Maßstab bietet aber auch Vorteile. Reaktionen können in

einer hochkontrollierten Umgebung stattfinden. Das gesamte System kann homogen temperiert werden, Reaktionen können unproblematisch überwacht und automatisiert gesteuert werden [50]. Durchflussreaktoren mit teils komplexen Strömungsgeometrien wurden bereits zur Durchführung verschiedenster chemischer Reaktionen additiv gefertigt [55-58]. Lederle *et al.* verdeutlichten in einer Studie die Eignung von aus Acrylnitril-Butadien-Styrol (ABS) gedruckten Reaktionsgefäßen zur Durchführung chemischer Reaktionen unter Inertgasatmosphäre selbst mit hochreaktiven Reagenzien. Sie demonstrierten damit die aus dem FDM-Fertigungsprozess resultierende Dichtigkeit, sowie die Chemikalienbeständigkeit von ABS [59]. Einen umfassenden Überblick über gegenwärtige Anwendungen der additiven Fertigung im chemischen Labor sind in den Ausführungen von Hübner und Lederle zu finden [60]. Im biotechnologischen Bereich entwickelten beispielsweise Krujatz *et al.* ein Bioreaktorsystem für die Kultivierung und Überwachung von Mikroalgen und photobiotechnologischen Prozessen, das aus Polyamid additiv gefertigt wurde und ein Arbeitsvolumen von 20 mL fasst [61]. Schmidt *et al.* entwarfen ein Perfusions-Bioreaktorsystem, das die Kultivierung von adhärenten Zellen in bis zu vier Sauerstoff-kontrollierten, additiv gefertigten Mikrobioreaktoren ermöglicht [62]. Durch Automatisierung des Systems konnte ein gleichmäßiges, reproduzierbares Aussäen der Zellen ermöglicht werden. Auch Rimington *et al.* realisierten Perfusions-Bioreaktoren mithilfe der additiven Fertigung [63]. Das 3D-gedruckte Perfusionssystem unterstützte die Differenzierung myogener Vorläuferzellen.

Für einen Einsatz im Bioreaktor wurden beispielsweise Rührer mit komplexen Geometrien additiv gefertigt oder Modelle entwickelt, die mit einer hohen spezifischen Oberfläche einen Biofilm im Reaktor vor vorzeitigem Ablösen schützen [31,64]. Khan *et al.* setzten die additive Fertigung zur Herstellung von Reaktoreinsätzen ein, die mit einer feinen gitterartigen und porösen Struktur auf *Beads* immobilisierte Mikroorganismen einschließen [65]. Die *Beads* konnten in die 3D-gedruckte poröse Struktur eindringen und wurden dort zurückgehalten, wodurch die Exposition der Mikroorganismen mit dem Kulturmedium erhöht werden sollte. Odeleye *et al.* optimierten das Wachstum von Stammzellen auf *Microcarrier* durch Integration von additiv gefertigten Strömungsverteilern in den Fließbettreaktor [66]. Die Strömungsverteiler stellten eine gleichmäßige Strömung, sowie einen ausreichenden Nährstofftransfer zu den Partikeln sicher.

Weitere Anwendung findet die additive Fertigung in der Sensorik, Analytik und Überwachung von (biotechnologischen) Prozessen. Durch den Einsatz von leitfähigen 3D-Druckmaterialien können zum Beispiel Elektroden für elektrochemische Sensoren maßgefertigt werden [67,68]. Die auf diese Weise hergestellten Elektroden können mit biologischen

Komponenten funktionalisiert und zur elektrochemischen Detektion von Analyten verwendet werden [69]. Nesaei *et al.* konnten durch Funktionalisierung der 3D-gedruckten Elektroden mit Glucose Oxidase sogar eine höhere Sensitivität gegenüber Glucose als mit funktionalisierten, konventionellen *Screen-printed electrodes* erreichen [70]. Eine andere Möglichkeit stellt die Verwendung des 3D-Drucks zur Fertigung von individuellen, häufig mikrofluidischen Plattformen und Geräteapparaturen für die Biosensorik und Analytik dar, in die kommerzielle Produkte, wie z.B. Smartphones, Elektroden, Membranen oder andere Sensorkomponenten integriert werden können [71-75]. In diesem Bereich gibt es zahlreiche Beispiele für 3D-gedruckte Sensorsysteme, die sich anhand ihrer biologischen Komponente in zellbasierte, enzymbasierte, antikörperbasierte, aptamerbasierte oder *bead*-basierte Sensoren einteilen lassen. Einen umfassenden Überblick über den Einsatz der additiven Fertigung in der Biosensorik geben Ni *et al.* [71]. Da im experimentellen Teil dieser Arbeit ein Biosensor mit elektrochemischem Detektionsprinzip beschrieben wird, fokussieren sich die nachfolgenden Ausführungen auf elektrochemische Biosensoren.

Dong *et al.* haben beispielsweise ein nahezu vollständig 3D-gedrucktes, enzymbasiertes Sensorsystem zur Detektion von Laktat vorgestellt [76]. Sie druckten mit verschiedenen 3D-Druckmaterialien sowohl die Elektroden als auch die Kabelanschlüsse und das Gehäuse des Systems. Einzig eine aus Polyethylenterephthalat (PET) bestehende Unterlage fertigten sie nicht mittels 3D-Druck. Für die online-Analyse von Glucose- und Laktatkonzentrationen haben Gowers *et al.* ein mikrofluidisches System entwickelt, in welches zwei enzymbasierte Biosensoren integriert werden können [77]. Aus einem festen, polymerbasierten Material druckten sie einen mikrofluidischen Chip und Halterungen für die Elektroden. Um eine hinreichende Abdichtung der Halterungen mit dem Chip zu gewährleisten, druckten sie zusätzlich Dichtungsringe aus einem weichen, elastischen 3D-Druckmaterial. Motaghi *et al.* setzten die 3D-Drucktechnologie zur Minimierung der notwendigen Probenmengen ein, indem sie eine bipolare Elektrode in einen mikrofluidischen Chip integrierten [78]. Auf diese Weise konnten sie sowohl das benötigte Volumen an Aptamerlösung zur Funktionalisierung der Elektrode als auch das Probenvolumen zur Detektion reduzieren. Die auch im Rahmen dieser Arbeit verwendeten, kommerziell erhältlichen *Screen-printed electrodes* (SPE) wurden von Damiati *et al.* in ein 3D-gedrucktes, mikrofluidisches Sensorsystem integriert. Die SPE und das mikrofluidische System wurden dabei durch eine doppelseitige Klebeschicht zusammengefügt. Li *et al.* stellten ein tragbares Biosensorsystem vor, das aus einem kleinen Impedanzdetektor und einem 3D-gedruckten Chipsystem besteht [79]. In das Chipsystem kann eine SPE und ein *Universal Serial Bus* (USB) Anschlussstück zur Verbindung mit dem Detektor integriert werden.

Es existieren verschiedene Ansätze, um polymerbasierte 3D-Druckmaterialien für analytische oder sensorische Zwecke zu funktionalisieren. Je nach gewählten additiven Fertigungsverfahren und Druckmaterial weist die 3D-gedruckte Struktur eine Topographie und Rauheit auf, die sich als Träger für katalytisch aktives Material eignet [60]. Zur Umsetzung chemischer Reaktionen können mit nasschemischen Methoden katalytische Beschichtungen auf das Material aufgetragen werden [60]. Ebenso können vorhandene reaktive Gruppen des verwendeten 3D-Druckmaterials für kovalente Funktionalisierungen genutzt werden [60]. Kazenwadel *et al.* entwickelten ein modular aufgebautes Reaktorsystem zur Implementierung und Testung von Enzym Kaskaden [80]. Zur Immobilisierung von Enzymen wurden in einem ersten Schritt die im acrylbasierten Druckmaterial vorhandenen Carboxylgruppen durch Zugabe eines Carbodiimids aktiviert und daran anschließend Enzyme über Amidbindungen kovalent gebunden. Durch ein ähnliches Verfahren erreichten auch Peris *et al.* eine Aldehyd-funktionalisierte Materialoberfläche eines mittels FDM gedruckten Nylons, an welche sie eine Transaminase kovalent immobilisierten [81]. Im Gegensatz zu einer Funktionalisierung von bereits gedruckten Materialteilen, fügten Manzano *et al.* dem Ausgangsmaterialgemisch (polymerbasiert) vor dem additiven Fertigungsprozess für ihre Anwendung funktionelle Monomere hinzu [82]. Auf diese Weise konnten sie Objekte mit einer intrinsischen chemischen Reaktivität additiv fertigen. Häufig ist es jedoch nicht möglich, Anpassungen des Ausgangspolymergemisches vorzunehmen, da viele 3D-Druckersysteme auf kommerziell erhältliche Materialkartuschen angewiesen sind, die nur ungeöffnet vom 3D-Druckersystem akzeptiert werden.

Ein weiterer Anwendungsbereich der additiven Fertigung, der hier nur der Vollständigkeit halber genannt werden soll, ist das *Bioprinting*. Besonders im biomedizinischen Bereich und im *Tissue Engineering* wurden durch das 3D *Bioprinting* neue Maßstäbe gesetzt. Lebende Zellen, wie beispielsweise Stammzellen, Zelllinien und vom Patienten stammende Zellen, können mit guter räumlicher Kontrolle in nahezu jede gewünschte strukturelle Anordnung gedruckt werden [83,84]. Infolgedessen ist es möglich, technische Konstruktionen nachzubilden, die die Form, Struktur, Architektur und/oder Funktion von nativen Geweben oder Organen imitieren [83-85]. Einen umfassenden Überblick über die Fortschritte des 3D *Bioprinting* und gegenwärtige Anwendungen sind in den Artikeln von Matai *et al.* sowie Jovic *et al.* zu finden [86,87].

3.4 Materialien für die additive Fertigung

Materialien und deren zugrunde liegenden Eigenschaften kommt bei der Frage, ob sich die additive Fertigung im Bereich der Biotechnologie bewähren kann, eine Schlüsselrolle zu. Die Auswahl an Materialien ist allerdings trotz starkem wirtschaftlichen Wachstum

der 3D-Druckbranche bisher sehr begrenzt [5,9]. Weiter verlangen Hersteller häufig die Verwendung ihrer eigenen, proprietären Materialien in ihren 3D-Druckern – ansonsten riskiert der Verbraucher den Verlust der Garantie [5]. Diese Situation schränkt den Materialpool zusätzlich ein.

Die Ausgangsmaterialien für den 3D-Druck werden je nach Fertigungstechnologie in Form von Pulvern, Schichten, Flüssigkeiten oder Filamenten verarbeitet (siehe **Abbildung 3-4**). Die verschiedenen additiven Fertigungstechnologien stellen dabei unterschiedliche Anforderungen an die Ausgangsmaterialien. Beispielsweise können mittels FDM ausschließlich thermoplastische Materialien verarbeitet werden und SLA sowie *Inkjet Printing* sind auf photosensitive Polymere angewiesen.
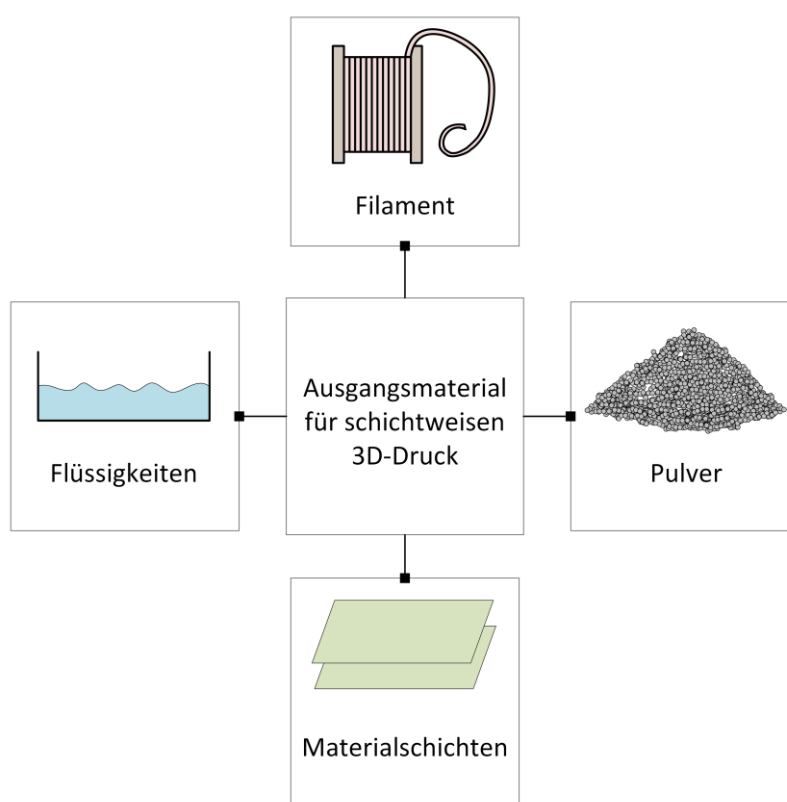
Abbildung 3-4 Schematische Darstellung der schichtweisen Fertigung bei Verwendung unterschiedlicher Ausgangsmaterialien (verändert nach [88]).

Die gebräuchlichsten Materialien für die additive Fertigung sind Metalle und Legierungen, Polymere und Keramiken [14,9]. In den letzten Jahren wurden außerdem zahlreiche Verbundwerkstoffe (*composites*) entwickelt, die mittels 3D-Druckverfahren verarbeitet werden können [9,89]. Verbundwerkstoffe bestehen in der Regel aus einem Polymer-Hauptmaterial und einem Verstärkungsmaterial, wie Carbonfaser oder Glasfaser. Im Rahmen

dieser Arbeit wurde ausschließlich mit Polymeren als Fertigungsmaterial gearbeitet, so-dass sich die folgenden Ausführungen auf diese fokussieren.

Als Polymer wird ein Stoff bezeichnet, dessen Struktur im Wesentlichen aus sich wieder-holenden Einheiten besteht [90]. Diese Einheiten leiten sich im Allgemeinen von Molekülen mit geringer relativer Molekülmasse ab [90]. Es werden natürliche und synthetische Poly-mere unterschieden [90,91]. Natürliche Polymere, auch Biopolymere genannt, werden in Le-bewesen synthetisiert [90]. Zu ihnen gehören sowohl Proteine und Nukleinsäuren, die aus den Monomer-Einheiten Aminosäuren und Nukleotide aufgebaut sind, als auch Cellulose und Chitosan, die aus β-D-Glucose- bzw. Glucosamin-Einheiten bestehen [91]. Als synthe-tische Polymere werden Stoffe bezeichnet, die durch Reaktionen (Polymerisation, Poly-kondensation, Polyaddition) künstlich hergestellt wurden [90]. Die in der additiven Ferti-gung am häufigsten verwendeten Polymere sind die synthetisch hergestellten Stoffe Ac-rylnitril-Butadien-Styrol (ABS) und Polylactid (PLA)[9]. Beide Materialien sind durch Wärmezufuhr in einem bestimmten Temperaturbereich verformbar (thermoplastisch) und werden auf Grund dieser Eigenschaft häufig für die additive Fertigung mittels FDM verwendet [9,92]. Synthetische, photosensitive Monomere bzw. Oligomere polymerisieren nach Aktivierung mittels UV-Licht und werden bei 3D-Drucktechnologien wie SLA oder *Inkjet Printing* verwendet [93]. Bei diesen Fertigungsverfahren umfasst das flüssige Poly-mer-Gemisch neben den Monomer- bzw. Oligomer-Einheiten weitere Komponenten wie Photoinitiatoren und Additive (z. B. Pigmente, (Licht-)Stabilisatoren oder Inhibito-ren) [93,94]. Photoinitiatoren agieren als Katalysatoren der Photopolymerisation, indem sie absorbierte Lichtenergie in reaktive Spezies (freie Radikale und/oder Kationen) umwan-deln [94]. Die reaktive Spezies initiiert über radikale oder kationische Reaktionsmechanis-men das Kettenwachstum der Polymerkette und ist daher von hoher Relevanz für den 3D-Druckprozess [94].

In der vorliegenden Arbeit wurden zwei verschiedene Materialien verwendet, die auf syn-thetischen Polymeren basieren und mittels *Inkjet Printing* verarbeitet wurden. In Kapitel 4.1 und 4.4 wird das Material „VisiJet® M2R-CL" (vertrieben von 3D Systems Inc.) und in Kapitel 4.2 und 4.3 das Material „AR-M2" (vertrieben von Keyence GmbH) charak-terisiert und in Anwendungen beschrieben. Bei beiden Materialien handelt es sich um feste, unbiegsame, transluzente Polyacrylate, die jeweils aus zwei verschiedenen Acrylat-monomeren bzw. -oligomeren aufgebaut sind [95,96]. Neben starren, unbiegsamen Druckob-jekten können ebenso elastische Bauteile gefertigt werden [97,98]. Das Polymergemisch be-steht in dem Fall zu einem hohen Anteil aus Silikonen (Poly(organo)siloxane).

Eine weitere Klasse von polymerbasierten Materialien wird durch das 3D *Bioprinting* beschrieben. Hier werden Materialien benötigt, die Gewebe- und Organstrukturen möglichst nah imitieren und/oder den *In-vivo*-Anforderungen hinsichtlich biologischer Verträglichkeit, Zersetzung und dem Erhalt der Zellfunktionalität gerecht werden [30]. Gleichzeitig sollten die Materialien „3D-druckbar" sein, d. h. sie sollten den Bedingungen des additiven Fertigungsprozesses standhalten. Als Hauptakteure in dieser Sparte haben sich hydrogelbasierte Systeme etabliert [30,45]. Der Begriff „Hydrogel" bezieht sich auf ein hydrophiles 3D-Netzwerk, das aus natürlichen oder synthetischen Polymeren mit hohem Wassergehalt besteht [30,99]. In den letzten Jahren haben sich verschiedene Polymere als Hydrogel-Komponenten bewährt, darunter sind Alginat, Collagen, Chitosan, Hyaluronsäure, Gelatine, methacrylierte Gelatine und Polyethylenglycol [30,100-102].

Gegenwärtige Entwicklungen zielen darauf ab, die mechanischen Eigenschaften 3D-gedruckter, polymerbasierter Materialien weiter zu verbessern. Reine Polymerprodukte weisen häufig nur eine geringe Festigkeit sowie Temperaturbeständigkeit auf, weswegen sie für einige Anwendungen ungeeignet sind [9,89]. Diese Eigenschaften können durch den Zusatz von Verstärkungsmaterialien wie Carbon- oder Glasfasern, verbessert werden [89]. Die resultierenden Verbundwerkstoffe werden bereits für die industrielle Fertigung anspruchsvoller Funktionsprototypen oder Automobilteilen verwendet [9,10].

3.4.1 Materialanforderungen

Ein Material unterliegt verschiedensten Anforderungen hinsichtlich des additiven Fertigungsprozesses oder der beabsichtigten Anwendung [9]. Wie bereits angesprochen, setzt die Fertigung mittels FDM beispielsweise thermoplastische und das *Inkjet Printing* photosensitive Materialien voraus. Der beabsichtigte Anwendungsbereich stellt weitere Forderungen an physikalische, chemische und biologische Eigenschaften eines Materials – oder aus anderer Sichtweise: die physikalischen, chemischen und biologischen Eigenschaften eines Materials bestimmen über dessen Anwendungsspektrum. **Abbildung 3-5** gibt einen Überblick über mögliche Materialeigenschaften, die speziell eine biotechnologische Anwendung beeinflussen und bestimmen können.
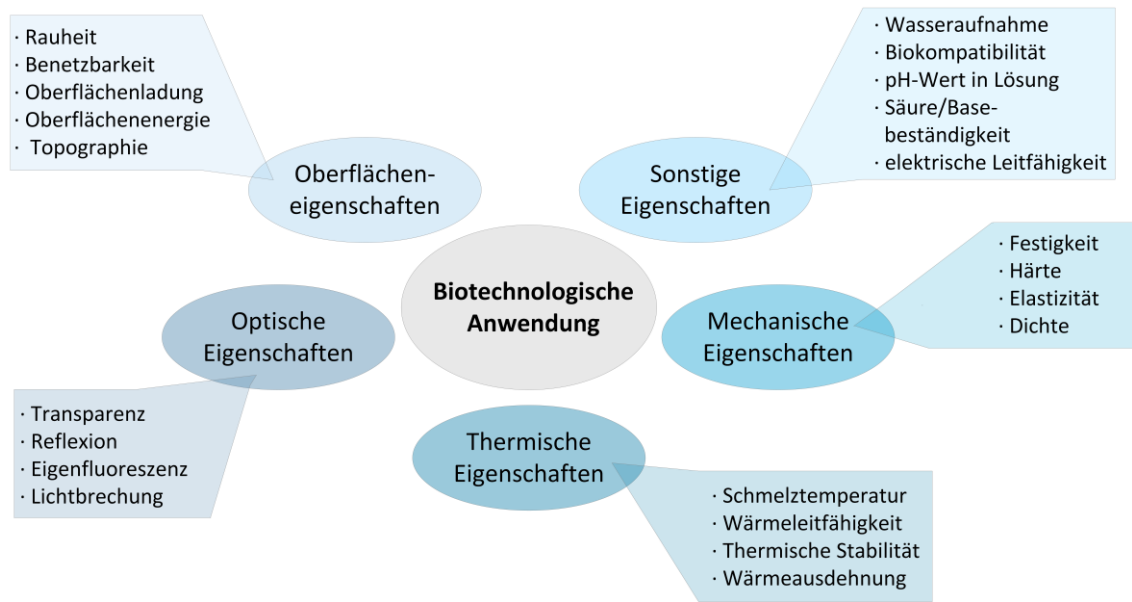
Abbildung 3-5 Auswahl von Materialeigenschaften, die eine Anwendung speziell im biotechnologischen Bereich bestimmen können.

Zur optischen Kontrolle und Analyse von Flüssigkeitsströmen oder stattfindenden Prozessen innerhalb eines Systems sind die optischen Materialeigenschaften wie Transparenz und Reflexion bedeutsam. In der Biotechnologie können dies Anwendungen als LoC-System oder die Überwachung von Bioprozessen in additiv gefertigten Bioreaktoren sein, die auf transparente Materialien angewiesen sind. Des Weiteren entscheidet die Eigenfluoreszenz eines Materials über die Möglichkeit der mikroskopischen Analyse mittels Fluoreszenzmikroskopie, welches eine Verwendung beispielsweise in der Zellanalytik einschränken kann. Mechanische Materialeigenschaften wie Härte, Festigkeit und Elastizität bestimmen maßgeblich den Anwendungsbereich als auch die Haltbarkeit des Materials in der jeweiligen Anwendung. Ist ein Material mit geringer Zugfestigkeit einer permanent hohen Kraft ausgesetzt, kann es frühzeitiger zu Verformungen oder zum Bruch kommen.

Soll ein Material in einer biologischen Umgebung (wie z. B. Anwendungen in der Zellkultur) eingesetzt werden, muss dieses gewisse Sterilitätsanforderungen erfüllen [103]. Ein Verfahren zur Sterilisation ist die thermische Behandlung mit feuchter Hitze im Autoklaven. Dabei wird das zu sterilisierende Material Temperaturen von meist 121 °C für mehrere Minuten ausgesetzt. Thermische Materialeigenschaften wie Schmelztemperatur, Wärmeausdehnung und thermische Verformung sind daher wichtige Parameter, die über die Verwendung eines thermischen Sterilisationsverfahrens bestimmen und ultimativ über den Einsatz eines Materials in biomedizinischen und biotechnologischen Anwendungen entscheiden können. Die Wärmeleitfähigkeit sowie Wärmeausdehnung eines Materi-

als können außerdem bei temperaturgeführten Prozessen, wie beispielsweise biotechnologischen Zellkultivierungen, von Relevanz sein und sollten mit in die Prozessplanung einbezogen werden [104]. Vor allem durch Zusatz von Verstärkungsmaterialien wie Carbon- oder Glasfasern im Polymergemisch können dabei veränderte thermische Eigenschaften erhalten werden [89].

Der additive Fertigungsprozess hat Auswirkungen auf Oberflächeneigenschaften wie Rauheit und Benetzbarkeit, sowie den Glanzgrad [32]. Durch den Fertigungsprozess können unterschiedliche Materialoberflächen mit unterschiedlichen Eigenschaften entstehen [32]. Mittels FDM und *Inkjet Printing* entstehen beispielsweise Modellseiten, die durch den schichtweisen Materialauftrag charakteristische Oberflächenprofile mit einer hohen Rauheit an bestimmten Objektseiten aufweisen. Die Oberflächentopographie kann das Strömungsverhalten von Flüssigkeiten innerhalb eines Systems beeinflussen. Außerdem haben Oberflächentopographie, Rauheit und Benetzbarkeit Einfluss auf die Zelladhäsion und Proliferation und entscheiden daher maßgeblich über die Anwendung eines Materials in der Zellkultur oder *in vivo* [105,106]. Für den Einsatz eines Materials in biologischen Anwendungen sind jedoch noch weitere Eigenschaften bedeutend, wie beispielsweise die Oberflächenladung und -energie sowie der pH-Wert in Lösung. Insgesamt muss die biologische Verträglichkeit (Biokompatibilität) gesichert sein [107,108]. Ein negativer Effekt von aus dem Material entweichenden Verbindungen (*leachables*) muss dabei ausgeschlossen werden. Besonders bei polymerbasierten Materialien ist das Austreten/Auslaugen von nicht auspolymerisierten (Acrylat) Monomeren, Reaktionsprodukten oder anderen Komponenten des Polymergemisches ein bekanntes Problem und häufig mit nachteiligen Effekten auf die biologische Umgebung verbunden [109-111]. Außerdem können sich Reagenzien, die zur Nachbearbeitung (*Post-Processing*) additiv gefertigter Objekte verwendet werden, negativ auf die biologische Umgebung auswirken [112]. Wird ein Material *in vivo*, in den menschlichen Körper eingebracht, sollte eine starke Immunreaktion ausgeschlossen werden [113,110]. So können zytotoxische Effekte ausgehend von Materialien Hautirritationen oder allergische Reaktionen auslösen [114,115]. Materialien werden je nach Verhalten *in vivo* als biostabil oder biodegradierbar klassifiziert [116]. Biodegradierbare Materialien dürfen dabei auch nach Resorption *in vivo* keine negativen Einflüsse auf den Organismus zeigen [116].

3.4.2 Aufarbeitung von 3D-gedruckten Objekten (*Post-Processing*)

Die Nachbearbeitung (*Post-Processing*) von additiv gefertigten Modellteilen bezieht sich auf die (in der Regel manuellen) Schritte, die zur Endbearbeitung und Fertigstellung der Modellteile für den Anwendungszweck notwendig sind [14]. Nach Beenden des *Post-Processing* sind die gefertigten Teile bereit für den Einsatz. Das *Post-Processing* kann

abrasive Bearbeitungsschritte, wie Polieren und Schleifen, aber auch das Aufbringen von Beschichtungen und Lackierungen umfassen [14]. Die notwendigen Bearbeitungsschritte sind sehr anwendungsspezifisch und abhängig von dem zugrunde liegenden additiven Fertigungsverfahren. Ziele des *Post-Processing* können beispielsweise Verbesserungen der Oberflächenstruktur oder der Genauigkeit von Endabmessungen sein. Sieht das Fertigungsverfahren außerdem eine Verwendung von Stützmaterial zur Unterstützung der Modellstrukturen vor, wird dieses im *Post-Processing* entfernt. Je nach Eigenschaft des Stützmaterials kann es mechanisch entfernt oder im Fall von löslichen Stützmaterial thermisch geschmolzen oder aufgelöst werden [14]. Die 3D-Drucktechnologien, die im Rahmen dieser Arbeit zur Fertigung von Objekten verwendet wurden, setzen wasserlösliche oder thermisch schmelzbare Stützmaterialien ein. Durch Verwendung solcher Stützmaterialien wird das Risiko von Beschädigungen am Modell während des *Post-Processing* im Vergleich zur Nutzung von mechanisch zu entfernenden Stützmaterialien stark reduziert. Abhängig von der intendierten Anwendung kann das *Post-Processing* aufwendige Nachbearbeitungsschritte oder eine thermische sowie chemische Behandlung des Modells umfassen [14]. Besonders bei der Nachbearbeitung von kleinen und komplexen Modelldetails, z. B. bei mikrofluidischen LoC-Systemen, kann das *Post-Processing* Herausforderungen bieten und zeitintensive Schritte umfassen. Außerdem stellen sowohl Rückstände des Stützmaterials, als auch weitere Reagenzien, die während des *Post-Processing* z. B. zur Desinfektion verwendet wurden, potentielle Gefahren für die biologische Umgebung dar und können sich negativ auf diese auswirken [112]. Aus diesem Grund sollten alle notwendigen Schritte des *Post-Processing* überlegt durchgeführt und in Hinblick auf die beabsichtigte Anwendung ausgewählt werden.

3.5 Biokompatibilität und *In-vitro*-Testverfahren für die biologische Beurteilung von Materialien

Werden Materialien in unmittelbaren Kontakt mit dem menschlichen Körper gebracht, müssen unerwünschte Nebenwirkungen und Risiken für die Person ausgeschlossen werden. Aus diesem Grund sollten beispielsweise jegliche Medizinprodukte zuvor eingehend auf die biologische Verträglichkeit (Biokompatibilität) untersucht werden [117]. Der Begriff „Biokompatibilität" beschreibt die Verträglichkeit zwischen einem Material (bzw. Endprodukt) und einem biologischen System [113,118]. Als offiziell anerkannte Definition wird häufig auf die Auslegung von David F. Williams auf der „Conference of the European Society of Biomaterials (1986)" verwiesen, der Biokompatibilität definierte als:

> *„The ability of a material to perform with an appropriate host response in a specific application"* [119],

welches in etwa bedeutet: „Biokompatibilität ist die Fähigkeit eines Materials, in einer spezifischen Anwendung bei angemessener Wirtsreaktion eine bestimmte Funktion auszuüben" [120]. Eine „angemessene Wirtsreaktion" umfasst beispielsweise einen normalen, unkomplizierten Heilungsprozess, Resistenz gegen bakterielle Kolonisation oder Biofilmbildung und die Verhinderung von Blutgerinnung [117]. Ein Endprodukt ist dementsprechend biokompatibel, wenn die verwendeten Materialien mit dem Gewebe, den Zellen und den Körperflüssigkeiten des Anwenders wechselseitig verträglich sind [117]. Die Biokompatibilität eines Materials (bzw. Endprodukts) wird dabei sowohl durch dessen Materialeigenschaften, als auch durch die Art und Dauer der intendierten Anwendung bestimmt [120].

Richtlinien und Prüfmethoden zur Beurteilung von Materialien (bzw. Endprodukten) hinsichtlich Biokompatibilität werden in der Normenreihe EN ISO 10993 beschrieben [121]. Die erforderlichen *In-vitro-* und *In-vivo*-Analysen sind dabei von der beabsichtigten Anwendung sowie Kontaktart und -dauer mit dem biologischen System abhängig [120]. Ein Implantat, das dauerhaft in den menschlichen Körper eingesetzt werden soll, muss sich so unter anderem Prüfungen auf Genotoxizität, Hämokompatibilität, Zytotoxizität, systemische Toxizität, Irritationen und Hautsensibilisierungen unterziehen [107]. Bereits in den frühen Phasen der Produktentwicklung können *In-vitro*-Testverfahren nützliche Informationen über die Sicherheit von Materialien liefern. Nur Materialien, die sich *in vitro* als biologisch verträglich erweisen, werden anschließend für eine *In-vivo*-Testung in Betracht gezogen und sind damit möglicherweise für eine klinische Anwendung geeignet. Die frühe Evaluation der Materialien bietet somit nicht nur die Möglichkeit geeignete Kandidaten für *In-vivo*-Studien auszuwählen, sondern spart zudem Ressourcen und Zeit ein [107]. Insgesamt stellt die biologische Beurteilung nach EN ISO 10993 einen ganzheitlichen Ansatz dar, der auf eine gründliche physikochemische Charakterisierung, *In-vitro*-Testverfahren und, nach Auswertung der zuvor erhaltenen Daten, begründeten *In-vivo*-Studien beruht [107,118,120].

Wie bereits in Kapitel 3.4.1 angesprochen, nehmen die physikalischen, chemischen und biologischen Materialeigenschaften Einfluss auf eine biologische Umgebung und damit auf die Biokompatibilität des Materials. Auch das Design und der Herstellungsprozess des Materials bzw. Endprodukts sollten so abgestimmt werden, dass toxikologische Risiken minimiert sind [122]. Im konkreten Fall eines 3D-gedruckten polymerbasierten Materials können sich etwa neben den eigentlichen physikochemischen Materialeigenschaften zahl-

reiche Aspekte auf die Biokompatibilität auswirken, wie z. B. aus dem Material austretende Komponenten des Polymergemisches, Rückstände des Stützmaterials, während des *Post-Processing* verwendete Reagenzien sowie das Desinfektions- bzw. Sterilisationsverfahren.

Es existieren eine Vielzahl von *In-vitro-* sowie *In-vivo*-Prüfmethoden, um die biologische Verträglichkeit eines Materials zu bewerten. Im Rahmen dieser Arbeit wurden 3D-gedruckte Materialien lediglich ersten Biokompatibilitätsprüfungen in *In-Vitro*-Testverfahren zur Analyse der Zytotoxizität unterzogen, um eine sichere Laboranwendung der Materialien in biotechnologischen/biomedizinischen Bereichen zu gewährleisten. Daher konzentrieren sich die folgenden Ausführungen allein auf *In-vitro*-Testverfahren zur Analyse der Zytotoxizität. Eine ausführliche Übersicht und Beschreibung sämtlicher *In-vitro-* sowie *In-vivo*-Prüfmethoden sind in den Ausführungen von Wintermantel *et al.* und der Norm EN ISO 10993 zu finden [118,121].

In Abhängigkeit der intendierten Anwendung des Materials werden vor Analyse der Zytotoxizität die zellulären Modelle (Zelllinien) für die *In-vitro*-Tests gewählt, die die *In-vivo*-Situation bestmöglich abbilden sollten [107,118]. Ferner stehen drei Kontaktmethoden zur Interaktion von Material und biologischem System zur Auswahl, von denen die weitere Probenvorbereitung und auch das anschließende Analyseverfahren abhängen kann: der direkte Materialkontakt, der indirekte Kontakt durch eine Schicht Agar oder Filter und Extraktionsmethoden, bei denen das Material zuvor für eine gewisse Zeit in Flüssigkeit gehalten wurde und diese anschließend mit dem biologischen System in Kontakt gebracht wird [107,121].

3.5.1 Mikroskopische Analysen zur Bewertung der Zytotoxizität

Nachdem das zu prüfende Material in direkten/indirekten Kontakt mit den Zellen gebracht wurde, gibt die mikroskopische Analyse der Zellmorphologie erste Hinweise auf die Zytotoxizität des Materials [107,118]. Eine mikroskopische Beobachtung der Zellproliferation oder zellspezifischer Verhaltensweisen im Verlauf der Kultivierung kann weitere Informationen über die biologische Verträglichkeit des Materials liefern. Mithilfe verschiedener Färbemethoden kann zudem die Integrität von Membranen, Organellen oder die Gegenwart von intrazellulären Molekülen mikroskopisch kontrolliert werden [118]. Der Farbstoff Trypanblau fungiert beispielsweise als Indikator für die Membranintegrität und wird verwendet, um Zellen mit beeinträchtigter Zellmembran visuell zu identifizieren [123]. Tote oder geschädigte Zellen besitzen eine eingeschränkte Membranintegrität, die es dem Farbstoff ermöglicht in die Zelle einzudringen und sie somit zu markieren [123]. Auf diese Weise ist eine quantitative Aussage über den Anteil lebender/toter Zellen möglich.

Mittels des in Kapitel 4.1 vorgestellten bildbasierten Analysesystems kann das Zellverhalten kontinuierlich, in Echtzeit, verfolgt werden. Es ermöglicht die mikroskopische Aufnahme mit Durchlicht, Phasenkontrast sowie roter und grüner Fluoreszenz. Das Gerät selbst wird in einen herkömmlichen Inkubator gestellt, um die Temperatur und CO_2-Bedingungen konstant zu halten. Die Steuerung erfolgt über einen zusätzlichen Computer außerhalb des Inkubators.

3.5.2 Biochemische Methoden zur Bewertung der Zytotoxizität

Biochemische Prüfmethoden liefern häufig ein zuverlässigeres und spezifischeres Ergebnis als mikroskopische Analysen zur Zytotoxizität [107,124]. Zahlreiche biochemische Testverfahren sind kommerziell erhältlich, die vielfältige Zellfunktionen analysieren und sich mit verschiedenen Prozessen des Zellstoffwechsels beschäftigen [107,125].

Im Rahmen dieser Arbeit wurden der Laktatdehydrogenase (LDH)-*Assay* und der Cell-TiterBlue® (CTB)-*Assay* zur Bestimmung der Viabilität verwendet. LDH ist ein in allen Körperzellen vorkommendes, intrazelluläres Enzym [126]. Durch die Schädigung der Zellmembran und den damit verbundenen Verlust der Membranintegrität gelangt das Enzym in die extrazelluläre Matrix, wo es mithilfe des LDH-*Assay* bestimmt werden kann. LDH katalysiert die Reduktion von Nicotinamid-Adenin-Dinukleotid (NAD)$^+$ zu NADH in Anwesenheit von Laktat (welches gleichzeitig zu Pyruvat oxidiert wird) [127]. In einer zweiten gekoppelten Reaktion wird das gebildete NADH oxidiert und das in dem Detektionsansatz ebenfalls enthaltene Tetrazolium-Salz zu einem roten Formazanprodukt reduziert. Die Bildung von Formazan kann bei 490 nm spektroskopisch bestimmt werden und ist direkt proportional zu der Anzahl an Zellen mit geschädigter Zellmembran [127].

Der CTB-Test gibt Aufschluss über das intrazelluläre Reduktionspotential der Zellen und beruht auf der Umwandlung von Resazurin in das fluoreszierende Produkt Resorufin [128,129]. Metabolisch inaktiven Zellen ist es nicht möglich Resazurin zu Resorufin zu reduzieren und entsprechend kann kein Fluoreszenzsignal detektiert werden [129]. Die Intensität des Fluoreszenzsignals steigt daher proportional zur Zellviabilität und kann spektrophotometrisch mittels Mikroplatten-Reader bestimmt werden [129].

Viele anerkannte Testmethoden zur Bewertung der Zytotoxizität bestimmen die mitochondriale Funktion von Zellen durch Messung der Aktivität mitochondrialer Enzyme wie Dehydrogenasen, welches häufig durch einen Reaktionsmechanismus mit Bildung von Formazan erfolgt [107]. Allgemein liefern biochemische Testmethoden in kurzer Zeit zuverlässige, quantitative Ergebnisse. All diese Methoden unterscheiden jedoch nicht zwischen

den Mechanismen, die zum Zelltod führen – sie basieren allein auf der Quantifizierung lebender und toter Zellen [107].

3.5.3 Durchflusszytometrische Verfahren zur Bewertung der Zytotoxizität

Eine noch differenziertere Analyse des Zellverhaltens und -zustandes ermöglicht die Durchflusszytometrie. Mithilfe der Durchflusszytometrie können Zellen bezüglich ihrer physikalischen und molekularen Eigenschaften analysiert werden. Für die Bewertung der Zytotoxizität eines Materials liefern Analysen der apoptotischen und nekrotischen Zellmechanismen wichtige Informationen über toxische Substanzen [107]. Apoptose beschreibt den Mechanismus eines intern „programmierten" Zelltods [130]. Im Gegensatz dazu ist die Nekrose ein zellulärer Mechanismus, der durch externe Faktoren wie Verletzungen oder toxische Substanzen ausgelöst wird [130,131]. Beide Signalwege führen zur Ausprägung expliziter morphologischer und biochemischer Zellmerkmale, die mit spezifischen Fluoreszenzmarkern detektiert und analysiert werden können [107]. Ein frühes Stadium der Apoptose ist beispielsweise durch die Translokation von Phosphatidylserin an die äußere Zelloberfläche gekennzeichnet [130,132]. Annexin V besitzt eine hohe Bindungsaffinität zu Phosphatidylserin und kann daher als Markerprotein für den Nachweis von Apoptose fungieren [132]. Die Detektion von fluoreszenzmarkiertem Annexin V stellt eine anerkannte und häufig verwendete durchflusszytometrische Methode zur Analyse der Apoptose dar [132]. Des Weiteren können beispielsweise Änderungen des mitochondrialen Transmembranpotentials Hinweise auf Apoptose geben und durchflusszytometrisch analysiert werden [107].

Die Durchflusszytometrie erlaubt zudem die Detektion zelltypspezifischer Moleküle und Proteine durch fluoreszenzmarkierte Antikörper [133]. Folglich kann der Einfluss eines Materials sehr spezifisch untersucht und analysiert werden.

4 Experimenteller Teil

Diese Doktorarbeit setzt sich aus vier verschiedenen Teilen zusammen, die sich mit der Integration von additiv gefertigten Systemen in biotechnologische Anwendungen befassen. Jeder Teil wurde separat in *peer-reviewed* Fachzeitschriften veröffentlicht.

Um den sicheren Einsatz zweier polymerbasierter 3D-Druckmaterialien in biologischen Applikationen zu gewährleisten, wurden diese zunächst umfassend charakterisiert. Die erste Publikation mit dem Titel „*Real-Time Live-Cell Imaging Technology Enables High-Throughput Screening to Verify in Vitro Biocompatibility of 3D Printed Materials*" beschäftigt sich mit dem Einfluss verschiedener Desinfektions- bzw. Sterilisationsverfahren auf die Zytotoxizität (und damit Biokompatibilität) additiv gefertigter Objekte, die aus dem Material VisiJet® M2R-CL von 3D Systems Inc. hergestellt wurden. Des Weiteren werden verschiedene *In-Vitro*-Testverfahren zur Analyse der Zytotoxizität vorgestellt und miteinander verglichen. Bei Anwendungen in der adhärenten Zellkultur steht ein Material über einen längeren Zeitraum in direktem Kontakt mit den Zellen. Aus diesem Grund wurden in der zweiten Publikation mit dem Titel „*Characterization of a customized 3D-printed cell culture system using clear, translucent acrylate that enables optical online monitoring*" neben *In-Vitro*-Zytotoxizitätstests auch Untersuchungen der Oberflächeneigenschaften des 3D-Druckmaterials AR-M2 von Keyence GmbH angestellt. Ferner wird ein additiv gefertigtes Zellkultursystem vorgestellt, in welchem adhärent wachsende Zellen kultiviert und mikroskopisch beobachtet werden können.

Nachdem die polymerbasierten 3D-Druckmaterialien in den ersten beiden Publikationen eingehend charakterisiert wurden, werden in der dritten und vierten Publikation Anwendungen der additiven Fertigung in der Biotechnologie beschrieben. In der Publikation mit dem Titel „*Customizable 3D-printed (co-)cultivation systems for in vitro study of angiogenesis*" wird ein Ko-Kultivierungssystem vorgestellt, welches zur Analyse der Angiogenese und der Wechselwirkungen unterschiedlicher Zelltypen entwickelt wurde. Überdies zeigen in dieser Publikation weitere maßgeschneiderte, 3D-gedruckte Plattformen und Systeme das große Potential der additiven Fertigung zur individuellen Anpassung an Experimente auf. Die vierte Publikation mit dem Titel „*3D-printed flow cells for aptamer-based impedimetric detection of E. coli Crooks strain*" beschreibt statische und dynamische Durchflusszellen, die für die Durchführung elektrochemischer Messungen entwickelt und additiv gefertigt wurden. Die Anwendung der statischen Durchflusszelle wird in aptamerbasierten Biosensor-Experimenten verdeutlicht. Der Einfluss integrierter Mikromischer auf die Mischverhältnisse vor einer elektrochemischen Messung wird mit Experimenten in der dynamischen Durchflusszelle veranschaulicht.

4.1 Vergleich dreier Verfahren zur Analyse der Biokompatibilität von 3D-gedruckten Elementen in einer Studie verschiedener Aufarbeitungsstrategien
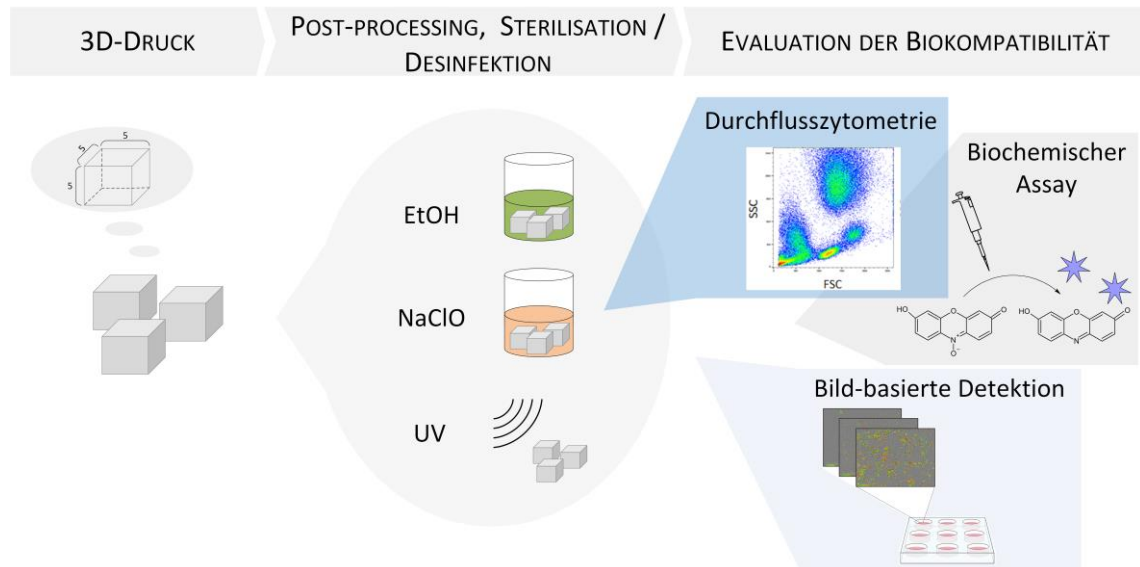

Abbildung 4-1 *Graphical abstract* von „*Real-Time Live-Cell Imaging Technology Enables High-Throughput Screening to Verify in Vitro Biocompatibility of 3D Printed Materials*".

Trotz steigendem Interesse an der Integration von additiv gefertigten Objekten in biotechnologischen und biomedizinischen Anwendungen, mangelt es an Informationen über den Einfluss von Druckmaterialien und deren Aufarbeitungsmethoden (*Post-Processing*) auf lebende Zellen. Neben den Aufarbeitungsschritten, die z. B. zur Entfernung von mitgedruckten, unterstützenden Strukturen (Stützmaterial) notwendig sind, können auch die Desinfektions- bzw. Sterilisationsverfahren große Auswirkungen auf die biologische Verträglichkeit des Materials haben.

Im nachfolgenden Artikel wird der Einfluss verschiedener Desinfektions- bzw. Sterilisationsstrategien auf die Zytotoxizität (und damit Biokompatibilität) 3D-gedruckter Elemente untersucht. Daneben werden drei unterschiedliche *In-Vitro*-Testverfahren zur Analyse der Zytotoxizität miteinander verglichen und hinsichtlich einer Eignung für *Screenings* hoher Probenanzahlen bewertet.

Bei dem innerhalb dieser Arbeit verwendeten 3D-Druckmaterial (VisiJet® M2R-CL, 3D Systems Inc.) handelt es sich um ein transluzentes, festes Polyacrylat, das mittels *Inkjet*

Printing mit hoher Auflösung gedruckt wurde. Das Material besteht aus zwei verschiedenen Acrylatmonomeren bzw. -oligomeren, wobei zum Zeitpunkt der Untersuchungen keine näheren Informationen zu den Materialeigenschaften vorlagen [95]. Nach obligatorischen Aufarbeitungsschritten, die zur Entfernung von mitgedruckten Stützstrukturen erforderlich sind, wurde das 3D-Druckmaterial mit drei unterschiedlichen Methoden desinfiziert bzw. sterilisiert. Eine Desinfektion bzw. Sterilisation ist für alle Materialien zwingend erforderlich, die in direktem oder indirektem Kontakt mit biologischer Umgebung stehen, um eine Kontamination derselben zu verhindern. In der hier präsentierten Arbeit wurden zwei chemische Reagenzien zur Desinfektion des 3D-Druckmaterials verwendet – Ethanol (v/v, 70 %) und Natriumhypochlorit (v/v, 2 %). Als physikalische Sterilisationsmethode wurde das Material mit UV-Licht ($\lambda = 266$ nm) bestrahlt. Nach weiterer Probenvorbereitung gemäß ISO 10993:2012 wurde der Einfluss der Materialproben auf adipogene, mesenchymale Stammzellen (AD-MSC) untersucht und die Biokompatibilität bewertet. Hierzu dienten neben einem biochemischen Testverfahren im Mikroplatten-Reader, eine durchflusszytometrische Methode sowie moderne bildbasierte Analysetechnologie.

Es konnte gezeigt werden, dass eine vorherige Desinfektion des Materials mit Ethanol weder negative Einflüsse auf die Zellen noch auf die Materialeigenschaften hat. Kontrollkulturen wiesen eine vergleichbare Zellmorphologie, Viabilität als auch ähnliches Zellwachstum auf, sodass die Aufarbeitungsstrategie mit Ethanol als Desinfektionsmittel als erfolgreich bewertet und das 3D-Druckmaterial als (*in vitro*) biokompatibel betrachtet werden kann. Diese Ergebnisse bilden damit einen Ausgangspunkt für vielseitige biotechnologische und biomedizinische Anwendungen des 3D-Druckmaterials.

In einem Vergleich der unterschiedlichen *In-Vitro*-Testverfahren zur Analyse der Biokompatibilität zeigt sich die Überlegenheit des bildbasierten Analysesystems hinsichtlich des Zeitaufwandes, der Benutzerfreundlichkeit und des wissenschaftlichen Informationsgehalts. Bildbasierte Echtzeitanalysen ermöglichen die gleichzeitige Beobachtung von Veränderungen der Zellmorphologie sowie kinetische Analysen und Quantifizierungen im Hochdurchsatz. Damit stellen bildbasierte Analysesysteme nicht nur ein ideales Werkzeug für die Untersuchung der Biokompatibilität dar, sondern erweisen sich außerdem als nützlich für den täglichen Gebrauch in zahlreichen Zellkulturanwendungen.

Im folgenden Artikel „*Real-Time Live-Cell Imaging Technology Enables High-Throughput Screening to Verify in Vitro Biocompatibility of 3D Printed Materials*" werden die Ergebnisse detailliert beschrieben und diskutiert.

materials

MDPI

Article

Real-Time Live-Cell Imaging Technology Enables High-Throughput Screening to Verify in Vitro Biocompatibility of 3D Printed Materials

Ina G. Siller [ID]**, Anton Enders** [ID]**, Tobias Steinwedel, Niklas-Maximilian Epping, Marline Kirsch, Antonina Lavrentieva, Thomas Scheper and Janina Bahnemann *** [ID]

Institute of Technical Chemistry, Leibniz University Hannover, Callinstraße 5, 30167 Hannover, Germany
* Correspondence: Jbahnemann@iftc.uni-hannover.de; Tel.: +49-511-762-2568

check for updates

Abstract: With growing advances in three-dimensional (3D) printing technology, the availability and diversity of printing materials has rapidly increased over the last years. 3D printing has quickly become a useful tool for biomedical and various laboratory applications, offering a tremendous potential for efficiently fabricating complex devices in a short period of time. However, there still remains a lack of information regarding the impact of printing materials and post-processing techniques on cell behavior. This study introduces real-time live-cell imaging technology as a fast, user-friendly, and high-throughput screening strategy to verify the in vitro biocompatibility of 3D printed materials. Polyacrylate-based photopolymer material was printed using high-resolution 3D printing techniques, post-processed using three different procedures, and then analyzed with respect to its effects on cell viability, apoptosis, and necrosis of adipogenic mesenchymal stem cells (MSCs). When using ethanol for the post-processing procedure and disinfection, no significant effects on MSCs could be detected. For the analyses a novel image-based live-cell analysis system was compared against a biochemical-based standard plate reader assay and traditional flow cytometry. This comparison illustrates the superiority of using image-based detection of in vitro biocompatibility with respect to analysis time, usability, and scientific outcome.

Keywords: real-time live-cell imaging technology; in vitro study; biocompatibility; 3D printing; flow cytometry; adipogenic mesenchymal stem cells

1. Introduction

3D printing has become a highly attractive tool with numerous different applications in the last decade. Already established technologies in the realm of rapid prototyping, 3D printing techniques are now increasingly being used to fabricate individually-designed devices in a comparatively easy, time and cost-effective way. Several 3D printing technologies are now available on the market, diverging mainly in the printing process and/or the physical state of the material bases utilized. The most established of these technologies create devices by melting and extruding thermoplastic filaments, fusing small particles of polymer powder together, or curing liquid resins via photopolymerization [1]. There are some fundamental similarities, however, for example, all 3D printing techniques make use of a "layer by layer" fabrication process, which facilitates almost unlimited complexity with respect to the final printed product.

Facilitated by 3D printing, the rise of rapid prototyping has great potential to accelerate the progression of biomedicine, biotechnology, and tissue engineering. Put differently, 3D printing permits the rapid fabrication of customized medical products and equipment, which can enable more individualized medical application [1–3]. The generation of implantable, highly porous 3D scaffolds

has become an increasingly important concept within the field of tissue engineering [3,4]. Such porous, personalized scaffolds provide a suitable surface for patient-specific cells to proliferate under ideal conditions. Nevertheless, despite these recent advances in medical applications involving 3D printing, the in vivo use of 3D printed materials should still be treated with some degree of caution, given the tremendous complexity of interactions within the human body. One major challenge associated with introducing foreign material into an organic system is the concept of "biological compatibility" or "biocompatibility" [1]. A generally accepted definition of this concept was given by D. F. Williams in 1987, "Biocompatibility is the ability of a material to perform with an appropriate host response in a specific application" [5].

An "appropriate host response" includes a normal healing process, resistances to bacterial colonization or biofilm formation and the prevention of blood clotting [6]. The biocompatibility of all materials being considered for use in real-world biomedical applications must first therefore be carefully assessed and confirmed via in vivo and in vitro studies [6,7]. If leachables or extractables show a negative impact on mammalian cells in vitro, then a material cannot be characterized as biologically compatible [8]. International standards—such as ISO 10993—provide extensive information, which can be used to develop appropriate assays and otherwise inform about biocompatibility testing methods [9].

A variety of cell culture-based in vitro assays are available for investigation of cytotoxicity of materials. These methods vary widely, from analysis and counting of viable/dead cells via microscope to biochemical-based assays and flow cytometric analyses. Microscopic observations of changes in cell morphology and counting of viable/dead cells form the basis [7]. As vital dyes such as Trypan blue can only enter—and thereby mark out—cells with disrupted cell membranes, use of these dyes in tissue cultures allows researchers to visually distinguish living and dead cells [10]. Biochemical-based assays provide a more reliable and specific outcome [7,11]. Numerous commercial assays are available, each one dealing with a different process of cellular metabolism [7,12]. For example, the CellTiter-Blue® assay (CTB assay) used within this study relies on the conversion of resazurin to the fluorescent product resorufin, which highlights the intracellular reduction potential of living cells [13]. However, although assays like this are widely used, they can only highlight the fundamental distinction between living and dead cells—they do not allow any further nuanced analysis into the different mechanisms by which cell death may occur [7]. Analyses of apoptosis and necrosis provide more detailed information on this front. The apoptotic pathway describes the mechanism of an internally "programmed" cell death [14,15]. By contrast, necrosis is a cellular death mechanism that has been triggered by external factors, such as injury or infection [14]. Both of these pathways display distinct morphological and biochemical features that can be observed and analyzed using specific fluorescence detection markers.

Due to the versatility of 3D printing technologies, a wide variety of printing materials—as well as post-processing procedures and surface finishing steps—are now being utilized. The materials can differ (for example) in their physical state, melting temperature, strength, and/or durability [1]. And the potential fields of application for any given method—as well as associated necessary post-processing or sterilization steps—are ultimately dependent on the properties of the underlying materials [7,16]. For example, materials with a high heat distortion temperature can be sterilized by thermal sterilization (autoclaving) for subsequent use in biological applications, while materials with a lower heat distortion tolerance require alternative sterilization procedures. Support materials such as wax are used by many 3D printing technologies to provide a scaffold with which to stabilize the building material. Following the printing process, this support material must be removed. The post-processing and removal of support material residues is also material-dependent, and can cause difficulties—especially with respect to detailed 3D structures and small channels (for example in microfluidic systems [17]. Depending on the post-processing and sterilization procedure, different end products with different properties can be obtained from the same material formulation. For applications in cell culture, every material formulation and post-processed product needs an individual investigation for biocompatibility. Accordingly, there is an apparent need for high-throughput screening assays.

This study seeks to help to fill in that gap by introducing real-time live-cell imaging technology as a fast, cost-effective and easy to use screening method to examine the in vitro biocompatibility of materials. To that end, a translucent clear, solid polyacrylate was printed via a high-resolution MultiJet 3D printing process, and was then post-processed to remove the supporting material. Following this post-processing procedure, three different disinfection and sterilization methods were examined, using ultra violet (UV) light as a physical sterilization method, as well as ethanol (70%, *v/v*) and sodium hypochlorite (2%, *v/v*) as chemical reagents. Afterwards, all of the post-processed objects were analyzed and screened for their suitability in cell culture applications by comparison of different in vitro biocompatibility methods. For biocompatibility evaluation, extraction media were obtained in accordance to ISO 10993:2012 standards and its impact on adipogenic mesenchymal stem cells (MSCs) was observed. Metabolic activity (representing cell viability) was assessed using a CellTiter-Blue® (CTB) cell viability assay. Analyses of apoptotic and necrotic responses as a measure of biocompatibility were also performed in a comparative study, using both modern image-based live-cell analysis technology and traditional flow cytometry.

2. Materials and Methods

2.1. Experimental Procedure

After 3D printing of a translucent polyacrylate material was completed, the printed parts are then cleaned in post-processing steps and sterilized or disinfected, respectively, using three different approaches. According to ISO 10993:12, extraction media are obtained for studying the influence of the 3D printed material on MSCs in in vitro biocompatibility assays. Three different methods to assess in vitro biocompatibility were compared in this study: (1) A biochemical-based viability assay (CTB assay) in a standard plate reader; (2) traditional flow cytometry; and (3) novel image-based live-cell analysis. A schematic overview of the experimental procedure is shown in Figure 1.
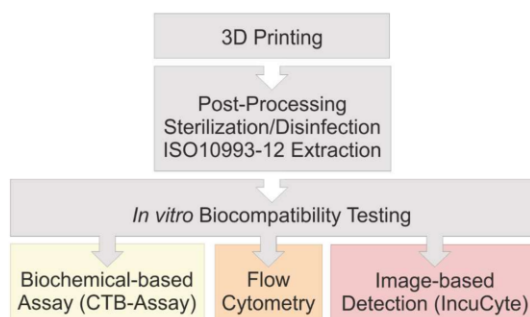

Figure 1. Flow chart of performed experiments. The in vitro biocompatibility of 3D printed material was evaluated using three different approaches.

2.2. 3D Printing

3D printed constructs were manufactured using the high-resolution MultiJet 3D printer ProJet® MJP 2500 Plus (3D Systems, Rock Hill, SC, USA). The 3D printing material analyzed in this study is VisiJet® M2R-CL (3D Systems, Rock Hill, SC, USA). It appears as a translucent clear, solid polyacrylate following a UV-curing process, and it is printed with a resolution of 800×900 dots per inch and a layer resolution of 32 μm [18,19]. As support material for the printing process, VisiJet® M2-SUP is used. For studying the success of the post-processing and the potential influence of leachables, $5 \times 5 \times 5$ mm cubes were printed—representing a total surface area of $1.5 \text{ cm}^2 \cdot \text{ml}^{-1}$. The known hazardous components in the liquid state of the present acrylic photopolymer material are 3-hydroxy-2,2-dimethylpropyl, 3-hydroxy-2,2-dimethylpropionate, the polymerization initiator diphenyl(2,4,6-trimethylbenzoyl) phosphine oxide, and monofunctional urethane acrylate.

Together with the constituent tricyclodecane dimethanol diacrylate, these components are all listed as being potentially harmful to aquatic organisms and/or as otherwise potentially causing adverse effects on aquatic environments in their liquid state (i.e., before polymerization) [19]. During the printing process, the polyacrylic material is polymerized by UV light—after which it can be declare harmless. No additional information regarding the material was provided by the manufacturer.

2.3. Post-Processing of 3D Printed Objects

All steps of the post-processing are shown in Figure 2, and they include freezing the printing plate for 15 min at −18 °C, and placing 3D printed objects in a heat steam bath of the EasyClean unit (3D systems, Rock Hill, SC, USA) for 45 min at 65 °C and incubation in an ultrasonic bath (Bandelin electronic, Berlin, Germany) with detergent (Fairy Ultra Plus, Procter and Gamble, CT, USA) for 30 min at 65 °C. Deionized water, provided by Arium® (Sartorius Stedim Biotech GmbH, Göttingen, Germany), was used in all experiments.
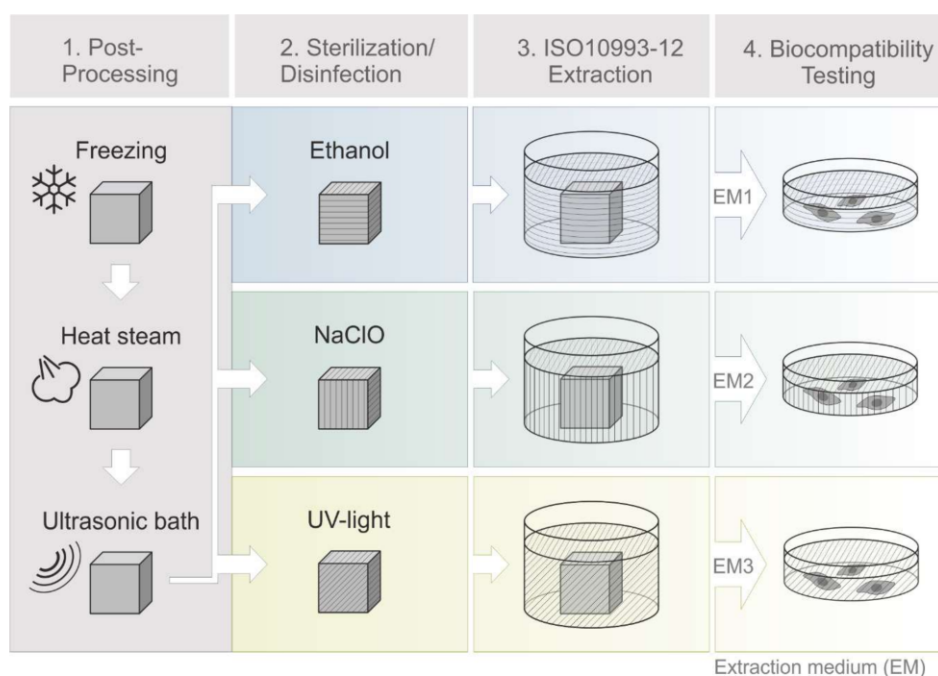

Figure 2. Schematic process of 3D printing, post-processing and extraction medium preparation. Cleaning steps (**1**): freezing of 3D printed objects (15 min, −18 °C), heat steam in a water bath (45 min, 65 °C), ultrasonic bath with detergent (30 min, 65 °C). Sterilization steps (**2**): disinfection in ethanol (70%, *v/v*, 1 h, RT) or sodium hypochlorite (2%, *v/v*, 1 h, RT) or UV light exposure (1 h, RT). Biocompatibility testing steps (**4**) then followed an incubation of 3D printed objects in cell culture medium according to EN ISO 10993-12 (2012) (**3**). (EM = extraction medium). EM 1: EM obtained by incubation of 3D printed material treated with ethanol (70%, *v/v*) in a disinfection process. EM 2: EM obtained by incubation of 3D printed material treated with sodium hypochlorite (2%, *v/v*) and EM 3: EM obtained by incubation of 3D printed material sterilized by UV light.

2.4. Sterilization/Disinfection of 3D Printed Objects

One disadvantage of many 3D printed materials is their relatively low heat distortion temperature and their corresponding incompatibility with thermal sterilization approaches [19–21]. However, a guaranteed sterile and disinfected product is necessary for the use in biomedical applications [22,23]. The polyacrylic material used in this study has a heat distortion temperature around 80 °C, as a result

the most common sterilization method (autoclaving) is not a possibility [19,24,25]. But physical and chemical procedures can also be used to sterilize and disinfect materials [24]. In this study, two different methods for chemical disinfection were used: The product was subjected to incubation in either ethanol (Carl Roth GmbH und Co. KG, Karlsruhe, Germany), 70%, *v/v*, or sodium hypochlorite, 2%, *v/v*, (Carl Roth GmbH und Co. KG, Karlsruhe, Germany), for 1 h at room temperature. In addition, UV irradiation (UV Sterilization Cabinet KT-09DC, Alexnld, Tiberias, Israel, 6 W, λ = 266 nm) was also used as a physical sterilization method. In order to cover every side of the 3D printed cubes with UV light, the cubes are turned around within a total of 1 h of UV light exposure at room temperature. After sterilization or disinfection procedure all cubes were washed thoroughly with sterile phosphate-buffered saline (PBS).

2.5. Preparation of Extraction Media (EM) for Biocompatibility Studies

Potential leaching properties of the 3D printed material, or remaining support material, were evaluated by obtaining extraction medium (EM) according to EN ISO 10993-12:2012 (Biological evaluation of medical devices—art 12: Sample preparation and reference materials). After post-processing, the aforementioned 3D printed cubes were incubated in cell culture medium Minimum Essential Medium Eagle, with alpha modification (α-MEM) (Thermo Fisher Scientific Inc., Waltham, MA, USA) containing 10% human serum (c.c.pro GmbH, Oberdorla, Germany) and 1% Gentamicin (PAA Laboratories GmbH, Pasching, Austria), for 72 h at 37 °C with a surface area/volume ratio of 3 $cm^2 \cdot ml^{-1}$. The obtained medium is referred to as extraction medium (EM). EM obtained by incubation of 3D printed material treated with ethanol (70%, *v/v*) in post-processing process is referred to as "EM 1." EM obtained by incubation of 3D printed material treated with sodium hypochlorite (2%, *v/v*) is hereafter referred to as "EM 2", and EM obtained by incubation of 3D printed material sterilized by UV light is referred to as "EM 3." Cell culture medium incubated for 72 h at 37 °C without 3D printed objects served as a control for all biocompatibility experiments.

2.6. Cell Line and Cell Culture Conditions

For all experiments, human adipogenic tissue-derived mesenchymal stem cells (MSCs) were used. After obtaining the donor's informed written consent, as approved by the Institutional Review Board (Hannover Medical School) with the reference number 3475-2017, adipose tissue was received following abdominoplasty surgery. After isolation, MSCs have been extensively characterized by surface marker analysis and functional properties as described earlier [26]. Cultivation of MSCs was performed in cell culture medium in a 5% CO_2, 21% O_2, humidified atmosphere at 37 °C (Heracell 150i incubator, Thermo Fisher Scientific Inc., Waltham, USA). The MSCs were routinely maintained in 75 cm^2 cell culture flasks (Corning, CellBind Surface, Corning, NY, USA), and then harvested at about 85% confluency by accutase treatment (Merck KGaA, Darmstadt, Germany) for detachment [26]. 24 h prior to the start of an experiment, cells were seeded in 6-, and 96-well plates (at a density of 18,000 $cells \cdot cm^{-2}$ and 1100 $cells \cdot cm^{-2}$, respectively) (Sarstedt AG and Co. KG, Nürnbrecht, Germany). Experiments were performed with cells of passages two to six.

2.7. CellTiter Blue® (CTB) Viability Assay in Fluorescence Plate Reader

For indirect evaluation of cell viability using a standard method, a CellTiter-Blue® cell viability assay (Promega, GmbH, Mannheim, Germany) was performed using the background and standard controls specified in the accompanying manual. Metabolically active cells are able to reduce blue resazurin into a purple, fluorescent resorufin via action of numerous redox enzymes in different intracellular compartments [13,27,28]. The fluorescence intensity produced by this reaction is therefore indicative of the number of viable cells. The product formation is monitored at an extinction wavelength of 544 nm, and an emission wavelength of 590 nm, using a fluorescence plate reader (Fluoroskan Acent, Thermo Fisher Scientific Inc., Waltham, MA, USA). MSCs were seeded in 96-well plates at a density of 8000 cells/well in 100 µl cell culture medium and incubated for 24 h at 37 °C in a humid atmosphere

supplemented with 5% CO_2. Subsequently, the MSCs were cultivated in the related extraction medium (see Section 2.5) or control medium for 24 h. After 24 h, extraction or control medium was removed, 100 µl fresh culture medium containing 10% CTB stock solution was added to each well and the MSCs were incubated for 1.5 h before measuring the fluorescence in a plate reader. Each experiment was repeated 13 times ($n = 13$).

2.8. Cell Viability Analysis by Flow Cytometry

Flow cytometry represents the traditional method used to monitor and quantitatively examine cell apoptosis and necrosis [29]. The BD FACSAria™ Fusion (Becton Dickinson, Franklin Lakes, NJ, USA) used in this study contains four lasers with numerous filters, which allow for a combination of multiple fluorescence markers within one sample. The basic principle of a flow cytometer is the analyses of hydrodynamically focused single cells that pass orthogonally through a bundled laser beam of a suitable wavelength. As they pass through the laser beam, the cells can be identified and classified by their physical characteristics (i.e., according to cell size, granularity, or specific fluorescence labeling) [30].

2.8.1. Sample Preparation

MSCs were seeded at a density of 18,000 cells·cm^{-2} in 6-well plates and then incubated for 24 h at 37 °C under 5% CO_2. Before related extraction media or control medium was used (as described below in Section 2.5), MSCs were washed once with PBS to remove non-adherent cells. MSCs were then cultivated in correspondent media for another 24 h. Cell samples for cell counting and flow cytometry experiments were obtained by detachment of adherent cells using accutase treatment. Before dyeing and analysis, the detached cells were sedimented by centrifugation for 5 min at 200× g and then resuspended in fresh culture medium [31,32]. The cell number and viability was estimated viw cell counting using a 0.4% Trypan blue stain ($n = 4$) in a haemocytometer (Brand GmbH + Co. KG, Wertheim, Germany) [10]. Trypan blue can be used to visually identify cells with disrupted cell membranes since dead or damaged cells possess a compromised membrane integrity which allows the dye to enter the cell and visibly mark it as distinct from a healthy living surrounding.

2.8.2. Measurement and Quantification of Apoptosis and Necrosis

MSCs were centrifuged for 5 min at 200× g, resuspended, and then washed with PBS twice. Necrotic cells were marked and identified using the SYTOX® AADvanced™ Dead Cell Stain, which is provided in the CellEvent™ Caspase-3/7 Green Flow Cytometry Assay Kit (Thermo Fisher Scientific Inc., Waltham, MA, USA). These cells were stained as instructed in the manual. Necrotic cells possess disrupted cell membranes which allow the Dead Cell Stain to enter the cell and intercalate in DNA structures, thereby visually marking out the cell. Necrosis can be measured at an excitation maximum of 546 nm and an emission maximum of 647 nm. Apoptotic cells express and activate the enzymes caspase-3 and caspase-7 [33]. Hence, apoptosis can be evaluated by the detection of active caspase-3/7 using the CellEvent™ Caspase-3/7 Green Stain, provided in the same assay kit. The corresponding green fluorescence signal has an excitation maximum of 511 nm and an emission maximum of 533 nm, and was captured with appropriate laser and filter settings using a BD FACSAria™ Fusion flow cytometer. The same number of cells were stained in each sample, in order to maintain an equal distribution of fluorescence reagents to cells. To represent a positive control for apoptosis, 50 µm cisplatin (cisplatin-induced apoptosis) was also added to the cells (control experiments were performed in triplicate). Cisplatin is a platin derivative that blocks DNA synthesis, induces apoptosis via p53-dependent and independent signaling mechanisms, and activates caspase-3. It is a well-known DNA-alkylating antitumor agent which is used as a chemotherapeutic drug [34,35]. MSCs cultivated in normal cell culture medium, without contact to 3D printing material, served as a negative control. The MSCs were cultivated for a period of 30 h, with cell samples taken every 4–6 h ($n = 6$). Cell samples were handled and counted via the Trypan blue exclusion method (described in Section 2.8.1). The BD

FACS Diva™ Software v8.0 (Becton Dickinson, Franklin Lakes, NJ, USA) was used for analysis. Flow cytometry analysis is predicated on the principle of "gating", by placing gates around cell populations with common characteristics, different cell populations can be segregated and selected for further investigation. Here, a uniform gating strategy was used for all experiments in order to separately analyze and quantify apoptotic, necrotic and living cells. Necrotic and apoptotic cells, respectively, possess higher red and green fluorescence signal intensities compared with living cells. Gates were determined based on both positive and negative cell controls. At least 10,000 events per sample were analyzed with an "event" being defined as a single particle detected by the system. The experiment was performed with three biological replicates.

2.9. Cell Viability Analysis by Real-Time Live-Cell Imaging System

The IncuCyte® Live-Cell Analysis System (Sartorius Stedim Biotech GmbH, Göttingen, Germany) is an image-based real-time system that allows for an automatic acquisition and analysis of cell images. With the use of two lasers, both phase contrast as well as fluorescence images can be captured. The entire system is placed inside a cell culture incubator in order to guarantee controlled cultivation conditions during real-time monitoring. Phase contrast and fluorescence images are automatically recorded and analyzed using customized software tools in the IncuCyte® S3 image analysis software (Sartorius Stedim Biotech GmbH, Göttingen, Germany). With pre-defined imaging masks, fluorescence signals of the recorded images are then analyzed and counted. Parameters such as minimum fluorescence signal intensity are considered and defined in advance (e.g., to exclude diffuse background noise from the evaluation). The same imaging masks are applied to all acquired images. The data is exported as Counts/Image, which represents the counted fluorescence signals with respect to a single image. The applied dynamic image processing and analysis enables quantitative real-time analyses of fluorescence signals in an imaging field. In addition, by using pre-defined cell-specific imaging masks containing information on cell size and shape, cell growth can be monitored in real-time, by analyzing the occupied area of an imaging field in phase contrast images. Accordingly, this system provides both quantitative and kinetic data. A schematic workflow of the real-time live-cell imaging system is shown in Figure 3.
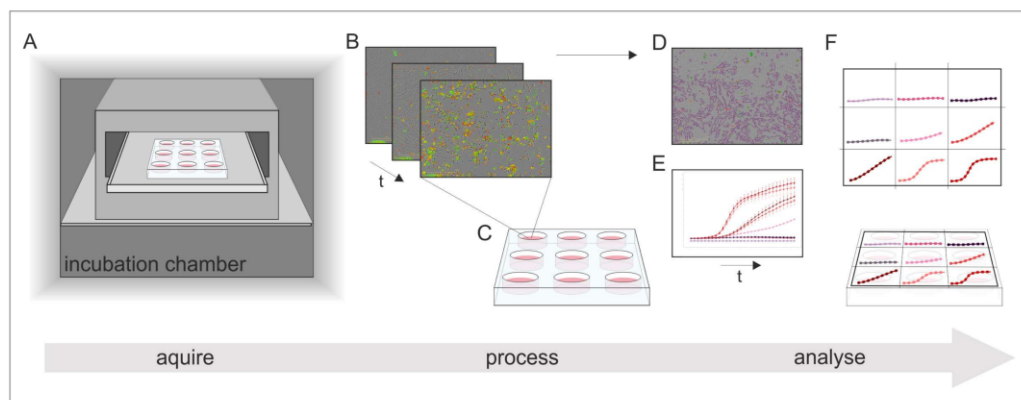
Figure 3. Schematic illustration of the working process of real-time live-cell analysis. (**A**) Placing of the real-time live-cell imaging system inside a cell culture incubator; (**B**) automatically acquire images over time; (**C**) receive images of all locations in the culture vessel at once; (**D**) imaging masks identify regions of interest; and (**E**) the results can be monitored in real-time and (**F**) display quantitative and kinetic analyses of all culture vessels at once.

2.9.1. Sample Preparation

MSCs were seeded in 96-well plates at a density of 8000 cells/well in 100 µl cell culture medium and then incubated for 24 h at 37 °C in a humid atmosphere supplemented with 5% CO_2. Staining reagents for quantification of apoptosis and necrosis were diluted in respective cell culture medium obtained as described in Section 2.5. Before the staining reagents containing media were added to these cultivation wells, the old medium was first discarded and all non-adherent cells were removed by a washing step with PBS.

2.9.2. Measurement and Quantification of Apoptosis and Necrosis

A quantitative analysis of apoptosis and necrosis of MSCs over time was ascertained during the cultivation in extraction medium 1 (EM 1) and extraction medium 2 (EM 2), with regular cell culture medium serving as a control. Staining of the cells was performed using the IncuCyte® Cytotoxicity and Apoptosis Detection Kits (Sartorius Stedim Biotech GmbH, Göttingen, Germany), according to the manufacturer's protocols. Real time measurement of necrosis is based on the cell membrane integrity—i.e., the same principle as used for necrosis detection in flow cytometry experiments. In the case of a damaged cell membrane, the IncuCyte® Cytotox dye enters the cell, intercalates into DNA, and thereby marks out the nuclei. Red fluorescence of the cytotoxicity dye can be measured at an excitation maximum of 612 nm and an emission maximum of 631 nm. As in flow cytometry experiments, apoptotic cells were analyzed by detection of active caspase-3/7. IncuCyte® Caspase-3/7 reagent was used for the detection of active caspase-3/7, which is expressed and activated in apoptotic cells. Apoptotic cells can be identified by measuring green fluorescence at an excitation maximum of 500 nm and an emission maximum of 530 nm. The apoptosis inducer cisplatin was added in three wells to a final concentration of 50 µm to regular cell culture medium, in order to represent a positive control for apoptosis. MSCs cultivated in regular cell culture medium, without contact to 3D printing material, served as a control. As soon as the staining reagents with the corresponding medium were added to the cell culture wells, the monitoring was started using the IncuCyte® S3 Live-Cell Analysis System. Phase contrast and fluorescence images were automatically captured every hour for a duration of 30 h. The experiment was performed with six biological replicates, every measurement in triplicates. Quantitative analyses of caspase-3/7 and cytotoxicity signals, as well as of cell proliferation were performed with pre-defined cell-specific masks in the IncuCyte® S3 image analysis software.

3. Results

3D printed polyacrylic material was post-processed using three different sterilization or disinfection methods. To evaluate the efficiency of each post-processing and disinfection method as well as to investigate potential leaching properties of the 3D printed polyacrylic material itself, a comparative study using a biochemical-based standard plate reader assay (CTB Assay), standard flow cytometry, and an image-based live-cell analysis system was conducted. The leaching of acrylate monomers, degradation products, or other components from polymer-based materials is a well-known problem that often has negative effects on the biological environment [7,36–38]. Leachables can lead to cytotoxic effects on cells (which can manifest as irritations and/or allergic reactions within the human body) [8,36,39].

3.1. Biochemical-Based CTB Cell Viability Assay

Metabolic activity as an indicator of cell viability of MSCs is analyzed by performing biochemical-based CTB cell viability assays during cultivation in extraction medium, which is prepared according to EN ISO 10993-12 (2012) (see Section 2.5). This CTB assay presents a biochemical-based method for assessing the cytotoxicity of a material. These results are summarized in Figure 4, where the cell viability observed during MSC cultivation in different extraction media is plotted. The cell viability is normalized to the control cultivation. Here, the use of ethanol (70%, *v/v*) (EM 1) as disinfectant did

36

not show a significant difference in metabolic capacity and cell viability compared to control cultures. By contrast, both chemical disinfection methods of the 3D printed objects with sodium hypochlorite (2%, *v/v*) (EM 2), and irradiation sterilization (EM 3), caused a significant decrease in metabolic activity—resulting in only 35.5 ± 13,0% and 25.4 ± 17.0% viable cells, respectively, when compared to the control culture. From these results, the following conclusions could be drawn: (1) cleaning and disinfection of the 3D printed parts using ethanol 70% was successful, and (2) EM 1 did not contain any toxic leachables.
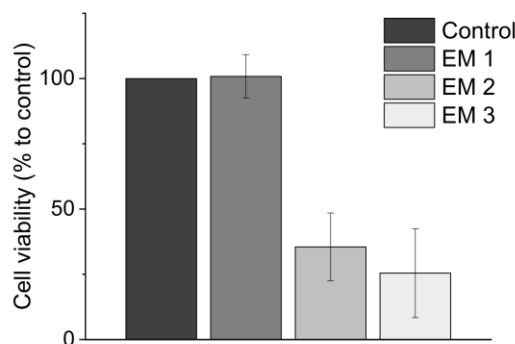

Figure 4. Results of CellTiter-Blue® cell viability assay (CTB assay) to analyze the metabolic capacity (shown as cell viability in %) of MSCs. (EM = extraction medium). EM 1: EM obtained by incubation of 3D printed material treated with ethanol (70%, *v/v*) in a disinfection process. EM 2: EM obtained by incubation of 3D printed material treated with sodium hypochlorite (2%, *v/v*). EM 3: EM obtained by incubation of 3D printed material sterilized by UV light. All experiments were repeated several times (*n* = 13) and compared to MSC cultivation in regular cell culture medium (Control).

It can further be concluded that UV light is not a suitable sterilization method for the 3D printed material used in this study. The negative effects of EM 3 on cell viability may be due to several factors. UV light can have an adverse effect on both the optical and mechanical properties of polymer materials [40,41]. In our experiments, a slight change in color and translucency, as well as an increased brittleness of the surface of the material, was noticed after only 1 h of UV light exposure. Applications involving polymers are restricted due to the capability of photo-degradation, particularly under exposure of UV light [41,42]. Photooxidative reactions aroused by UV light are also associated with the formation of free radicals, which can lead to a radical chain mechanism and ultimately result in the rupture of a polymer structure. The degree of impact depends on the UV light intensity and duration—but this process initially manifests as a change in the color and an increased degree of "mistiness" observed in the polymer material [41,43]. These reactions may also lead to a release of leachables, which can have cytotoxic effects on cells. It should also be noted that the UV sterilization method was also rather impractical in this instance, because the 3D printed parts had to be rotated permanently in order to ensure uniform UV exposure. Since it would be difficult to maintain uniform UV irradiation across all surfaces of complex 3D printed structures—such as embedded channels in microfluidic systems—they would therefore be difficult to sterilize using this procedure.

Similarly, although sodium hypochlorite is the most widely used disinfectant in the food industry and a commonly used irritant in endodontic practice, a significant decrease in cell viability of MSCs was observed in our CTB assays after cultivation in EM 2 using sodium hypochlorite as a disinfection agent in the post-processing process [10,44–46]. This is perhaps not surprising; a study on mesenchymal stem cells of the human bone marrow from Alkahtani et al. has previously shown that even low concentrations of sodium hypochlorite exhibit cytotoxicity [47]. Treatment of sodium hypochlorite can thus damage cell membrane proteins and lead to cell lysis [48]. Such damage might have been responsible for the decreased metabolic activity observed in our MSCs. In contrast, the use of ethanol

(70%, *v/v*) as a disinfection agent in the post-processing process of the 3D printed polyacrylic material has no negative impact on metabolic capacity of MSCs. Ethanol functioned as an effective disinfectant here without impacting either the optical or mechanical properties of the material. In addition, ethanol (70%, *v/v*) is also already a commonly used disinfectant in the health services field [23,49].

The CTB assay can score with its fast and user-friendly implementation while also allowing for high-throughput screenings. As a method performed in a standard plate reader, there is no need of sophisticated instruments. However, there is one important limitation on the CTB assay: it only provides information about the count of viable cells, and it is not sensitive to measuring the different mechanisms that can lead to cellular death, which present important information about the material formulation under investigation. Accordingly, to more precisely consider the impact of the post-processed 3D printed material on cell behavior, further studies aimed at measuring the rate of specific death mechanisms (i.e., apoptosis and necrosis) were also necessary. The use of specific dyes which mark out particular apoptotic and necrotic intracellular signals allowed for more detailed evaluations of cellular behavior and cytotoxicity mechanisms to assess in vitro biocompatibility. The standard plate reader used for CTB assays is not capable of detecting multiple fluorescence signals simultaneously. The follow section therefore considers the practicability of performing apoptosis and necrosis staining and analyses in a flow cytometry study vs. using a novel high-throughput image-based analysis system.

3.2. Analysis of Cell Death Responses via Flow Cytometry

Flow cytometry is a standard method used to monitor and quantitatively examine cell death via apoptosis and necrosis [29]. As cells undergoing necrosis experience a disruption of the cell membrane, the use of a red fluorescence dye that enters and labels the DNA of damaged cells with disrupted cell membranes is an elegant and effective way to visibly mark out such cells [33]. Specific fluorescence labeling can also be used to visually detect apoptotic cells, which express and activate the enzymes caspase-3 and caspase-7 [33]. Here, a green fluorescence dye that is sensitive to active caspase-3/7 was used to identify apoptosis (see Section 2.8.2). The relative percentage of necrotic vs. apoptotic MSCs within a sample can then be assessed and used to analyze the biocompatibility of the 3D printed material after post-processing and disinfection (see Section 2.5). Figure 5 shows the flow cytometric analysis of MSCs cultivated over a period of 30 h.
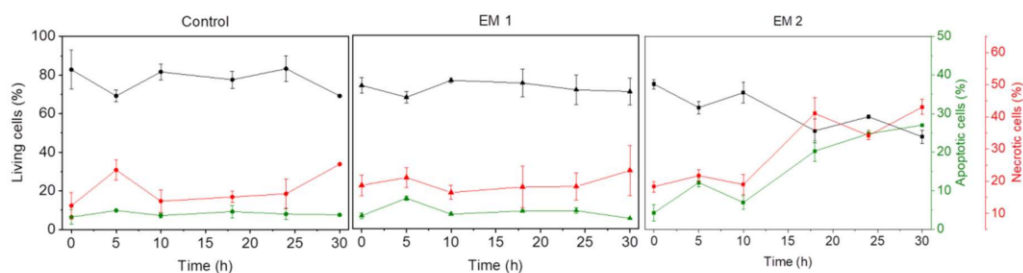

Figure 5. Results of flow cytometric studies on apoptosis and necrosis of MSCs over a period of 30 h. The percentage of living, apoptotic and necrotic cells are analyzed per cultivation. A caspase 3/7 signal (green) represents apoptotic cells; the cytotox-signal (red) is correlated to necrotic cells. (EM = extraction medium). EM 1: EM obtained by incubation of 3D printed material treated with ethanol (70%, *v/v*) in a disinfection process. EM 2: EM obtained by incubation of 3D printed material treated with sodium hypochlorite (2%, *v/v*). The experiments are compared to MSC cultivation in regular cell culture medium (Control) and were performed three times (*n* = 3).

As explained above (see Section 3.1), UV light is not a suitable sterilization method for the 3D printed material used in this study. Therefore, as shown in Figure 5, UV light as sterilization method was no longer analyzed. MSCs that were cultivated in extraction medium 1 (EM 1), obtained by

incubation of 3D printed material disinfected by ethanol (2%, *v/v*), showed no significant difference with respect to the relative percentages of living, apoptotic, and necrotic cells when compared to control cultures; in both cases, the percentage of apoptotic cells was about 4%, the percentage of necrotic cells was about 16%, and the balance were living cells. Since the same number of cells was stained and used for each measurement, the data does not show any increase in the count of living cells due to cell growth. In contrast to the MSCs in EM 1 and the control cultures, the cultivation of MSCs in extraction medium 2 (EM 2)—obtained by incubation of 3D printed material disinfected by sodium hypochlorite (2%, *v/v*)—resulted in a strong increase in both apoptotic and necrotic cells. In this medium, the percentage of apoptotic and necrotic cells increased over time from 4% and 18%, respectively, to approximately 30% and 45%, while the percentage of living cells correspondingly decreased from 80% to 50%. Each experiment showed a slight increase in the percentage of apoptotic and necrotic cells, as well as a simultaneous decrease in the count of living cells (after 5 h). This occurrence may be related to the change of cell culture medium to relevant extraction or control medium, and adaption of the cells to their new environment—which is associated with cellular stress [50].

Figure 6 illustrates the calculated cell growth over a cultivation period of 30 h. For MSCs cultivated in EM 1, no significant difference in cell growth was observed when compared to control cultures. Over the cultivation period, the number of living cells increased by a factor of approximately 2, both for cultivation in control medium and in EM 1. By contrast, cultivation in EM 2 leads to a strong decrease in cell viability, which resulted in a significant decrease in the number of living cells (by more than half) within 30 h.
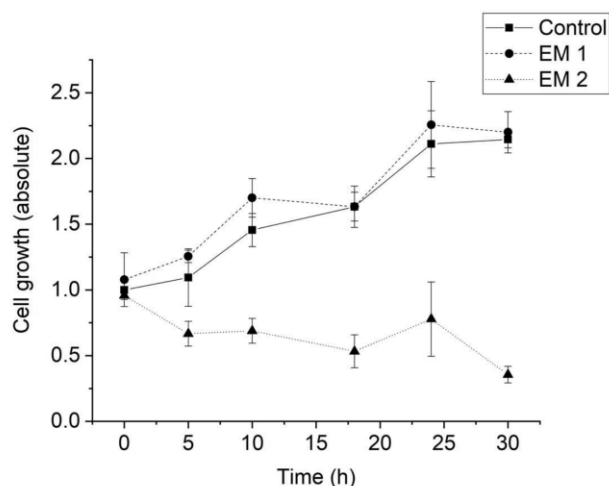

Figure 6. Cell growth of MSCs determined by cell counting using Trypan blue staining. (EM = extraction medium). EM 1: EM obtained by incubation of 3D printed material treated with ethanol (70%, *v/v*) in a disinfection process. EM 2: EM obtained by incubation of 3D printed material treated with sodium hypochlorite (2%, *v/v*). The experiments are compared to MSC cultivation in regular cell culture medium (Control) and were performed three times (*n* = 3).

In summary, then, apoptosis/necrosis analyses over 30 h reveal no evidence of any behavior in MSCs cultivated in EM 1 that could be attributed to potential toxic leachables in the 3D printed material. And a post-processing procedure that included disinfection with ethanol (70%, *v/v*) proved to be the most advisable approach tested for handling this high-resolution polyacrylic 3D printed material. In general, the flow cytometry results confirm the results of the CTB assay, but it provides more detailed information about the mechanism of cell death that was observed.

3.3. Analysis of Cell Death Responses via Image-Based Live-Cell Analysis System

Another approach for analyzing apoptotic and necrotic responses of cells in order to assess in vitro biocompatibility of a material is represented by comparatively novel image-based live-cell analysis systems. The IncuCyte® Live-Cell Analysis System used in this study is an image-based real-time system that allows the automatic acquisition and analysis of phase contrast and fluorescence images of cells using customized software tools.

Using this system, MSCs cultivated either in extraction or in a control medium (see Section 2.5) were monitored and analyzed automatically over a period of 30 h. Phase contrast, as well as fluorescence images, were captured every 1 h following the addition of fluorescence reagents for the purpose of highlighting apoptosis and necrosis. A contrasting juxtaposition—representing the cell phenotype data of individual cell populations cultivated in extraction or control medium—is shown in Figure 7 Green fluorescence signals show apoptotic cells; red fluorescence signals show necrotic cells. As a positive apoptosis control, MSCs were cultivated with the addition of the apoptosis inducer cisplatin. In keeping with previous investigations (see Sections 3.1 and 3.2 above), no differences in cell morphology, cell growth, or layer formation was observed for MSCs cultivated in EM 1 compared with control cultures. By contrast, MSCs cultivated in EM 2 show similar characteristics compared to the cultivation of MSCs with cisplatin (positive apoptosis control). After 15 h of incubation in EM 2 or cisplatin, large gaps in cell layer, less connected cells, and cell rounding as well as shrinkage were all observed. These are common characteristics associated with cell apoptosis [51]. After 30 h of MSC cultivation in EM 2 and the positive apoptosis control, a high increase in apoptotic and necrotic signals was observed via measurements of corresponding fluorescence signals.
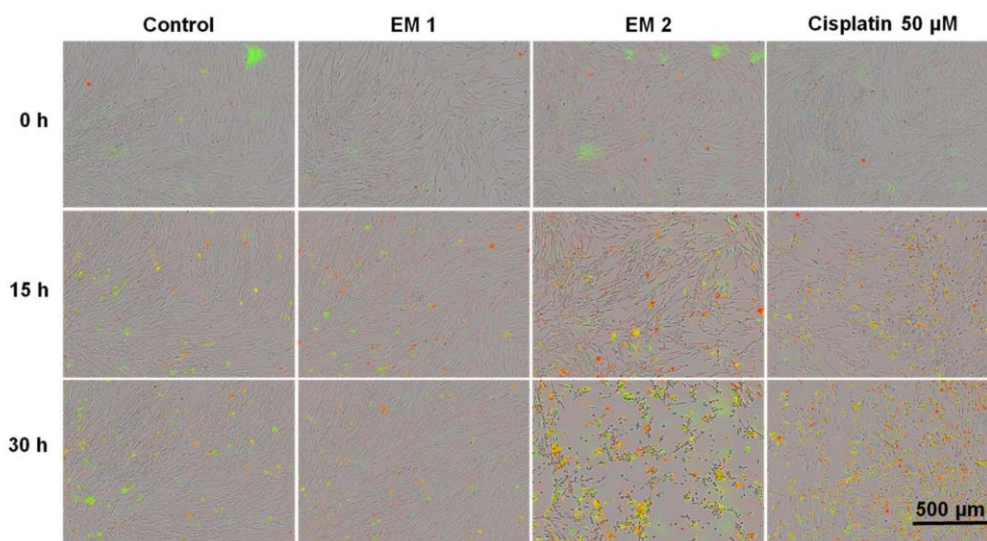

Figure 7. Fluorescence images of MSCs over time by image-based live-cell analysis system (IncuCyte). Green fluorescence is related to apoptotic cells; red fluorescence shows necrotic cells. (EM = extraction medium). EM 1: EM obtained by incubation of 3D printed material treated with ethanol (70%, *v/v*) in a disinfection process. EM 2: EM obtained by incubation of 3D printed material treated with sodium hypochlorite (2%, *v/v*). The experiments are compared to MSC cultivation in regular cell culture medium (Control) and were performed three times (*n* = 3). Cisplatin 50 μm: Positive control for apoptosis.

Figure 8 shows kinetic analyses of MSC growth, as well as apoptotic and necrotic signals obtained by dynamic image processing of phase contrast and fluorescence images, as described in Section 2.9. In this Figure, the unit Counts/Image was based on fluorescence signals provoked by apoptotic or

40

necrotic cells in a specific imaging field. MSCs were cultivated in corresponding extraction media or control medium (see Section 2.5, above). As was to be expected from the previous investigations, there was no relevant difference observed in the cell behavior of MSCs cultured with EM 1 compared to the control cell culture medium. Over the duration of the experiment, cell confluency (representing the cell growth) increased. Living cells grow, expand, and divide. Furthermore, the number of apoptotic and necrotic cells per image field during MSC cultivation in EM 1 and control medium remained minimal. By contrast, MSC cultivation in EM 2 stagnated, and a strong relative increase in apoptotic and cytotoxic signals was also observed. A subsequent decline in cell proliferation after 10 h in EM 2 was likely related to the changes in cell morphology (e.g., cell rounding, shrinkage) and detachment of dead cells from the surface as a result of increased apoptosis and necrosis [14]. Detached dead cells might migrate into the supernatant, beyond the focal point of the laser, where they cannot be recognized and counted adequately.
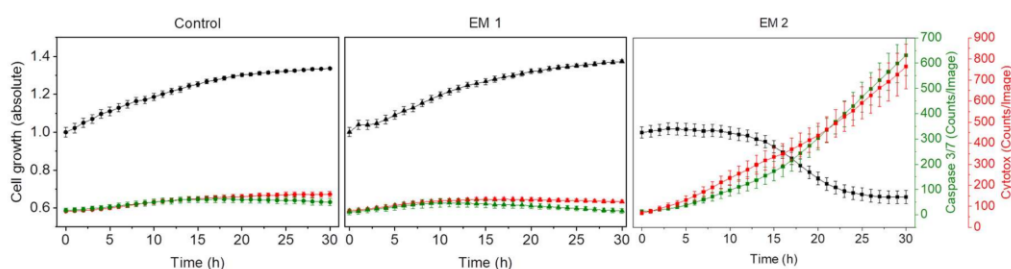

Figure 8. Analysis of cytotoxicity of the 3D printing polyacrylic material and apoptosis of MSCs by an image-based live-cell analysis system (IncuCyte). Cell growth, apoptosis and necrosis of MSCs are analyzed per cultivation. A caspase 3/7 signal (green) represents apoptotic cells; the cytotox-signal (red) is correlated to necrotic cells. (EM = extraction medium). EM 1: EM obtained by incubation of 3D printed material treated with ethanol (70%, *v/v*) in a disinfection process. EM 2: EM obtained by incubation of 3D printed material treated with sodium hypochlorite (2%, *v/v*). The experiments are compared to MSC cultivation in regular cell culture medium (Control) and were performed eighteen times ($n = 18$).

4. Discussion

The results obtained from the image-based evaluation conducted via live-cell analysis system were in full agreement with the results obtained via both the CTB assay and flow cytometry method—and all three methods confirmed that EM 1 had no significant influence on MSCs. It can therefore be assumed that the post-processing procedure including disinfection with ethanol (70%, *v/v*) was successful, and no critical amount of cytotoxic substances leached out of the 3D printed polyacrylic material. Since the 3D printed polyacrylic material had no negative impact on cell behavior or cell morphology of MSCs, it can be considered in vitro biocompatible. These findings collectively mark out a solid starting point for further investigations, and open the door for potential biological and biomedical applications using the analyzed 3D printed high-resolution polyacrylic material, which is promising not only for micro-scale and microfluidic applications, but also for rapid prototyping of various devices for cell culture and lab scale experiments [17].

Comparing the three methodologies used to evaluate in vitro biocompatibility here reveals some major disadvantages of both the flow cytometry and CTB assay methods. In both oh those cases, cell sample preparation and analysis must take place outside the cell culture incubator, which is designed to ensure a constant temperature and high humidity to facilitate cell growth under a CO_2 atmosphere. Such handling of the cells outside the incubator disrupts these optimal conditions, which may impose cellular stress and could also potentially impact cell growth, apoptosis, and/or necrosis [52,53]. Furthermore, as noted above, analysis of biocompatibility via biochemical-based CTB assay only provides information about cell viability in general. As a result, it can at best be considered a

41

first analysis assay useful to obtaining a general sense of the cytotoxicity potential of a material, before continuing with further considerations. Flow cytometry and the image-based analysis system both allow for more detailed and specific analyses of cellular behavior and reactions on potential cytotoxic material constituents in assessing biocompatibility. For flow cytometry experiments, the cells of an individual cultivation well were harvested and examined for each measuring point. This means that in flow cytometry analyses, different cell populations are compared with each other, and therefore temporal investigation based only on a single cell population is not possible (this applies to adherent growing cells). Attempting to track dynamic functional cellular processes and morphology over the whole time frame of an experiment accordingly becomes an arduous task; and flow cytometry is particularly ill-suited to the task of monitoring rapid cellular changes (e.g., in response to external influences). Due to well-to-well variations and differences in cell treatment and seeding, the comparability of the obtained data cannot be guaranteed [54]. In addition, sample preparation for flow cytometry studies is laborious, requiring substantial time expenditure and good cell culture practices [54]. The extensive sample handling also results in a substantial delay from cell detachment to analyses. Additionally, the multiple centrifugation steps required during sample preparation and dyeing procedures expose the cells to mechanical stress [54]. Disruption and damage of the cell membrane triggered by stress factors can lead to apoptotic or necrotic responses and thus to false-positive results.

In contrast, image-based live-cell analysis gives the ability to visualize cellular phenotypes images as well as to perform kinetic analyses and quantifications of apoptotic and necrotic cell responses simultaneously in high-throughput. Based on microscopic data, numerous cell specific analyses can be performed directly, using customized tools and software. Live-cell imaging technology offers the possibility to monitor and study the same cell population for an indefinite period of time by analyzing the same imaging field. Since the imaging and analysis is realized fully automated inside a cell culture incubator, there is no need to physically move cells and risk exposing them to lower temperatures and potential cellular stress. Culture perturbations in performing assays with traditional methods such as flow cytometry and CTB viability assays are affecting cellular behavior and provoke cellular stress [52–54]. That includes the physical movement of cultures by removing cell culture flasks or plates from the laboratory cell culture incubator as well as changes in temperature and atmospheric conditions while performing the experiment. The real-time analysis system does not have to take into account any of the aforementioned disturbances.

5. Conclusions

This study presents a comprehensive comparison of three different methodologies for the in vitro evaluation of biocompatibility of 3D printed polyacrylic material. The superiority of an image-based live-cell analysis system with respect to time, usability, and scientific outcome was shown. Image-based real-time analyses allow for simultaneous observations of changes in cell morphology via microscopic imaging as well as kinetic analyses and quantifications of apoptotic and necrotic cell responses. Conventional methods for testing in vitro biocompatibility—such as microscopy or biochemically based assays—were comparatively outshone. The fast and simple handling; the potential of performing screenings in high throughput; and the high quantity and informative value of cellular data all make real-time live-cell imaging technology an ideal tool not only for the study of biocompatibility, but also for the usage in numerous cell culture applications on a daily basis. With the possibility of integrating up to two fluorescence channels in addition to phase contrast, and the choice between three different objective nosepieces, countless image-based cell assays can potentially be performed and monitored in real-time. Long term assays for studying chemotaxis, angiogenesis or stem cell differentiation are just as simple to realize as measurements of cellular health in drug screenings.

At the same time, this study also highlighted the importance of analyzing and comparing different post-processing procedures of 3D printed materials considered for biological applications Even though the tested material itself is in vitro biocompatible, remaining support material or contaminations due to insufficient post-processing methods could still potentially lead to adverse effects on surrounding

cellular environment. 3D printing materials produced for a specific printer system are often not considered for use in cell culture or biomedical applications where biocompatibility is a central demand [3]. Manufacturers often give no suggestions for a proper disinfection and sterilization of their numerous material formulations. It is accordingly up to the researcher to investigate the materials in terms of biocompatibility and appropriate post-processing and sterilization protocols. On that account, high-throughput screening methods as the image-based live-cell analysis system are critical for both finding biocompatible material formulations, and also finding the best solution of post-processing for one given material.

References

1. Gross, B.C.; Erkal, J.L.; Lockwood, S.Y.; Chen, C.; Spence, D.M. Evaluation of 3D Printing and Its Potential Impact on Biotechnology and the Chemical Sciences. *Anal. Chem.* **2014**, *86*, 3240–3253. [CrossRef] [PubMed]
2. Ventola, C.L. Medical Applications for 3D Printing: Current and Projected Uses. *Pharm. Ther.* **2014**, *39*, 704–711.
3. Chia, H.N.; Wu, B.M. Recent advances in 3D printing of biomaterials. *J. Biol. Eng.* **2015**, *9*, 4. [CrossRef] [PubMed]
4. Derby, B. Printing and Prototyping of Tissues and Scaffolds. *Sci.* **2012**, *338*, 921. [CrossRef] [PubMed]
5. Williams, D.F. Definitions in biomaterials. In Proceedings of the Consensus of the European Society for Biomaterials Conference, Chester, UK, 3–5 March 1986.
6. Ratner, B.D.; Hoffman, A.S.; Schoen, F.J.; Lemons, J.E. *Biomaterials Science. An Introduction to Materials in Medicine*, 3rd ed.; Academic Press: San Diego, CA, USA.
7. Bernard, M.; Jubeli, E.; Pungente, M.D.; Yagoubi, N. Biocompatibility of polymer-based biomaterials and medical devices—regulations, in vitro screening and risk-management. *Biomater. Sci.* **2018**, *6*, 2025–2053. [CrossRef] [PubMed]
8. Badylak, S. The Impact of Host Response on Biomaterial Selection. In *Host Response to Biomaterials*; Academic Press: San Diego, CA, USA.
9. NSAI Standards. *I. S. EN ISO 10993-12:2012 Biological Evaluation of Medical Devices*; National Standards Authority of Ireland: Dublin, Ireland, 2012.
10. Strober, W. Trypan Blue Exclusion Test of Cell Viability. *Curr. Protoc. Immunol.* **2001**, *21*, A.3B.1–A.3B.2.
11. Eisenbrand, G.; Pool-Zobel, B.; Baker, V.; Balls, M.; Blaauboer, B.J.; Boobis, A.; Carere, A.; Kevekordes, S.; Lhuguenot, J.C.; Pieters, R.; et al. Methods of in vitro toxicology. *Food Chem. Toxicol.* **2002**, *40*, 193–236. [CrossRef]
12. Single, A.; Beetham, H.; Telford, B.J.; Guilford, P.; Chen, A. A Comparison of Real-Time and Endpoint Cell Viability Assays for Improved Synthetic Lethal Drug Validation. *J. Biomol. Screen.* **2015**, *20*, 1286–1293. [CrossRef] [PubMed]

13. O'Brien, J.; Wilson, I.; Orton, T.; Pognan, F. Investigation of the Alamar Blue (resazurin) fluorescent dye for the assessment of mammalian cell cytotoxicity. *Eur. J. Biochem.* **2000**, *267*, 5421–5426. [CrossRef]

14. Fiers, W.; Beyaert, R.; Declercq, W.; Vandenabeele, P. More than one way to die: apoptosis, necrosis and reactive oxygen damage. *Oncogene* **1999**, *18*, 7719–7730. [CrossRef]

15. Norbury, C.J.; Hickson, I.D. Cellular responses to DNA damage. *Annu. Rev. Pharmacol. Toxicol.* **2001**, *41*, 367–401. [CrossRef]

16. Walczak, R. Inkjet 3D printing—towards new micromachining tool for MEMS fabrication. *Bull. Pol. Acad. Sci. Tech. Sci.* **2018**, *66*, 179–186.

17. Enders, A.; Siller, I.G.; Urmann, K.; Hoffmann, M.R.; Bahnemann, J. 3D Printed Microfluidic Mixers—A Comparative Study on Mixing Unit Performances. *Small* **2019**, *15*, 1804326. [CrossRef] [PubMed]

18. 3D Systems. Projet MJP 2500 MultiJet Plastic Printers Tech. Specs. Available online: https://de.3dsystems.com/3d-printers/projet-mjp-2500-series/specifications (accessed on 6 June 2019).

19. 3D Systems. Safety Data Sheet: VisiJet M2R-CL. Available online: http://infocenter.3dsystems.com/materials/mjp/visijet-m2r-cl (accessed on 6 June 2019).

20. 3D Systems. Safety Data Sheet: VisiJet M3 Crystal. Available online: http://infocenter.3dsystems.com/materials/mjp/visijet-m3-crystal (accessed on 6 June 2019).

21. 3D Systems. Safety Data Sheet: VisiJet M2G-CL. Available online: http://infocenter.3dsystems.com/materials/mjp/visijet-m2g-cl?_ga=2.257034957.758772822.1561980611-943946801.1561980611 (accessed on 6 June 2019).

22. Block, S.S. *Disinfection, Sterilization, and Preservation*, 5th ed.; Lippincott Williams & Wilkins: Philadelphia, PA, USA, 2001.

23. Smith, P.N.; Palenik, C.J.; Blanchard, S.B. Microbial contamination and the sterilization/disinfection of surgical guides used in the placement of endosteal implants. *Int. J. Oral Maxillofac. Implants* **2011**, *26*, 274–281. [PubMed]

24. Rutala, W.A.; Weber, D.J. Disinfection and sterilization: An overview. *Am. J. Infect. Control* **2013**, *41*, S2–S5. [CrossRef]

25. Rutala, W.A.; Weber, D.J.; HICPAC. *Guideline for Disinfection and Sterilization in Healthcare Facilities*; Centers for Disease Control and Prevention: Chapel Hill, NC, USA, 2008.

26. Pepelanova, I.; Kruppa, K.; Scheper, T.; Lavrentieva, A. Gelatin-Methacryloyl (GelMA) Hydrogels with Defined Degree of Functionalization as a Versatile Toolkit for 3D Cell Culture and Extrusion Bioprinting. *Bioengineering (Basel)* **2018**, *5*, 55. [CrossRef] [PubMed]

27. Niles, A.L.; Moravec, R.A.; Riss, T.L. In vitro viability and cytotoxicity testing and same-well multi-parametric combinations for high throughput screening. *Curr. Chem. Genom.* **2009**, *3*, 33–41. [CrossRef]

28. Gonzalez, R.J.; Tarloff, J.B. Evaluation of hepatic subcellular fractions for Alamar blue and MTT reductase activity. *Toxicol. In Vitro* **2001**, *15*, 257–259. [CrossRef]

29. Wlodkowic, D.; Skommer, J.; Darzynkiewicz, Z. Flow cytometry-based apoptosis detection. *Methods Mol. Boil.* **2009**, *559*, 19–32.

30. Adan, A.; Alizada, G.; Kiraz, Y.; Baran, Y.; Nalbant, A. Flow cytometry: basic principles and applications. *Crit. Rev. Biotechnol.* **2017**, *37*, 163–176. [CrossRef]

31. Bajpai, R.; Lesperance, J.; Kim, M.; Terskikh, A.V. Efficient propagation of single cells accutase-dissociated human embryonic stem cells. *Mol. Reprod. Dev.* **2007**, *75*, 818–827. [CrossRef] [PubMed]

32. Salzig, D.; Leber, J.; Merkewitz, K.; Lange, M.C.; Köster, N.; Czermak, P. Attachment, Growth, and Detachment of Human Mesenchymal Stem Cells in a Chemically Defined Medium. *Stem Cells Int.* **2016**, *2016*, 1–10. [CrossRef] [PubMed]

33. Elmore, S. Apoptosis: A review of programmed cell death. *Toxicol. Pathol.* **2007**, *35*, 495–516. [CrossRef] [PubMed]

34. Dasari, S.; Tchounwou, P.B. Cisplatin in cancer therapy: molecular mechanisms of action. *Eur. J. Pharmacol.* **2014**, *740*, 364–378. [CrossRef] [PubMed]

35. Florea, A.M.; Büsselberg, D. Cisplatin as an Anti-Tumor Drug: Cellular Mechanisms of Activity, Drug Resistance and Induced Side Effects. *Cancers* **2011**, *3*, 1351–1371. [CrossRef] [PubMed]

36. Kopperud, H.M.; Kleven, I.S.; Wellendorf, H. Identification and quantification of leachable substances from polymer-based orthodontic base-plate materials. *Eur. J. Orthod.* **2011**, *33*, 26–31. [CrossRef] [PubMed]

37. Oesterreicher, A.; Wiener, J.; Roth, M.; Moser, A.; Gmeiner, R.; Edler, M.; Pinter, G.; Griesser, T. Tough and degradable photopolymers derived from alkyne monomers for 3D printing of biomedical materials. *Polym. Chem.* **2016**, *7*, 5169–5180. [CrossRef]

38. Amato, S.F.; Ezzell, R.M. *Regulatory Affairs for Biomaterials and Medical Devices: Woodhead Publishing Series in Biomaterials*; Woodhead Publishing: Sawston, UK, 2015.

39. Rashid, H.; Sheikh, Z.; Vohra, F. Allergic effects of the residual monomer used in denture base acrylic resins. *Eur. J. Dent.* **2015**, *9*, 614–619. [CrossRef]

40. Goddard, J.M.; Hotchkiss, J.H. Polymer surface modification for the attachment of bioactive compounds. *Prog. Polym. Sci.* **2007**, *32*, 698–725. [CrossRef]

41. Rudko, G.; Kovalchuk, A.; Fediv, V.; Chen, W.M.; Buyanova, I.A. Enhancement of polymer endurance to UV light by incorporation of semiconductor nanoparticles. *Nanoscale Res. Lett.* **2015**, *10*, 81. [CrossRef]

42. Vijayalakshmi, S.P.; Madras, G. Photodegradation of poly (vinyl alcohol) under UV and pulsed-laser irradiation in aqueous solution. *J. Appl. Polym. Sci.* **2006**, *102*, 958–966. [CrossRef]

43. Gogotov, I.N.; Barazov, S.K. The Effect of Ultraviolet Light and Temperature on the Degradation of Composite Polypropylene. *Int. Polym. Sci. Technol.* **2014**, *41*, 55–58. [CrossRef]

44. Fukuzaki, S. Mechanisms of actions of sodium hypochlorite in cleaning and disinfection processes. *Biocontrol Sci.* **2006**, *11*, 147–157. [CrossRef] [PubMed]

45. Rutala, W.A.; Weber, D.J. Uses of inorganic hypochlorite (bleach) in health-care facilities. *Clin. Microbiol. Rev.* **1997**, *10*, 597–610. [CrossRef] [PubMed]

46. Spencer, H.R.; Ike, V.; Brennan, P.A. Review: the use of sodium hypochlorite in endodontics—potential complications and their management. *Bdj open* **2007**, *202*, 555. [CrossRef]

47. Alkahtani, A.; Alkahtany, S.M.; Anil, S. An in vitro evaluation of the cytotoxicity of varying concentrations of sodium hypochlorite on human mesenchymal stem cells. *J. Contemp. Dent. Pract.* **2014**, *15*, 473–481. [CrossRef]

48. Hidalgo, E.; Bartolome, R.; Dominguez, C. Cytotoxicity mechanisms of sodium hypochlorite in cultured human dermal fibroblasts and its bactericidal effectiveness. *Chem. Biol. Interact.* **2002**, *139*, 265–282. [CrossRef]

49. Graziano, M.U.; Graziano, K.U.; Pinto, F.M.G.; Bruna, C.Q.M.; Souza, R.Q.S.; Lascala, C.A. Effectiveness of disinfection with alcohol 70% (w/v) of contaminated surfaces not previously cleaned. *Rev. Lat. Am. Enfermagem* **2013**, *21*, 618–623. [CrossRef]

50. Garcia-Montero, A.; Vasseur, S.; Mallo, G.V.; Soubeyran, P.; Dagorn, J.C.; Iovanna, J.L. Expression of the stress-induced p8 mRNA is transiently activated after culture medium change. *Eur. J. Cell Biol.* **2001**, *80*, 720–725. [CrossRef]

51. Rello, S.; Stockert, J.C.; Moreno, V.; Gámez, A.; Pacheco, M.; Juarranz, A.; Cañete, M.; Villanueva, A. Morphological criteria to distinguish cell death induced by apoptotic and necrotic treatments. *Apoptosis* **2005**, *10*, 201–208. [CrossRef]

52. Watanabe, I.; Okada, S. Effects of temperature on growth rate of cultured mammalian cells (L5178Y). *J. Cell Biol.* **1967**, *32*, 309–323. [CrossRef] [PubMed]

53. Tchao, R. Fluid shear force and turbulence-induced cell death in plastic tissue culture flasks. *In Vitro Toxicol.* **1996**, *9*, 93–100.

54. Gelles, J.D.; Chipuk, J.E. Robust high-throughput kinetic analysis of apoptosis with real-time high-content live-cell imaging. *Cell Death Dis.* **2016**, *7*, e2493. [CrossRef] [PubMed]

4.2 Entwicklung und Charakterisierung eines 3D-gedruckten Zellkultursystems für die adhärente Zellkultur

Abbildung 4-2 *Graphical abstract* von „*Characterization of a customized 3D-printed cell culture system using clear, translucent acrylate that enables optical online monitoring*".

Im vorherigen Kapitel konnte verdeutlicht werden, wie unerlässlich und bedeutsam eine geeignete *Post-Processing*-Strategie für die biologische Verträglichkeit eines Materials ist. Die einzelnen Komponenten, aus denen das 3D-Druckmaterial besteht, können dabei ebenfalls einen entscheidenden Einfluss auf die Biokompatibilität haben. Das Auslaugen von Acylatmonomeren, Degradationsprodukten oder anderen Bestandteilen ist ein bekanntes Problem bei polymerbasierten Materialien und geht häufig mit zytotoxischen Effekten auf eine biologische Umgebung einher [109,111,107]. Außerdem werden je nach Anwendung neben der Gewährleistung von Biokompatibilität weitere Anforderungen an das Material gestellt. Chemische, mechanische und physikalische Materialeigenschaften können kritische Faktoren darstellen, die den Einsatzbereich eines Materials potentiell einschränken können.

Nachfolgend wird ein additiv gefertigtes Zellkultursystem vorgestellt, das als Kultivierungsgefäß in der adhärenten Zellkultur eingesetzt werden kann. Da bisher keine Informationen über die biologische Verträglichkeit und Materialeigenschaften vorliegen, wurde das verwendete 3D-Druckmaterial vorweg eingehend charakterisiert.

Ähnlich zu dem im vorherigen Kapitel untersuchten 3D-Druckmaterial, handelt es sich bei dem hier verwendeten Material (AR-M2, Keyence GmbH) ebenso um ein transluzentes, festes Polyacrylat, das mittels *Inkjet Printing* hochauflösend gedruckt wurde. Der Einfluss des 3D-Druckmaterials auf Säugetierzellen wurde in Studien zur Zellproliferation, Viabilität, Zellmorphologie und Apoptose/Nekrose-Verteilungen umfassend untersucht. Adipogene, mesenchymale Stammzellen (AD-MSCs) dienten dabei als sensible, humane Modellzellen. Weder in indirektem Kontakt über das Zellkulturmedium noch in direktem Kontakt zu den Zellen konnte ein negativer Einfluss des Materials festgestellt werden – alle Untersuchungen zeigten keine signifikanten Unterschiede zu durchgeführten Kontrollkultivierungen in handelsüblichen Kulturgefäßen. Aus diesem Grund kann das 3D-Druckmaterial als (*in vitro*) biokompatibel bewertet werden.

Werden Zellen in direktem Kontakt zu einem Material kultiviert, sind die Oberflächeneigenschaften des Materials von großer Bedeutung. Die Oberflächenrauheit, Topographie und Benetzbarkeit können einen entscheidenden Einfluss auf die Adhärenz und Proliferation der Zellen haben [134,105]. Aus diesem Grund wurden die Oberflächenstrukturen des 3D-Druckmaterials mittels eines hochauflösenden 3D-Mikroskopes untersucht. Bedingt durch den zugrunde liegenden Druckprozess werden verschiedene Oberflächenstrukturen erzeugt. Durch Anpassen der Orientierung des CAD-Modells vor dem Druck kann eine ausgewählte Oberflächenstruktur für bestimmte Modelldetails festgelegt werden. Für das entwickelte Zellkultursystem wurde das CAD-Modell derart orientiert, sodass die Oberfläche, die mit den Zellen in direkten Kontakt kommt, eine glatte und homogene Struktur aufweist.

Das entworfene Zellkultursystem passt in eine Vertiefung einer regulären *6-Well Plate*. Dadurch können nicht nur sterile Bedingungen geschaffen werden – es wird zudem eine benutzerfreundliche Handhabung erreicht. AD-MSCs wurden in die 3D-gedruckte Zellkulturkammer ausgesät und über mind. 70 h kultiviert. Die klare, transluzente Erscheinung des Materials erlaubt zugleich eine mikroskopische Beobachtung der Kultivierung. Insgesamt konnten keine Nachteile des 3D-gedruckten Systems zu handelsüblichen Kulturgefäßen festgestellt werden. Vielmehr eröffnen die beachtlichen Eigenschaften des untersuchten 3D-Druckmaterials die Türen zu unzähligen Einsatzmöglichkeiten, insbesondere in der adhärenten Zellkultur.

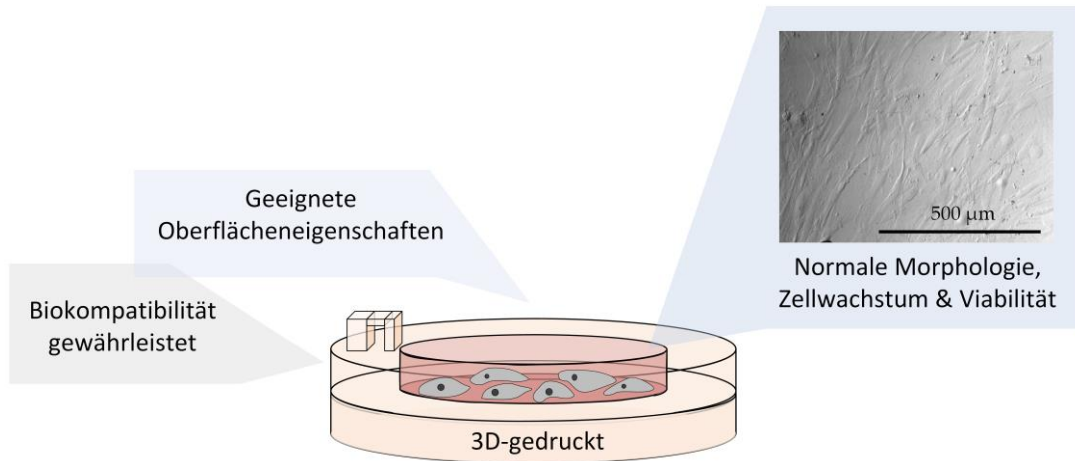Im folgenden Artikel „*Characterization of a customized 3D-printed cell culture system using clear, translucent acrylate that enables optical online monitoring*" werden die Ergebnisse ausführlich beschrieben und diskutiert.

PAPER • OPEN ACCESS

Characterization of a customized 3D-printed cell culture system using clear, translucent acrylate that enables optical online monitoring

View the article online for updates and enhancements.

Biomedical Materials

CrossMark

OPEN ACCESS

PAPER

Characterization of a customized 3D-printed cell culture system using clear, translucent acrylate that enables optical online monitoring

Ina Gerhild Siller [iD]**, Anton Enders, Pia Gellermann, Steffen Winkler, Antonina Lavrentieva, Thomas Scheper and Janina Bahnemann**

Institute of Technical Chemistry, Leibniz University Hannover, Callinstraße 5, Hannover 30167, Germany

E-mail: jbahnemann@iftc.uni-hannover.de

Abstract

Cells are very sensitive to their direct environment—they place high demands, for example, on ambient culture medium, adjacent cell types, and the properties of surrounding material parts. As a result, mechanical and physical material properties—such as surface roughness, swelling, electrostatic effects, etc—can all have a significant impact on cell behaviour. In addition, a material's composition also impacts whether that material meets biocompatibility requirements and can thus be considered for potential use in biomedical applications. The entry of high-resolution 3D printing technology in biotechnology has opened the door to individually-designed experiment-adaptable devices of almost unlimited complexity that can be manufactured within just a few hours. 3D printing materials are frequently lacking in the characteristics that make them suitable for biomedical applications, however.

This study introduces a high-resolution polyacrylic 3D printing material as a potential alternative material for use in cultivation systems with indirect or direct contact to cells. Viability analyses, studies of apoptotic/necrotic cell death response, and surface studies all suggest that this material meets the requirements for (*in vitro*) biocompatibility, and has surface properties sufficient to permit uninhibited cell proliferation for cells in direct contact to the material. Moreover, the translucency of this material facilitates the type of optical monitoring required for performing experiments in a microfluidic environment, or for facilitating microscopic observations.

1. Introduction

In 1983, the US American engineer Charles 'Chuck' Hull came up with the idea of the first 3D printing apparatus, which was capable of creating objects in a layer-by-layer fashion [1]. Shortly thereafter, he filed a patent for his revolutionary idea. 3D printing (also known as additive manufacturing) has since transformed traditional manufacturing, enabling the fabrication of individually designed complex systems in an astonishingly short amount of time. After Hull's initial patents expired, 3D printing technology quickly became widespread across a variety of industries and disciplines. 3D printing technology also soon found its way into scientific applications, and it is now established in the medical sector, where it facilitates modern-day 'miracles' including complex surgical models and customized patient-specific prostheses based upon medical imaging data [2, 3]. In the wet lab environment, 3D printing has turned out to be a valuable tool for creating experiment-specific labware and individually adjusted prototypes ('rapid prototyping') [4, 5]. And with more recent developments in advanced 3D printers that permit printing in high resolution of under 100 μm, this technology has also found important applications in microfluidics and biomedical engineering [6–8]. In microfluidics, high-definition 3D printing technology now

allows researchers to manufacture 3D geometries with almost unlimited complexity in virtually no time.

As diverse as these applications are, so are the underlying 3D printing technologies that have been developed. The material bases can vary from photosensitive liquid acrylates (which are cured via photopolymerization) to rigid thermoplastic materials (which are fused and extruded in strands) to powdered material particles (which are selectively sintered with a laser)—to give just a few illustrative examples. Regardless of their differences, however, all 3D printing technologies have one thing in common: they utilize a 'layer-by-layer' fabrication process. In this study, objects were printed via inkjet 3D printing technology. The printer uses ultraviolet (UV) light curable material in liquid form that is ejected from the inkjet head as it moves forward. During the subsequent backward movement, the material is flattened by a roller and cured via a UV lamp. This process is then repeated, layer-by-layer, until the desired object is fully built up.

For integration of 3D-printed objects into biomedical applications, the biological environment needs to be in compliance with specific material properties. Whenever a biological system (such as a cell) is brought into direct contact with a material, interface interactions can transpire. Properties of the material can provoke changes in the biological environment—which can in turn have an additional effect on the material, etc, creating a feedback loop effect. As a result, the chemical, mechanical, and physical properties of a material are all critical factors that can each potentially limit the incorporation of that material into biological applications. Aside from consideration of the general non-toxicity of a material, however, two surface characteristics have been identified in the literature as having critical parameters for influencing cellular behaviour: wettability, and surface topography/roughness [9–11]. Surface wettability plays a major role in cell attachment and growth, because it can impact protein adsorption. Cell attachment is regulated via proteins—giving one reason for using serum-enriched cell culture medium, which is containing these specific proteins [9]. The proteins adsorb onto the materials surface, and then provide binding sites for cell anchorage. Surface topography at both micro- and nano-scales also has implicated for cell adhesion and proliferation. After studying surface wettability and topography independently, Yang *et al* have shown the dependency of osteoblast adhesion and spreading on surface roughness of polystyrene films [10]. But other material properties can also potentially affect the surrounding biological environment: these include (to name just a few) material tensile strength, flexibility, hardness, durability, surface charge, and energy or electrostatics [12]. To overcome potential adverse material properties of 3D printi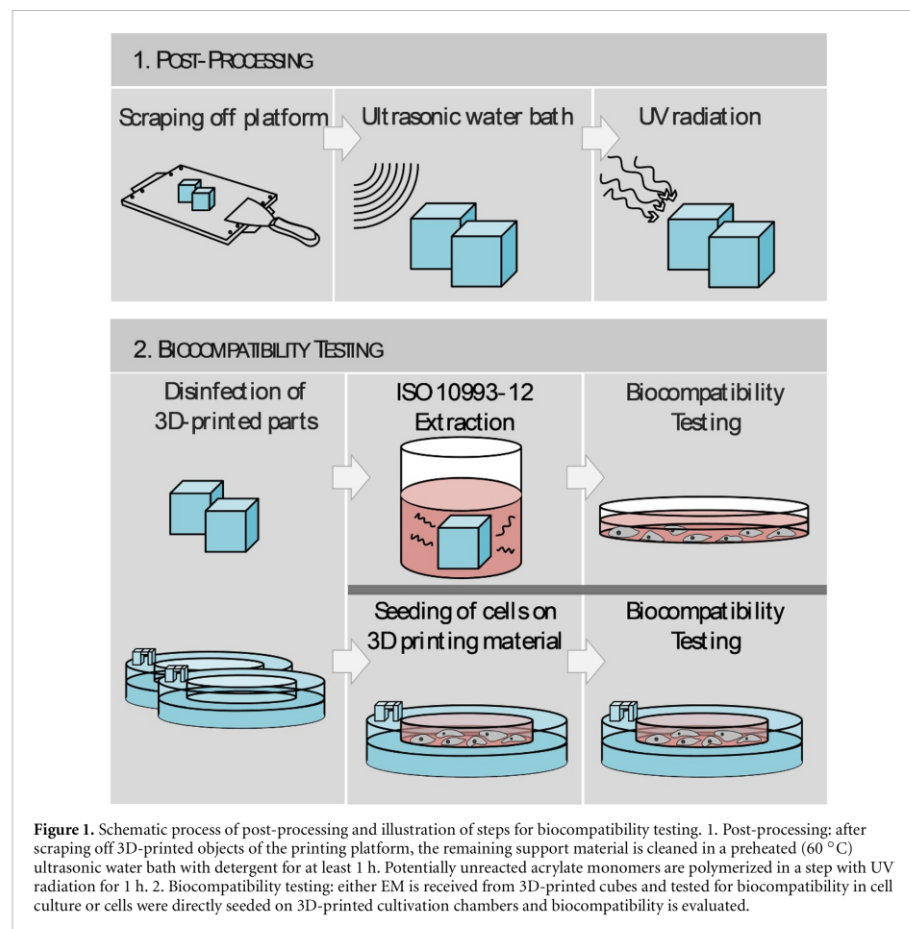ng resins, Lu *et al* have illustrated the effectiveness of using waterborne polyurethane as a coating material [13]. This improved both cell adhesion and proliferation compared to uncoated material. It should be apparent that there are many factors to consider in this equation. But even if all mechanical, physical, and physico-chemical properties of a material meet the desired requirements, enhanced cytotoxicity may *still* disqualify the material for any biological studies. Put differently (and simply): in order to qualify for use in biological studies, it must be shown that a material has no negative influence on cell growth and proliferation compared to certified cell culture materials. The biocompatibility of a material must be established within restrictions or limitations.

Against this backdrop, then, this work represents a comprehensive investigation of a rigid, clear 3D-printed acrylic resin for potential use in biological applications and highlights the application in adherent cell culture by designing and characterizing a customized 3D-printed cell culture system. This study not only demonstrates the applicability of the 3D printing material in countless biological fields with regard to biocompatibility, but also emphasizes its suitability for the cultivation of adherent growing cells. Due to the printing process used, different surface topographies are formed. Depending on the desired application, the surface structure may have an impact. For that reason, the surface roughness and 3D profile of structures formed by the 3D printing process were analysed. And the potential influence of ethanol on these surface properties was also investigated—since ethanol is commonly used for disinfection of the 3D-printed objects. As mentioned above, biocompatibility is a central and prerequisite requirement for the use of any material in biological applications. The 3D printing material used in this study has not yet been certified as biocompatible, and to the best of our knowledge, there are no studies published yet that integrate additive manufactured systems into biological applications printed with this material. Accordingly, in order to evaluate as a matter of first impression the biocompatibility of this material, standard viability analyses based on biochemical assays as well as flow cytometric studies of apoptotic and necrotic cell responses were conducted. A customized cell culture system for adherent cell cultivation was designed, 3D-printed and examined for its suitability in biomedical applications. Since translucency of the 3D-printed material allows for optical observations, morphological changes in response to direct cell-material contact could be monitored by microscopic experiments.

2. Methods

2.1. 3D printing and post-processing
The analysed objects, cubes, and co-cultivation chambers were constructed with the computer-aided design (CAD) software SolidWorks 2018 (Dassault

Figure 1. Schematic process of post-processing and illustration of steps for biocompatibility testing. 1. Post-processing: after scraping off 3D-printed objects of the printing platform, the remaining support material is cleaned in a preheated (60 °C) ultrasonic water bath with detergent for at least 1 h. Potentially unreacted acrylate monomers are polymerized in a step with UV radiation for 1 h. 2. Biocompatibility testing: either EM is received from 3D-printed cubes and tested for biocompatibility in cell culture or cells were directly seeded on 3D-printed cultivation chambers and biocompatibility is evaluated.

Systèmes, Waltham, MA, USA). The printing material analysed in this study is named AR-M2 (Keyence Deutschland GmbH, Neu-Isenburg, Germany), and it is a rigid translucent polyacrylate resin printed using the high-resolution 3D printer AGILISTA-3200 W (Keyence Deutschland GmbH, Neu-Isenburg, Germany). Via a UV curing process, and using inkjet printing technology, a layer thickness of 15 μm and a resolution of 635×400 dots per inch can be achieved. The material appears as stable and translucently clear, enabling optical microscopic analyses. The known material components in a liquid state of the polyacrylate are two acrylate monomers, a photoinitiator, a stabilisator, and a urethane-acrylate-oligomer. AR-S1 (Keyence Deutschland GmbH, Neu-Isenburg, Germany) was used as support material during the printing process.

The support material is removed via several additional post-processing steps (figure 1). After roughly scraping the 3D-printed objects off the printing platform, remaining support material is removed by placing the objects for at least 1 h in a pre-warmed (60 °C) ultrasonic water bath (Banedlin electronic, Berlin, Germany) with detergent (Fairy Ultra Plus, Procter and Gamble, CT, USA). This water bath is filled with deionized water provided by Arium® (Sartorius Stedim Biotech GmbH, Göttingen, Germany). To ensure proper photo polymerization of the materials acrylate monomers, the 3D-printed objects are additionally exposed to UV light (UV Sterilization Cabinet KT-09DC, Alexnld, Tiberias, Israel) for 1 h.

Since the 3D-printed material deforms at temperatures around 80 °C, thermal sterilization approaches are not applicable here [14, 15]. Instead, a chemical disinfection procedure with ethanol was used in this study. The 3D-printed objects were immersed for 1 h in ethanol (Carl Roth GmbH und Co. KG, Karlsruhe, Germany), 70%, v/v, placed for at least 30 min in a sterile environment (safety bench hood cabinet) allowing residues of ethanol to evaporate and washed thoroughly with sterile phosphate-buffered saline (PBS, Carl Roth GmbH und Co. KG, Karlsruhe, Germany) afterwards.

2.2. Chemical stability testing and surface analysis

To determine chemical stability, $5 \times 5 \times 5$ mm cubes with a total surface area-to-volume-ratio of 1.5 cm$^2 \cdot$ ml^{-1} were 3D-printed, post-processed, and incubated for 1 h, 24 h, 7 d and 14 d, respectively, in three different chemical solvents at RT. Isopropyl alcohol (70%, v/v) and ethanol (70%, v/v) were selected as chemical solvents since they are all commonly used in disinfection approaches for cell culture applications. Both before and after incubation, the 3D objects were dried (70 °C, 60 min), weighed, and subjected to surface studies (i.e. roughness, etc). The mass difference was then calculated, and both the color and the roughness parameters were observed using a digital microscope (VHX-5000, Keyence Corp., Osaka, Japan).

2.3. Preparation of extraction media for biocompatibility studies

To evaluate the biocompatibility of the aforementioned material, extraction medium (EM) is obtained according to EN ISO 10993-12:2012 (Biological evaluation of medical devices—art 12: Sample preparation and reference materials). $5 \times 5 \times 5$ mm cubes with a total surface area of 1.5 cm^2 were 3D-printed, post-processed, disinfected with ethanol (70%, v/v), and incubated in a cell culture medium (Minimum Essential Medium Eagle, with alpha modification (α-MEM) (Thermo Fisher Scientific Inc. Waltham, USA), 10% human serum (c.c.pro GmbH, Oberdorla, Germany), and 0.5% Gentamicin (PAA Laboratories GmbH, Pasching, Austria)). The 3D-printed cubes were incubated in cell culture medium for 72 h at 37 °C in a 5% CO$_2$, 21% O$_2$, humidified atmosphere (Heracell 150i incubator, Thermo Fisher Scientific Inc. Waltham, USA) with a surface area/volume ratio of 3 cm$^2 \cdot$ ml^{-1}. The obtained medium is referred to as EM. As a control, cell culture medium was also incubated for 72 h at 37 °C in a 5% CO$_2$, 21% O$_2$, humidified atmosphere in the absence of any 3D-printed cubes.

2.4. Cell line and cell culture conditions

In this study, experiments with human adipose tissue-derived mesenchymal stem/stromal cells (AD-MSCs) were performed. Following isolation from adipose tissue after abdominoplasty surgery, these cells were expanded and cryopreserved in passage 2 until used for biocompatibility studies. The donor has given informed written consent as approved by the Institutional Review Board (Hannover Medical School) with the reference number 3475–2017. The isolated cells have been previously extensively characterized as AD-MSCs [16]. AD-MSCs were cultivated in cell culture medium (described in 2.3.) at 37 °C in a 5% CO$_2$, 21% O$_2$, humidified atmosphere and harvested at about 85% confluency by accutase treatment (Merck KGaA, Darmstadt, Germany). All experiments were performed with cells of passages three to nine. Cell proliferation was also monitored, and images were taken, via live cell imaging microscopy in the cell imaging multi-mode reader Cytation-5 (BioTek Instruments, Inc. Winooski, VT, USA).

2.5. CellTiter-Blue® viability assay

To evaluate cell viability, CellTiter-Blue® (CTB) cell viability assay (Promega, GmbH, Mannheim, Germany) was performed as instructed by the manual, including background and standard controls. Viable cells possess the ability to convert an indicator dye, the blue resaruzin, into a purple, fluorescent product (resorufin) [17, 18]. Metabolically inactive cells are not able to reduce resaruzin, and, as a result, they do not produce any florescent signal. Therefore, the detection of fluorescence intensity gives an indication on cell viability in the sample.

The fluorescent product formation is monitored at an extinction wavelength of 544 nm, and an emission wavelength of 590 nm, using a fluorescence plate reader (Fluoroskan Acent, Thermo Fisher Scientific Inc. Waltham, USA). Cells were seeded in 96-well plates (Sarstedt AG & Co. KG, Nürnbrecht, Germany) (at a density of 1100 cells $\cdot$ cm^{-2}) 24 h prior to the start of an experiment, and thereafter maintained at 37 °C in a 5% CO$_2$, 21% O$_2$, humidified atmosphere. The cell culture medium is exchanged to EM or control medium for another cultivation period of 24 h. After 24 h, the medium was removed from each well, 100 μl fresh culture medium containing 10% CTB stock solution was added to each well and the cells were incubated at 37 °C in a 5% CO$_2$, 21% O$_2$, humidified atmosphere for 1.5 h before measuring the fluorescence signal.

2.6. Lactate dehydrogenase based viability assay

Another colorimetric method commonly used to determine cell viability is the evaluation of lactate dehydrogenase (LDH) activity in the cell culture supernatant. Damaged or dead cells with compromised membrane integrity release LDH from the cytosol into the cell culture medium. Here, the Cytotoxicity Detection Kit (Roche, Basel, Switzerland) was used, and a spectrophotometric microplate reader (BioTek Instruments, Inc. Winooski, VT, USA) allowed for simultaneous measurement of multiple samples. The amount of leaked, active LDH is measured by the conversion of tetrazolium salt into the red formazan, which possess an absorption maximum at 500 nm. Therefore, the amount of formazan is directly proportional to the count of damaged cells, and can thus be used to measure cell viability. The LDH assay was performed as instructed by the manual, including controls. Cells were seeded as described in section 2.5 and 100 μl supernatant from each well were used for the calculation of cell viability by LDH assay.

2.7. Cell growth on 3D printing material

Cell cultivation chambers were designed via CAD software; 3D-printed; post-processed; disinfected with ethanol (70 %, v/v); and then washed thoroughly with sterile PBS for the use in cell culture. Figure 5 illustrates the dimensions and handling of the 3D-printed system. The whole system fits in a well of a regular 6-well plate, which facilitates user-friendly handling without compromising sterility. A cultivation surface for adherent cell growth is placed in a cavity in the middle of the system that is hereafter referred to as the 'cell cultivation well'. The growth surface area of the cell cultivation well is adapted to the growth area of a regular well in a 24-well plate and is 1.89 cm^2. Therefore, experiments in regular 24-well plates served as a control, an ideal cultivation. However, it should be noted that the regular 24-well plates used are coated with unknown formulations, designed by the manufacturer to provide an optimum culture substrate (Sarstedt AG & Co. KG, Nürnbrecht, Germany). Accordingly, the 3D-printed system is actually being compared to ideal cultivation conditions.

Before the start of an experiment, the 3D-printed cell cultivation chambers were immersed in ethanol (70 %, v/v; 1 h) for disinfection. Afterwards, they were placed in a sterile environment on a sterile surface for at least 30 min allowing residues of ethanol to evaporate. Finally, the 3D-printed systems were washed thoroughly with sterile PBS. Cells were seeded in cell cultivation wells at a density of 15.000 cells · cm^{-2}. As control cultures, cells were seeded at the same density in 24-well plates (Sarstedt AG & Co. KG, Nürnbrecht, Germany), which have the same growth surface area of 1.89 cm^2 as the 3D-printed cultivation wells. All cultures were maintained at 37 °C in a 5% CO_2, 21% O_2, humidified atmosphere. After 24 h and 48 h, cell viability was evaluated via a CTB viability assay (see section 2.5). Cell proliferation was also determined via Trypan blue exclusion method. The Trypan blue stain can enter and thereby mark dead or damaged cells, as they possess compromised membrane integrity. On that account, living and dead or damaged cells can be distinguished. Cells were stained with 0.4% Trypan blue stain (n = 3) and living just as dead cells counted in a haemocytometer (Brand GmbH + Co. KG, Wertheim, Germany). In addition, apoptosis and necrosis of cells were analysed by flow cytometry after seeding of cells directly onto 3D-printed material. Figure 1 presents an overview of the conducted method steps for analysing biocompatibility of the 3D-printed material.

2.8. Contact angle measurement

The contact angle between water droplets and the 3D-printed material surfaces was determined using a contact angle meter (OCA 50 15EC, DataPhysics Instruments GmbH, Filderstadt, Germany). 1 μl of deionized water was dropped onto the material surface.

The measurement (optical recording by camera) was started immediately and corresponding software (SCA 20, DataPhysics Instruments GmbH, Filderstadt, Germany) was used to estimate the contact angles. All sides of the surface structure formed by the 3D printing process and the surface of a commercial cell culture well plate were analysed. For each material surface five independent measurements were performed.

2.9. Cell viability analysis by flow cytometry

Flow cytometry is a technique used to identify cell phenotype and characteristics by using light-scattering properties of cells and their fluorescence activity. Flow cytometry renders it possible to not only differentiate between living and dead cells, but also to draw correlations between cell apoptosis vs. necrosis using specific fluorescence detection markers. Analyses of apoptosis vs. necrosis is particularly useful because it provides a researcher with more detailed information regarding the influences of the 3D printing material on cell behaviour and cell death. Single cells are hydrodynamically focused in a liquid stream, and, as they pass the interrogation point, a light beam of suitable wavelengths is directed to hit single cells—permitting the research to analyse the light scattering effect caused by that cell's physical characteristics.

The BD FACSAria™ Fusion (Becton Dickinson, Franklin Lakes, NJ, USA) flow cytometer was used in this study. Cells were seeded in 3D-printed cultivation chambers or regular 24-well plates, respectively, with a density of 15.000 cells · cm^{-2} and incubated at 37 °C in a 5% CO_2, 21% O_2, humidified atmosphere. After a defined period of time, cells were detached via accutase treatment, centrifuged for 5 min at 200 xg, and washed with PBS twice. Apoptotic and necrotic cells were then visualized via specific fluorescence staining. An early event happening during apoptosis is the translocation of phosphatidylserine to the cell surface. The detection of these residues on the surface of the cell can therefore be considered to constitute a clear sign of apoptosis. Annexin V has a high binding affinity for phosphatidylserine and therefore can be used as a marker protein for detecting apoptosis. Here, apoptotic cells were identified using a PE Annexin V stain (Becton Dickinson, Franklin Lakes, NJ, USA). The corresponding green fluorescence signal has an excitation maximum of 496 nm, and an emission maximum of 578 nm. Necrotic cells are visually marked using a red fluorescent dead cell stain—here, propidium iodide (Becton Dickinson, Franklin Lakes, NJ, USA). As in the Trypan blue exclusion method, propidium iodide enters cells with disrupted cell membranes, resulting in a fluorescent label of dead cells as a consequence of DNA intercalation. The red fluorescent signal was then measured at an excitation maximum of 493 nm and an emission maximum of 636 nm.
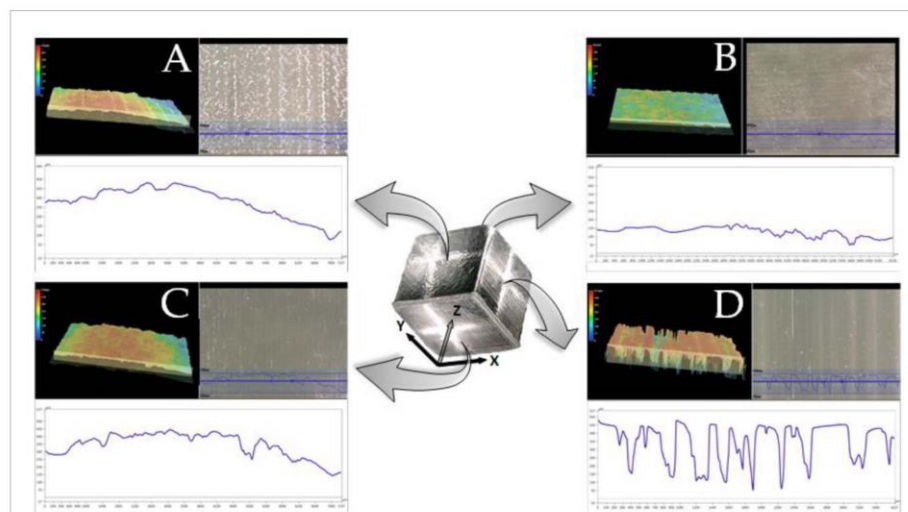
Figure 2. Characteristics of the different surface structures evidenced on the sides of the 3D-printed material. A microscopic image of the analysed surface (50x), the corresponding 3D surface profile, and roughness profile are shown for each printing side. (A) Illustrates the side that is defining the start/end point of the ink nozzles forming the layers; (B) illustrates the smooth, flat upper side; (C) illustrates the bottom side, which is placed on the printing platform, and (D) illustrates the layer-by-layer-structure side.

As a negative control, cells were cultivated in original cell culture medium, without any contact to 3D-printed material. For analysing flow cytometry data, the BD FACS Diva™ Software v8.0 (Becton Dickinson, Franklin Lakes, NJ, USA) was used. The basic principle of analysing flow cytometry data is predicated on 'gating' cell populations of interests. Cells with common characteristics will appear in one population, and can be analysed and quantified separately from other cells. In this way, living, apoptotic, and necrotic cell populations have been identified. In order to ensure a sufficient sample size to draw accurate conclusions, a uniform gating strategy was maintained and at least 10 000 events per sample were analysed, with an 'event' being defined as a single particle being detected.

3. Results and discussion

3.1. Analysis of the 3D printing materials' surface topography

In order to use a material in cell culture applications, the material must not only be sterile and biologically compatible, but it must also have a surface structure and other properties, which are suitable for the intended application. The surface topography and properties of a material can therefore have a high impact on potential applications for that material [19, 20]. For example, an opaque material would not be a good choice for any applications requiring optical analyses. For this reason, the investigation of the surface structures of individual cultivation vessels produced by rapid prototyping is of great importance.

Here, the 3D printing process creates four different surface structures. The specific characteristics of each surface structure with regard to the objective appearance and surface roughness are presented in figure 2. The first surface structure is the bottom side, which is directly placed on the printing platform (see figure 2(C)). The stripes visible in this surface structure are generated by the ink nozzles of the 3D printer, and are therefore entirely dependent on the distance that exists between those nozzles. As shown in the roughness profile of figure 2(C), this first surface exhibits small irregularities in height due to the structure of the printing platform. During forward movement of the printing head, the ink is pushed through the nozzles. A roller sitting right behind the nozzles smooth the printed bands into a flat layer before a UV-lamp cures the ink. The smoothing of the roller creates a flat layer, which constitutes the second surface structure (see figure 2(B)). This upper side always has the flattest surface structure in any object printed using this process. In the further course of the printing process, layer upon layer is stacked to form the desired object. This creates a striped appearance on two sides of the cured material resulting in a third surface structure type—as defined as the layer-by-layer structure side (see figure 2(D)). These structures evidence highest surface roughness. Figure 2(A) represents the fourth formed surface structure, which results from the start and end points of the ink nozzles forming the layers. It also shows a slightly striped appearance generated by the different ink layers.

For applications with direct cell-material interaction, the materials' surface topography must allow

6

for cell adhesion and proliferation *without* influencing cell morphology [21]. Distinct irregularities in height of the material's structure can result in accumulations and detachment of cells at specific locations, and thereby cause problematic inhomogeneity of cell growth on the surface [21, 22]. For this reason, the upper material side smoothed by the roller of the 3D printer was chosen for growth experiments with cells. Here, the printing process did not cause any distinct height irregularities, neither in the direction parallel to the printing direction nor at a 90° angle to the printing direction, as the roughness profiles show (see figure S3 in supporting information (available online at stacks.iop.org/BMM/15/055007/mmedia)). By regulating the orientation of the intended 3D-printed object before printing, the desired surface structure can be selected for specific object details. In this study, we orientated the CAD model—and thus the resulting 3D-printed system—in order to ensure that the smoothed, uniform surface structure was located at the area where cells would be seeded. In contrast to our application—*e.g.* general cultivation with simultaneous observation of cells growing on 3D printing material—other applications may actually require surfaces with a higher relative degree of roughness, so the extent that an increased adhesion or accumulation of cells and corresponding cellular behaviour could be deemed beneficial in other contexts [23–25].

Furthermore, the physical shape of an object may have a significant impact on a biological application, just as hardness and flexibility are important values that must be taken into account [12]. For all biomedical applications, sterile systems are absolutely mandatory. Previous published work has demonstrated the importance of a suitable sterilization or disinfection procedure for 3D-printed objects used in cell culture applications [26]. Many 3D-printed materials lack a high heat distortion temperature, which forecloses the possibility of using any thermal sterilization techniques (*e.g.* autoclaving) [14, 15]. Because the polyacrylate material used in this study deforms at temperatures around 80 °C, thermal sterilization is not possible. Therefore, a chemical disinfection method using ethanol (70 %, v/v) was used in this study.

However, contact with chemical solvents as ethanol can affect the surface properties of a material. Thus, a surface study using different organic solvents used in conventional laboratory routine was also conducted. Treatment with isopropyl alcohol (70 %) and ethanol (70 %) were shown to have no significant impact on the surface roughness, weight, colour, or overall appearance of the investigated 3D-printed material up to an incubation period of 24 h. The corresponding results can be found in the supporting information in figures S1 and S2. Furthermore, previous work demonstrated the suitability of ethanol as an effective disinfectant without influencing optical or mechanical properties of a 3D-printed material [26].

Many 3D-printed materials also evidence a high water uptake and associated swelling—which can result in deformations of the printed systems, and may have a corresponding impact on durability and strength of the material [12]. Especially for devices where small details are of critical importance (for example, microfluidic channels), deformations should be avoided at all costs since they can render the printed device unfunctional. The 3D-printed material used in this study was particularly developed by the manufacturer (Keyence Deutschland GmbH, Neu-Isenburg, Germany) to minimize water uptake and swelling. Indeed, no water uptake was detected for an incubation period of 14 d in performed weight experiments (figure S2 in supporting information).

3.2. Testing the biocompatibility of the 3D printing material in accordance to ISO 10993-12:2012
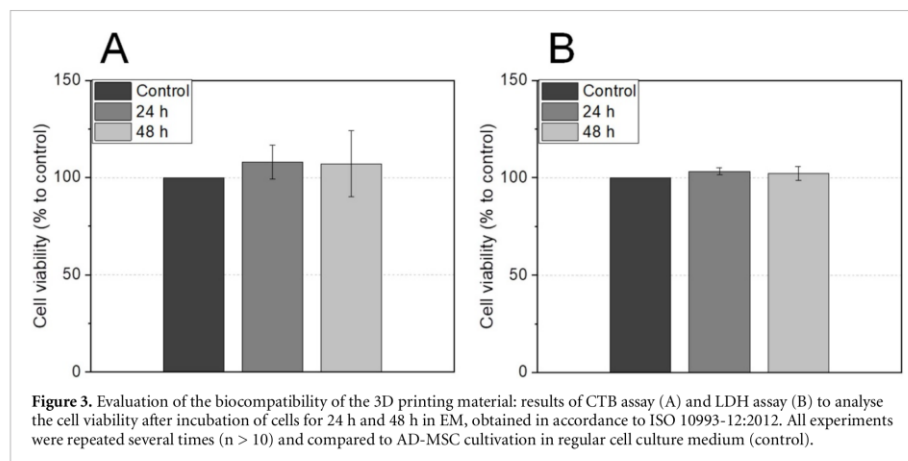
Whenever foreign material is considered for use in biomedical applications, guaranteed biological compatibility is also an absolute prerequisite. For polymer-based materials, potentially cytotoxic effects on cells can emanate from leaching of remaining acrylate monomers or degradation, and can result in irritations and/or allergic reactions within the human body [12, 27, 28]. The 3D printing material used has not yet been certified as biocompatible, nor has it been introduced to a biological environment with mammalian cells. Therefore, general biocompatibility studies were initially carried out.

To investigate the potential cytotoxicity of the 3D-printed polyacrylic material, two different *in vitro* viability assays were conducted—each relying on a different process in the cellular metabolism. Both assays are biochemical-based and widely used, providing results that are both reliable and specific in nature [12, 29]. For both the CTB assay and the LDH assay, AD-MSCs were cultivated in EM, which was prepared beforehand according to EN ISO 10993-12 (2012) (see section 2.3). The results of both viability assays are presented in figure 3, in which cell viability is normalised to the control.

Neither assay revealed any significant differences in cell viability when compared with control cultures (cell viabilities of cells incubated in the EM of around 107% in CTB assay and 102% in LDH assay). In summary, then, this EM does not contain any toxic substances leading to negative effects on the cell's viability. Therefore, the analysed 3D printing material can be considered as (*in vitro*) biocompatible according to ISO 10993-12:2012.

3.3. Cell growth in 3D-printed cultivation chambers

Depending on the application, biological systems may be in either direct or indirect contact with the material of a cultivation vessel or other equipment. In the case of direct contact, many material's properties can influence the suitability of the material

7

Figure 3. Evaluation of the biocompatibility of the 3D printing material: results of CTB assay (A) and LDH assay (B) to analyse the cell viability after incubation of cells for 24 h and 48 h in EM, obtained in accordance to ISO 10993-12:2012. All experiments were repeated several times (n > 10) and compared to AD-MSC cultivation in regular cell culture medium (control).
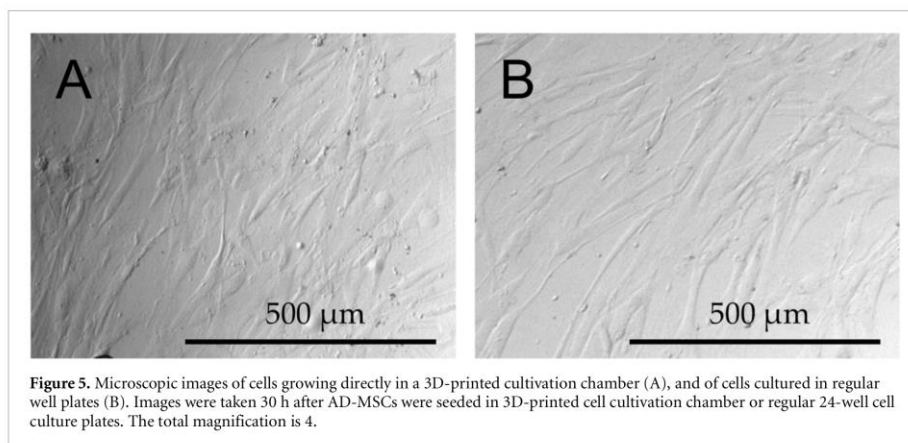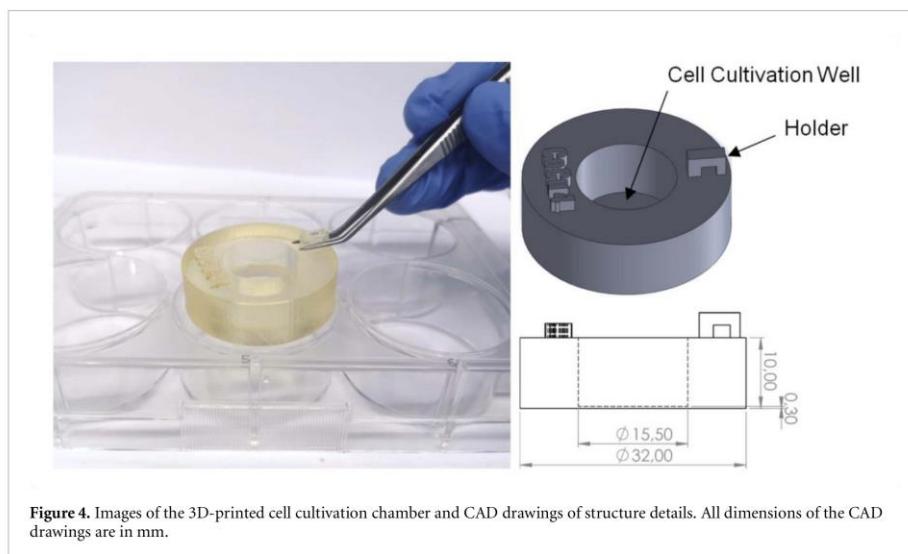
in the desired biological application, since cells are very sensitive to their direct environment [12]. As mentioned above, mechanical and physical properties such as surface roughness, swelling, and wettability can all have a major impact on cell adhesion and proliferation [19, 20]. Optical properties such as transparency and color of the material are also of great importance for microscopic applications. Here, a transparent solid cultivation chamber was 3D-printed. Depending on the thickness of the 3D-printed object, the cured material can take on a slightly yellowish tinge—however, the transparency of the 3D-printed material still allows for direct microscopic monitoring of cell cultures even when this tinge is present. Application fields, that partially require optical monitoring of experiments—such as microfluidics or cell culture technology—can benefit from the material's optical properties [30].

Figure 4 illustrates a 3D-printed prototype of a cell cultivation chamber. The dimensions of this system are adapted to fit in a well of a regular 6-well plate. By placing the system within a sterile 6-well plate, not only sterile conditions but also a user-friendly handling approach can be achieved. AD-MSCs were seeded in a cavity in the middle of the system—the cell cultivation well—which has a material thickness of 0.3 mm to the bottom. The growth surface area of the cell cultivation well is 1.89 cm², and is designed to match the growth area of regular 24-well plates. Thus, it is possible to perform control cell cultivations in regular 24-well plates with equal growth surface area for comparison. However, it should be noted that control cultivations represent the optimal growth of AD-MSCs as the regular 24-well plates used in this study are coated with an unknown formulation in order to obtain an optimal culture substrate on the part of the manufacturer.

Figure 5 demonstrates representative microscopic images of cells growing directly on 3D-printed

material in the cell cultivation chamber and control cells plated in regular well plates after a cultivation period of 30 h. Microscopic analyses of cell growth, cell morphology, and layer formation showed no differences for AD-MSCs growing on 3D-printed material when compared with control cultures in regular well plates. In addition, contact angle measurements were performed on the different sides of the material surfaces formed by the 3D printing process. The contact angle quantifies the wettability of a surface and can be used as an indicator for cell adhesion [31]. All surfaces analysed, including the control surface of regular cell culture well plates, exhibited comparable water contact angles around 80° (78.41°–83.73°). The comparable contact angles thus indicate similar cell adhesion tendency to the 3D printing material as well as the regular cell culture plates. However, other material properties such as surface charge and energy can also potentially affect cellular adhesion and proliferation.

In addition, the cell growth and viability of AD-MSCs cultured in 3D-printed cultivation chamber was determined by cell counting using Trypan blue staining and CTB assays (see sections 2.7 and 2.5). Results of both analyses are presented in figure 6. Both analyses showed no significant differences—regardless of whether AD-MSCs grew on the 3D-printed material or on the material surface of regular well plates. Up to a cultivation period of 44 h, the number of living cells increased in the average by a factor of 4.5 for control cultivations, and 4.1 for cells growing on 3D-printed material (see figure 6(A)). After 44 h, only minor additional changes in cell growth can be observed (since a cell confluency of 100% has been achieved by that point). Furthermore, viability analyses of cells growing in direct contact to the 3D-printed material showed no significant differences to control cultures—resulting in 95 ± 7.4% after a cultivation period of 24 h and

8

Figure 4. Images of the 3D-printed cell cultivation chamber and CAD drawings of structure details. All dimensions of the CAD drawings are in mm.

Figure 5. Microscopic images of cells growing directly in a 3D-printed cultivation chamber (A), and of cells cultured in regular well plates (B). Images were taken 30 h after AD-MSCs were seeded in 3D-printed cell cultivation chamber or regular 24-well cell culture plates. The total magnification is 4.
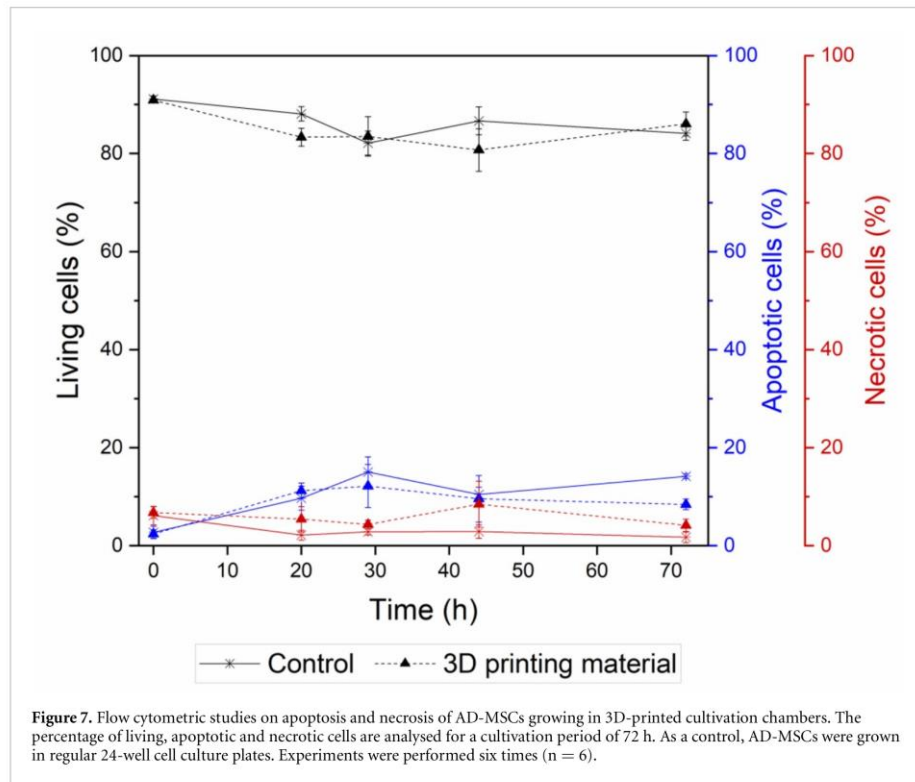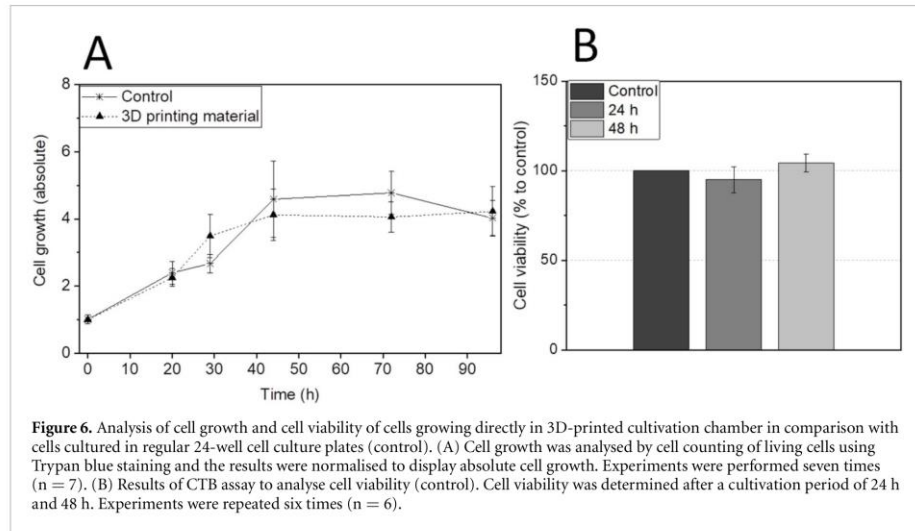
$104.5 \pm 4.95\%$ after 48 h of cultivation on 3D-printed material. In summary, neither cell growth nor cell viability appears to be restricted by this 3D-printed material.

However, CTB assay only allows for conclusions based on the fundamental distinction between living and dead cells—it does not provide any more general information about the different mechanisms by which cell death may occur. Apoptosis and necrosis analyses contain important additional data, which can help a researcher to assess the impact of the 3D-printed material on cell behaviour. As a result, additional apoptosis and necrosis analyses were also conducted via flow cytometry. While apoptosis represents the endogenous mechanism of a regulated or 'programmed' cell death, the necrosis pathway is often described as an unregulated form of cell death occurring in response to external stresses

such as physical injuries, chemical substances, or pathogens [32, 33]. Both pathways present divergent morphological and biochemical characteristics, from which specific fluorescent detection markers for flow cytometry analyses can allow conclusions to be drawn.

3.4. Characterization of cell state using flow cytometry

Physical cell characteristics such as size and information about the internal complexity (i.e. granularity), as well as fluorescent signals, can easily be analysed via flow cytometry. By using specific fluorescent markers to detect and differentiate between apoptotic and necrotic cell features, cell death response can be monitored and quantitatively investigated (see section 2.9). Cells undergoing apoptosis can be identified by using a fluorescence annexin V dye, which

9

Figure 6. Analysis of cell growth and cell viability of cells growing directly in 3D-printed cultivation chamber in comparison with cells cultured in regular 24-well cell culture plates (control). (A) Cell growth was analysed by cell counting of living cells using Trypan blue staining and the results were normalised to display absolute cell growth. Experiments were performed seven times (n = 7). (B) Results of CTB assay to analyse cell viability (control). Cell viability was determined after a cultivation period of 24 h and 48 h. Experiments were repeated six times (n = 6).

Figure 7. Flow cytometric studies on apoptosis and necrosis of AD-MSCs growing in 3D-printed cultivation chambers. The percentage of living, apoptotic and necrotic cells are analysed for a cultivation period of 72 h. As a control, AD-MSCs were grown in regular 24-well cell culture plates. Experiments were performed six times (n = 6).

is detecting the translocation of phosphatidylserine to the cell surface—a typical attribute of apoptosis [33]. Since necrotic cells possess a compromised cell membrane, specific fluorescence dyes (here propidiumiodide) can enter the cell and intercalate in DNA structures [33]. As a result, cells with disrupted cell membranes can be visually detected and quantified using this method. The relative percentages of living, apoptotic, and necrotic cells—cultured directly in 3D-printed cultivation chambers and in regular well plates as a control—is presented in figure 7.

10

Across both cultivation systems (i.e. AD-MSCs growing in direct contact to 3D-printed material, and AD-MSCs cultivated on regular well plate surfaces), no obvious difference with respect to the relative percentages of living, apoptotic, and necrotic cells was detected. The relative percentages of living cells decreased for both cultivation systems from about 91% at the beginning of the experiment to percentages ranging between 81% and 86% during the further cultivation process. The relative percentage of apoptotic cells increased from 2.5% at the beginning of the cell cultivations to about 15% after 29 h of cultivation. In the further cultivation process, a decline of 4% in respect to the relative percentage of apoptotic cells cultured 3D-printed cultivation chambers was observed—while control cultures again showed a slight increase of the percentage of apoptotic cells after 72 h. The simultaneous decrease in the count of living cells and increase in the percentage of apoptotic cells at the beginning of the experiment may be related to the adaption of the AD-MSCs to their new environment and cell culture medium. Changes of cell culture medium and environment can be associated with cellular stress, which causes a decrease in cell viability [34, 35]. Except for a point of time of 44 h after AD-MSCs were seeded in the respective cultivation wells, both cultivation systems showed similar courses of the relative percentages of necrotic cells. After a cultivation time of 44 h, AD-MSCs growing in 3D-printed cultivation chambers showed a slightly increased count of necrotic cells but no significant differences to the control cultivation.

In keeping with previous investigations, no significant differences in regard to apoptotic and necrotic cell death responses were observed between cells cultured directly in 3D-printed cell cultivation systems and in regular well cell culture plates. The 3D printing material used here has no negative effect on the AD-MSCs. It is important to mention that the used material has not yet been certified as biocompatible and there have been no publications demonstrating the use of this material for biological applications. Therefore, our results show for the first time that the 3D printing material used here has a high potential for the production and application of customized cell culture vessels and devices.

4. Conclusions

This study not only presents a thorough examination of a not yet certified 3D printing material with regard to surface quality and biocompatibility, but also it shows a comprehensive characterization of a customized 3D-printed cell culture system for potential use in biological applications. Considered collectively, the experiments discussed above demonstrated that this 3D-printed material *is* suitable for applications requiring either direct or indirect cell contact—which

opens the door for its use in countless applications in the fields of biotechnology and biomedicine. Because no significant differences in cell behaviour and response, morphology, or proliferation could be identified between this material and control cultivations, this material can also be characterized as (*in vitro*) biocompatible. Moreover, the translucent clear appearance of the 3D-printed material enables optical experiments—such as microscopic monitoring of cell cultures, or tracing of liquids within microfluidic applications.

The relevance of the 3D printing material analysed here is indisputable: taking into account both the benefits of 3D printing technology and the outstanding properties of this material, we believe that this study should open the door to a wide range of biological applications going forward—in particular in the field of personalized cell culture technology and 3D cell culture.

Ethics approval and consent to participate

The use of donated tissues and cells is approved by the local ethics committee of Hannover Medical School (reference number 3475-2017). Patients gave their written consent for tissue donations. Consents were archived within the patients' charts. All donations were performed anonymously and were not traceable by the scientists. The set of information for the scientists contained only age and gender. Patients with severe co-morbidities were not included in the study at hand.

11

Conflicts of interest

The authors declare no conflict of interest.

ORCID iD

Ina Gerhild Siller ● https://orcid.org/0000-0002-5755-7550

References

[1] Hull C W 2015 *Res.-Technol. Manag.* **58** 25–30
[2] Jones D B, Sung R, Weinberg C, Korelitz T and Andrews R 2015 *Surg. Innov.* **23** 189–95
[3] Ventola C L 2014 *Pharm. Ther.* **39** 704–11
[4] Coakley M and Hurt D E 2016 *J. Lab. Autom.* **21** 489–95
[5] Raddatz L, Vries I D, Austerjost J, Lavrentieva A, Geier D, Becker T, Beutel S and Scheper T 2017 *Eng. Life Sci.* **17** 931–9
[6] Enders A, Siller I G, Urmann K, Hoffmann M R and Bahnemann J 2019 *Small* **15** 1804326
[7] Brimmo A, Goyette P-A, Alnemari R, Gervais T and Qasaimeh M A 2018 *Sci. Rep.* **8** 10995
[8] Macdonald N P, Cabot J M, Smejkal P, Guijt R M, Paull B and Breadmore M C 2017 *Anal. Chem.* **89** 3858–66
[9] Papenburg B J, Rodrigues E D, Wessling M and Stamatialis D 2010 *Soft. Matter.* **6** 4377–88
[10] Yang S Y, Kim E-S, Jeon G, Choi K Y and Kim J K 2013 *Mater. Sci. Eng. C: Mater. Biol. Appl.* **33** 1689–95
[11] Lourenco B N, Marchioli G, Song W, Reis R L, van Blitterswijk C A, Karperien M, van Apeldoorn A and Mano J F 2012 *Biointerphases* **7** 46
[12] Bernard M, Jubeli E, Pungente M D and Yagoubi N 2018 *Biomater. Sci.* **6** 2025–53
[13] Lu Z, Jiang X, Zuo X and Feng L 2016 *RSC Adv.* **6** 102381–8
[14] 3D Systems I 2016 *Safety Data Sheet: VisiJet EX 200, VisiJet M3 Crystal: According to Regulation (EC) No 1907/2006 and 1272/2008, Hazard Communication Standard 29 CFR 1910 (USA), WHS Regulations Australia, JIS Z 7253 (2012) Japan (3D Systems I)*
[15] 3D Systems I 2018 *Safety Data Sheet: VisiJet M2R-CL: According to Regulation (EC) No 1907/2006 and 1272/2008, Hazard Communication Standard 29 CFR 1910 (USA), WHS Regulations Australia, JIS Z 7253 (2012) Japan (3D Systems I)*
[16] Pepelanova I, Kruppa K, Scheper T and Lavrentieva A 2018 *Bioengineering* **5** 55
[17] O'Brien J, Wilson I, Orton T and Pognan F 2000 *Eur. J. Biochem.* **267** 5421–6
[18] Niles A L, Moravec R A and Riss T L 2009 *Curr. Chem. Genomics* **3** 33–41
[19] Thevenot P, Hu W and Tang L 2008 *Curr. Top. Med. Chem.* **8** 270–80
[20] Wang Y-X, Robertson J L, Spillman W B J R and Claus R O 2004 *Pharm. Res.* **21** 1362–73
[21] Kocijan A, Conradi M and Hočevar M 2019 *Materials* **12** 1877
[22] Lampin M, Warocquier-Clérout R, Legris C, Degrange M and Sigot-Luizard M F 1997 *J. Biomed. Mater. Res.* **36** 99–108
[23] Angelova N and Hunkeler D 1999 *Trends Biotechnol.* **17** 409–21
[24] Pattanaik B, Pawar S and Pattanaik S 2012 *Indian J. Dent. Res.* **23** 398–406
[25] van Midwoud P M, Janse A, Merema M T, Groothuis G M M and Verporte E 2012 *Anal. Chem.* **84** 3938–44
[26] Siller I G, Enders A, Steinwedel T, Epping N-M, Kirsch M, Lavrentieva A, Scheper T and Bahnemann J 2019 *Materials* **12** 2125
[27] Kopperud H M, Kleven I S and Wellendorf H 2011 *Eur. J. Orthod.* **33** 26–31
[28] Rashid H, Sheikh Z and Vohra F 2015 *Eur. J. Dent.* **9** 614–9
[29] Eisenbrand G *et al* 2002 *Food Chem. Toxicol.* **40** 193–236
[30] Walczak R 2018 *Bull. Pol. Acad. Sci., Tech. Sci.* **66** 179–86
[31] Dowling D P, Miller I S, Ardhaoui M and Gallagher W M 2011 *J. Biomater. Appl.* **26** 327–47
[32] Tang D, Kang R, Berghe T V, Vandenabeele P and Kroemer G 2019 *Cell Res.* **29** 347–64
[33] Wlodkowic D, Telford W, Skommer J and Darzynkiewicz Z 2011 *Methods Cell Biol.* **103** 55–98
[34] Garcia-Montero A, Vasseur S, Mallo G V, Soubeyran P, Dagorn J C and Iovanna J L 2001 *Eur. J. Cell Biol.* **80** 720–5
[35] Young J W, Locke J C W and Elowitz M B 2013 *Proc. Natl. Acad. Sci. USA* **110** 4140–5

Supplementary Information for

Characterization of a customized 3D-printed cell culture system using clear, translucent acrylate that enables optical online monitoring

Authors:

Ina Gerhild Siller [1], Anton Enders [1], Pia Gellermann [1], Steffen Winkler [1], Antonina Lavrentieva [1], Thomas Scheper [1] and Janina Bahnemann [1, *]

[1] Institute of Technical Chemistry, Leibniz University Hannover, Callinstraße 5, 30167 Hannover, Germany

* Correspondence: jbahnemann@iftc.uni-hannover.de; Tel.: +49-511-762-2568

Influence of organic solvents on surface properties of the 3D printing material

The 3D printing material analyzed in this study lacks a high heat distortion temperature, which prohibits for use of thermal sterilization techniques (*e.g.* autoclaving). Since sterile systems are mandatory for all biological application, a suitable sterilization or disinfection procedure had to be found for systems printed with the 3D printing material. Therefore, the chemical disinfectants ethanol (70 %, v/v) and isopropyl alcohol (70 %, v/v) were analyzed with regard to their influence on surface properties of the 3D printing material.
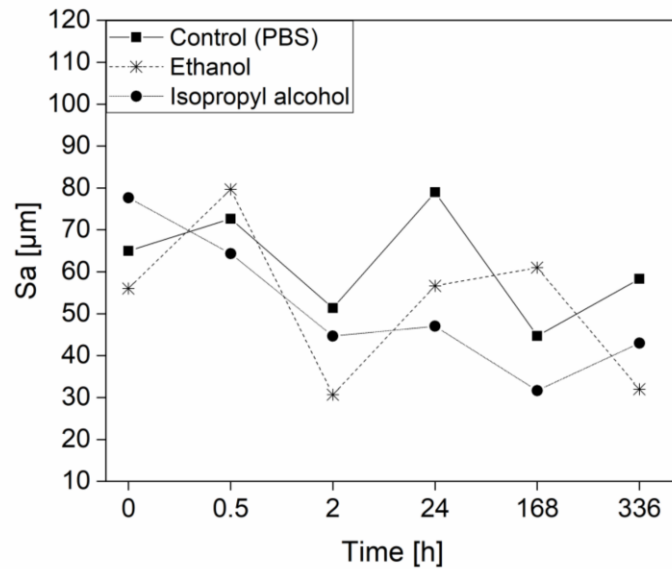
Figure S1. Analysis of the materials upper sides surface by determining the area roughness parameter Sa. Sa is defined as the arithmetical mean deviation of the assessed area of a materials surface. The assessed area was 9.81 mm^2. The 3D printed material was incubated in PBS, ethanol (70 %, v/v) and isopropyl alcohol (70 %, v/v) for a total of 14 days (336 h).

The results of determining the surface roughness of the upper material side formed in the 3D printing process are shown in Figure S1. In addition to an incubation with the chemical solvents ethanol and isopropyl alcohol, the 3D-printed material was incubated in phosphate buffered saline (PBS) as a control. In comparison with the control, no noteworthy influences of ethanol and isopropyl alcohol on the surface roughness can be identified over an incubation period of 14 days.
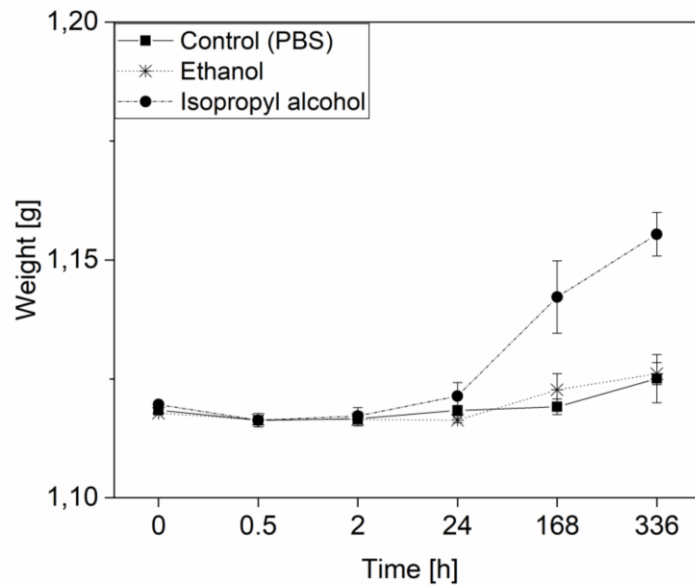
Figure S2. Analysis of weight differences before and after incubation of 3D printed material in PBS, ethanol (70 %, v/v) and isopropyl alcohol (70 %, v/v) for a total of 14 days (168 h).

In order to determine the water uptake and associated swelling of the 3D printing material, weight experiments were conducted (Figure S2). In addition to an incubation in PBS as a control, 3D-printed cubes were incubated in ethanol and isopropyl alcohol. Up to an incubation period of 24 h, no significant differences between the different fluids can be seen. After 168 h, an incubation of 3D-printed material parts in isopropyl alcohol resulted in an increased weight of the corresponding material parts. This is an evidence for water uptake or swelling and deformations of the 3D printing material cannot be excluded. However, incubation in ethanol or PBS did not lead to any conspicuous weight differences over an incubation period of up to 14 days. Taken together, both – analysis of the surface roughness as well as weight experiments – show, that ethanol can be used without any concerns as a disinfectant for the 3D printing material.

Analysis of surface roughness on the surface selected for interaction with cells

As mentioned in this study, the 3D printing process creates four different surface structures each holding different topography details. Furthermore, each surface side can be analyzed in two directions: in the direction parallel to the print direction and at a 90° angle to the print direction.
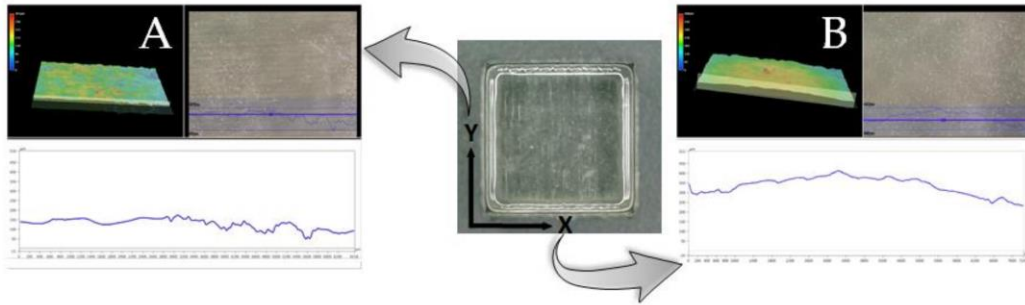
Figure S3. Analysis of surface topography on the 3D printing material surface selected for interaction with cells. (A) shows the roughness profile in the direction parallel to the print direction. (B) indicate the roughness profile at a 90° angle to the print direction.

For the cultivation of adherent cells, the flattest surface structure was chosen – the surface structure representing the upper side of a model, which is smoothed by the roller in the printing process. Both surface roughness profiles of this structure side are shown in figure S3 and possess comparable topographies. Neither the roughness profile in the direction parallel to the print direction nor the profile at a 90° angle to the print direction present irregularities in height of more than 100 µm. Correspondingly, the printing process did not cause any distinct irregularities in height.

4.3 Individuell anpassbare 3D-gedruckte Ko-Kultivierungssysteme für die Analyse von Angiogenese *in vitro*
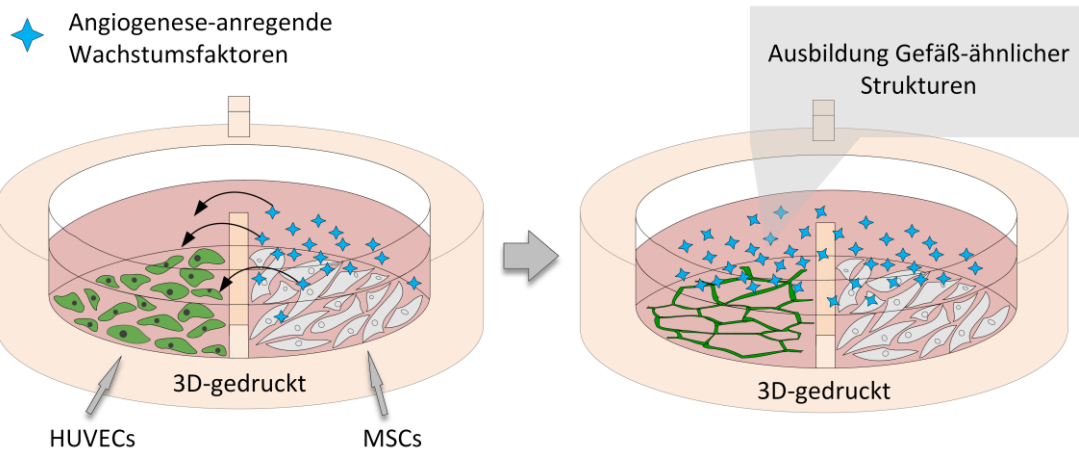
Abbildung 4-3 *Graphical abstract* von „*Customizable 3D-printed (co-)cultivation systems for in vitro study of angiogenesis*".

Die Bearbeitung naturwissenschaftlicher Fragestellungen erfordert häufig die Entwicklung geeigneter, individueller Methoden und Verfahren. Für diese Entwicklungen sind Wissenschaftler jedoch oft auf kommerziell erhältliche Versuchsgeräte und zugehöriges Equipment angewiesen, welche nicht zwangsläufig den tatsächlich gewünschten Anforderungen entsprechen. Die Einführung hochauflösender additiver Fertigungstechnologien kann diese Einschränkungen in einigen Wissenschaftsbereichen überwinden, indem sie die individuelle, passgenaue und schnelle Erstellung verschiedenster Objekte ermöglicht. So erlaubt die 3D-Drucktechnologie die Fertigung von komplexen, experiment-spezifischen und individuell-anpassbaren Versuchssystemen und zugehörigem Equipment.

Im folgenden Kapitel werden die Möglichkeiten der additiven Fertigung in einem Anwendungsbeispiel zur Analyse der Angiogenese verdeutlicht. Ein 3D-gedrucktes Ko-Kultivierungssystem wird vorgestellt, das die Ausbildung gefäßähnlicher Strukturen von Endothelzellen und deren Beobachtung ermöglicht. Zudem werden weitere additiv gefertigte Plattformen vorgestellt, die *In-vitro*-Studien (der Angiogenese) unterstützen.

Der Prozess der Angiogenese ist an der Ausbildung und Steuerung des menschlichen Gefäßsystems beteiligt und beschreibt sowohl das Wachstum und die Bildung neuer Blutgefäße aus bereits vorhandenen Gefäßstrukturen als auch die Reorganisation und Umgestaltung des vaskulären Netzwerks [135,136]. Sie wirkt daher maßgeblich an Regenerationsprozessen mit und nimmt somit eine wichtige Rolle im Bereich des *Tissue Engineerings* ein – ein Grund, weswegen das Interesse an neuartigen Analyseverfahren und Methodiken immens ist [137].

Das entwickelte Ko-Kultivierungssystem wurde mit dem im vorherigen Kapitel 4.2 charakterisierten 3D-Druckmaterial (AR-M2, Keyence GmbH) gedruckt. Um eine sterile und einfache Handhabung zu gewährleisten, wurden die Dimensionen des Ko-Kultivierungssystems an eine Vertiefung einer *6-Well Plate* angepasst, sodass es darin platziert werden kann. Eine mittige Barriere teilt die Kultivierungsfläche in zwei Bereiche. Jeder Bereich präsentiert die Kultivierungsfläche für einen Zelltyp, sodass zwei Zelltypen gleichzeitig im System ko-kultiviert werden können. Die Barriere trennt die beiden Zelltypen physisch voneinander, erlaubt aber ab einem bestimmten Volumen die gleichzeitige Kultivierung in einem gemeinsamen Zellkulturmedium (indirekte Ko-Kultivierung).

In einer indirekten Ko-Kultivierung von AD-MSCs und Endothelzellen aus humanen Nabelschnurvenen (HUVECs) in dem 3D-gedruckten System konnte gezeigt werden, dass die Endothelzellen mit der Zeit gefäßähnliche Strukturen ausbilden. Dies kann auf das angiogene Potential von AD-MSCs zurückgeführt werden [138,137]. Während der Ko-Kultivierung geben die AD-MSCs Angiogenese-anregende Wachstumsfaktoren und Hormone ab, die über das Zellkulturmedium zu den HUVECs gelangen und dort die Gefäßbildung anregen. Besonders hervorzuheben ist, dass dies ohne zusätzliche Verwendung von unterstützenden Matrixsubstraten erreicht wurde. Da das 3D-Druckmaterial nur eine geringe Eigenfluoreszenz besitzt, konnte die Bildung gefäßähnlicher Strukturen von HUVECS, die das grün fluoreszierende Protein (GFP) exprimieren, nicht nur durch Phasenkontrast- sondern auch mittels Fluoreszenzmikroskopie beobachtet werden.

Die Studie zeigt das enorme Potential von individuell-anpassbaren 3D-gedruckten Plattformen auf und signalisiert, dass die additive Fertigung das Spektrum der den Forschern zur Verfügung stehenden Versuchssystemen und Laborequipment erweitern kann.

Im folgenden Artikel „*Customizable 3D-printed (co-)cultivation systems for in vitro study of angiogenesis*" werden die Ergebnisse detailliert ausgeführt und diskutiert.

materials

MDPI

Article

Customizable 3D-printed (co-)cultivation systems for in vitro study of angiogenesis

Ina G. Siller [1], Niklas-Maximilian Epping [1], Antonina Lavrentieva [1], Thomas Scheper [1] and Janina Bahnemann [1],*

[1] Institute of Technical Chemistry, Leibniz University Hannover, Callinstraße 5, 30167 Hannover, Germany
* Janina Bahnemann: jbahnemann@iftc.uni-hannover.de

Abstract: Due to the ever-increasing resolution of 3D printing technology, additive manufacturing is now even used to produce complex devices for laboratory applications. Personalized experimental devices or entire cultivation systems of almost unlimited complexity can potentially be manufactured within hours from start to finish—an enormous potential for experimental parallelization in a highly controllable environment. This study presents customized 3D-printed co-cultivation systems, which qualify for angiogenesis studies. In these systems, endothelial and mesenchymal stem cells (AD-MSC) were indirectly co-cultivated—that is, both cell types were physically separated through a rigid, 3D-printed barrier in the middle, while still sharing the same cell culture medium that allows for the exchange of signalling molecules. Biochemical-based cytotoxicity assays initially confirmed that the 3D printing material does not exert any negative effects on cells. Since the material also enables phase contrast and fluorescence microscopy, the behaviour of cells could be observed over the entire cultivation via both. Microscopic observations and subsequent quantitative analysis revealed that endothelial cells form tubular-like structures as angiogenic feature when indirectly co-cultured alongside AD-MSCs in the 3D-printed co-cultivation system. In addition, further 3D-printed devices are also introduced that address different issues and aspire to help in varying experimental setups. Our results mark an important step forward for the integration of customized 3D-printed systems as self-contained test systems or equipment in biomedical applications.

Keywords: additive manufacturing; co-cultivation; mammalian cell culture; angiogenesis; biomaterials; biomedical application

---

1. Introduction

One of the major goals in the field of tissue engineering is the generation of artificial tissue grafts for replacement and/or reconstitution of damaged tissues and organs [1]. Maintaining adequate oxygen and nutrient supply within the tissue graft poses a particular challenge—and the use of diffusion as the main underlying transport principle of soluble nutrients is often insufficient in this context (especially in larger and dense tissues) [2]. To overcome this diffusion limit and to facilitate a fine distribution, a well-organized vascular vessel network must be generated [3]. The development of the human vascular system is mainly controlled by two different mechanisms: vasculogenesis and angiogenesis. Vasculogenesis describes the formation of new vessels from endothelial progenitor cells. In contrast, the reorganization and remodelling of an existing vascular network is mostly driven by angiogenic processes [3]. Angiogenesis is defined as the formation and growth of new blood vessels from existing vessels, as well as the restructuring of the vascular network [3]. As such, angiogenesis plays a fundamental role in numerous regeneration processes within the human body—and, consequently, a key act in tissue engineering [4]. The process of angiogenesis is determined by several cell types and the surrounding matrix (in particular, the basement membrane). Endothelial

cells are the primary cell type involved [5]. After endothelial cells received signalling and activation, key steps in the subsequent generation of new vessel structures include the degradation of basement membrane, as well as the proliferation and cell migration of endothelial cells before they form and stabilize tubular structures and loops [5,6]. The alignment and arrangement of endothelial cells in tubes is referred to as tubular-like structures in this study.

There are numerous methods for assessing angiogenesis – all of which vary drastically in the particular part of the angiogenic cascade to which they refer, and in their clinical relevance [7]. Whereas *in vivo* approaches possess high potential to capture the complex processes of the human body, *in vitro* assays tend to be less laborious, achieving faster results and providing great quantification possibilities [6,7]. However, although *in vivo* assays are more time-consuming, expensive and limited in quantification, their high clinical relevance makes them indispensable in many respects [7]. But before taking the steps towards conducting *in vivo* tests, *in vitro* assays can be beneficial in providing valuable initial information about test conditions. Since *in vitro* angiogenesis assays often focus on only one particular step in the angiogenic cascade, they exhibit high potential to consider the specific effects, interactions and role of tested drugs in the process of angiogenesis [6,8].

Traditionally, *in vitro* cell culture assays have been performed using only one single cell type— although the cells' natural environment *in vivo* often comprises of various cell types [9]. Even if cells of different cell types are not in direct contact *in vivo*, they may at least be able to communicate with other cell types [9]. A common attempt to imitate an *in vivo* environment is represented in the simultaneous cultivation of several cell types within *in vitro* co-cultures. In principle, co-culture systems allow the cultivation of two or more cell types with a certain degree of contact/communication facilitated between them [10]. Especially for studying angiogenesis, co-culture approaches frequently prove beneficial, since angiogenic processes are stimulated by intercellular factors [3,11]. A well-known known and clinically relevant co-culture model for analysis of angiogenesis involves the co-cultivation of mesenchymal stem cells and endothelial cells [12,13]. Mesenchymal stem cells possess an angiogenic potential supporting the formation of tubular-like structures and characteristics in endothelial cells by releasing angiogenic factors [12–14]. Therefore, these cell types were selected as co-culture models in this study. In general, co-culture models cover direct cultivations of different cell types, which enables both direct cell-cell contact and interaction as well as indirect co-cultivation approaches, where different cell types are physically separated but sharing one cell culture medium that permits an intercellular communication and exchange of molecules [10,15,16]. Different co-culture models are commercially available—including co-culture inserts for well plates which facilitate the cultivation of two cell types that are physically separated from each other in one cell culture medium (for example, those distributed by ibidi GmbH, Germany or Thermo Fisher Scientific, USA) [17]. Petri dishes are also commercially available that have a surface separated in two, three, or even four compartments by a small barrier—a design which allows for a shared use of cell culture medium (for example, those distributed by Thermo Fisher Scientific Inc., USA). Numerous experimental co-culture setups have been developed and found their application in virtually all biological disciplines [10].

For studying vascularization and angiogenesis, *in vitro* approaches include indirect co-cultivation in commercial transwell inserts via use of membranes or in micropatterned systems [18–21]. Especially useful for analysing endothelial tube formation, one basic method involves seeding cells onto a layer of gel matrix, which provides those cells with nutrients and stimulates angiogenesis by releasing angiogenic factors [11,22]. Common matrix substances in such systems are collagen, fibrin, and Matrigel®, whereas Matrigel® comprises of a solubilized basement membrane (from Engelbreth-Holm-Swarm mouse sarcoma) and evolved to be a standard substrate material in all kind of angiogenic tube formation assays in co- or mono-cultures [11,23]. Carter *et al.* have taken another approach and developed a porous and permeable membrane, which is similar in thickness to the vascular basement membrane and functions as a barrier or growth surface in co-cultivations [24]. Intensive research on cell-cell interactions, communication, and behaviour has also been conducted in direct co-cultivation studies *in vitro*—for example, through the use of endothelial and stromal

cells [22,25,26]. More recent studies in the field of regenerative medicine have aimed to mimic the *in vivo* environment by (co-)culturing cells in 3D hydrogel or matrix structures, as well as on scaffold materials and beads [22,27–30]. These methods show a great potential for imitating the *in vivo* situation, but are often regrettably limited in their capacity to ensure efficient oxygen and nutrient supply within the hydrogel or scaffold. In addition, analysis of cell behaviour and interaction in three dimensions still poses a considerable challenge [22]. Several approaches have been undertaken in microfluidics in recent years in an attempt to address this problem [11,18,31].

Importantly, however, all of these studies require appropriate experimental equipment, test beds, or – in the case of microfluidics and scaffolds – suitable microfluidic chambers and scaffolding elements. Indeed, the vast majority of reported microfluidic chambers have been fabricated by laborious, traditional manufacturing processes that require special training and are particularly time-consuming. And unless they wish to fabricate their own chambers, researchers currently have no choice but to revert to commercially available test equipment. Nowadays, additive manufacturing technology does enable the rapid production of customized labware and high definition experiment-specific equipment—but limitations remain. Even though many 3D printing materials are commercially available, not all of them are suitable for biomedical applications, due to the lack of biocompatibility or sufficient surface properties, for example [32,33].

Against this backdrop, this study introduces a customized 3D-printed co-cultivation system for use with indirect co-culture assays. Together with further developed 3D-printed (co-)cultivation platforms, this study illustrates the high potential of the 3D printing material in question – not only for the *in vitro* study of angiogenesis, but also for potential integration in biomedical applications more generally. To analyse the applicability of the customized co-cultivation system in angiogenesis studies, mesenchymal stem cells and endothelial cells were indirectly co-cultivated in the system. The release of angiogenic factors into the cell culture medium is expected to result in the formation of tubular-like structures by the endothelial cells. Endothelial tube formation was monitored via microscopic observation which was facilitated by the transparent appearance of the 3D printing material. Recently published work already indicated the great potential of the material in question with respect to proliferation and biocompatibility studies with mesenchymal stem cells [34]. Here, we further illustrate other excellent application possibilities for this versatile and highly promising material.

2. Materials and Methods

2.1. Design, 3D Printing and Post-Processing

As a first step in the manufacturing process, a 3D computer-aided design model was constructed. 3D computer-aided design (CAD) software SolidWorks 2018 (Dassault Systems, Waltham, MA, USA) was used for the design of all 3D-printed devices. The constructed CAD model was then directly sent to the 3D printer, where it is fabricated. A rigid, translucent, clear polyacrylate resin named AR-M2 (Keyence Deutschland GmbH, Neu-Isenburg, Germany) was selected as the 3D printing material, and processed using high-resolution 3D printer AGILISTA-3200 W (Keyence Deutschland GmbH, Neu-Isenburg, Germany). This printer manufactures objects via inkjet technology using an ultraviolet (UV) curing process, which results in a layer thickness of 15 μm and a resolution of 635 x 400 dots per inch.

Since surrounding supporting material must ultimately be removed from 3D-printed parts, a final "post-processing" phase is required after the printing phase is completed. Because the support material used (AR-S1; Keyence Deutschland GmbH, Neu-Isenburg, Germany) is soluble in water, the printed parts were placed for at least 1 h in a pre-warmed (60°C) ultrasonic water bath (Bandelin electronic, Berlin, Germany) filled with deionized water and detergent (Fairy Ultra Plus, Procter and Gamble, Petit-Lancy, Switzerland), which was sufficient to remove all support material. After washing the parts thoroughly with deionized water, they were then "post-cured" with UV light (UV

Sterilization Cabinet KT-09DC, Alexnld, Tiberias, Israel) for 1 h, in order to ensure full photo polymerization of the materials acylate monomers.

Immediately prior to its deployment in the biological environment, all 3D-printed parts were chemically disinfected via incubation in ethanol (70 %, v/v) (Carl Roth GmbH und Co. KG, Karlsruhe, Germany) for 1 h; then placed on a sterile surface for 1 h to allow the ethanol to evaporate; and, finally, washed thoroughly with sterile phosphate-buffered saline (PBS) (Carl Roth GmbH und Co. KG, Karlsruhe, Germany).

As highlighted in previous published work, the 3D printing material in question has a translucent clear appearance which facilitates optical microscopic observations. Known material components in the liquid state of the polyacrylate are two acrylate monomers, a photoinitiator, a stabilizer, and a urethane-acrylate-oligomer [34].

2.2. Cell Lines and Cell Culture Conditions

Two different cell lines were used in this study: GFP Human Umbilical Vein Endothelial Cells (HUVECs), and human adipose tissue-derived mesenchymal stem/stromal cells (AD-MSCs). HUVECs were purchased from Cellworks (Caltag Medsystems Limited, Buckingham, UK) and cryopreserved until usage. These cells are an angiogenesis co-culture that has been validated by the manufacturer. They were cultivated in basal Endothelial Cell Growth Medium 2 (EGM-2), with added supplement mix as instructed by the manufacturer (Promocell, Heidelberg, Germany), 8 % fetale kalv serum (FKS) (Sigma Aldrich Chemie GmbH, Munich, Germany) and 0.5 % gentamycin (PAA Laboratories GmbH, Pasching, Austria), at 37°C in a 5 % CO_2 and 21 % O_2 humidified atmosphere. The AD-MSCs were isolated from adipose tissue following abdominoplasty surgery, extensively characterized as AD-MSCs, and cryopreserved in passage two until usage [35]. The donor provided informed written consent as approved by the Institutional Review Board (Hannover Medical School), with the reference number 3475-2017. For cultivation of AD-MSCs, a cell culture medium containing Minimum Essential Medium Eagle with alpha modification (α-MEM) (Thermo Fisher Scientific Inc., Waltham, USA), 10 % human serum (c.c.pro GmbH, Oberdorla, Germany) and 0.5 % gentamycin (PAA Laboratories GmbH, Pasching, Austria) was prepared, and the cells were cultivated at 37°C in a 5 % CO_2 and 21 % O_2 humidified atmosphere. Both cell lines were sub-cultivated with a confluence of 80 % - 90 % via accutase treatment (Merck KGaA, Darmstadt, Germany). All experiments were performed with cells of passages lower than nine.

2.3. CellTiter Blue (CTB) Viability Assay

The CellTiter Blue® (CTB) cell viability assay was performed according to the manufacturer's protocol (Promega GmbH, Mannheim, Germany). In brief, cell culture medium was removed from each sample under examination, and 200 μl of fresh cell culture medium containing 10 % CTB stock solution was then added, respectively. Samples were subsequently incubated at 37°C in a 5 % CO_2 and 21 % O_2 humidified atmosphere for 1.5 h, and fluorescence signal was thereafter measured using a fluorescence plate reader (Fluoroskan Ascent, Therma Fisher Scientific Inc., Waltham, USA). Viable, metabolically active cells are able to convert resazurin—which is contained in the reagent solution—into the fluorescent product resorufin. This conversion to resorufin can be monitored at an extinction wavelength of 544 nm and an emission wavelength of 590 nm.

2.4. Lactate Dehydrogenase (LDH) based Viability Assay

Using the Cytotoxicity Detection Kit (Roche, Basel, Switzerland), the release of lactate dehydrogenase (LDH) into the culture supernatant was measured. Lactate dehydrogenase is a cytosolic enzyme which is released upon cell lysis or damage of the cell membrane. That way, the assay can be used to determine cell viability. The amount of LDH in the culture supernatant is measured by a coupled enzymatic reaction that causes tetrazolium salt to convert into a red formazan. The red formazan product holds an absorption maximum at 500 nm, which can be monitored. The assay kit was performed as specified by the manufacturer's protocol, and a spectrophotometric

microplate reader (BioTek Instruments, Inc., Winooski, VT, USA) was used to measure formazan formation.

2.5. Cell proliferation studies

Cell proliferation was monitored by performing the Trypan blue exclusion method. The Trypan blue stain is able to enter cells with compromised membrane integrity (i.e., damaged or lysed cells) and marks them with a blue colour. This allows for the differentiation between living and damaged/dead cells. After staining of the cells with 0.4 % Trypan blue stain, the cell suspension is then pipetted in a haemocytometer (Brand GmbH + Co. KG, Wertheim, Germany), and a count of blue cells is taken.

Viability and proliferation studies of AD-MSCs and HUVECS growing on 3D printing material were performed as described in detail in previous published work [34]. While AD-MSCs were seeded in 3D-printed wells at a density of 15.000 cells·cm^{-2}, HUVECs were seeded at a density of 25.000 cells·cm^{-2} (since these cells are smaller).

2.6. Co-cultivation of AD-MSCs and HUVECs, separated through dividing barrier

For indirect co-cultivation experiments, a cell cultivation system was designed that allows for separate cultivation of two adherent growing cell types within a single shared cell culture medium. The growth surface area is divided into two spaces by a rigid barrier wall. Each side represents the surface area for cell adhesion and growth of one cell type. The 3D-printed barrier provides a sufficient height (2 mm) to prevent cell-cell contact among the different cell types but still simultaneously enable both sides to share the same cell culture medium. This allows endothelial cells (here: HUVECs) to be physically separated from stromal cells (here: AD-MSCs), and to develop tubular-like structures due to stimulating substances released from feeder cells. The separate cultivation of AD-MSCs and HUVECs using a physical barrier within a single shared cell culture medium is referred to as "indirect co-cultivation" in this study. The designed co-cultivation system fits in a well of a commercially available 6-well cell cultivation plate, which provides sterile and user-friendly handling. Cultivation surfaces for adherent cell growth of two cell types are separated through a barrier. The CAD-design, dimensions, and the handling are all illustrated in Figure 1.

Following 3D printing, post-processing, disinfection, and an evaporation procedure, the co-cultivation systems were washed thoroughly with PBS. Both cell types were then seeded separately and independently from each other within a cell-type-specific culture medium. HUVECs were seeded at a density of 30.000 cells per side within the co-cultivation chambers, while AD-MSCs were seeded at a density of 20.000 cells per side. Cells were seeded in a volume of 200 µl cell culture medium. This volume allowed for discrete seeding, without overflowing the barrier. For cell seeding and adhesion, cells were kept in their regular cell-type-specific culture medium. After 24 h, the medium of both cell types was removed, and a co-cultivation medium was added. The co-cultivation medium contains half EGM-2 and half α-MEM, at 3 % human serum and 0.5 % gentamycin. A volume of 550 µl of co-cultivation medium permits an overflow and exchange of the medium across the physical barrier. The cultivations were maintained at 37°C in a 5 % CO_2 and 21 % O_2 humidified atmosphere. Cell growth, behaviour, and angiogenesis were all subsequently monitored using a cell imaging multi-mode reader (Cytation 5; BioTek Instruments, Inc., Winooski, VT, USA).
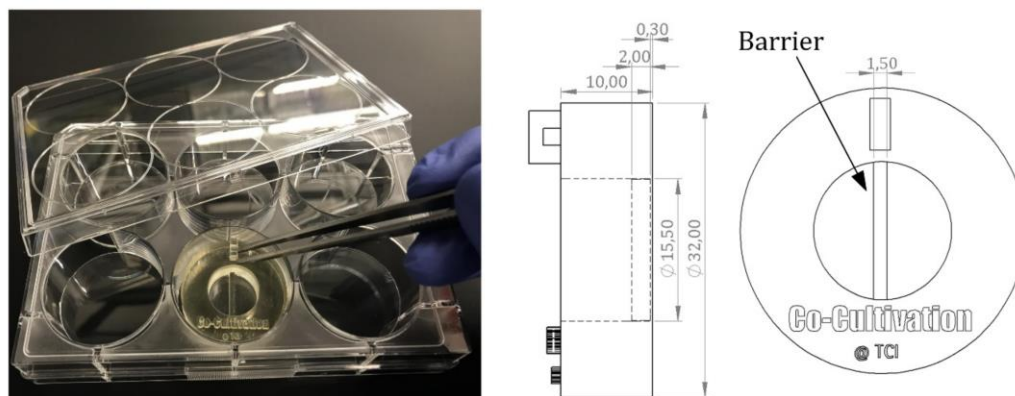
Figure 1. Illustration of a 3D-printed co-cultivation system that is separating two cell types through a dividing barrier. Both cell types can still share one cell culture medium and thereby enable exchange of substances. All dimensions in CAD drawing are in mm.

2.7. Co-cultivation of AD-MSCs and HUVECs without physical separation

For further co-cultivation and screening approaches, co-cultivations of AD-MSCs and HUVECs in which both cell types were not physically separated from each other were also performed. The collective cultivation of AD-MSCs and HUVECs without a physical barrier is referred to as "direct co-cultivation" in this study. Within this experimental setup, AD-MSCs and HUVECs were seeded in different cell mixture ratios in a screening assay. A screening platform was designed and 3D-printed, and then fitting into a regular 60 mm petri dish, in order to facilitate sterile and user-friendly handling. In a first approach, a cell count of 70.000 cells per cultivation well was set, and the correspondence ratios were respectively calculated. Chosen cell mixture ratios were 1:1, 1:2, 1:3, 1:5, 2:1, 3:1, and 5:1 (HUVEC:AD-MSC). The 3D-printed cultivation platform was maintained at 37°C in a 5 % CO_2 and 21 % O_2 humidified atmosphere. Cell growth, behaviour, and angiogenesis were all subsequently monitored using a cell imaging multi-mode reader (Cytation 5; BioTek Instruments, Inc., Winooski, VT, USA).

2.8. Crystal Violet Staining Method

All attached cells were marked using a method of crystal violent staining. Crystal violet is a triarylmethane dye that can bind to DNA and proteins [36]. For staining, the cell culture medium was removed, and the cells themselves were washed with PBS. 200 µl of a prewarmed crystal violet staining solution (Merck KGaA, Darmstadt, Germany), which was added to each well and incubated for 10 min at room temperature. Afterwards, the staining solution was removed, and the chambers thoroughly washed with PBS. Microscopic images were then taken with a 3D digital microscope (VHX; Keyence Deutschland GmbH, Neu-Isenburg, Germany).

2.9. Evaluation of Angiogenesis

To detect and quantitative analyse angiogenic tube formation, the free open source software AngioTool® (National Institute of Health, National Cancer Institute, Bethesda, MD, USA) was utilized [37]. For analysis of experiments, AngioTool® can detect the output of various morphometric parameters related to angiogenesis (such as the vessel area, total number of junctions, or the average vessel length). Vessel profiles and networks were then identified according to the parameters set. In this study, fluorescence images were analysed using the following settings present in AngioTool®: vessel diameter = 12 µm; vessel intensity = 15-255; and fill holes = 240. These parameters were selected because they had previously proven to be suitable.

For better imagination, a figure demonstrating the output of AngioTool® and a detailed description of analysis parameters are given in the supplementary material (see Figure S1, supplementary material).

3. Results and Discussion

3.1. Viability and Growth Analyses of Cells growing on 3D Printing Material

Guaranteed biocompatibility is an essential prerequisite for all materials that are introduced to a biological environment (for example, within biomedical applications). Any potential negative effects on cells—for example, via leaching of substitutes or degradation of products—must be definitively ruled out, since these characteristics can induce irritations and/or allergic reactions [38–40].

Recently published work in studies using AD-MSCs had already demonstrated the general biocompatibility of the 3D printing material in question [34]. As co-cultivations are generally performed with various cell types, further biocompatibility studies of the printing material with HUVECs were also conducted. Therefore, AD-MSCs—just as HUVECs—were cultured in direct contact with the 3D printing material, and cell viability, morphology, and proliferation were all carefully monitored. HUVEC cell viability and proliferation was compared to AD-MSCs viability, as well as to the cell growth on the cell culture-treated surfaces of commercially 24-well plates (as a control). For these experiments, cell cultivation chambers were 3D printed. The cultivation chambers are designed to fit into the well of a regular 6-well cell cultivation plate, which helped to ensure sterile and user-friendly handling. By adapting the growth surface area of the 3D-printed cultivation chamber to the growth surface area of a commercial 24-well cell cultivation well, control cultivations can be performed using commercially available 24-well cell cultivation plates. The growth surface area of both of the cultivation systems that were used was 1.89 cm². Here, cultivations in commercial 24-well cell cultivation plates represent the optimal cell growth with optimal conditions.

In order to ensure that the 3D-printed material in question has no toxic effects on the cells, two biochemical-based *in vitro* viability assays were also performed—each based on a different metabolic activity and function in the cellular metabolism (see Sections 2.3 and 2.4). Figure 2 shows the results of these viability assays, as well as proliferation studies of both cell types that were grown directly on the 3D-printed material. No significant differences in cell viability for either cell types (in comparison to the control cultures) were observed. In fact, over a cultivation period of 72 h, the average cell viability observed within the 3D-printed chambers was slightly higher than that observed within the commercial 24-well plates. Furthermore, an analysis of cell growth showed no significant differences in growth rates for either cell types—regardless of whether cells were cultivated in 3D-printed systems or in commercial cell cultivation well plates.

The transparent clear appearance of the 3D-printed material also allows for optical microscopic monitoring of the cell morphology. Such observation did not reveal any changes in either the cell morphology or behaviour for cells that were cultivated in direct contact with the 3D-printed material. Taken together, neither cell viability and proliferation nor morphology appears to have been influenced by the 3D printing material for either of the cell types that were analysed.
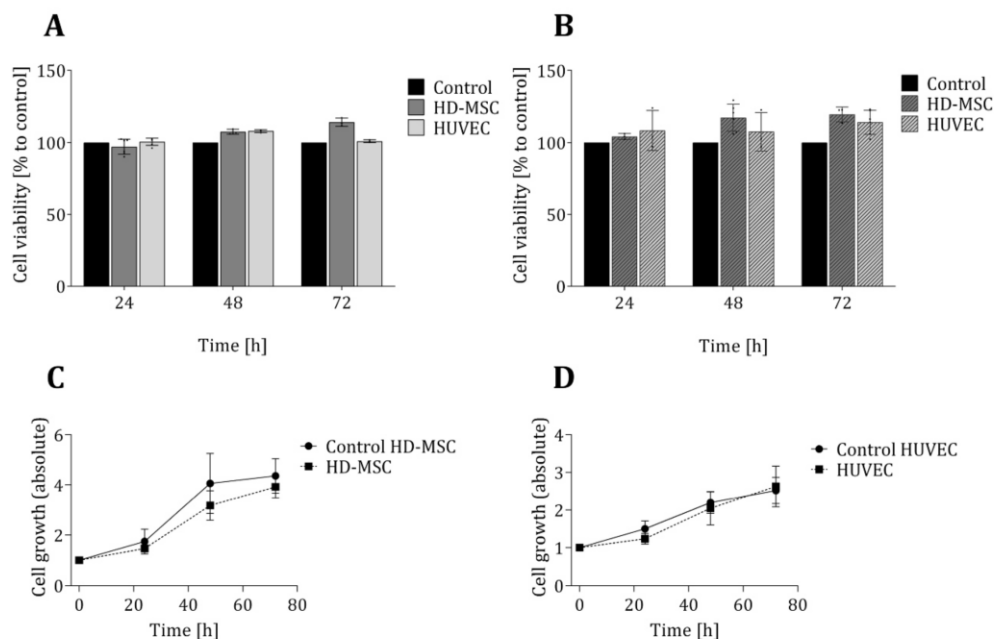
Figure 2. Evaluation of cell viability and proliferation of cells growing in direct contact to the 3D printing material. Cell viability of both cell types (AD-MSCs and HUVECs) was analysed in LDH assays (a) and CTB assays (b) after cultivation of cells for 24 h, 48 h and 72 h in 3D-printed chambers. Control cultures of both cell types were performed in commercially available regular 24-well cell culture plates and are considered to present cell growth under optimal conditions. Cell viability is normalized to the corresponding control, respectively. Cell growth was determined by cell counting of living cells using Trypan blue staining and illustrated for HD-MSCs (c) and HUVECs (d). All experiments were repeated several times (n > 6), and compared to control.

3.2. Co-cultivation of HUVECs and AD-MSCs in 3D-printed Cell Cultivation Systems

A common approach to mimicking an *in vivo* environment for the purposes of studying intercellular interactions is the *in vitro* cultivation of different cell types in co-cultures, which implies a simultaneous cultivation of several cell types. There are many such approaches: For example, direct co-cultivation systems enable both cell-cell contact and interaction between different cell types. By contrast, in indirect co-cultivations, the different cell types are physically separated but still share one culture medium, which allows for the exchange of signalling molecules via the medium.

3D printing represents an ideal, flexible tool to satisfy the widely varying demands of different experimental setups. For an indirect co-cultivation of AD-MSCs and HUVECs, a cultivation system was designed and 3D-printed (see Figure 1). The cavity in the middle was divided into two spaces by a rigid, 3D-printed barrier. Each side represents the surface area for cell adhesion to facilitate the growth of one cell type. The barrier was high enough to physically separate the two cell types but still simultaneously allow both sides to share a single cell culture medium. To maintain a sterile environment while still enabling user-friendly and convenient handling, the dimensions of the co-cultivation system were also adapted to fit in the well of a commercially available 6-well cell cultivation plate (see Figure 1).

One of the most well-known and clinically relevant *in vitro* co-culture models facilitates cultivation of mesenchymal stem cells and endothelial cells [12,13]. These models are frequently used (for example) to study the angiogenic potential of MSCs from different sources and donors, as one of the required potency assays [14,41,42]. Such assays evaluate MSCs supporting the formation of tubular-like structures of endothelial cells through release of angiogenic factors [13,42]. In this work, we analysed the suitability of using a 3D-printed co-cultivation platform for the development and

assessment of endothelial tubes in the presence of AD-MSCs. Figure 3 demonstrates the principle of an indirect co-cultivation within the 3D-printed chamber. While HUVECs cultured in mono-culture do not display characteristics of angiogenesis, HUVECs cultured in a shared medium alongside AD-MSCs form tubular-like structures that are considered a characteristic of angiogenesis.
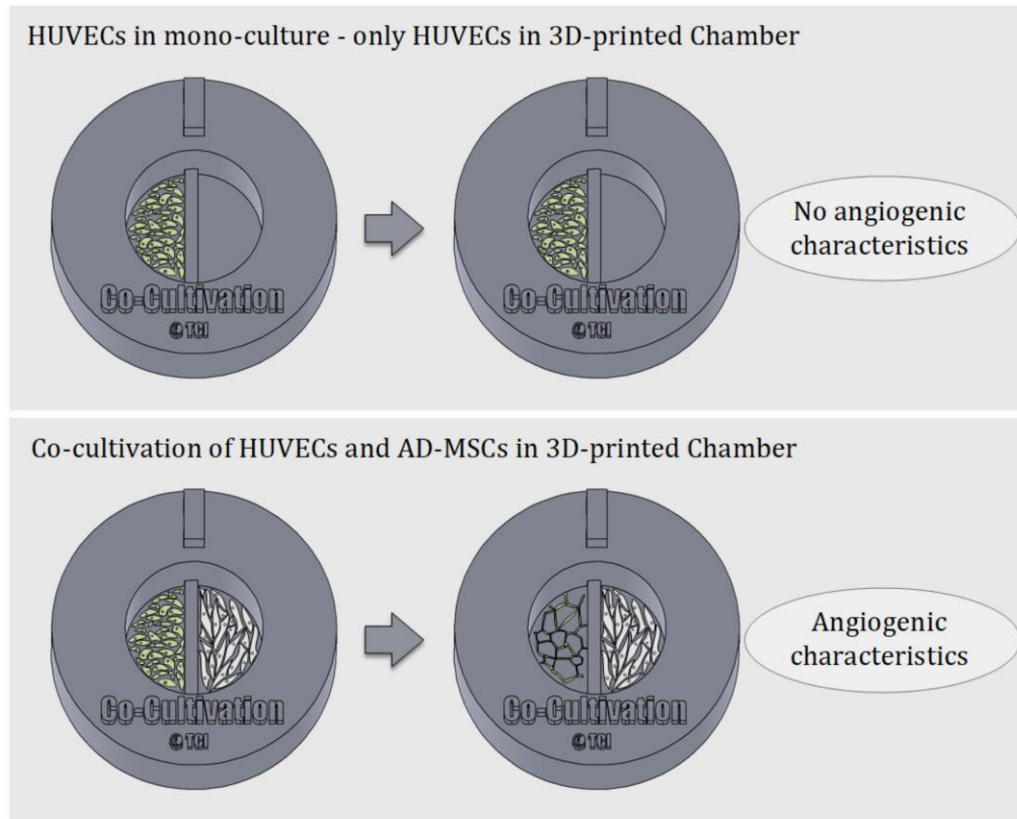

Figure 3. Schematic illustration of the underlying principle of indirect co-cultivation pointed out. While HUVECs cultured alone in the 3D-printed chamber show no signs of angiogenesis, HUVECs cultured in co-cultivation with AD-MSCs in 3D-printed chambers develop characteristics of angiogenesis.

To analyse the suitability of the 3D printing material, as well as the customized 3D-printed co-cultivation system in the context of indirect co-cultivation approaches, co-cultures of HUVECs and AD-MSCs were conducted over a period of 144 h (6 d), and endothelial tube formation was carefully monitored. In this study, all experiments were performed with HUVECs expressing *green fluorescent protein* (GFP) to facilitate monitoring via fluorescence. Because the 3D printing material in question holds no notable degree of autofluorescence, it readily permitted microscopic monitoring of fluorescence. Figure 4 shows fluorescence images of HUVECs grown in the 3D-printed co-cultivation chamber taken over a cultivation period of 144 h, as well as a quantitative analysis of tubular-like structures. Both cell types were seeded independently in their cell specific cell culture medium, in a volume that allowed for discrete seeding without overflowing the barrier in the middle. After a cultivation period of 24 h, culture media were removed and changed to co-cultivation medium in a volume that permitted the indirect interaction of both cell types via the transmission of signalling molecules.
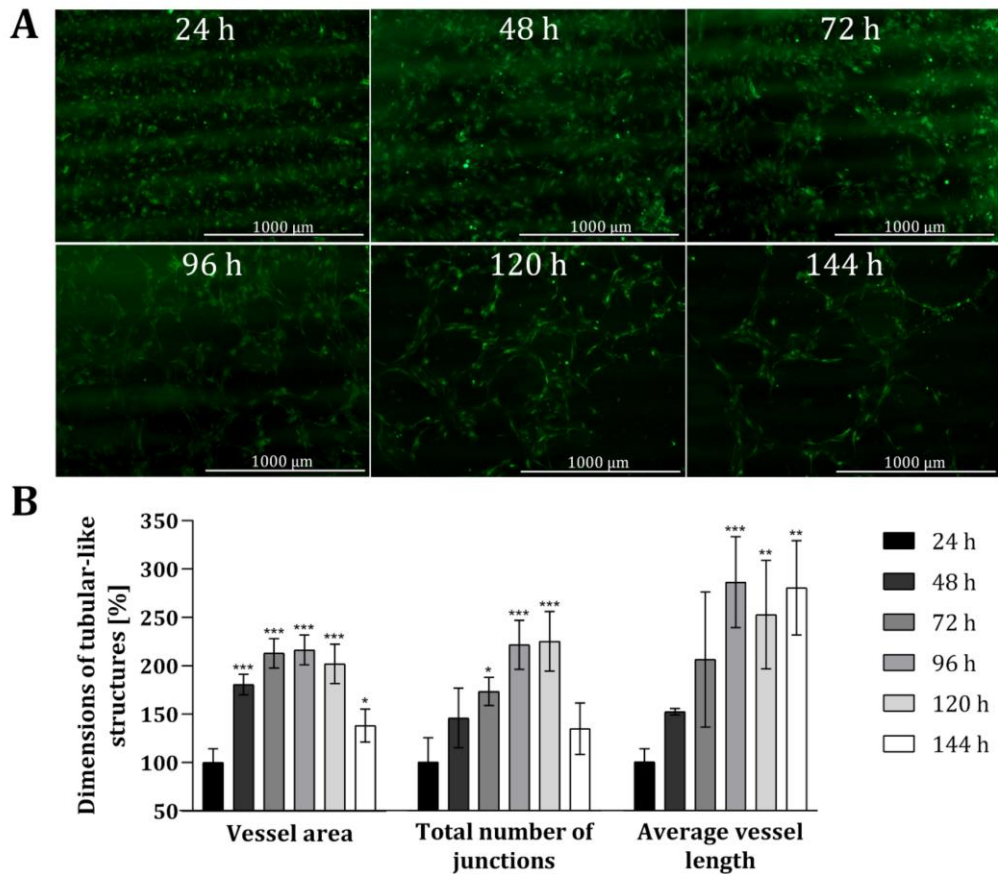
Figure 4. Analysis of angiogenic tube formation in indirect co-cultivation in 3D-printed system. (a): Fluorescence images of HUVECs cultivated in co-cultivation with AD-MSCs, physically separated through a barrier. After 24 h, the medium was changed to co-cultivation medium. In all, cells were co-cultivated for 144 h. (b): Results of quantitative analysis of the vessel area, total number of junctions and average vessel length of tubular-like structures of HUVECs using the software AngioTool®. HUVECs cultured in monoculture in 3D-printed system served as negative control. All experiments were repeated several times in independent experiments ($n > 3$) and significant differences to negative control are indicated: *$p < 0.05$. **$p < 0.01$, ***$p < 0.001$.

The obtained fluorescence images illustrate that a tubular network was, indeed, formed in the course of time (see Figure 4 (A)). Already after 48 h the slow migration and the associated accumulation of HUVECs can be seen, as smaller gaps are formed in the cell layer. These gaps become much wider after 72 h and over time, as the HUVECs accumulate more and more in a tubular structure. The cells gradually develop into a tubular-like network with increasing vessel or tube length, while the thickness of the formed tubes is declining. Quantitative analyses also revealed that the dimensions of tubular-like structures increased over time (see Figure 4 (B)) when compared to HUVECs only cultured in mono-culture within 3D-printed systems. The dimensions of the vessel area, the total number of junctions, and the average vessel length was more than doubled after around 72 h. The average length of the vessel in particular notably continued to extend as time progressed (i.e., to 286 % ± 47 % after 96 h, and ultimately to 280 % ± 48 % after 144 h). By contrast, the vessel area and total number of junctions both decreased again after 144 h – with a p-value of 0.0399, the dimensions of the vessel area are only slightly significant different, and no significant difference was observed for the total number of junctions compared to the dimensions after 24 h. Fluorescence

images taken after 144 h of co-cultivation also highlighted that the tubular-like networks formed wide holes, while the thickness of the developed tubes declined. One potential reason for the reduced vessel area and thickness of tubular structures after 144 h could be due to the loss of cells via detachment of dead cells.

In all, this experiment demonstrates that endothelial cells form tubular-like networks within the context of an indirect co-cultivation approach with AD-MSCs in a customized 3D-printed system. There was no need of applying Matrigel® or any other substrate materials to stimulate angiogenesis; rather, due to the angiogenic potential of AD-MSCs, and a potential release of angiogenic factors in the cell culture medium, co-culture alongside AD-MSCs facilitated the development of angiogenic features within endothelial cells [4]. The process of angiogenic tube formation may of course be accelerated by applying matrix substances (which could easily be coated onto the 3D-printing material). The material used for 3D printing has also been proven to be suitable for cell cultivation—particularly in the context of this customized 3D-printed co-cultivation system. This could represent a promising starting point for further investigations of intercellular interactions, or for assessing the effects of potential regulators on vessel formation. To the best knowledge of the authors, this experiment marks one of the first indirect co-cultivation assay in this vein that has been performed within a 3D-printed system—and thereby represents an important step towards the integration of customized 3D-printed devices in biomedical and/or tissue engineering applications [43,44].

3.3. Further customizable, experiment-specific 3D-printed platforms for the study of angiogenesis

In vitro angiogenesis studies provide valuable initial information about (for example) drug substances, suitable test concentrations, and cell therapy candidates, to name just a few applications. Essential test variants can be performed *in vitro* before considering their use in *in vivo* experiments. In addition, *in vitro* angiogenesis assays often address only one particular step in the angiogenic cascade—such as the degradation of

basement membrane or endothelial cell proliferation and migration—and thus hold the potential to provide relevant information about specific interactions, or classify roles of tested drugs in a particular phase of the angiogenesis process [6]. For these reasons, there are numerous studies reporting on *in vitro* angiogenesis assays [7,22].

However, general *in vitro* test setups and requirements in research can vary widely between experiments. Suitable experimental equipment, test beds, or supporting scaffold structures may be needed—which can pose a significant challenge for researchers. Unless they are prepared to produce their own labware, researchers are dependent on commercially available products. At this point, 3D printing technology represents an advantageous tool to fabricate individually and experiment-specific products in high-resolution and with almost unlimited complexity. Some possible applications of 3D-printed systems supporting *in vitro* studies (of angiogenesis) are illustrated in Figure 5 and 6.

One example of how 3D printing can be used to create new opportunities or circumvent limitations imposed by existing commercially-available equipment is demonstrated in the following. As a proof of concept, a platform with seven cell cultivation wells was specifically designed and 3D-printed for a direct co-cultivation approach with endothelial cell (HUVECs) and stromal cells (AD-MSCs). For the direct co-cultivation, the wells were not divided by a barrier and, consequently, the two cell types were cultivated with direct cell-cell contact. This custom 3D-printed system was then fitted into a commercial petri dish (Ø 60 mm) as pictured in Figure 6 (C), to ensure sterility and user-friendly handling of the 3D-printed platform. It must be emphasized that the chosen design format represents only one of many design possibilities and shows the great potential of the 3D printing technology used in this study for cell culture applications.
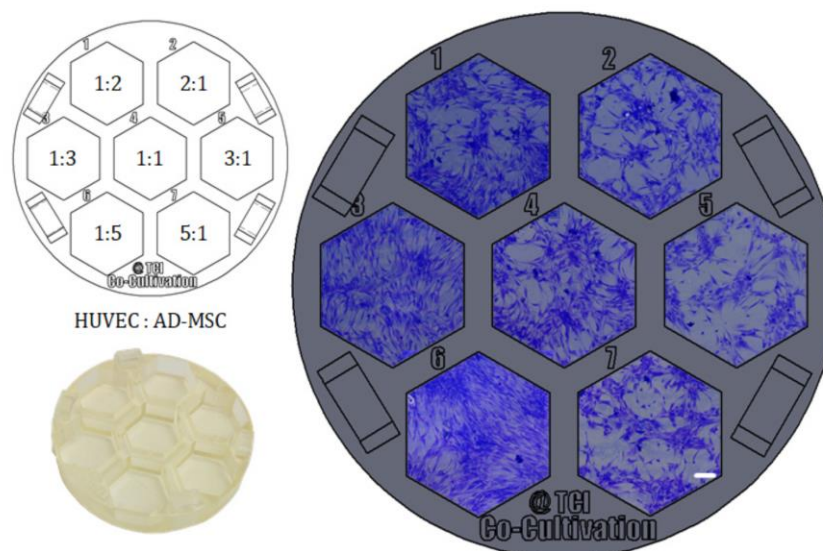
Figure 5. Example of direct co-cultivations (without physical barrier) performed in a 3D-printed screening platform fitting in a commercial petri dish. HUVECs and AD-MSCs were seeded in different cell mixture ratios (1:2, 1:3, 1:5, 1:1, 2:1, 3:1, 5:1), while cell density per well was held constant and co-cultivated in co-cultivation medium for 96 h. Images of cells were taken with a 3D digital microscope after crystal violet staining; scale bar is 150 μm.

With the goal of finding the most promising cell mixture ratio, HUVECs and AD-MSCs were thereafter seeded into the cell cultivation wells in different ratios, while the cell density per well was held constant. Here, variation of cell mixture ratios led to different degrees of formation of holes and tubular-like structures as angiogenic features—probably in response to different local concentrations of pro- or anti-angiogenic signalling molecules secreted by AD-MSCs. In this experimental approach, a high ratio of AD-MSCs caused overgrowth or domination over the endothelial cells as the whole cell cultivation well became pervaded by AD-MSC-typical cell layer morphologies (see cell mixture ratios of 1:5 and 1:3 in Figure 5). In conclusion, a cell mixture ratio of 2:1 (HUVEC:AD-MSC) was determined to be advisable for future experiments.

This experiment illustrates what a useful tool 3D printing technology can be for meeting experiment-specific challenges. As long as the 3D printing material in question is biocompatible and can also fulfil all experimental requirements with respect to mechanical and optical material properties, it can function as a self-contained test system; supporting scaffold structures for 3D cell culture experiments; individually-designed labware; or even a high-throughput system and cell culture vessel.

Figure 6 illustrates further variations of 3D-printed (co-) cultivation platforms and approaches designed to study angiogenesis *in vitro*. These screening platforms were again fitted in commercial petri dishes to function as a test bed – with the possibility to apply Matrigel® or other hydrogel matrix substances as a supporting base, if desired – and proved helpful in finding a suitable test concentration of a pro- or anti-angiogenic drug in more complex 3D culture systems. Screening platforms with co-cultivation wells – i.e., where the growth area is divided through a rigid barrier – may help to facilitate the study of angiogenic potential of stromal cells from different sources and donors (see Section 2.2.). 3D-printed Co-culture systems with printed barriers dividing the growth area into thirds enable the separate growth of three different cell types even as the cells continue to still share one cell culture medium.
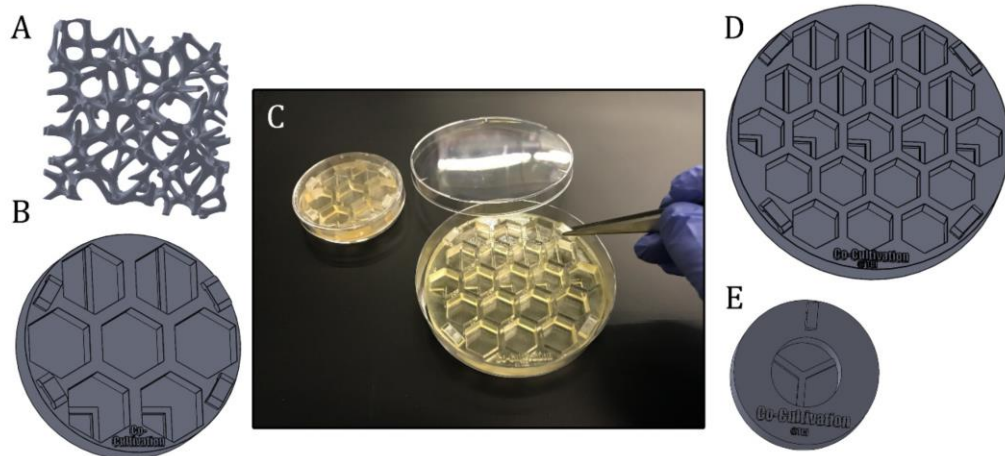
Figure 6. Presentation of different experiment-specific co-cultivation platforms and approaches. (a): Scaffold structure that can directly be seeded with cells, coated or filled with matrix substrates (b): Screening platform, which is fitting in a regular petri dish Ø 60 mm. (c): Illustration of the handling of 3D-printed screening platforms, which are fitting in commercial petri dishes with diameters of 60 mm or 90 mm. (d): Example of a co-cultivation platform with 19 wells for screening approaches. The system is fitting in a regular petri dish with a diameter of 90 mm. (e): Co-cultivation system allowing separate growth of three different cell types, while sharing still one cell culture medium.

The provision of adequate nutrient and oxygen supply within a tissue graft continues to constitute a significant challenge in the field of tissue engineering [3]. Indeed, overcoming limitations on diffusion is a major goal in modern graft engineering [3]. In order to achieve this, both the physiologic and pathologic appearance of the vascular system must be carefully analysed and replicated [45]. In an attempt to mimic vascular networks, Kang *et al.* fabricated porous scaffolds via stereolithography, coated them with a collagen layer, seeded cells onto the matrix, and then integrated the construct in a perfusion system to imitate blood flow through the scaffold [45]. Similar approaches could potentially be pursued and enhanced via 3D-printed scaffolds printed with the material used in this study. Scaffold structures of almost unlimited complexity (indeed, even in microscale format) can be 3D-printed, and cells can be grown directly on the scaffold, on coating matrix substances (e.g. hydrogels or Matrigel®), or in hydrogel substances in pores. The whole system can then be integrated into a flow chamber. Customizable 3D-printed platforms therefore hold tremendous promise to broaden the spectrum of *in vitro* systems available to researchers.

4. Conclusions

This study introduces a customized 3D-printed co-cultivation system useful for indirect co-cultivation approaches, as well as further 3D-printed devices useful for the *in vitro* study of angiogenesis. The results first confirmed that the 3D printing material does not exert any negative influences on cell behaviour. The customized 3D-printed co-cultivation system was then proven to be a suitable platform for performing and monitoring indirect co-cultivations. Angiogenic tube formation of endothelial cells was observed to develop within this system in response to the potential release of angiogenic factors by co-cultured mesenchymal stem cells—without the need for any supporting substrates (such as, for example, Matrigel®). Since the 3D printing material also enables phase contrast and fluorescence microscopy, the behaviour of cells could be observed over the entire cultivation period via both. To the best of the authors' knowledge, there have been only few work published that demonstrates how 3D-printed systems can be used as customizable platforms in indirect 2D co-cultivation approaches [43,44]. We believe this paper therefore marks an important step forward for the integration of customized 3D-printed systems as self-contained test systems or equipment in biomedical applications.

Angiogenesis studies, and indeed cell culture work in general, frequently confront researchers not only with difficult scientific questions but also profound implementation challenges. Researchers are forced to find suitable assays and methods to address and assess complicated experimental problems. But all too frequently, researchers are already restricted even in the very first phase of problem-solving (i.e., formulating experimental design) because they are reliant on commercially available experimental equipment. The rise of experiment-specific, customized 3D-printed labware can remove this artificial and regrettable limitation. Moreover, high-resolution 3D printing technology can open the door to manufacturing even complex devices at a micro scale [46]. Personalized experimental equipment or whole cultivation systems of almost limitless complexity can potentially be produced from start to finish within just a few hours—offering for a tremendous potential for pursuing experimental parallelization within a highly controllable environment. The 3D printing material used in this study outshines and also convinces by its suitability in cell cultivation experiments, as it can be exposed to ethanol (without negative effect on the material or later on the cells). Furthermore, autoclavable 3D printing materials are also commercially available. Thus, the sterility of the 3D-printed parts can be assured. Moreover, the mechanical and optical properties of the 3D printing material used here make it a very promising candidate for producing customized cell culture products. Whether as customized test system (as highlighted in this study) or as a high-throughput screening platform, as scaffold material or as experiment-specific labware – the 3D printing material in question may have almost unlimited application in future research setups.

References

1. Shafiee, A.; Atala, A. Tissue Engineering: Toward a New Era of Medicine. *Annu. Rev. Med.* **2017**, *68*, 29–40, doi:10.1146/annurev-med-102715-092331.

2. Rouwkema, J.; Rivron, N.C.; van Blitterswijk, C.A. Vascularization in tissue engineering. *Trends Biotechnol.* **2008**, *26*, 434–441, doi:10.1016/j.tibtech.2008.04.009.

3. Rouwkema, J.; Khademhosseini, A. Vascularization and Angiogenesis in Tissue Engineering: Beyond Creating Static Networks. *Trends Biotechnol.* **2016**, *34*, 733–745, doi:10.1016/j.tibtech.2016.03.002.

4. Saberianpour, S.; Heidarzadeh, M.; Geranmayeh, M.H.; Hosseinkhani, H.; Rahbarghazi, R.; Nouri, M. Tissue engineering strategies for the induction of angiogenesis using biomaterials. *J Biol Eng* **2018**, *12*, 36, doi:10.1186/s13036-018-0133-4.

5. Auerbach, R.; Auerbach, W.; Polakowski, I. Assays for angiogenesis: A review. *Pharmacology & Therapeutics* **1991**, *51*, 1–11, doi:10.1016/0163-7258(91)90038-N.

6. Donovan, D.; Brown, N.J.; Bishop, E.T.; Lewis, C.E. Comparison of three in vitro human 'angiogenesis' assays with capillaries formed in vivo. *Angiogenesis* **2001**, *4*, 113–121, doi:10.1023/A:1012218401036.

7. Auerbach, R.; Lewis, R.; Shinners, B.; Kubai, L.; Akhtar, N. Angiogenesis Assays: A Critical Overview. *Clin Chem* **2003**, *49*, 32–40, doi:10.1373/49.1.32.

8. Bootle-Wilbraham, C.A.; Tazzyman, S.; Marshall, J.M.; Lewis, C.E. Fibrinogen E-fragment inhibits the migration and tubule formation of human dermal microvascular endothelial cells in vitro. *Cancer Res.* **2000**, *60*, 4719–4724.

9. Horvath, P.; Aulner, N.; Bickle, M.; Davies, A.M.; Nery, E.D.; Ebner, D.; Montoya, M.C.; Östling, P.; Pietiäinen, V.; Price, L.S.; et al. Screening out irrelevant cell-based models of disease. *Nature Reviews Drug Discovery* **2016**, *15*, 751–769, doi:10.1038/nrd.2016.175.

10. Goers, L.; Freemont, P.; Polizzi, K.M. Co-culture systems and technologies: taking synthetic biology to the next level. *J R Soc Interface* **2014**, *11*, 20140065, doi:10.1098/rsif.2014.0065.

11. Yang, G.; Mahadik, B.; Choi, J.Y.; Fisher, J.P. Vascularization in tissue engineering: fundamentals and state-of-art. *Tissue Engineering* **2020**, *2*, 12002, doi:10.1088/2516-1091/ab5637.

12. Koob, S.; Torio-Padron, N.; Stark, G.B.; Hannig, C.; Stankovic, Z.; Finkenzeller, G. Bone Formation and Neovascularization Mediated by Mesenchymal Stem Cells and Endothelial Cells in Critical-Sized Calvarial Defects. *Tissue Eng. Part A* **2010**, *17*, 311–321, doi:10.1089/ten.tea.2010.0338.

13. Kasper, G.; Dankert, N.; Tuischer, J.; Hoeft, M.; Gaber, T.; Glaeser, J.D.; Zander, D.; Tschirschmann, M.; Thompson, M.; Matziolis, G.; et al. Mesenchymal Stem Cells Regulate Angiogenesis According to Their Mechanical Environment. *STEM CELLS* **2007**, *25*, 903–910, doi:10.1634/stemcells.2006-0432.

14. Kang, Y.; Kim, S.; Fahrenholtz, M.; Khademhosseini, A.; Yang, Y. Osteogenic and angiogenic potentials of monocultured and co-cultured human-bone-marrow-derived mesenchymal stem cells and human-umbilical-vein endothelial cells on three-dimensional porous beta-tricalcium phosphate scaffold. *Acta Biomaterialia* **2013**, *9*, 4906–4915, doi:10.1016/j.actbio.2012.08.008.

15. Zhang, Y.; Guo, W.; Wang, M.; Hao, C.; Lu, L.; Gao, S.; Zhang, X.; Li, X.; Chen, M.; Li, P.; et al. Co-culture systems-based strategies for articular cartilage tissue engineering. *J Cell Physiol* **2018**, *233*, 1940–1951, doi:10.1002/jcp.26020.

16. Li, W.; Khan, M.; Mao, S.; Feng, S.; Lin, J.-M. Advances in tumor-endothelial cells co-culture and interaction on microfluidics. *Journal of Pharmaceutical Analysis* **2018**, *8*, 210–218, doi:10.1016/j.jpha.2018.07.005.

17. Renaud, J.; Martinoli, M.-G. Development of an Insert Co-culture System of Two Cellular Types in the Absence of Cell-Cell Contact. *J. Vis. Exp.* **2016**, doi:10.3791/54356.

18. Huang, C.P.; Lu, J.; Seon, H.; Lee, A.P.; Flanagan, L.A.; Kim, H.-Y.; Putnam, A.J.; Jeon, N.L. Engineering microscale cellular niches for three-dimensional multicellular co-cultures. *Lab on a Chip* **2009**, *9*, 1740–1748, doi:10.1039/b818401a.

19. Khademhosseini, A.; Ferreira, L.; Blumling, J.; Yeh, J.; Karp, J.M.; Fukuda, J.; Langer, R. Co-culture of human embryonic stem cells with murine embryonic fibroblasts on microwell-patterned substrates. *Biomaterials* **2006**, *27*, 5968–5977, doi:10.1016/j.biomaterials.2006.06.035.

20. Kaji, H.; Camci-Unal, G.; Langer, R.; Khademhosseini, A. Engineering systems for the generation of patterned co-cultures for controlling cell-cell interactions. *Biochim. Biophys. Acta* **2011**, *1810*, 239–250, doi:10.1016/j.bbagen.2010.07.002.

21. Kubosch, E.J.; Heidt, E.; Bernstein, A.; Bottiger, K.; Schmal, H. The trans-well coculture of human synovial mesenchymal stem cells with chondrocytes leads to self-organization, chondrogenic differentiation, and secretion of TGFbeta. *Stem Cell Res. Ther.* **2016**, *7*, 64, doi:10.1186/s13287-016-0322-3.

22. Staton, C.A.; Reed, M.W.R.; Brown, N.J. A critical analysis of current in vitro and in vivo angiogenesis assays. *International Journal of Experimental Pathology* **2009**, *90*, 195–221, doi:10.1111/j.1365-2613.2008.00633.x.

23. Ponce, M.L. Tube formation: an in vitro matrigel angiogenesis assay. *Methods in molecular biology (Clifton, N.J.)* **2009**, *467*, 183–188, doi:10.1007/978-1-59745-241-0_10.

24. Carter, R.N.; Casillo, S.M.; Mazzocchi, A.R.; DesOrmeaux, J.-P.S.; Roussie, J.A.; Gaborski, T.R. Ultrathin transparent membranes for cellular barrier and co-culture models. *Biofabrication* **2017**, *9*, 15019, doi:10.1088/1758-5090/aa5ba7.

25. Bishop, E.T.; Bell, G.T.; Bloor, S.; Broom, I.J.; Hendry, N.F.; Wheatley, D.N. An in vitro model of angiogenesis: basic features. *Angiogenesis* **1999**, *3*, 335–344, doi:10.1023/a:1026546219962.

26. Montesano, R.; Pepper, M.S.; Orci, L. Paracrine induction of angiogenesis in vitro by Swiss 3T3 fibroblasts. *J. Cell Sci.* **1993**, *105 (Pt 4)*, 1013–1024.

27. Gershovich, J.G.; Dahlin, R.L.; Kasper, F.K.; Mikos, A.G. Enhanced osteogenesis in cocultures with human mesenchymal stem cells and endothelial cells on polymeric microfiber scaffolds. *Tissue Eng. Part A* **2013**, *19*, 2565–2576, doi:10.1089/ten.TEA.2013.0256.

28. Unterleuthner, D.; Kramer, N.; Pudelko, K.; Burian, A.; Hengstschläger, M.; Dolznig, H. An Optimized 3D Coculture Assay for Preclinical Testing of Pro- and Antiangiogenic Drugs. *SLAS DISCOVERY: Advancing the Science of Drug Discovery* **2017**, *22*, 602–613, doi:10.1177/2472555216686529.

29. Nakatsu, M.N.; Hughes, C.C.W. Chapter 4 An Optimized Three‐Dimensional In Vitro Model for the Analysis of Angiogenesis. *Methods in Enzymology : Angiogenesis*; Academic Press, 2008; pp 65–82, ISBN 0076-6879.

30. Sun, W.; Motta, A.; Shi, Y.; Seekamp, A.; Schmidt, H.; Gorb, S.N.; Migliaresi, C.; Fuchs, S. Co-culture of outgrowth endothelial cells with human mesenchymal stem cells in silk fibroin hydrogels promotes angiogenesis. *Biomed. Mater.* **2016**, *11*, 35009, doi:10.1088/1748-6041/11/3/035009.

31. Hsu, Y.-H.; Moya, M.L.; Hughes, C.C.W.; George, S.C.; Lee, A.P. A microfluidic platform for generating large-scale nearly identical human microphysiological vascularized tissue arrays. *Lab on a Chip* **2013**, *13*, 2990–2998, doi:10.1039/C3LC50424G.

32. Ho, C.M.B.; Ng, S.H.; Yoon, Y.-J. A review on 3D printed bioimplants. *International Journal of Precision Engineering and Manufacturing* **2015**, *16*, 1035–1046, doi:10.1007/s12541-015-0134-x.

33. Siller, I.G.; Enders, A.; Steinwedel, T.; Epping, N.-M.; Kirsch, M.; Lavrentieva, A.; Scheper, T.; Bahnemann, J. Real-Time Live-Cell Imaging Technology Enables High-Throughput Screening to Verify in Vitro Biocompatibility of 3D Printed Materials. *Materials (Basel)* **2019**, *12*, doi:10.3390/ma12132125.

34. Siller, I.G.; Enders, A.; Gellermann, P.; Winkler, S.; Lavrentieva, A.; Scheper, T.; Bahnemann, J. Characterization of a customized 3D-printed cell culture system using clear, translucent acrylate that enables optical online monitoring. *Biomed. Mater.* **2020**, doi:10.1088/1748-605X/ab8e97.

35. Lavrentieva, A.; Majore, I.; Kasper, C.; Hass, R. Effects of hypoxic culture conditions on umbilical cord-derived human mesenchymal stem cells. *Cell Commun. Signal.* **2010**, *8*, 18, doi:10.1186/1478-811X-8-18.

36. Feoktistova, M.; Geserick, P.; Leverkus, M. Crystal Violet Assay for Determining Viability of Cultured Cells. *Cold Spring Harb. Protoc.* **2016**, *2016*, pdb.prot087379, doi:10.1101/pdb.prot087379.

37. Zudaire, E.; Gambardella, L.; Kurcz, C.; Vermeren, S. A computational tool for quantitative analysis of vascular networks. *PLoS ONE* **2011**, *6*, e27385, doi:10.1371/journal.pone.0027385.

38. Bernard, M.; Jubeli, E.; Pungente, M.D.; Yagoubi, N. Biocompatibility of polymer-based biomaterials and medical devices - regulations, in vitro screening and risk-management. *Biomater. Sci.* **2018**, *6*, 2025–2053, doi:10.1039/C8BM00518D.

39. Kopperud, H.M.; Kleven, I.S.; Wellendorf, H. Identification and quantification of leachable substances from polymer-based orthodontic base-plate materials. *European Journal of Orthodontics* **2011**, *33*, 26–31, doi:10.1093/ejo/cjq020.

40. Rashid, H.; Sheikh, Z.; Vohra, F. Allergic effects of the residual monomer used in denture base acrylic resins. *Eur. J. Dent.* **2015**, *9*, 614–619, doi:10.4103/1305-7456.172621.

41. Li, Q.; Wang, Z. Influence of Mesenchymal Stem Cells with Endothelial Progenitor Cells in Co-culture on Osteogenesis and Angiogenesis: An In Vitro Study. *Archives of Medical Research* **2013**, *44*, 504–513, doi:10.1016/j.arcmed.2013.09.009.

42. Gurel Pekozer, G.; Torun Kose, G.; Hasirci, V. Influence of co-culture on osteogenesis and angiogenesis of bone marrow mesenchymal stem cells and aortic endothelial cells. *Microvascular Research* **2016**, *108*, 1–9, doi:10.1016/j.mvr.2016.06.005.

43. Giglio, E. de; Bonifacio, M.A.; Ferreira, A.M.; Cometa, S.; Ti, Z.Y.; Stanzione, A.; Dalgarno, K.; Gentile, P. Multi-compartment scaffold fabricated via 3D-printing as in vitro co-culture osteogenic model. *Scientific Reports* **2018**, *8*, 15130, doi:10.1038/s41598-018-33472-1.

44. Lerman, M.J.; Lembong, J.; Gillen, G.; Fisher, J.P. 3D printing in cell culture systems and medical applications. *Appl. Phys. Rev.* **2018**, *5*, 41109, doi:10.1063/1.5046087.

45. Kang, T.-Y.; Hong, J.M.; Jung, J.W.; Kang, H.-W.; Cho, D.-W. Construction of Large-Volume Tissue Mimics with 3D Functional Vascular Networks. *PLoS ONE* **2016**, *11*, e0156529, doi:10.1371/journal.pone.0156529.

46. Enders, A.; Siller, I.G.; Urmann, K.; Hoffmann, M.R.; Bahnemann, J. 3D Printed Microfluidic Mixers—A Comparative Study on Mixing Unit Performances. *Small* **2019**, *15*, 1804326, doi:10.1002/smll.201804326.

84

Supplementary Material for

Customizable 3D-printed (co-)cultivation systems for in vitro study of angiogenesis

Authors:

Ina G. Siller [1], Niklas-Maximilian Epping [1], Antonina Lavrentieva [1], Thomas Scheper [1] and Janina Bahnemann [1, *]

[1] Institute of Technical Chemistry, Leibniz University Hannover, Callinstraße 5, 30167 Hannover, Germany
*   Correspondence: jbahnemann@iftc.uni-hannover.de; Tel.: +49-511-762-2568

Evaluation of Angiogenesis by using AngioTool® software

For quantitative analysis of angiogenesis, the open source software AngioTool® (National Institute of Health, National Cancer Institute, Bethesda, MD, USA) was used. Images were analysed regarding different parameters that are related to angiogenesis. As one of the parameters, the vessel area was analysed, which is defined as the area of all segmented vessels while a vessel is defined in AngioTool® as a segment between two branching points. Furthermore, the total number of junctions or branching points between vessels was determined as well as the average vessel length of all vessels in the image. Figure S1 illustrates the output of AngioTool® for an exemplary image. Additionally, an Excel sheet with the calculated results for the analysis parameters was issued by the software.
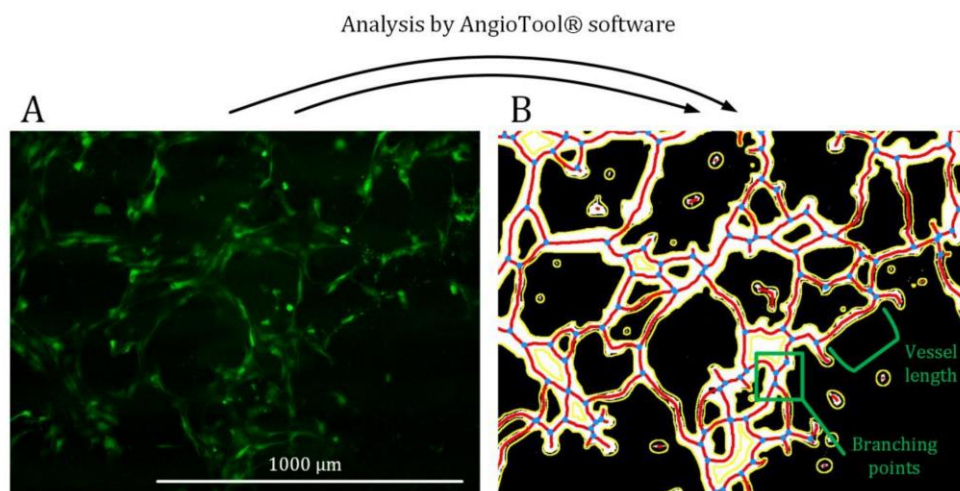

Figure S1. Exemplary images of cell analysis using AngioTool®. (A): Fluorescent image of GFP Human Umbilical Vein Endothelial Cells (HUVECs) cultivated for 120 h in the 3D-printed co-cultivation system. Total magnification is 4. (B): Output of AngioTool®. All vessels that are considered by the software are marked in red and all branching points are highlighted in blue.

4.4 Entwicklung 3D-gedruckter statischer und dynamischer Durchflusszellen für elektrochemische (Bio)Sensoren
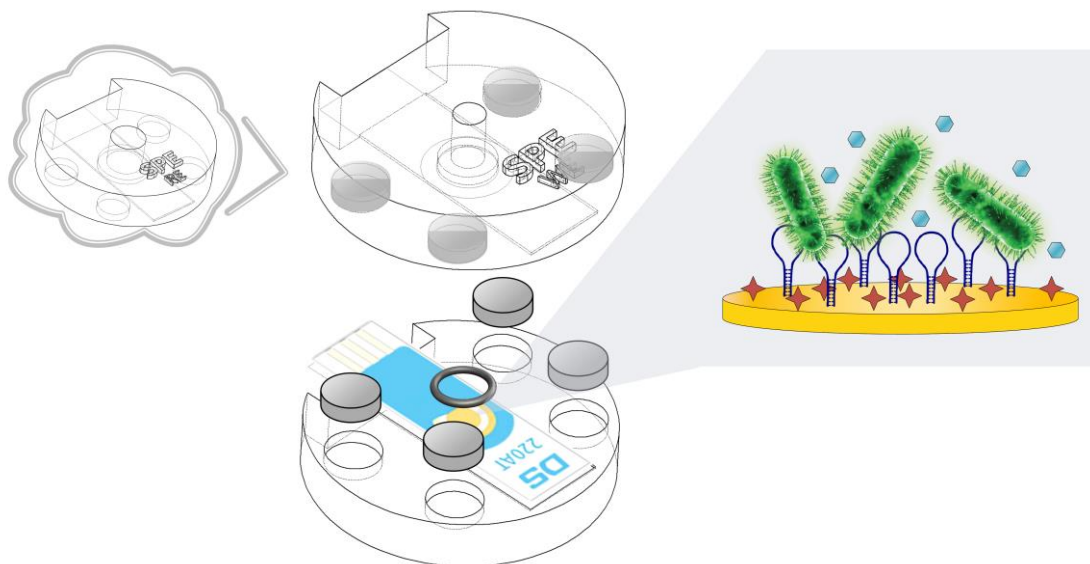
Abbildung 4-4 *Graphical abstract* von „*3D-printed Flow Cells for Aptamer-Based Impedimetric Detection of E. coli Crooks Strain*".

Wie bereits in Kapitel 3.3 angesprochen, gibt es vielfältige Anwendungsmöglichkeiten von 3D-Druck in der (Bio)Sensorik. Es können nicht nur maßgeschneiderte Versuchsgehäuse oder Apparaturen gefertigt werden, sondern sogar Elektroden mit geeigneten Materialien 3D-gedruckt werden [71]. Dabei bietet die additive Fertigung die Möglichkeit, konventionelle Sensorkomponenten, wie Elektroden, in das System zu integrieren. Sogenannte *Screen-printed electrodes* (SPEs) stellen hierbei eine attraktive Alternative zu konventionellen Elektroden dar. Mit einer Größe von nur wenigen Zentimetern unterstützen sie insbesondere die fortschreitende Entwicklung zu miniaturisierten, sensitiven und tragbaren Sensorsystemen. Außerdem stellen sie im Gegensatz zu herkömmlichen Elektroden eine kostengünstige Einweg-Variante dar [139].

SPEs können „blank", d. h. ohne weitere Hilfsmittel, für elektrochemische Messungen verwendet werden – sie benötigen einzig eine Verbindung zu einem Potentiostaten. Viele Anwendungen erfordern jedoch die Integration von SPEs in Geräteapparaturen oder Inkubations- und Waschschritte, die mit der „blanken" SPE nur schwierig realisiert werden können. Zur Umsetzung dieser Anwendungen bietet die additive Fertigung herausragende Möglichkeiten um experiment-spezifisch maßgefertigte Systeme herzustellen.

Nachfolgend werden 3D-gedruckte statische und dynamische Durchflusszellen vorgestellt, in die eine SPE passgenau montiert und entsprechende elektrochemische Messungen durchgeführt werden können. Die Anwendung wird als *proof-of-concept* in einem aptamerbasierten, impedimetrischen Biosensor zur Detektion eines *E. coli* Crooks Stammes demonstriert und die Vorteile eines automatisierbaren, dynamischen Systems sowohl in CFD (*Computational Fluid Dynamics*) Simulationen als auch praktischen Mischexperimenten aufgezeigt.

Die additiv gefertigten Systeme bestehen aus zwei Bauelementen: einem Deckelaufsatz und einem Bodenteil. In beiden Elementen befindet sich eine speziell auf die Abmessungen einer SPE angepasste Vertiefung, die einen festen Halt der SPE in der Durchflusszelle gewährleistet. Der Deckelaufsatz besitzt eine Öffnung bzw. Kammer, die die Elektroden der SPE umschließt und diese einem definierten Flüssigkeitsvolumen, wie z. B. Pufferlösungen oder Bakterienproben, aussetzt. Während der Durchführung eines Biosensor-Experiments muss der obere Aufsatz ausgetauscht werden – nur die Arbeitselektrode soll mit Aptameren funktionalisiert werden, während bei den elektrochemischen Messungen alle Elektroden in Kontakt mit der jeweiligen Pufferlösung stehen sollen. Daher wurden für die statische Durchflusszelle zwei austauschbare Deckelaufsätze konstruiert, die sich im Durchmesser der Öffnung zur Flüssigkeitszugabe unterscheiden: ein Aufsatz umschließt einzig die Arbeitselektrode der SPE, der andere Aufsatz alle Elektroden (Arbeits-, als auch Referenz- und Gegenelektrode) der SPE. Das System wird durch einen Verschlussmechanismus mit Magneten sowie O-Ringen abgedichtet.

In der aptamerbasierten Biosensor-Anwendung konnte erfolgreich eine impedimetrische Detektion eines *E. coli* Crooks Stammes in der statischen Durchflusszelle demonstriert werden. Die entwickelte statische Durchflusszelle hat die Durchführung des Biosensor Experiments maßgeblich unterstützt – die Wasch- und Inkubationsschritte wären ohne Durchflusszelle, mit der „blanken" SPE, in dem Umfang nicht möglich gewesen. Darüber hinaus veranschaulichen Experimente in einer speziell für SPE-Anwendungen entwickelten, dynamischen Durchflusszelle die Vorteile von integrierten Mikromischern. Durch sie konnte eine homogene Vermischung der Analytprobe vor der Messung gewährleistet werden. Die Kopplung des Systems an eine Spritzenpumpe ermöglicht eine automatisierte und zeitgesteuerte Inkubation, bspw. von Puffer- oder Probenlösungen. Ebenso könnte das System an einen Bioprozess gekoppelt werden, um bspw. eine kontinuierliche Detektion von Zielanalyten aus einem laufenden Kultivierungsprozess zu ermöglichen.

Im folgenden Artikel „*3D-printed Flow Cells for Aptamer-Based Impedimetric Detection of E. coli Crooks Strain*" werden die Ergebnisse detailliert beschrieben und diskutiert.

sensors **MDPI**

Article

3D-Printed Flow Cells for Aptamer-Based Impedimetric Detection of *E. coli* Crooks Strain

Ina G. Siller [1,†] , **John-Alexander Preuss** [1,†] , **Katharina Urmann** [2] , **Michael R. Hoffmann** [2] ,
Thomas Scheper [1] **and Janina Bahnemann** [1,*]

[1]   Institute of Technical Chemistry, Leibniz University Hannover, Callinstraße 5, 30167 Hannover, Germany;
   siller@iftc.uni-hannover.de (I.G.S.); preuss@iftc.uni-hannover.de (J.-A.P.); scheper@iftc.uni-hannover.de (T.S)
[2]   Department of Environmental Science and Engineering, California Institute of Technology, 1200 E. California
   Blvd., Pasadena, CA 91125, USA; urmann.k@gmail.com (K.U.); mrh@caltech.edu (M.R.H.)
*   Correspondence: jbahnemann@iftc.uni-hannover.de; Tel.: +49-511-762-2568
†   Co-first author, these authors contributed equally to this work.

check for
updates

Abstract: Electrochemical spectroscopy enables rapid, sensitive, and label-free analyte detection without the need of extensive and laborious labeling procedures and sample preparation. In addition, with the emergence of commercially available screen-printed electrodes (SPEs), a valuable, disposable alternative to costly bulk electrodes for electrochemical (bio-)sensor applications was established in recent years. However, applications with bare SPEs are limited and many applications demand additional/supporting structures or flow cells. Here, high-resolution 3D printing technology presents an ideal tool for the rapid and flexible fabrication of tailor-made, experiment-specific systems. In this work, flow cells for SPE-based electrochemical (bio-)sensor applications were designed and 3D printed. The successful implementation was demonstrated in an aptamer-based impedimetric biosensor approach for the detection of *Escherichia coli* (*E. coli*) Crooks strain as a proof of concept. Moreover, further developments towards a 3D-printed microfluidic flow cell with an integrated micromixer also illustrate the great potential of high-resolution 3D printing technology to enable homogeneous mixing of reagents or sample solutions in (bio-)sensor applications.

Keywords: additive manufacturing; impedimetric biosensor; aptasensor; screen-printed electrodes

1. Introduction

Electrochemical biosensors are widely used in areas such as health care, food control, or environmental analysis [1]. Especially the high selectivity of the biological recognition element and the sensitivity of electrochemical measuring methods (transducers) are potential key benefits of such sensors. Besides biorecognition elements like antibodies [2], lectin molecules [3], or bacteriophages [4], aptamers are of high interest [1]. In brief, aptamers are single-stranded nucleic acids that can display a high affinity to a target analyte. They are selected in vitro by an evolutionary process (SELEX, Systematic Evolution of Ligands by Exponential Enrichment) [5–7]. This class of biorecognition elements is often compared to antibodies. Aptamers benefit from their high stability in different chemical environments and to temperature changes [7]. Moreover, commercial, in vitro synthesis of nucleic acids enables a cost-efficient and flexible production and even allows site-specific modifications for attachment chemistries (e.g., thiol, amine, or biotin groups). Owing to their stability, consistent quality, small size, and broad possible target range, many assays can be designed utilizing aptamers as receptor molecules.

Electrochemical measurements, such as electrochemical impedance spectroscopy, offer label-free, rapid, and sensitive detection—a real benefit towards point-of-care testing. For instance, detection

limits close to single-molecule detection have been reported (lipopolysaccharide concentration of 0.01 attomolar) [8]. Herein, we focused on impedimetric aptamer sensors. Previously reported targets include: Small molecules like progesterone [9] or Ochratoxin A (OTA) [10], proteins such as clinically relevant Vascular Endothelial Growth Factor (VEGF) [11,12] or carcinoembryonic antigen (CEA) [13], spore simulants of *Bacillus anthracis* [14], and various bacterial pathogens (e.g., *Salmonella typhimurium* [15,16], *Escherichia coli* (*E. coli*) [17–20], *Staphylococcus aureus* [21,22]). Infections with specific pathogenic *E. coli*, for instance, are the cause of multiple severe medical conditions [23]. Thus, rapid and reliable testing is needed to validate the safety of food or environmental samples. However, this presents only one example of why rapid detection methods are needed. Traditional methods based on bacterial culturing are laborious and take days, while specific amplification (e.g., polymerase chain reaction-based detection) needs only a few hours but does not differentiate between dead and living cells and requires costly devices and reagents. In comparison, electrochemical methods offer rapid and sensitive testing. Combined with aptamers as biorecognition element, the binding of whole cells enables selective detection of bacteria with no or little sample preprocessing. Besides electrochemical biosensors with antibodies and other biorecognition elements [24] with detection limits down to single-digit CFU (colony-forming units) mL^{-1}, also a few electrochemical aptamer-based biosensors have been reported for the detection of *E. coli* [25–27]. However, they all have in common that electrodes are either self-made or custom-made, which hampers simple and open-access transfer to in-field applications, due to a lack of standardization of the electrode setup.

In recent years, an increasing number of publications—focused on screen-printed electrodes (SPE)—have been presented. SPEs are a disposable alternative to bulk electrodes. Besides in-house screen-printing facilities, different commercial suppliers are established, offering cost-efficient mass production [10,28,29]. Their products encompass disposable SPEs with different electrode materials (e.g., graphite, gold, platinum) or even nano-engineered surfaces (e.g., deposited gold nanoparticles or carbon nanotubes). Working electrodes with a diameter of only a few millimeters enable miniaturized assays [30].

Several authors state that a specific volume of reagents or sample of interest is placed onto the working electrode [31–33]. However, for many applications a static or dynamic flow cell might be of interest. Potential advantages include the handling of samples with defined volumes, a controlled environment, or, especially with regard to flow cells, an automation of experiments. A few authors mounted the electrode setup/screen-printed electrodes into dynamic flow cells or open/static cells. Polydimethylsiloxane (PDMS) [34,35] or 3D printing-based cells [36,37] are the most common, but also electrochemical cells based on glass [38], polypropylene [39], or poly(methyl methacrylate) (PMMA) [10] have been reported. Especially research laboratories may benefit from 3D printing as a flexible small-manufacturing tool not limited to flow cells or open cells. Instead, it opens access to a range of useful laboratory tools, while no special training is needed for the manufacturing process [40–45]. In brief, based on CAD (computer-aided design) modelling, a 3D model is structured into a finite number of layers to be printed layer by layer. In this way, a range of even complex 3D structures can be manufactured. The 3D-printed open cells may include a chamber for screen-printed microinterdigitated electrodes, which also enable a connection via Universal Serial Bus (USB) [30] and a chamber for bipolar electrodes [46]. An example of a 3D-printed microfluidic chamber was presented by Damiati et al. The SPE and the microfluidic chamber were bonded by a double-sided adhesive layer [37]. Moreover, there are some examples for open cells which are not based on 3D printing. Those include an open cell for the SPEs made of glass [38] and a one-compartment cell made of a not-further-specified material [47].

The potential of flow cells is illustrated by a study by Rhouati et al. [10]. They developed an automated aptamer-based detection of ochratoxin A in a custom PMMA flow cell for SPEs, which included a multiple-step processing of beer sample and reagents. For other flow cells, 3D printing has been utilized to manufacture master molds for PDMS and to provide (complex) housing for microfluidic channels made of PDMS [48].

In this study, we present 3D-printed cells that allow direct assembly of commercially available SPEs. Since there are different suppliers of SPEs of different size and shape, 3D printing offers customized integration of electrodes dependent on the specific needs for the experiments. The advantage of a static 3D-printed flow cell is demonstrated in an impedimetric and label-free aptamer-based biosensor approach for the detection of *E. coli* Cook's strain as a proof of concept. An aptamer-based biosensing experiment involves several incubation and washing steps. Therefore, a system that allows the treatment of the SPE with defined volumes of liquids would be beneficial. In addition, for aptamer functionalization an exclusive exposure of only the working electrode is required. The static flow cell was designed and 3D-printed to meet these demands.

Moreover, this study also presents a 3D-printed microfluidic dynamic flow cell with an integrated micromixer, which can be operated automatically. Automated mixing of reagents or sample solutions before electrochemical measurements would not only ensure homogeneous mixing of the sample applied to the electrodes, but also contribute to reproducibility. A comparison of the mixing performance with and without micromixer unit in the flow cell demonstrates the great effect of integrated micromixers.

2. Materials and Methods

2.1. Design, 3D Printing, and Post-Processing

Flow cells were constructed with the computer-aided design (CAD) software SolidWorks (Dassault Systems, Waltham, MA, USA) and 3D printed using a high-resolution 3D printer (ProJet® MJP 2500 Plus, 3D Systems, SC, USA). As printing material, a rigid translucent polyacrylate resin was used (VisiJet® M2R-CL, 3D Systems, SC, USA) via MultiJet printing technology, involving a UV-curing process. The 3D parts were printed with a resolution of 800×900 dots per inch and a layer thickness of 32 μm. VisiJet® M2-SUP functioned as the supporting material for the printing process. For removal of support material after printing, 3D-printed parts were placed for 15 min at −18 °C, then removed from the printing platform and placed for 45 min in a heat steam bath and paraffin oil bath at 65 °C (EasyClean unit, 3D Systems, SC, USA). Afterwards, the parts were rinsed in an ultrasonic water bath with the use of detergent (Fairy Ultra Plus, Procter and Gamble, CT, USA) for 30 min at 65 °C. The microfluidic structures of the dynamic flow cells were additionally flushed with paraffin oil (Carl Roth GmbH, Karlsruhe, Germany), soapy water, and water at the respective steps to remove remaining wax and oil residues.

Both constructed 3D-printed cell systems consisted of two parts—a bottom and a top part. Two exchangeable top parts were designed—one enclosing only the working electrode of the SPE and one enclosing all electrodes. For sufficient sealing, disc magnets (diameter: 6.4 mm, length: 1.6 mm; National Imports LLC, dba Magcraft, Vienna, VA, USA) and the corresponding electrodes enclosing O-rings (11×2 mm; 7×2 mm; Marco Rubber & Plastics, LLC, Seabrook, NH, USA) were embedded in the 3D-printed parts. The Standard Triangle Language (STL) files of the 3D-printed parts are provided as supporting information.

2.2. Biosensing Experiment in 3D-Printed Static Flow Cell

2.2.1. Cultivation of Bacteria and Sample Preparation

Escherichia coli (*E. coli*) (Crooks strain, ATCC® 8739, American Type Culture Collection, Manassas, VA, USA) was cultivated in appropriate nutrient broth and incubated at 37 °C, 150 rpm. To estimate the concentration of bacteria, optical density (OD) was measured at a wavelength of 600 (OD_{600}) with a spectrophotometer. As the optical density (OD_{600}) reached 0.5 (equals approximately 10^8 cells/mL), 1-mL samples of the culture were taken and spun down in a regular lab centrifuge for 10 min at $5000 \times g$. Supernatant was carefully discarded and the pellet was resuspended in 1 mL fresh nutrient medium. Centrifugation and washing steps were repeated twice and cells were diluted in ferri-/ferrocyanide buffer (FeSB) (see Section 2.2.4) to receive the required dilution.

2.2.2. Preparation of Screen-Printed Electrodes (SPE)

Screen-printed gold electrodes (SPE) (DRP-220AT SPE) were purchased from Metrohm DropSens (Oviedo, Spain). The SPE consisted of a gold working electrode (4 mm in diameter), a gold counter electrode, and a silver pseudo-reference electrode and was made of high-temperature curing inks. The SPE was connected via a cable (CAC, Metrohm DropSens, Oviedo, Spain) to a potentiostat (VSP-300 with ultra-low current cable, BioLogic, Seyssinet-Pariset, France). All measurements were conducted at room temperature in an air-conditioned laboratory.

Before the start of a biosensing experiment, the SPE was mounted in the 3D-printed static cell with the top part enclosing all electrodes, cleaned, and activated according to the procedure described and optimized by Henihan et al. [49]. In brief, 100 µL of 0.1 mol L^{-1} sulfuric acid (H_2SO_4) was applied on all electrodes of the SPE. Then, 10 electrochemical cyclic voltammetry (CV) cycles with a voltage between 0 and 1.6 V, followed by three CV cycles with a voltage between 0 and 1.3 V, were run. After a biosensing experiment was done, the SPE was washed thoroughly with deionized nuclease-free water (Millipore Milli-Q® system, Merck KGaA, Darmstadt, Germany) and cleaned with the same CV procedure.

2.2.3. Aptamer Functionalization of the SPE

DNA oligonucleotides were purchased from Integrated DNA Technologies, Inc. (Coralville, IA, USA), with a thiol modification at 5. The oligonucleotide sequence of the used aptamer was described by Bruno et al. and was as follows: 5–ATC CGT CAC ACC TGC TCT GTC TGC GAG CGG GGC GCG GGC CCG GCG GGG GAT GCG TGG TGT TGG CTC CCG TAT–3 [50]. Until the start of an experiment, aptamer stock solution of 300 µM in deionized nuclease-free water was stored at 4 °C.

Chemical modification of oligonucleotides with thiol groups is a simple and often-used method for aptamer immobilization on gold surfaces [51]. Due to chemisorption of the activated thiol-modified aptamers on the gold surface, self-assembled monolayers were created.

For aptamer immobilization on the SPE, oligonucleotides were diluted to 1 µM in aptamer selection buffer (SB) containing 0.5 M sodium chloride (NaCl), 10 mM Tris buffer (Tris-hydrogen chloride (HCl)), 1 mM magnesium chloride ($MgCl_2$); pH was set to pH 7.5. All buffer constituents used in this study were purchased from Sigma-Aldrich (St. Louis, MO, USA), unless noted differently. Furthermore, all buffer and solutions were diluted with deionized nuclease-free water. One µM aptamer solution was preconditioned with 200 µM Tris-(2-carboxyethyl)-phosphine-hydrochloride (TCEP) for 20 min for the reduction of disulfides, as described by Reich et al. [21]. Afterwards, the mixture was heated up to 95 °C for 5 min to break up hybridizations and potentially avoid incorrect folding. Cooling to room temperature then enabled the correct and functional folding of the oligonucleotides.

Only the working electrode should be functionalized with oligonucleotides. Thus, the top part of the 3D-printed cell was chosen, which was only enclosing the working electrode of the SPE.

When functionalizing the SPE with oligonucleotides, a balance has to be found between a high surface coverage density, which allows for a high capture capacity, and correct folding of the aptamer, which can be hampered at high immobilization density and, thus, hinder target binding [52]. Co-immobilization with mercaptohexanol (MCH) can be beneficial for a functional and well-ordered oligonucleotide monolayer. As a co-immobilized chemical, MCH has been found to support an upright position of immobilized DNA strands and can be used to control the aptamer density on the surface. Both contribute to correctly folded and functional aptamers. Another purpose is to fill in gaps on the gold surface. MCH blocks possible interaction sites and, thus, supports proper folding of the DNA oligonucleotides [21,53]. However, MCH can also displace aptamers. Therefore, a balance of concentration and incubation time has to be found [21]. The organization of the DNA strands to an ordered monolayer can take more than 8 h [21,54]. Therefore, to ensure a correct arrangement, the co-immobilization of aptamer and MCH was performed in an incubation step over night (for at least 15 h). Furthermore, in previous studies a ratio of 1:20 (1 µM aptamer and 20 µM MCH) was indicated as most suitable. Thus, this ratio was used for biosensing experiments [55].

In brief, reduced aptamer solution was mixed with 20 µM 6-mercapto-1-hexanol (MCH, 99%) for co-immobilization and 100 µL were applied on the working electrode in the corresponding 3D-printed static flow cell. As a precautionary measure, the system was placed in a wet chamber to additionally prevent evaporation. After immobilization was carried out at room temperature overnight, the solution was removed and electrodes were washed three times with SB. As an additional blocking step, the working electrode was exposed to 1 mM MCH for 15 min and subsequently washed again three times with SB [55].

After the MCH blocking step, all electrodes were exposed to boiling water for 2 min to break up hybridizations and then washed three times with SB (see Figure 1). As illustrated in Figure 1, aptamer structures could still possess incorrect folding or interactions. Breaking up the hybridizations can rectify incorrect folding and, thus, nonfunctioning aptamers. The next step was the incubation in SB for 30 min at room temperature to promote correct folding of the aptamer. Subsequently, electrochemical impedance spectroscopy (EIS) measurements were performed (see Section 2.2.4).
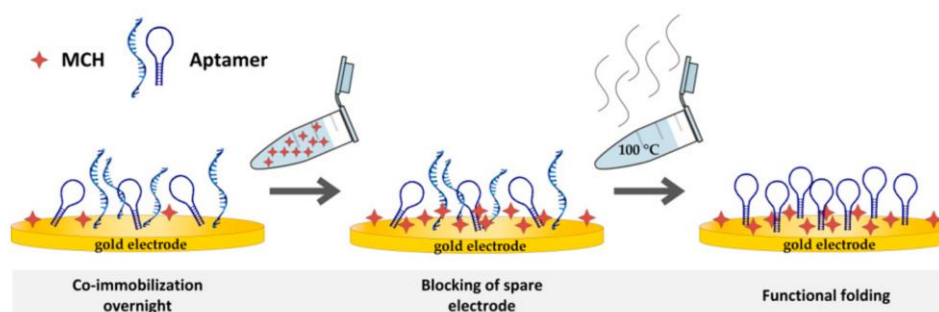

Figure 1. Schematic illustration of biosensor preparation. Co-immobilization step overnight, mercaptohexanol (MCH) blocking, and boiling step.

2.2.4. Biosensor Experiment with Bacteria in 3D-Printed Static Flow Cell

With the aptamer-functionalized SPE mounted in the 3D-printed static flow cell, kinetic EIS measurements were conducted. As described in previous studies, all EIS measurements were performed in ferri-/ferrocyanide buffer (FeSB) containing 2 mM potassiumhexacyanoferrate (II) and (III) ($K_3[Fe(CN)_6]$; $K_4[Fe(CN)_6]$, equimolar) in SB [21,49]. For all biosensor measurements, the top part enclosing all electrodes for the 3D-printed static flow cell was used. Impedance was measured at open circuit potential at an amplitude of 10 mV Root Mean Square (RMS) at 7 logarithmic spaced frequencies per decade in the range of 200.000–0.1 Hz, as these parameters have proven to be suitable in previous studies related to this subject [21,49]. Measurements were repeated four times, whereas the last three cycles were included in fitting and analysis. Spectra were fitted to the modified Randles circuit, which describes the present circuit between the electrodes [3]. Here, R_{sol} represents the solution resistance, R_{ct} is the charge transfer (interface) resistance, W represents the Warburg element (diffusion of ions to electrodes), and CPE is the constant phase element for the double layer at the surface. R_{ct} was chosen for further analysis since a binding event on the surface especially affects the charge transfer [21,49,56].

As a control for the biosensing experiment, electrochemical impedance was measured of the aptamer-functionalized SPE (before *E. coli* samples were applied on electrodes). Afterwards, electrodes on the SPE were washed with SB and dried before the prepared *E. coli* cell sample (100 µL) was applied to the working electrode and incubated for 1 h. Electrodes were thoroughly washed three times with SB and EIS was performed subsequently.

For regeneration of the aptamer-functionalized SPEs, the bacterial sample was removed, electrodes were washed thoroughly with SB, and the surfaces were exposed to boiling water for 2 min. After washing steps and incubation in SB (30 min, room temperature), SPEs were ready for another biosensing experiment.

2.3. Experiments in Dynamic 3D-Printed Microfluidic Flow Cell

The 3D-printed flow cell presented here features a micromixer upstream of the system, which ensures a homogeneously mixed solution before it reaches the electrodes. The mixer, known as HC-mixer, makes use of a split-and-recombine technique and H-shaped channel modules to intensify and enhance mixing performance [57,58]. The mixer was designed according to Enders et al. and connections to the tube and pump system were set up [58]. Right behind the micromixer unit, a fluid chamber enclosing the relevant electrodes of the SPE was integrated. The fluid chamber enclosing all electrodes of the SPE holds a volume of 30 µL. For connection of the microfluidic system to syringes and the pump system, the design of the system was adapted to the dimensions of a Dolomite 4-way microfluidic connector (Dolomite Center Ltd., Royston, UK). A syringe pump (AL-100, World Precision Instruments, Sarasota, FL, USA) was taken for this study.

The mixing performance of the integrated micromixer unit was determined by computational fluid dynamics (CFD) simulation experiments and compared with a reference design (T-mixer). CFD simulations were performed using COMSOL Multiphysics 5.4 (COMSOL Inc., Stockholm, Sweden). For the simulation, an aqueous liquid with a corresponding density (1 g cm $^{-1}$) and dynamic viscosity (1000×10^6 kg m^{-1} s^{-1}) was set. Flow rate of 3 µL s^{-1} for both inlets was chosen and a laminar flow as present in microfluidic channels was assumed. To simulate mixing, a solute concentration of 1 mol m^{-3} at one inlet and 0 mol m^{-3} at the other inlet was defined. A diffusion coefficient of 10^{-9} m^2 s^{-1} was set, presenting a commonly used constant [58,59]. Remaining simulation settings were chosen according to Enders et al. [58].

Practical experiments with the two-mixer designs (T-mixer and HC-mixer) were performed to confirm the results of the simulations. Acidic 100 mM sodium dihydrogen phosphate and basic 50 mM di-potassium hydrogen phosphate (both from Carl Roth GmbH, Karlsruhe, Germany) with 50% (v/v) (volume concentration) bromothymol blue solution (Sigma-Aldrich, St. Louis, MO, USA) were used to visualize mixing. Bromothymol blue indicates acidic pH by a yellow color, neutral pH by a green color, and basic pH by a blue color. In selecting the concentrations, care was taken to ensure that equal proportions of both solutions resulted in a neutral pH value (green). For the experiments, a flow rate of 3 µL s^{-1} was set at each inlet for 1 min to ensure a steady state. Pictures were taken using a digital microscope (VHX-6000 digital microscope, KEYENCE Deutschland GmbH, Neu-Isenburg, Germany). The magnification was set to 30×.

3. Results and Discussion

3.1. Introduction of Static 3D-Printed Flow Cell

For performing biosensing experiments with SPEs, a static cell was designed and 3D printed. It consisted of two parts—a bottom and a top part. Both parts held a slot specifically adapted to the dimensions of the SPE that was providing the necessary support and ensured a firm fit in the static flow cell. The top part included a cavity, focusing the corresponding electrodes of the SPE, which enabled the exposure of electrodes to a defined volume of liquid, such as buffer solutions or bacteria samples. During the biosensing experiment, the top part of the static flow cell has to be exchanged. Only the working electrode should be functionalized with aptamers, whereas for electrochemical measurements all electrodes have to be in contact with the respective buffer solution. Therefore, two exchangeable top parts were designed—one enclosing only the working electrode of the SPE and one enclosing all electrodes. Changing the top parts required easy (dis)assembly while holding sufficient sealing at the same time. This was guaranteed by magnets and an O-ring, which was perfectly enclosing the corresponding electrodes (see Figure 2).
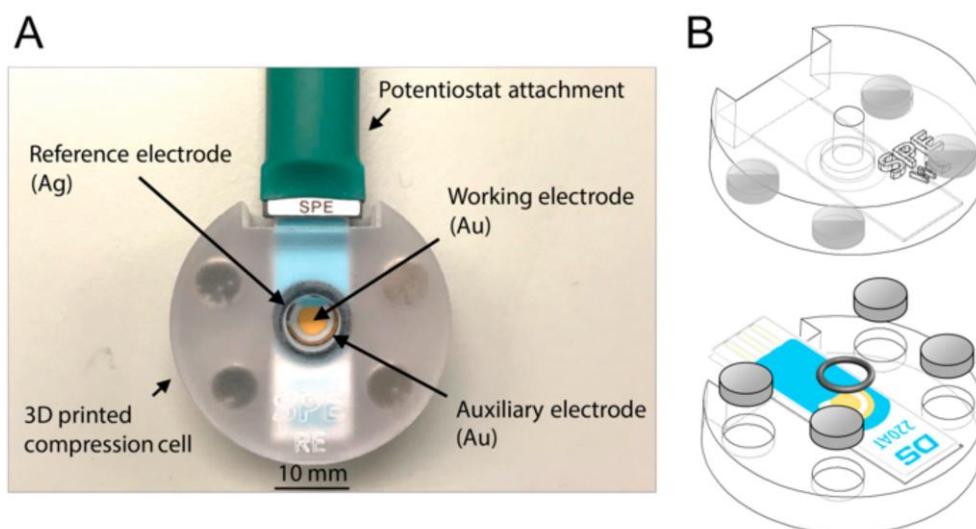
Figure 2. Image of the 3D-printed static flow cell with mounted screen-printed electrode (SPE) and connected cable (**A**) and illustration of the setup (here with top part enclosing only the working electrode of SPE) (**B**).

3D printing technology not only opened the door to the production of small batches or prototypes in a short amount of time, it also allows researchers to create individually designed experimental setups and devices of almost unlimited complexity, leaving them no longer reliant on commercially available goods. There are several reports on custom cell systems, for example, made of methyl methacrylate material or glass, that supported electrochemical measurements [10,60]. However, traditional manufacturing methods are often disadvantageous as they involve time-consuming process steps that often require special training, resulting in an overall laborious and cost-intensive process.

The 3D printing material used in this study is considered to be (in vitro) biocompatible, as has been shown in previous publication [61]. Therefore, the material is suitable for biotechnological applications. Furthermore, the chemical stability against ethanol or isopropyl alcohol solvents, which are frequently used in the laboratory for material disinfection, was also shown [61]. Since a variety of different 3D printing materials are already commercially available, compatible material with suitable properties can be selected for the most diverse applications and experimental requirements. Autoclavable 3D printing materials are also available, ensuring sterility of 3D-printed parts for biological applications.

3.2. Biosensing Experiments

To verify the successful aptamer immobilization on the working electrode, EIS measurements were conducted. Impedance is a mathematically complex value that consists of a real and an imaginary part. A common presentation of the data is to plot the real and imaginary parts against each other (Nyquist plot). Each point on the plot presents the impedance parts at one frequency. A comparison of Nyquist plots before and after aptamer functionalization is shown in Figure 3. A significant increase in impedance can be observed after aptamer is immobilized. Due to the immobilized oligonucleotides on the gold surface, the electron transfer is hindered and impedance increases.
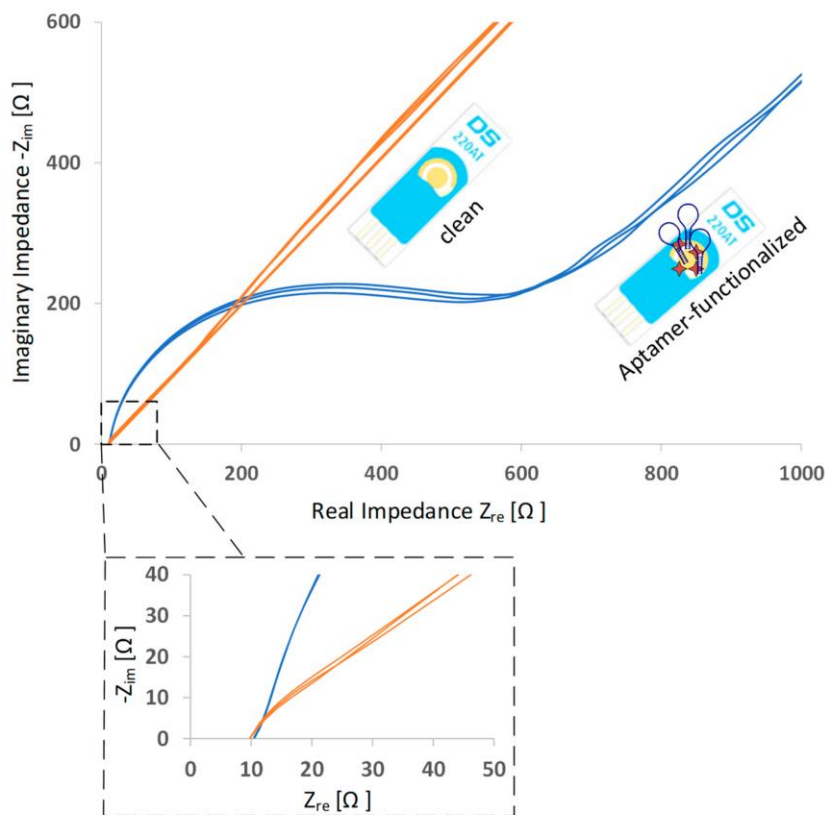
Figure 3. Typical electrochemical impedance spectra (Nyquist plots) before and after aptamer immobilization. The number of spectra curves in one graph indicate the number of EIS cycles.

The general principle of an aptamer-based impedimetric detection of a target involves a redox probe, which is supplied in a buffer solution. The redox probe is responsible for the electron transfer from the working electrode to the counter electrode. Here, the ferri-/ferrocyanide couple was used as a redox probe due to its fast electron transfer rate [62]. To assess the applicability of the 3D-printed static flow cell in combination with the SPE for detection of *E. coli* Crooks strain, direct capture experiments with *E. coli* were performed as proof of concept (see Figure 4).

Figure 4. Schematic illustration of aptasensor experiment.

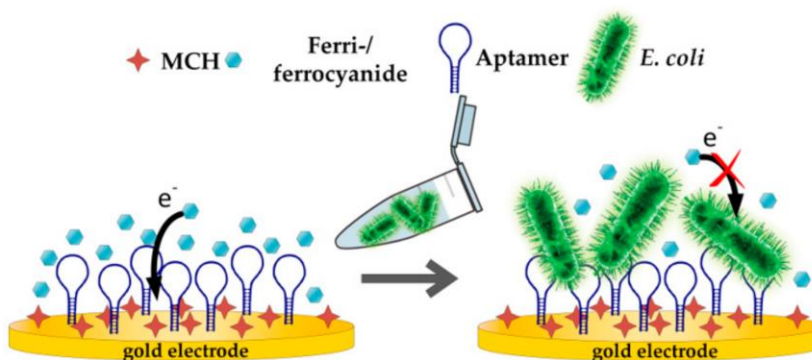After the SPE was functionalized and prepared, samples with varying *E. coli* Crooks strain concentrations were loaded onto the electrodes by means of the 3D-printed static flow cell and EIS was conducted. As mentioned in Section 2.2.4. electrochemical impedance data were fitted to the modified Randles circuit, subsequently, and the charge transfer (interface) resistance (R_{ct}) was chosen as parameter for analysis (see Figure 5). It was expected that upon binding of *E. coli* Crooks strain, the electron transfer between electrode and buffer solution containing the redox probe was influenced and that this was reflected in an altered R_{ct}.
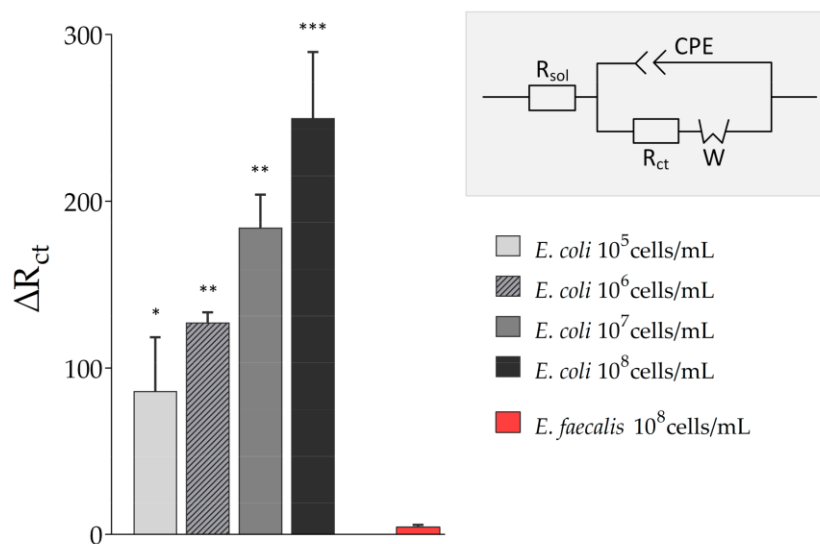

Figure 5. Results of biosensing experiments. Electrochemical Impedance Spectroscopy (EIS) measurements of biosensor experiments with varying *Escherichia coli* Crooks and *Enterococcus faecalis* (*E. faecalis*) concentrations were fitted to the modified Randles circuit with R_{sol}: solution resistance, R_{ct}: charge-transfer resistance, W: Warburg impedance, and CPE: constant phase element. Extracted charge transfer resistance ΔR_{ct} is displayed. All experiments were repeated several times in independent experiments (technical replicates, n = 3) and significant differences to *Enterococcus faecalis* as a control are indicated: * $p < 0.05$, ** $p < 0.01$, *** $p < 0.001$.

The charge transfer resistance (R_{ct}) increased with the concentration of *E. coli* in the sample solution (from $\Delta R_{ct} = 86.25 \pm 32.31$ at 10^5 cells/mL *E. coli* to $\Delta R_{ct} = 249.99 \pm 39.58$ at 10^8 cells/mL *E. coli*). The more *E. coli* cells that were present in the sample, the higher and more substantial was the influence on the electron transfer between electrode and redox probe. However, even low concentrations of *E. coli* Crooks strain were detectable. In addition, no cross-reactivity of the aptamer used in this study was observed, here to *Enterococcus faecalis*, and other previous published work already reported no or no significant binding of the used aptamer to *Staphylococcus aureus*, *Salmonella typhimurium*, or *E. coli* K12 [25].

After one biosensing run was done, the aptamer-functionalized SPE was regenerated in a cleaning step with boiling water. Thereby, aptamer structures unfold and potential captured targets (here, whole *E. coli*) can be released. A subsequent incubation step in aptamer selection buffer allowed the oligonucleotides to fold again in functional conformation and the biosensor was ready for another biosensing experiment. Nyquist plots of EIS indicated that the regeneration step successfully restored the SPE: The electrochemical condition of the regenerated SPE was identical to the status before sample incubation (see Figure 6). Aptamer structures were successfully regenerated.
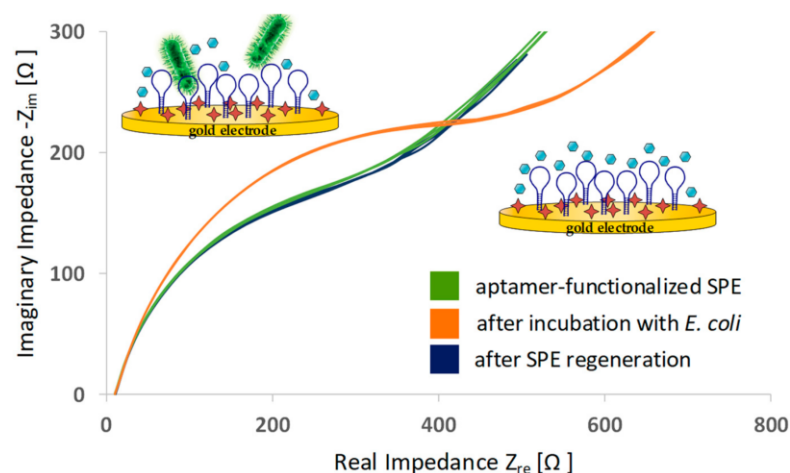
Figure 6. Typical electrochemical impedance data (Nyquist plots) of aptamer-functionalized SPE, after a biosensing run with *E. coli* and after regeneration of the SPE. The number of spectra curves in one graph indicates the number of EIS cycles.

The custom-designed, 3D-printed static flow cell has proven to be a prerequisite for performing the biosensing experiment—the 3D-printed system not only provides a stable fit of the SPE and thereby facilitates the handling, it also enables accurate washing and incubations with defined volumes of liquids. An exchangeable top part allows for the selective treatment of only the working electrode or all electrodes by the choice of top. Without this feature, a biosensing experiment following the approach of this study would have been difficult to carry out.

In all, aptamer functionalization of the mounted SPE and subsequent direct capture experiments with *E. coli* Crooks strain were successfully performed in a 3D-printed static flow cell. Due to the electrochemical detection method, bacteria were detected label-free, without the need of laborious and costly labeling procedures. With the use of aptamers as biological recognition element, a highly selective and sensitive biosensor was created. The aptamer used in this study has already been intensively characterized [25,26,63] but, to the best knowledge of the authors, it has never been used in combination with a 3D-printed chamber. The 3D printing material, in general and particularly the customized 3D-printed static flow cell, have proven to be expedient and beneficial in the context of electrochemical sensors. In fact, the 3D-printed static cell could find application in all kinds of SPE-based electrochemical studies.

3.3. Investigation of 3D-Printed Microfluidic Dynamic Flow Cell for SPE Applications

The 3D-printed static flow cell introduced in this study is based on manually performed washing and incubation steps. However, an automated flow cell system may be profitable in other aspects or for other applications. There are several reports demonstrating the advantages of flow systems for SPE applications [10,64]. A consistent, continuous liquid flow may improve washing or lower the limit of detection (LOD) of aptasensors. In addition, an automated system has great potential to improve reproducibility and lower the workload. Here, 3D printing technology offers tremendous potential for the rapid fabrication of complex flow systems that can be integrated in pump systems for automation.

A 3D-printed dynamic flow cell for SPE applications is shown in Figure 7A. The flow cell has three inlets and an outlet, which can be connected directly to sample and reagent solutions via tubing. The inflow and outflow into the flow cell can thus be controlled and enables reproducible and continuous sample processing. To enable mixing-dependent applications with the flow cell, a microfluidic HC-mixer was integrated upstream of the fluid chamber and the mixing performance was compared with an integrated T-mixer, referring to a T-shaped channel module [58].
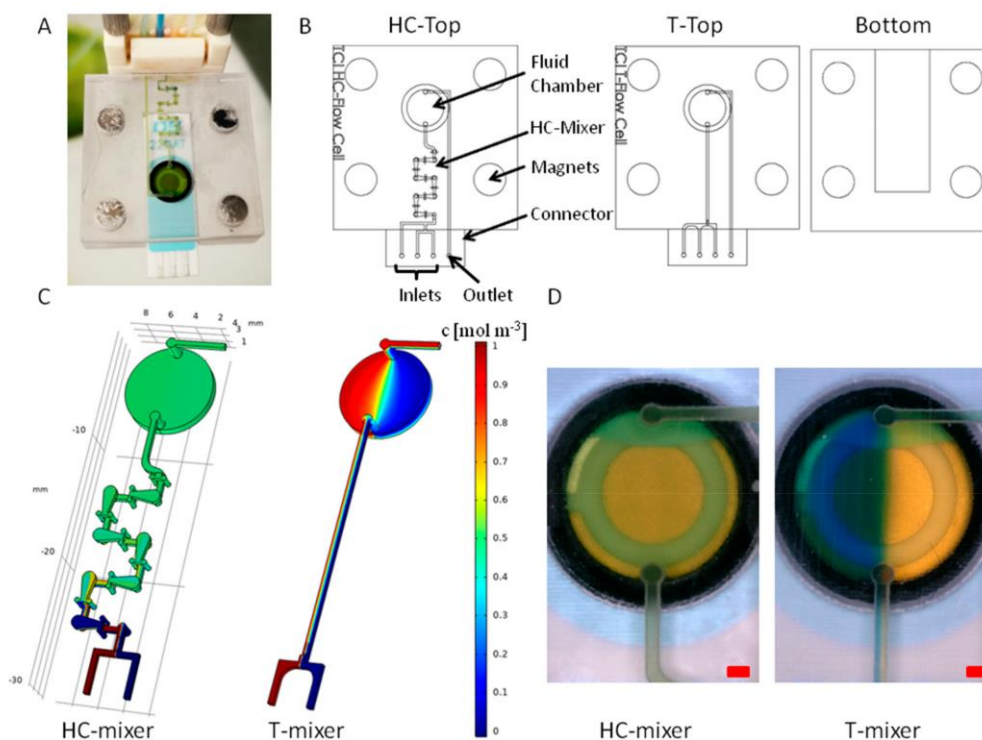
Figure 7. (**A**) Image of a 3D-printed dynamic flow cell with an integrated SPE. (**B**) computer-aided design (CAD) drawings of the top parts with HC-mixer and T-mixer and the bottom part of the flow cells. (**C**) COMSOL simulation of the interior structure of the dynamic flow cells (inlet flow rates of each 3 μL s^{-1}). The left inlet and the right inlet were simulated with concentrations of 1 mol m^{-3} and 0 mol m^{-3}, respectively (see legend). (**D**) Pictures of the fluid chambers during mixing experiments with flow rates of 3 μL s^{-1} for both inlets. Yellow-colored solution was pumped into the left inlet and blue-colored solution into the right inlet. The red scale bar represents 1 mm width.

The mixing performance of the integrated micromixer units was analyzed in both by CFD simulation and in practical experiments. For an overview, Figure 7A,B shows a picture of an assembled dynamic flow cell and CAD drawings of the individual parts, respectively. The mixing efficiency was determined by simulation (see Figure 7C). A homogeneous mixing is shown as green (0.5 mol m^{-3}), while no mixing is shown as blue (0 mol m^{-3}) and red (1 mol m^{-3}). After four of seven subunits of the HC-mixer, a homogeneous mixing was evident. The simulation with a T-mixer showed that there was almost no mixing of the liquids within the channel. Therefore, most parts of the liquid chamber appeared blue and red. This is due to the laminar flow present in microfluidic channels, which is why diffusion is the only mixing effect in straight microfluidic channels [58]. These results were confirmed by practical experiments. Since a homogeneous mixing with equal proportions of the solutions used resulted in a neutral pH value, a color change from blue or yellow to green is an indicator of successful mixing. The integration of an HC-mixer resulted in a uniform green color inside of the fluid chamber (see Figure 7A,D). In contrast, the T-mixer showed a mostly two-part segmentation of the liquids (right side is yellow, left side is blue). Between the segments, a narrow, green transition area was visible, which indicates a certain diffusive mixing, but not a homogeneous mixing within the fluid chamber of the flow cell.

Both the simulation and the practical experiments demonstrated the excellent and superior performance of the HC-mixer. The HC-mixer ensures a rapid and homogeneous mixing and is, therefore, of great interest for integration into 3D-printed flow cells–especially when using small

sample volumes. A possible application of the flow cell presented here is the automated and time-controlled incubation of buffers, aptamer, and sample solutions. Concentration gradients can be run or sample concentrations can be adjusted automatically. The integrated micromixer allows for a fast and efficient mixing of reagents and/or mixing of the sample before it comes into contact with the electrodes of a mounted SPE. In future work, sensor experiments with real samples have to be performed to validate the functionality of the 3D-printed dynamic flow cell.

4. Conclusions

This work demonstrates the successful development of a 3D-printed static flow cell for SPE-based applications. An aptamer-based impedimetric detection of *E. coli* Crooks strain as a proof of concept served to demonstrate the successful implementation of the system. With the use of commercially available SPEs, we presented not only a cost-effective and disposable alternative to bulk electrodes, but, moreover, demonstrated regeneration and reuse of the biosensor. Electrochemical biosensing experiments performed in 3D-printed static flow cell showed sensitive and selective binding to the target, even after multiple SPE regenerations. In summary, the direct capture biosensor presented rapid and sensitive detection without the need of costly labeling procedures or laborious sample preparation. The customized 3D-printed static flow cell proved to be indispensable for performing a biosensing experiment. The intensive/various washing and incubation steps required would have been difficult to perform without the 3D-printed system. In fact, the 3D-printed cells could serve as a fundamental base for SPE-based biosensors of any kind. The basic design allows easy fabrication with almost all 3D printing technologies and also allows researchers to customize the system to their applications and specifications.

A dynamic, 3D-printed microfluidic flow cell was presented, which enabled automated control of the fluid flow. By integration of a micromixer unit into the design, a homogeneous mixing of solutions prior to electrochemical measurement was provided. This not only replaces intensive, manually performed mixing steps, but also contributes to reproducible measurements and experiments. In combination with an automated pumping system, the fluid flow can be controlled from continuous (e.g., for washing the electrodes) to paused flow (e.g., to allow time-dependent incubations).

Compared to commercially available static and dynamic flow cells, the 3D-printed cells presented here are much more cost-effective. Depending on the 3D printing technology and printer system used, fabrication and labor costs may vary. The production of the ready-to-use 3D-printed cells in the proposed printer system cost a total of about \$18, taking into account material consumption and all consumables used, whereas comparable commercially available systems made of polytetrafluoroethylene (PTFE) are more than 50 times more expensive. As the operation of most 3D printers and the design of objects with CAD software is easy to use and does not require special training, the entire manufacturing process can be carried out with little training. In addition, 3D printing technology enables fabrication of experiment-specific devices on demand, directly on site in the laboratory. In case no 3D printer is available on site, commercial or academic 3D printing services offer contract printing at low cost.

This study demonstrated the great potential of customizable 3D-printed devices. Holding almost unlimited design options, 3D printing technology is of incredible interest for rapid fabrication of experiment-specific labware, test equipment, or whole test systems. With immense flexibility, 3D printing technology provides a platform for individual adaptations or system integrations, as well as the parallelization of complex systems. That way, not only electrochemical biosensing can benefit from 3D printing technology, but all scientific disciplines.

References

1. Preuß, J.A.; Reich, P.; Bahner, N.; Bahnemann, J. Impedimetric Aptamer-Based Biosensors: Applications. *Adv. Biochem. Eng. Biotechnol.* **2020**, *174*, 1–49.
2. Dastider, S.G.; Barizuddin, S.; Dweik, M.; Almasri, M.F. Impedance Biosensor Based on Interdigitated Electrode Array for Detection of *E. coli* O157:H7 in Food Products. In *Sensing for Agriculture and Food Quality and Safety Iv*; Kim, M.S., Tu, S.I., Chao, K., Eds.; Spie-Int Soc Optical Engineering: Bellingham, WA, USA, 2012.
3. Gamella, M.; Campuzano, S.; Parrado, C.; Reviejo, A.J.; Pingarron, J.M. Microorganisms Recognition and Quantification by Lectin Adsorptive Affinity Impedance. *Talanta* **2009**, *78*, 1303–1309. [CrossRef] [PubMed]
4. Bhardwaj, N.; Bhardwaj, S.K.; Mehta, J.; Mohanta, G.C.; Deep, A. Bacteriophage Immobilized Graphene Electrodes for Impedimetric Sensing of Bacteria (Staphylococcus arlettae). *Anal. Biochem.* **2016**, *505*, 18–25. [CrossRef] [PubMed]
5. Stoltenburg, R.; Reinemann, C.; Strehlitz, B. Selex-a (R)Evolutionary Method to Generate High-Affinity Nucleic Acid Ligands. *Biomol. Eng.* **2007**, *24*, 381–403. [CrossRef] [PubMed]
6. Ellington, A.D.; Szostak, J.W. In Vitro Selection of Rna Molecules That Bind Specific Ligands. *Nature* **1990**, *346*, 818–822. [CrossRef] [PubMed]
7. O'Sullivan, C.K. Aptasensors—The Future of Biosensing. *Anal. Bioanal. Chem.* **2002**, *372*, 44–48. [CrossRef] [PubMed]
8. Posha, B.; Nambiar, S.R.; Sandhyarani, N. Gold Atomic Cluster Mediated Electrochemical Aptasensor for the Detection of Lipopolysaccharide. *Biosens. Bioelectron.* **2018**, *101*, 199–205. [CrossRef]
9. Jimenez, G.C.; Eissa, S.; Ng, A.; Alhadrami, H.; Zourob, M.; Siaj, M. Aptamer-Based Label-Free Impedimetric Biosensor for Detection of Progesterone. *Anal. Chem.* **2015**, *87*, 1075–1082. [CrossRef]
10. Rhouati, A.; Hayat, A.; Hernandez, D.B.; Meraihi, Z.; Munoz, R.; Marty, J.L. Development of an Automated Flow-Based Electrochemical Aptasensor for on-Line Detection of Ochratoxin A. *Sens. Actuators B Chem.* **2013**, *176*, 1160–1166. [CrossRef]
11. Qureshi, A.; Gurbuz, Y.; Niazi, J.H. Capacitive Aptamer-Antibody Based Sandwich Assay for the Detection of Vegf Cancer Biomarker in Serum. *Sens. Actuators B Chem.* **2015**, *209*, 645–651. [CrossRef]
12. Tabrizi, M.A.; Shamsipur, M.; Farzin, L. A High Sensitive Electrochemical Aptasensor for the Determination of Vegf (165) in Serum of Lung Cancer Patient. *Biosens. Bioelectron.* **2015**, *74*, 764–769. [CrossRef] [PubMed]
13. Shekari, Z.; Zare, H.R.; Falahati, A. Developing an Impedimetric Aptasensor for Selective Label-Free Detection of Cea as a Cancer Biomarker Based on Gold Nanoparticles Loaded in Functionalized Mesoporous Silica Films. *J. Electrochem. Soc.* **2017**, *164*, B739–B745. [CrossRef]
14. Mazzaracchio, V.; Neagu, D.; Porchetta, A.; Marcoccio, E.; Pomponi, A.; Faggioni, G.; D'Amore, N.; Notargiacomo, A.; Pea, M.; Moscone, D.; et al. A Label-Free Impedimetric Aptasensor for the Detection of Bacillus Anthracis Spore Simulant. *Biosens. Bioelectron.* **2019**, *126*, 640–646. [CrossRef] [PubMed]
15. Jia, F.; Duan, N.; Wu, S.J.; Dai, R.T.; Wang, Z.P.; Li, X.M. Impedimetric Salmonella Aptasensor Using a Glassy Carbon Electrode Modified with an Electrodeposited Composite Consisting of Reduced Graphene Oxide and Carbon Nanotubes. *Microchim. Acta* **2016**, *183*, 337–344. [CrossRef]
16. Ranjbar, S.; Shahrokhian, S.; Nurmohammadi, F. Nanoporous Gold as a Suitable Substrate for Preparation of a New Sensitive Electrochemical Aptasensor for Detection of Salmonella typhimurium. *Sens. Actuators B Chem.* **2018**, *255*, 1536–1544. [CrossRef]
17. Burrs, S.L.; Bhargava, M.; Sidhu, R.; Kiernan-Lewis, J.; Gomes, C.; Claussen, J.C.; McLamore, E.S. A Paper Based Graphene-Nanocauliflower Hybrid Composite for Point of Care Biosensing. *Biosens. Bioelectron.* **2016**, *85*, 479–487. [CrossRef]

18. Yao, L.; Wang, L.; Huang, F.C.; Cai, G.Z.; Xi, X.G.; Lin, J.H. A Microfluidic Impedance Biosensor Based on Immunomagnetic Separation and Urease Catalysis for Continuous-Flow Detection of *E. coli* O157:H7. *Sens. Actuators B Chem.* **2018**, *259*, 1013–1021. [CrossRef]

19. Vanegas, D.C.; Rong, Y.; Schwalb, N.; Hills, K.D.; Gomes, C.; McLamore, E.S. Rapid Detection of Listeria Spp. Using an Internalin a Aptasensor Based on Carbon-Metal Nanohybrid Structures. In *Smart Biomedical and Physiological Sensor Technology Xii*; Cullum, B.M., McLamore, E.S., Eds.; Spie-Int Soc Optical Engineering: Bellingham, WA, USA, 2015.

20. Lee, Y.J.; Han, S.R.; Maeng, J.S.; Cho, Y.J.; Lee, S.W. In Vitro Selection of *Escherichia coli* O157:H7-Specific Rna Aptamer. *Biochem. Biophys. Res. Commun.* **2012**, *417*, 414–420. [CrossRef]

21. Reich, P.; Stoltenburg, R.; Strehlitz, B.; Frense, D.; Beckmann, D. Development of an Impedimetric Aptasensor for the Detection of Staphylococcus aureus. *Int. J. Mol. Sci.* **2017**, *18*, 18. [CrossRef]

22. Jia, F.; Duan, N.; Wu, S.J.; Ma, X.Y.; Xia, Y.; Wang, Z.P.; Wei, X.L. Impedimetric Aptasensor for Staphylococcus Aureus Based on Nanocomposite Prepared from Reduced Graphene Oxide and Gold Nanoparticles. *Microchim. Acta* **2014**, *181*, 967–974. [CrossRef]

23. Zhao, Y.W.; Wang, H.X.; Jia, G.C.; Li, Z. Application of Aptamer-Based Biosensor for Rapid Detection of Pathogenic Escherichia coli. *Sensors* **2018**, *18*, 16. [CrossRef] [PubMed]

24. Cesewski, E.; Johnson, B.N. Electrochemical Biosensors for Pathogen Detection. *Biosens. Bioelectron.* **2020**, *159*, 29. [CrossRef] [PubMed]

25. Brosel-Oliu, S.; Ferreira, R.; Uria, N.; Abramova, N.; Gargallo, R.; Munoz-Pascual, F.X.; Bratov, A. Novel Impedimetric Aptasensor for Label-Free Detection of *Escherichia coil* O157:H7. *Sens. Actuators B Chem.* **2018**, *255*, 2988–2995. [CrossRef]

26. Abdelrasoul, G.N.; Anwar, A.; MacKay, S.; Tamura, M.; Shah, M.A.; Khasa, D.P.; Montgomery, R.R.; Ko, A.I.; Chen, J. DNA Aptamer-Based Non-Faradaic Impedance Biosensor for Detecting *E. coli*. *Anal. Chim. Acta* **2020**, *1107*, 135–144. [CrossRef]

27. Queiros, R.B.; de-los-santos-Alvarez, N.; Noronha, J.P.; Sales, M.G.F. A Label-Free DNA Aptamer-Based Impedance Biosensor for the Detection of *Escherichia coli* Outer Membrane Proteins. *Sens. Actuators B Chem.* **2013**, *181*, 766–772. [CrossRef]

28. Campuzano, S.; Yanez-Sedeno, P.; Pingarron, J.M. Electrochemical Biosensing for the Diagnosis of Viral Infections and Tropical Diseases. *Chemelectrochem* **2017**, *4*, 753–777. [CrossRef]

29. Tudorache, M.; Bala, C. Biosensors Based on Screen-Printing Technology, Their Applications in Environmental and Food Analysis. *Anal. Bioanal. Chem.* **2007**, *388*, 565–578. [CrossRef]

30. Li, Z.M.; Ye, Z.Z.; Fu, Y.C.; Xiong, Y.H.; Li, Y.B. A Portable Electrochemical Immunosensor for Rapid Detection of Trace Aflatoxin B-1 in Rice. *Anal. Methods* **2016**, *8*, 548–553. [CrossRef]

31. Ding, J.N.; Zhang, D.W.; Liu, Y.; Yu, M.L.; Zhan, X.J.; Zhang, D.; Zhou, P. An Electrochemical Aptasensor for Detection of Lead Ions Using a Screen-Printed Carbon Electrode Modified with Au/Polypyrrole Composites and Toluidine Blue. *Anal. Methods* **2019**, *11*, 4274–4279. [CrossRef]

32. Tabrizi, M.A.; Shamsipur, M.; Saber, R.; Sarkar, S.; Besharati, M. An Electrochemical Aptamer-Based Assay for Femtomolar Determination of Insulin Using a Screen Printed Electrode Modified with Mesoporous Carbon and 1,3,6,8-Pyrenetetrasulfonate. *Microchim. Acta* **2018**, *185*, 7.

33. Hashkavayi, A.B.; Raoof, J.; Ojani, R. Construction of a Highly Sensitive Signal-on Aptasensor Based on Gold Nanoparticles/Functionalized Silica Nanoparticles for Selective Detection of Tryptophan. *Anal. Bioanal. Chem.* **2017**, *409*, 6429–6438. [CrossRef] [PubMed]

34. Berdat, D.; Rodriguez, A.C.M.; Herrera, F.; Gijs, M.A.M. Label-Free Detection of DNA with Interdigitated Micro-Electrodes in a Fluidic Cell. *Lab Chip* **2008**, *8*, 302–308. [CrossRef] [PubMed]

35. Wang, Y.X.; Ye, Z.Z.; Ping, J.F.; Jing, S.R.; Ying, Y.B. Development of an Aptamer-Based Impedimetric Bioassay Using Microfluidic System and Magnetic Separation for Protein Detection. *Biosens. Bioelectron.* **2014**, *59*, 106–111. [CrossRef] [PubMed]

36. Krejcova, L.; Nejdl, L.; Rodrigo, M.A.M.; Zurek, M.; Matousek, M.; Hynek, D.; Zitka, O.; Kopel, P.; Adam, V.; Kizek, R. 3d Printed Chip for Electrochemical Detection of Influenza Virus Labeled with Cds Quantum Dots. *Biosens. Bioelectron.* **2014**, *54*, 421–427. [CrossRef]

37. Damiati, S.; Kupcu, S.; Peacock, M.; Eilenberger, C.; Zamzami, M.; Qadri, I.; Choudhry, H.; Sleytr, U.B.; Schuster, B. Acoustic and Hybrid 3d-Printed Electrochemical Biosensors for the Real-Time Immunodetection of Liver Cancer Cells (Hepg2). *Biosens. Bioelectron.* **2017**, *94*, 500–506. [CrossRef]

38. Kuralay, F.; Campuzano, S.; Haake, D.A.; Wang, J. Highly Sensitive Disposable Nucleic Acid Biosensors for Direct Bioelectronic Detection in Raw Biological Samples. *Talanta* **2011**, *85*, 1330–1337. [CrossRef]

39. Cheng, M.S.; Lau, S.H.; Chan, K.P.; Toh, C.S.; Chow, V.T. Impedimetric Cell-Based Biosensor for Real-Time Monitoring of Cytopathic Effects Induced by Dengue Viruses. *Biosens. Bioelectron.* **2015**, *70*, 74–80. [CrossRef]

40. Dirkzwager, R.M.; Liang, S.L.; Tanner, J.A. Development of Aptamer-Based Point-of-Care Diagnostic Devices for Malaria Using Three-Dimensional Printing Rapid Prototyping. *ACS Sens.* **2016**, *1*, 420–426. [CrossRef]

41. Zhang, C.G.; Chang, S.J.; Settu, K.; Chen, C.J.; Liu, J.T. High-Sensitivity Glycated Hemoglobin (Hba1c) Aptasensor in Rapid-Prototyping Surface Plasmon Resonance. *Sens. Actuators B Chem.* **2019**, *279*, 267–273. [CrossRef]

42. Ude, C.; Hentrop, T.; Lindner, P.; Lucking, T.H.; Scheper, T.; Beutel, S. New Perspectives in Shake Flask Ph Control Using a 3d-Printed Control Unit Based on Ph Online Measurement. *Sens. Actuators B Chem.* **2015**, *221*, 1035–1043. [CrossRef]

43. Coakley, M.; Hurt, D.E. 3d Printing in the Laboratory: Maximize Time and Funds with Customized and Open-Source Labware. *JALA* **2016**, *21*, 489–495. [CrossRef] [PubMed]

44. Lucking, T.H.; Sambale, F.; Beutel, S.; Scheper, T. 3d-Printed Individual Labware in Biosciences by Rapid Prototyping: A Proof of Principle. *Eng. Life Sci.* **2015**, *15*, 51–56. [CrossRef]

45. Siller, I.G.; Enders, A.; Gellermann, P.; Winkler, S.; Lavrentieva, A.; Scheper, T.; Bahnemann, J. Characterization of a Customized 3d-Printed Cell Culture System Using Clear, Translucent Acrylate That Enables Optical Online Monitoring. *Biomed. Mater.* **2020**, *15*, 055007. [CrossRef] [PubMed]

46. Motaghi, H.; Ziyaee, S.; Mehrgardi, M.A.; Kajani, A.A.; Bordbar, A.K. Electrochemiluminescence Detection of Human Breast Cancer Cells Using Aptamer Modified Bipolar Electrode Mounted into 3d Printed Microchannel. *Biosens. Bioelectron.* **2018**, *118*, 217–223. [CrossRef] [PubMed]

47. Tran, H.V.; Piro, B.; Reisberg, S.; Nguyen, L.H.; Nguyen, T.D.; Duc, H.T.; Pham, M.C. An Electrochemical Elisa-Like Immunosensor for Mirnas Detection Based on Screen-Printed Gold Electrodes Modified with Reduced Graphene Oxide and Carbon Nanotubes. *Biosens. Bioelectron.* **2014**, *62*, 25–30. [CrossRef] [PubMed]

48. Ilkhani, H.; Zhang, H.; Zhou, A.H. A Novel Three-Dimensional Microtas Chip for Ultra-Selective Single Base Mismatched Cryptosporidium DNA Biosensor. *Sens. Actuators B Chem.* **2019**, *282*, 675–683. [CrossRef]

49. Henihan, G.; Schulze, H.; Corrigan, D.K.; Giraud, G.; Terry, J.G.; Hardie, A.; Campbell, C.J.; Walton, A.J.; Crain, J.; Pethig, R.; et al. Label- and Amplification-Free Electrochemical Detection of Bacterial Ribosomal Rna. *Biosens. Bioelectron.* **2016**, *81*, 487–494. [CrossRef]

50. Bruno, J.G.; Carrillo, M.P.; Phillips, T.; Andrews, C.J. A Novel Screening Method for Competitive Fret-Aptamers Applied to *Escherichia coli* Assay Development. *J. Fluoresc.* **2010**, *20*, 1211–1223. [CrossRef]

51. Balamurugan, S.; Obubuafo, A.; Soper, S.A.; Spivak, D.A. Surface Immobilization Methods for Aptamer Diagnostic Applications. *Anal. Bioanal. Chem.* **2008**, *390*, 1009–1021. [CrossRef]

52. Katharina, U.; Modrejewski, J.; Scheper, T.; Walter, J.-G. Aptamer-Modified Nanomaterials: Principles and Applications. *BioNanoMaterials* **2016**, *18*, 20160012.

53. Keighley, S.D.; Li, P.; Estrela, P.; Mighorato, P. Optimization of DNA Immobilization on Gold Electrodes for Label-Free Detection by Electrochemical Impedance Spectroscopy. *Biosens. Bioelectron.* **2008**, *23*, 1291–1297. [CrossRef] [PubMed]

54. DeBono, R.F.; Loucks, G.D.; DellaManna, D.; Krull, U.J. Self-Assembly of Short and Long-Chain N-Alkyl Thiols onto Gold Surfaces: A Real-Time Study Using Surface Plasmon Resonance Techniques. *Can. J. Chem.* **1996**, *74*, 677–688. [CrossRef]

55. Urmann, K.; Bahnemann, J.; Chikneyan, Z.; Kasmaee, L.M.; Hoffmann, M.R. Electromechanical Detection of Pathogens with Self-Assembled Nucleic Acid Biosensors. TechConnect Briefs 2, Materials for Energy, Efficiency and Sustainability. *Techconnect Briefs* **2018**, *2018*, 153–156.

56. Corrigan, D.K.; Schulze, H.; Henihan, G.; Ciani, I.; Giraud, G.; Terry, J.G.; Walton, A.J.; Pethig, R.; Ghazal, P.; Crain, J.; et al. Impedimetric Detection of Single-Stranded Pcr Products Derived from Methicillin Resistant Staphylococcus Aureus (Mrsa) Isolates. *Biosens. Bioelectron.* **2012**, *34*, 178–184. [CrossRef]

57. Viktorov, V.; Mahmud, M.R.; Visconte, C. Design and Characterization of a New H-C Passive Micromixer up to Reynolds Number 100. *Chem. Eng. Res. Des.* **2016**, *108*, 152–163. [CrossRef]

58. Enders, A.; Siller, I.G.; Urmann, K.; Hoffmann, M.R.; Bahnemann, J. 3d Printed Microfluidic Mixers—A Comparative Study on Mixing Unit Performances. *Small* **2019**, *15*, 9. [CrossRef]

59. Kim, D.S.; Lee, S.H.; Kwon, T.H.; Ahn, C.H. A Serpentine Laminating Micromixer Combining Splitting/Recombination and Advection. *Lab Chip* **2005**, *5*, 739–747. [CrossRef]

60. Salgado-Figueroa, P.; Gutierrez, C.; Squella, J.A. Carbon Nanofiber Screen Printed Electrode Joined to a Flow Injection System for Nimodipine Sensing. *Sens. Actuators B Chem.* **2015**, *220*, 456–462. [CrossRef]

61. Siller, I.G.; Enders, A.; Steinwedel, T.; Epping, N.M.; Kirsch, M.; Lavrentieva, A.; Scheper, T.; Bahnemann, J. Real-Time Live-Cell Imaging Technology Enables High-Throughput Screening to Verify in Vitro Biocompatibility of 3d Printed Materials. *Materials* **2019**, *12*, 17. [CrossRef]

62. Angell, D.H.; Dickinso, T. Kinetics of Ferrous/Ferric and Ferro/Ferricyanide Reactions at Platinum and Gold Electrodes .1. Kinetics at Bare-Metal Surfaces. *J. Electroanal. Chem. Interfacial Electrochem.* **1972**, *35*, 55–72. [CrossRef]

63. Demirkol, D.O.; Timur, S. A Sandwich-Type Assay Based on Quantum Dot/Aptamer Bioconjugates for Analysis of *Escherichia coli* O157:H7 in Microtiter Plate Format. *Int. J. Polym. Mater. Polym. Biomater.* **2016**, *65*, 85–90. [CrossRef]

64. Prieto-Simon, B.; Campas, M.; Andreescu, S.; Marty, J.L. Trends in Flow-Based Biosensing Systems for Pesticide Assessment. *Sensors* **2006**, *6*, 1161–1186. [CrossRef]

5 Zusammenfassung und Ausblick

In der vorliegenden Doktorarbeit wurden die Möglichkeiten, Herausforderungen und Perspektiven der additiven Fertigung in biotechnologischen/biomedizinischen Fragestellungen und Anwendungen betrachtet. Das Ziel war es die Eignung verschiedener polymerbasierter 3D-Druckmaterialien für biologische Anwendungen zu analysieren, zu evaluieren und das Potential der additiven Fertigungstechnologie anhand individuell-entwickelter Systeme für die biotechnologische sowie biomedizinische Forschung aufzuzeigen.

Wird ein Objekt mit einem biologischen System, wie beispielsweise lebenden Zellen, in Kontakt gebracht, so ist eine umfassende Charakterisierung des verwendeten Objektmaterials von großer Bedeutung. Die physikalischen, chemischen und biologischen Materialeigenschaften können einen Einfluss auf die biologische Umgebung haben und bestimmen über die Anwendbarkeit des Materials in einer biologischen Applikation. Im ersten Kapitel des praktischen Teils dieser Arbeit (Kapitel 4.1) konnte gezeigt werden, dass die Bearbeitungsschritte des *Post-Processing* die Materialeigenschaften und die biologische Verträglichkeit eines 3D-Druckmaterials maßgeblich beeinflussen. Die untersuchten Desinfektions- bzw. Sterilisationsverfahren zeigten unterschiedlich starke Auswirkungen auf die Zytotoxizität (und damit Biokompatibilität) des Materials auf. Eine überlegte Auswahl der nötigen *Post-Processing*-Schritte, insbesondere eines geeigneten Desinfektions- bzw. Sterilisationsverfahrens, ist somit unerlässlich und sollte in Hinblick auf die beabsichtigte Anwendung erfolgen.

Es existieren zahlreiche Prüfmethoden, um die Biokompatibilität eines Materials zu evaluieren und damit Risiken für die biologische Umgebung auszuschließen. Im Rahmen dieser Arbeit dienten biochemische Testverfahren, eine durchflusszytometrische Methode sowie ein bildbasiertes Analysesystem zur *In-Vitro*-Analyse der Zytotoxizität. Dabei erwies sich das bildbasierte Analysesystem hinsichtlich des nötigen Arbeits- und Zeitaufwandes, der Benutzerfreundlichkeit und des wissenschaftlichen Informationsgehalts als besonders vorteilhaft. Mit Hilfe des Systems konnten gleichzeitig sowohl Veränderungen der Zellmorphologie beobachtet als auch kinetische Analysen und Quantifizierungen in Echtzeit und im Hochdurchsatz realisiert werden – Attribute, die das Analysesystem zu einem wertvollen Werkzeug für den täglichen Gebrauch im Labor machen. Insgesamt konnte mit den *In-Vitro*-Testverfahren die Eignung beider untersuchter 3D-Druckmaterialien für biologische Anwendungen festgestellt werden.

Je nach Einsatzgebiet additiv gefertigter Systeme in der Laborumgebung sind neben einer gewährleisteten Biokompatibilität weitere Materialeigenschaften bedeutend. Als entscheidende Einflussfaktoren für das Adhäsions- und Proliferationsverhalten von Zellen gelten Oberflächeneigenschaften wie Rauheit und Benetzbarkeit. Umfassende Materialuntersuchungen, welche in Kapitel 4.2 aufgeführt sind, zeigten dabei auf, dass das 3D-Druckmaterial „AR-M2" (Keyence GmbH) nicht nur biologisch verträglich ist, sondern auch geeignete Oberflächeneigenschaften für eine Kultivierung von adhärenten Zellen in direktem Kontakt mit dem Material besitzt. Es konnte verdeutlicht werden, dass der zugrunde liegende additive Fertigungsprozess zur Ausbildung unterschiedlicher Oberflächenstrukturen führt, die das Zellwachstum und -verhalten beeinflussen können. Außerdem konnte in dieser Arbeit die Relevanz optischer Eigenschaften, wie die Transluzenz und die Eigenfluoreszenz des Materials, für Anwendungen in der Zellkulturtechnik hervorgehoben werden. So konnte die Kultivierung adhärent wachsender Zellen in einem individuell-designten Kultivierungssystem durch die vorteilhaften optischen Materialeigenschaften (fluoreszenz-)mikroskopisch beobachtet werden.

Nachdem die polymerbasierten 3D-Druckmaterialien in den Kapiteln 4.1 und 4.2 eingehend charakterisiert worden waren, konnten die breiten Anwendungsmöglichkeiten der additiven Fertigung in der Biotechnologie und Biomedizin in den Kapiteln 4.3 und 4.4 verdeutlicht werden. Mit Hilfe eines entwickelten Ko-Kultivierungssystems konnten die Wechselwirkungen zweier adhärent wachsender Zelltypen im Kontext der Angiogenese analysiert werden (Kapitel 4.3). Darüber hinaus wurden weitere additiv gefertigte Plattformen vorgestellt, die *In-vitro*-Studien (der Angiogenese) in der Zellkultur unterstützen. Es konnte verdeutlicht werden, dass die additive Fertigung das Spektrum der den Forschern zur Verfügung stehenden, kommerziellen Versuchssystemen und Laborequipment erheblich erweitern kann. Die Vorzüge der additiven Fertigung konnten innerhalb dieser Arbeit zudem für Anwendungen in der Biosensorik genutzt werden. Für die Durchführung elektrochemischer Messungen mit kommerziell erhältlichen *Screen-printed electrodes* wurden statische und dynamische Durchflusszellen entwickelt (Kapitel 4.4). Mit Hilfe einer statischen Durchflusszelle konnte eine aptamerbasierte, impedimetrische Detektion eines *E. coli* Crooks Stammes realisiert werden. Ohne die maßgefertigte Durchflusszelle wären die dafür notwendigen Wasch- und Inkubationsschritte nur mit hohem Energie- und Zeitaufwand umzusetzen gewesen. Die entwickelte dynamische Durchflusszelle verdeutlicht die Möglichkeiten des hochauflösenden 3D-Drucks zur Fertigung von komplexen mikrofluidischen Kanalstrukturen. Durch integrierte Mikromischer-Einheiten konnte eine homogene Vermischung von bspw. Puffer- und Probenlösungen vor der elektrochemischen Messung gewährleistet werden. Zudem konnte durch Kopplung des Systems an eine Spritzenpumpe ein automatisierter und zeitgesteuerter Ablauf ermöglicht werden.

Die Fülle an Anwendungsmöglichkeiten zeigt auf, dass die additive Fertigung großes Potential für die biotechnologische und biomedizinische Forschung besitzt, sei es zur Herstellung von individuellen, experiment-spezifischen Laborequipment, Hilfsapparaturen oder ganzen Versuchssystemen. Noch birgt die additive Fertigung jedoch einige Herausforderungen, besonders in Bezug auf biologische Anwendungen. Die auf dem Markt befindlichen, kommerziell erhältlichen Materialien sind oftmals nur unvollständig charakterisiert oder können aufgrund ihrer Eigenschaften für eine biologische Anwendung direkt ausgeschlossen werden. Toxische Materialkomponenten, sowie die Suche nach geeigneten Sterilisationsverfahren für spezifische Materialien stellen weiter Herausforderungen dar, die die unmittelbare Integration von 3D-Druck in biotechnologische/biomedizinische Prozesse verlangsamen. Ferner ist die generelle Fertigung eines Objekts durch das additive Verfahren zwar sehr schnell, die Nachbearbeitungsschritte im *Post-Processing* können jedoch viel Zeit in Anspruch nehmen. Insbesondere die Entfernung von Stützmaterial bei kleinen Modelldetails und komplexen Kanalstrukturen kann sich als problematisch erweisen. Weiterentwicklungen der additiven Fertigungstechnologien könnten diesbezüglich neue Stützmaterialien hervorbringen, die effizienter und einfacher im *Post-Processing* entfernt werden und keine Behandlung mit weiteren Reagenzien erfordern, welche sich negativ auf die biologische Verträglichkeit des Materials auswirken könnten.

Auch wenn weitere Forschungsaufwendungen hinsichtlich der Optimierung von Materialeigenschaften und der Nachbearbeitungsschritte des *Post-Processing* für die Integration in biologische Systeme dienlich wären, so sind die Vorteile der additiven Fertigung unverkennbar. Schon heute vermag es die additive Fertigung einen wertvollen Beitrag in der biotechnologischen Forschung zu leisten. Allein die in dieser Arbeit vorgestellten Anwendungen reichen von der Entwicklung individueller Kultivierungssysteme über die Erstellung maßgefertigter Hilfsapparaturen bis hin zur Realisierung automatisierter Versuchssysteme. Solange die Materialeigenschaften der beabsichtigten Anwendung entsprechen, sind Applikationen für additiv gefertigte Objekte in jedem Bereich des biotechnologischen/biomedizinischen Labors denkbar und dem Forscher kaum Grenzen gesetzt. Zukünftig könnten 3D-Drucker zur Ausstattung eines jeden Labors gehören und die Fertigung von individuellen, spezialisierten Versuchssystemen sowie Laborartikeln nach Bedarf und direkt vor Ort ermöglichen. Dadurch könnte sowohl ein Beitrag zur Nachhaltigkeit und Reduktion von Kunststoffen geleistet, als auch zeitintensive Transportwege eingespart werden.

6 Literaturverzeichnis

1. Fastermann P. Nachhaltigkeit – 3D-Druck als umweltfreundliche Technologie? In: Fastermann P, ed. *3D-Drucken*. Berlin, Heidelberg: Springer Berlin Heidelberg; 2016, 117–127.

2. Wohlers Associates / Statista. Global 3D printing products and services market size from 2020 to 2024. Verfügbar auf: https://www.statista.com/statistics/315386/global-market-for-3d-printers/. Abgerufen am 13. Juli 2020.

3. Kodama H. Automatic method for fabricating a three-dimensional plastic model with photo-hardening polymer. *Review of Scientific Instruments* 1981, 52(11), 1770–1773.

4. Molitch-Hou M. Overview of additive manufacturing process. In: *Additive Manufacturing*: Elsevier; 2018, 1–38.

5. Gross BC, Erkal JL, Lockwood SY, Chen C, Spence DM. Evaluation of 3D Printing and Its Potential Impact on Biotechnology and the Chemical Sciences. *Analytical Chemistry* 2014, 86(7), 3240–3253.

6. Noorani R. 3D printing: technology, applications, and selection: *CRC Press*; 2017.

7. Garrett B. 3D Printing: New Economic Paradigms and Strategic Shifts. *Glob Policy* 2014, 5(1), 70–75.

8. Bourell DL, Leu MC, Rosen DW. Roadmap for Additive Manufacturing: Identifying the Future of Freeform Processing. Austin, TX; 2009.

9. Ngo TD, Kashani A, Imbalzano G, Nguyen KTQ, Hui D. Additive manufacturing (3D printing): A review of materials, methods, applications and challenges. *Composites Part B: Engineering* 2018, 143, 172–196.

10. AMFG Autonomous Manufacturing. Die Entwicklung des Marktes für 3D-Druckmaterialien: Trends und Möglichkeiten in 2019. Verfügbar auf: https://amfg.ai/2020/01/11/die-entwicklung-des-marktes-fuer-3d-druckmaterialien-trends-und-moeglichkeiten-in-2019/. Abgerufen am 17. Juni 2020.

11. MarketsandMarkets Research Private Ltd. 3D Printing Materials Market - Global Forecast to 2024. Verfügbar auf: https://www.marketsandmarkets.com/Market-Reports/3d-printing-materials-market-1295.html. Abgerufen am 17. Juni 2020.

12. Almudhaf TI. Design of Automotive engine components by cad software; Autodesk Inventor and Solidworks; a comparative study. *Journal of Engineering Research and Application* 2020, 10(01), 25–31.

13. Ito Y, Nakahashi K. Surface triangulation for polygonal models based on CAD data. *Int. J. Numer. Meth. Fluids* 2002, 39(1), 75–96.

14. Gibson I, Rosen D, Stucker B, eds. Additive Manufacturing Technologies. New York, NY: *Springer New York*; 2015.

15. Raddatz L, Austerjost J, Beutel S. 3D-Druck: Chancen, Möglichkeiten, Risiken. *Chem. Unserer Zeit* 2018, 52(1), 42–50.

16. IPytics GmbH / Statista. Anzahl der Patente im Bereich 3D-Druck weltweit in den Jahren von 2007 bis 2019. Verfügbar auf: https://de.statista.com/statistik/daten/studie/989479/umfrage/anzahl-der-3d-druck-patente-weltweit/#professional. Abgerufen am 17. Juni 2020.

17. Mohr S, Khan O. 3D printing and its disruptive impacts on supply chains of the future. *Technology Innovation Management Review* 2015, 5(11), 20.

18. Manyika J, Chui M, Bughin J, Dobbs R, Bisson P, Marrs A. Disruptive technologies: Advances that will transform life, business, and the global economy: *McKinsey Global Institute San Francisco, CA*; 2013.

19. Micallef J. Beginning Design for 3D Printing. New York: *Apress*; 2015.

20. Austerjost J. Entwicklung und Evaluation innovativer Automations- und Digitalisierungslösungen für die chemische und biotechnologische Laborumgebung. *Dissertation*, 2019.

21. Godoi FC, Prakash S, Bhandari BR. 3d printing technologies applied for food design: Status and prospects. *Journal of Food Engineering* 2016, 179, 44–54.

22. Wu P, Wang J, Wang X. A critical review of the use of 3-D printing in the construction industry. *Automation in Construction* 2016, 68, 21–31.

23. Müller, E. / Manager Magazin. 3D-Druck - Weltmarktführer aus der deutschen Provinz. Verfügbar auf: https://www.manager-magazin.de/magazin/artikel/industrie-4-0-deutsche-entwickeln-3-d-druck-zur-industriereife-a-1202190.html. Abgerufen am 17. Juni 2020.

24. Leukers B, Gülkan H, Irsen SH, Milz S, Tille C, Schieker M, Seitz H. Hydroxyapatite scaffolds for bone tissue engineering made by 3D printing. *Journal of Materials Science: Materials in Medicine* 2005, 16(12), 1121–1124.

25. Mironov V, Boland T, Trusk T, Forgacs G, Markwald RR. Organ printing: computer-aided jet-based 3D tissue engineering. *Trends Biotechnol* 2003, 21(4), 157–161.

26. Ventola CL. Medical Applications for 3D Printing: Current and Projected Uses. *P T* 2014, 39(10), 704–711. Verfügbar auf: https://pubmed.ncbi.nlm.nih.gov/25336867.

27. Tack P, Victor J, Gemmel P, Annemans L. 3D-printing techniques in a medical setting: a systematic literature review. *BioMedical Engineering OnLine* 2016, 15(1), 115.

28. Klein GT, Lu Y, Wang MY. 3D printing and neurosurgery--ready for prime time? *World Neurosurgery* 2013, 80(3-4), 233–235.

29. Ramiah P, Du Toit LC, Choonara YE, Kondiah PPD, Pillay V. Hydrogel-Based Bioinks for 3D Bioprinting in Tissue Regeneration. *Front. Mater.* 2020, 7, 2997.

30. Unagolla JM, Jayasuriya AC. Hydrogel-based 3D bioprinting: A comprehensive review on cell-laden hydrogels, bioink formulations, and future perspectives. *Applied Materials Today* 2020, 18, 100479.

31. Lücking TH, Sambale F, Beutel S, Scheper T. 3D-printed individual labware in biosciences by rapid prototyping: A proof of principle. *Eng. Life Sci.* 2014, 15(1), 51–56.

32. Siller IG, Enders A, Gellermann P, Winkler S, Lavrentieva A, Scheper T, Bahnemann J. Characterization of a customized 3D-printed cell culture system using clear, translucent acrylate that enables optical online monitoring. *Biomed Mater* 2020.

33. Enders A, Siller IG, Urmann K, Hoffmann MR, Bahnemann J. 3D Printed Microfluidic Mixers—A Comparative Study on Mixing Unit Performances. *Small* 2019, 15(2), 1804326.

34. DIN EN ISO/ASTM 52900:2018-06, Additive Fertigung - Grundlagen - Terminologie (ISO/ASTM DIS 52900:2018); Deutsche und Englische Fassung prEN ISO/ASTM 52900:2018. Berlin: *Beuth Verlag GmbH.*

35. All3DP GmbH. 3D-Druck-Technologie 2020: Alle 3D-Druck-Verfahren. Verfügbar auf: https://all3dp.com/de/1/3d-druck-verfahren-3d-druck-technologie/. Abgerufen am 21. Juni 2020.

36. Chohan JS, Singh R, Boparai KS, Penna R, Fraternali F. Dimensional accuracy analysis of coupled fused deposition modeling and vapour smoothing operations for biomedical applications. *Composites Part B: Engineering* 2017, 117, 138–149.

37. Bhushan B, Caspers M. An overview of additive manufacturing (3D printing) for microfabrication. *Microsystem Technologies* 2017, 23(4), 1117–1124.

38. Gibson I, Rosen D, Stucker B. Material Jetting. In: Gibson I, Rosen D, Stucker B, eds. *Additive Manufacturing Technologies*. Vol. 42. New York, NY: Springer New York; 2015, 175–203.

39. Mao M, He J, Li X, Zhang B, Lei Q, Liu Y, Li D. The Emerging Frontiers and Applications of High-Resolution 3D Printing. *Micromachines* 2017, 8(4), 113.

40. Brunet A, Müller T, Scholz S, eds. Mikrofertigungstechnologien und ihre Anwendungen: Ein theoretischer und praktischer Leitfaden. Karlsruhe, Baden: *KIT Scientific Publishing*; 2017.

41. Schneider J, Rohner P, Thureja D, Schmid M, Galliker P, Poulikakos D. Electrohydrodynamic NanoDrip Printing of High Aspect Ratio Metal Grid Transparent Electrodes. *Adv. Funct. Mater.* 2016, 26(6), 833–840.

42. Coakley M, Hurt DE. 3D Printing in the Laboratory: Maximize Time and Funds with Customized and Open-Source Labware. *J Lab Autom* 2016, 21(4), 489–495.

43. Ude C, Hentrop T, Lindner P, Lücking TH, Scheper T, Beutel S. New perspectives in shake flask pH control using a 3D-printed control unit based on pH online measurement. *Sensors and Actuators B: Chemical* 2015, 221, 1035–1043.

44. Raddatz L, Vries I de, Austerjost J, Lavrentieva A, Geier D, Becker T, Beutel S, Scheper T. Additive manufactured customizable labware for biotechnological purposes. *Eng. Life Sci.* 2017, 17(8), 931–939.

45. Krujatz F, Lode A, Seidel J, Bley T, Gelinsky M, Steingroewer J. Additive Biotech—Chances, challenges, and recent applications of additive manufacturing technologies in biotechnology. *New Biotechnology* 2017, 39, 222–231.

46. Bhattacharjee N, Urrios A, Kang S, Folch A. The upcoming 3D-printing revolution in microfluidics. *Lab on a Chip* 2016, 16(10), 1720–1742.

47. Sochol RD, Sweet E, Glick CC, Wu S-Y, Yang C, Restaino M, Lin L. 3D printed microfluidics and microelectronics. *Microelectronic Engineering* 2018, 189, 52–68.

48. Yazdi AA, Popma A, Wong W, Nguyen T, Pan Y, Xu J. 3D printing: an emerging tool for novel microfluidics and lab-on-a-chip applications. *Microfluidics and Nanofluidics* 2016, 20(3), 50.

49. Ho CMB, Ng SH, Li KHH, Yoon Y-J. 3D printed microfluidics for biological applications. *Lab on a Chip* 2015, 15(18), 3627–3637.

50. Reschetilowski W. Handbuch Chemische Reaktoren. Berlin, Heidelberg: *Springer Berlin Heidelberg*; 2020.

51. González-Henríquez CM, Sarabia-Vallejos MA, Rodriguez-Hernandez J. Polymers for additive manufacturing and 4D-printing: Materials, methodologies, and biomedical applications. *Progress in Polymer Science* 2019, 94, 57–116.

52. Lee W, Kwon D, Choi W, Jung GY, Jeon S. 3D-printed microfluidic device for the detection of pathogenic bacteria using size-based separation in helical channel with trapezoid cross-section. *Scientific Reports* 2015, 5, 7717.

53. van den Driesche S, Lucklum F, Bunge F, Vellekoop MJ. 3D Printing Solutions for Microfluidic Chip-To-World Connections. *Micromachines* 2018, 9(2).

54. Su C-K, Hsia S-C, Sun Y-C. Three-dimensional printed sample load/inject valves enabling online monitoring of extracellular calcium and zinc ions in living rat brains. *Analytica Chimica Acta* 2014, 838, 58–63.

55. Capel AJ, Wright A, Harding MJ, Weaver GW, Li Y, Harris RA, Edmondson S, Goodridge RD, Christie SDR. 3D printed fluidics with embedded analytic functionality for automated reaction optimisation. *Beilstein J Org Chem* 2017, 13, 111–119.

56. Rossi S, Porta R, Brenna D, Puglisi A, Benaglia M. Stereoselective Catalytic Synthesis of Active Pharmaceutical Ingredients in Homemade 3D-Printed Mesoreactors. *Angew Chem Int Ed Engl* 2017, 56(15), 4290–4294.

57. Rao ZX, Patel B, Monaco A, Cao ZJ, Barniol-Xicota M, Pichon E, Ladlow M, Hilton ST. 3D-Printed Polypropylene Continuous-Flow Column Reactors: Exploration

of Reactor Utility in S N Ar Reactions and the Synthesis of Bicyclic and Tetracyclic Heterocycles. *Eur. J. Org. Chem.* 2017, 2017(44), 6499–6504.

58. Okafor O, Weilhard A, Fernandes JA, Karjalainen E, Goodridge R, Sans V. Advanced reactor engineering with 3D printing for the continuous-flow synthesis of silver nanoparticles. *React. Chem. Eng.* 2017, 2(2), 129–136.

59. Lederle F, Kaldun C, Namyslo JC, Hübner EG. 3D-Printing inside the Glovebox: A Versatile Tool for Inert-Gas Chemistry Combined with Spectroscopy. *Helv Chim Acta* 2016, 99(4), 255–266.

60. Hübner EG, Lederle F. Spezielle labortechnische Reaktoren: 3D-gedruckte Reaktoren. In: Freeden W, Rummel R, eds. *Handbuch der Geodäsie.* Vol. 2. Berlin, Heidelberg: Springer Berlin Heidelberg; 2019, 1–29.

61. Krujatz F, Fehse K, Jahnel M, Gommel C, Schurig C, Lindner F, Bley T, Weber J, Steingroewer J. MicrOLED-photobioreactor: Design and characterization of a milliliter-scale Flat-Panel-Airlift-photobioreactor with optical process monitoring. *Algal Research* 2016, 18, 225–234.

62. Schmid J, Schwarz S, Meier-Staude R, Sudhop S, Clausen-Schaumann H, Schieker M, Huber R. A Perfusion Bioreactor System for Cell Seeding and Oxygen-Controlled Cultivation of Three-Dimensional Cell Cultures. *Tissue Eng Part C Methods* 2018, 24(10), 585–595.

63. Rimington RP, Capel AJ, Chaplin KF, Fleming JW, Bandulasena HCH, Bibb RJ, Christie SDR, Lewis MP. Differentiation of Bioengineered Skeletal Muscle within a 3D Printed Perfusion Bioreactor Reduces Atrophic and Inflammatory Gene Expression. *ACS Biomaterials Science & Engineering* 2019, 5(10), 5525–5538.

64. Elliott O, Gray S, McClay M, Nassief B, Nunnelley A, Vogt E, Ekong J, Kardel K, Khoshkhoo A, Proaño G, Blersch DM, Carrano AL. Design and Manufacturing of High Surface Area 3D-Printed Media for Moving Bed Bioreactors for Wastewater Treatment. *Journal of Contemporary Water Research & Education* 2017, 160(1), 144–156.

65. Khan MH, Kana EG. Design, implementation and assessment of a novel bioreactor for fermentative biohydrogen process development. *International Journal of Hydrogen Energy* 2016, 41(24), 10136–10144.

66. Odeleye AOO, Baudequin T, Chui C-Y, Cui Z, Ye H. An additive manufacturing approach to bioreactor design for mesenchymal stem cell culture. *Biochemical Engineering Journal* 2020, 156, 107515.

67. Cardoso RM, Kalinke C, Rocha RG, dos Santos PL, Rocha DP, Oliveira PR, Janegitz BC, Bonacin JA, Richter EM, Munoz RAA. Additive-manufactured (3D-printed) electrochemical sensors: A critical review. *Analytica Chimica Acta* 2020, 1118, 73–91.

68. Han T, Kundu S, Nag A, Xu Y. 3D Printed Sensors for Biomedical Applications: A Review. *Sensors (Basel)* 2019, 19(7).

69. Muñoz J, Pumera M. 3D-printed biosensors for electrochemical and optical applications. *TrAC Trends in Analytical Chemistry* 2020, 128, 115933.

70. Nesaei S, Song Y, Wang Y, Ruan X, Du D, Gozen A, Lin Y. Micro additive manufacturing of glucose biosensors: A feasibility study. *Analytica Chimica Acta* 2018, 1043, 142–149.

71. Ni Y, Ji R, Long K, Bu T, Chen K, Zhuang S. A review of 3D-printed sensors. *Applied Spectroscopy Reviews* 2017, 52(7), 623–652.

72. Cevenini L, Calabretta MM, Tarantino G, Michelini E, Roda A. Smartphone-interfaced 3D printed toxicity biosensor integrating bioluminescent "sentinel cells". *Sensors and Actuators B: Chemical* 2016, 225, 249–257.

73. Kadimisetty K, Mosa IM, Malla S, Satterwhite-Warden JE, Kuhns TM, Faria RC, Lee NH, Rusling JF. 3D-printed supercapacitor-powered electrochemiluminescent protein immunoarray. *Biosensors and Bioelectronics* 2016, 77, 188–193.

74. Au AK, Bhattacharjee N, Horowitz LF, Chang TC, Folch A. 3D-printed microfluidic automation. *Lab Chip* 2015, 15(8), 1934–1941.

75. Takenaga S, Schneider B, Erbay E, Biselli M, Schnitzler T, Schöning MJ, Wagner T. Fabrication of biocompatible lab-on-chip devices for biomedical applications by means of a 3D-printing process. *Phys. Status Solidi A* 2015, 212(6), 1347–1352.

76. Dong Y, Min X, Kim S. A 3-D-Printed Integrated PCB-Based Electrochemical Sensor System. *EEE Sensors Journal* 2018, 18(7), 2959–2966.

77. Gowers SAN, Curto VF, Seneci CA, Wang C, Anastasova S, Vadgama P, Yang G-Z, Boutelle MG. 3D Printed Microfluidic Device with Integrated Biosensors for

Online Analysis of Subcutaneous Human Microdialysate. *Analytical Chemistry* 2015, 87(15), 7763–7770.

78. Motaghi H, Ziyaee S, Mehrgardi MA, Kajani AA, Bordbar A-K. Electrochemiluminescence detection of human breast cancer cells using aptamer modified bipolar electrode mounted into 3D printed microchannel. *Biosens Bioelectron* 2018, 118, 217–223.

79. Li Z, Ye Z, Fu Y, Xiong Y, Li Y. A portable electrochemical immunosensor for rapid detection of trace aflatoxin B 1 in rice. *Anal. Methods* 2016, 8(3), 548–553.

80. Kazenwadel F, Biegert E, Wohlgemuth J, Wagner H, Franzreb M. A 3D-printed modular reactor setup including temperature and pH control for the compartmentalized implementation of enzyme cascades. *Eng. Life Sci.* 2016, 16(6), 560–567.

81. Peris E, Okafor O, Kulcinskaja E, Goodridge R, Luis SV, Garcia-Verdugo E, O'Reilly E, Sans V. Tuneable 3D printed bioreactors for transaminations under continuous-flow. *Green Chem.* 2017, 19(22), 5345–5349.

82. Manzano JS, Weinstein ZB, Sadow AD, Slowing II. Direct 3D Printing of Catalytically Active Structures. *ACS Catalysis* 2017, 7(11), 7567–7577.

83. Ahangar P, Cooke ME, Weber MH, Rosenzweig DH. Current Biomedical Applications of 3D Printing and Additive Manufacturing. *Applied Sciences* 2019, 9(8), 1713.

84. Zhang YS, Yue K, Aleman J, Mollazadeh-Moghaddam K, Bakht SM, Yang J, Jia W, Dell'Erba V, Assawes P, Shin SR, Dokmeci MR, Oklu R, Khademhosseini A. 3D Bioprinting for Tissue and Organ Fabrication. *Annals of Biomedical Engineering* 2017, 45(1), 148–163.

85. Jammalamadaka U, Tappa K. Recent Advances in Biomaterials for 3D Printing and Tissue Engineering. *J Funct Biomater* 2018, 9(1).

86. Matai I, Kaur G, Seyedsalehi A, McClinton A, Laurencin CT. Progress in 3D bioprinting technology for tissue/organ regenerative engineering. *Biomaterials* 2020, 226, 119536.

87. Jovic TH, Kungwengwe G, Mills AC, Whitaker IS. Plant-Derived Biomaterials: A Review of 3D Bioprinting and Biomedical Applications. *Front. Mech. Eng.* 2019, 5, E1.

88. Zhai Y, Lados DA, LaGoy JL. Additive Manufacturing: Making Imagination the Major Limitation. *JOM* 2014, 66(5), 808–816.

89. Holmes M. Additive manufacturing continues composites market growth. *Reinforced Plastics* 2019, 63(6), 296–301.

90. Kumbar SG, Laurencin CT, Deng M. Natural and Synthetic Biomedical Polymers. Amsterdam: *Elsevier*; 2014.

91. Sionkowska A. Current research on the blends of natural and synthetic polymers as new biomaterials: Review. *Progress in Polymer Science* 2011, 36(9), 1254–1276.

92. Peterson AM. Review of acrylonitrile butadiene styrene in fused filament fabrication: A plastics engineering-focused perspective. *Additive Manufacturing* 2019, 27, 363–371.

93. Carve M, Wlodkowic D. 3D-Printed Chips: Compatibility of Additive Manufacturing Photopolymeric Substrata with Biological Applications. *Micromachines* 2018, 9(2).

94. Bagheri A, Jin J. Photopolymerization in 3D Printing. *ACS Applied Polymer Materials* 2019, 1(4), 593–611.

95. 3D Systems I. Safety Data Sheet: VisiJet M2R-CL: according to Regulation (EC) No 1907/2006 and 1272/2008, Hazard Communication Standard 29 CFR 1910 (USA), WHS Regulations Australia, JIS Z 7253 (2012) Japan; 2018. http://infocenter.3dsystems.com/materials/sites/default/files/sds-files/professional/VisiJet_M2R-CL/24218-S12-03-A%2CSDS%20GHS%2CEnglish%2CVisiJet%20M2R-CL.pdf. Abgerufen am 20. November 2019.

96. KEYENCE Deutschland GmbH. AR-M2 Sicherheitsdatenblatt: Druckmaterial für 3D-Drucker.

97. O'Bryan CS, Bhattacharjee T, Hart S, Kabb CP, Schulze KD, Chilakala I, Sumerlin BS, Sawyer WG, Angelini TE. Self-assembled micro-organogels for 3D printing silicone structures. *Science advances* 2017, 3(5), e1602800.

98. Liravi F, Salarian M, Dal Castel C, Simon L, Toyserkani E. High-speed material jetting additive manufacturing of silicone structures: mechanical characterization. *Progress in Additive Manufacturing* 2019, 4(4), 479–495.

99. Ullah F, Othman MBH, Javed F, Ahmad Z, Akil HM. Classification, processing and application of hydrogels: A review. *Mater Sci Eng C Mater Biol Appl* 2015, 57, 414–433.

100. Drury JL, Mooney DJ. Hydrogels for tissue engineering: scaffold design variables and applications. *Biomaterials* 2003, 24(24), 4337–4351.

101. Parveen FK, ed. Recent advances in biopolymers. [Rijeka, Croatia]: *InTech*; 2016.

102. Aljohani W, Ullah MW, Zhang X, Yang G. Bioprinting and its applications in tissue engineering and regenerative medicine. *International Journal of Biological Macromolecules* 2018, 107, 261–275.

103. Rutala WA, Weber DJ, HICPAC. Guideline for Disinfection and Sterilization in Healthcare Facilities. Chapel Hill, NC 2018.

104. Wang X, Jiang M, Zhou Z, Gou J, Hui D. 3D printing of polymer matrix composites: A review and prospective. *Composites Part B: Engineering* 2017, 110, 442–458.

105. Papenburg BJ, Rodrigues ED, Wessling M, Stamatialis D. Insights into the role of material surface topography and wettability on cell-material interactions. *Soft Matter* 2010, 6(18), 4377–4388.

106. Lourenco BN, Marchioli G, Song W, Reis RL, van Blitterswijk CA, Karperien M, van Apeldoorn A, Mano JF. Wettability influences cell behavior on superhydrophobic surfaces with different topographies. *Biointerphases* 2012, 7(1-4), 46.

107. Bernard M, Jubeli E, Pungente MD, Yagoubi N. Biocompatibility of polymer-based biomaterials and medical devices - regulations, in vitro screening and risk-management. *Biomater Sci* 2018, 6(8), 2025–2053.

108. Thevenot P, Hu W, Tang L. Surface chemistry influences implant biocompatibility. *Curr Top Med Chem* 2008, 8(4), 270–280.

109. Kopperud HM, Kleven IS, Wellendorf H. Identification and quantification of leachable substances from polymer-based orthodontic base-plate materials. *European Journal of Orthodontics* 2011, 33(1), 26–31.

110. Amato SF, Ezzell RM, eds. Regulatory Affairs for Biomaterials and Medical Devices : Woodhead Publishing Series in Biomaterials: *Woodhead Publishing*; 2015.

111. Oesterreicher A, Wiener J, Roth M, Moser A, Gmeiner R, Edler M, Pinter G, Griesser T. Tough and degradable photopolymers derived from alkyne monomers for 3D printing of biomedical materials. *Polym. Chem.* 2016, 7(32), 5169–5180.

112. Siller IG, Enders A, Steinwedel T, Epping N-M, Kirsch M, Lavrentieva A, Scheper T, Bahnemann J. Real-Time Live-Cell Imaging Technology Enables High-Throughput Screening to Verify in Vitro Biocompatibility of 3D Printed Materials. *Materials (Basel)* 2019, 12(13).

113. Ratner BD. Chapter 3 - The Biocompatibility of Implant Materials. In: Badylak SF, ed. *Host Response to Biomaterials.* Oxford: Academic Press; 2015, 37–51.

114. Badylak SF, ed. Host Response to Biomaterials. Oxford: *Academic Press*; 2015.

115. Rashid H, Sheikh Z, Vohra F. Allergic effects of the residual monomer used in denture base acrylic resins. *Eur J Dent* 2015, 9(4), 614–619.

116. Epple M. Biomaterialien und Biomineralisation: Eine Einführung für Naturwissenschaftler, Mediziner und Ingenieure. Wiesbaden: *Vieweg+Teubner Verlag*; 2003.

117. Ratner BD, Hoffman AS, Schoen FJ, Lemons JE. Biomaterials Science: An Introduction to Materials in Medicine. 3rd ed. Saint Louis: *Elsevier Science*; 2014.

118. Wintermantel E, Ha S-W. Medizintechnik: Life Science Engineering (German Edition). 4th ed. Dordrecht: *Springer*; 2008.

119. Williams DF. Definitions in biomaterials: Proceedings of a consensus conference of the European Society for Biomaterials, Chester, England, March 3-5, 1986. Amsterdam, New York: *Elsevier*; 1987.

120. Morgenstern U, Kraft M. Biomedizinische technik - faszination, einführung, überblick: Band 1. Berlin, Germany: *De Gruyter*; 2014.

121. DIN EN ISO 10993-1:2017-04, Biologische Beurteilung von Medizinprodukten_-Teil_1: Beurteilung und Prüfungen im Rahmen eines Risikomanagementsystems (ISO/DIS_10993-1:2017); Deutsche und Englische Fassung prEN_ISO_10993-1:2017. Berlin: *Beuth Verlag GmbH*.

122. Di Silvio L. Cellular response to biomaterials. Boca Raton, FL, Cambridge: *CRC Press*; 2009.

123. Strober W. Trypan Blue Exclusion Test of Cell Viability. *Current Protocols in Immunology* 2001, 21(1), A.3B.1-A.3B.2.

124. Eisenbrand G, Pool-Zobel B, Baker V, Balls M, Blaauboer BJ, Boobis A, Carere A, Kevekordes S, Lhuguenot J-C, Pieters R, Kleiner J. Methods of in vitro toxicology. *Food and Chemical Toxicology* 2002, 40(2), 193–236.

125. Single A, Beetham H, Telford BJ, Guilford P, Chen A. A Comparison of Real-Time and Endpoint Cell Viability Assays for Improved Synthetic Lethal Drug Validation. *Journal of Biomolecular Screening* 2015, 20(10), 1286–1293.

126. Gressner AM, Arndt T. Lexikon der medizinischen Laboratoriumsdiagnostik; 2019.

127. Kumar P, Nagarajan A, Uchil PD. Analysis of cell viability by the lactate dehydrogenase assay. *Cold Spring Harb Protoc* 2018, 2018(6), pdb-prot095497.

128. O'Brien J, Wilson I, Orton T, Pognan F. Investigation of the Alamar Blue (resazurin) fluorescent dye for the assessment of mammalian cell cytotoxicity. *Eur J Biochem* 2000, 267(17), 5421–5426.

129. Niles AL, Moravec RA, Riss TL. In vitro viability and cytotoxicity testing and same-well multi-parametric combinations for high throughput screening. *Curr Chem Genomics* 2009, 3, 33–41.

130. Fiers W, Beyaert R, Declercq W, Vandenabeele P. More than one way to die: apoptosis, necrosis and reactive oxygen damage. *Oncogene* 1999, 18, 7719 EP -.

131. Norbury CJ, Hickson ID. Cellular responses to DNA damage. *Annu Rev Pharmacol Toxicol* 2001, 41, 367–401.

132. Overbeeke R, Steffens-Nakken H, Vermes I, Reutelingsperger C, Haanen C. Early Features of Apoptosis Detected by Four Different Flow Cytometry Assays. *Apoptosis* 1998, 3(2), 115–121.

133. Shapiro HM. Practical flow cytometry. 4th ed. New York: *Wiley-Liss*; 2003.

134. Yang SY, Kim E-S, Jeon G, Choi KY, Kim JK. Enhanced adhesion of osteoblastic cells on polystyrene films by independent control of surface topography and wettability. *Mater Sci Eng C Mater Biol Appl* 2013, 33(3), 1689–1695.

135. Patan S. Vasculogenesis and angiogenesis as mechanisms of vascular network formation, growth and remodeling. *J Neurooncol* 2000, 50(1-2), 1–15.

136. Rouwkema J, Khademhosseini A. Vascularization and Angiogenesis in Tissue Engineering: Beyond Creating Static Networks. *Trends Biotechnol* 2016, 34(9), 733–745.

137. Saberianpour S, Heidarzadeh M, Geranmayeh MH, Hosseinkhani H, Rahbarghazi R, Nouri M. Tissue engineering strategies for the induction of angiogenesis using biomaterials. *J Biol Eng* 2018, 12, 36.

138. Kasper G, Dankert N, Tuischer J, Hoeft M, Gaber T, Glaeser JD, Zander D, Tschirschmann M, Thompson M, Matziolis G, Duda GN. Mesenchymal Stem Cells Regulate Angiogenesis According to Their Mechanical Environment. *STEM CELLS* 2007, 25(4), 903–910.

139. Hayat A, Marty JL. Disposable screen printed electrochemical sensors: tools for environmental monitoring. *Sensors (Basel)* 2014, 14(6), 10432–10453.

140. Pichler J, Galosy S, Mott J, Borth N. Selection of CHO host cell subclones with increased specific antibody production rates by repeated cycles of transient transfection and cell sorting. *Biotechnol Bioeng* 2011, 108(2), 386–394.

141. Fischer S, Handrick R, Otte K. The art of CHO cell engineering: A comprehensive retrospect and future perspectives. *Biotechnol Adv* 2015, 33(8), 1878–1896.

142. Pichler J, Hesse F, Wieser M, Kunert R, Galosy SS, Mott JE, Borth N. A study on the temperature dependency and time course of the cold capture antibody secretion assay. *J Biotechnol* 2009, 141(1-2), 80–83.

143. Kumar N, Borth N. Flow-cytometry and cell sorting: an efficient approach to investigate productivity and cell physiology in mammalian cell factories. *Methods* 2012, 56(3), 366–374.

Anhang

Weitere Projekte, die während der Promotionszeit bearbeitet wurden

A.1 Entwicklung eines additiv gefertigten, mikrofluidischen Zelltransfektionssystems

Der Bedarf an (personalisierter) Biopharmazeutika, die mit immer höherer Produktivität und gleichzeitig niedrigen Herstellungskosten produziert werden können, steigt stetig [140]. Um dabei eine möglichst hohe Wirksamkeit und Verträglichkeit für den Menschen zu gewährleisten, werden für die Produktion von Biopharmazeutika oftmals Säugetierzellen verwendet [141]. Die dafür am häufigsten genutzte Zelllinie sind *Chinese Hamster Ovary* (CHO)-Zellen. Diese erzeugen ein human ähnliches Glykosylierungsmuster, wodurch Immunreaktionen vermieden werden. Um eine flexible Produktion von Zielproteinen in CHO-Zellen zu ermöglichen, wurde im Rahmen dieser Arbeit an einem Projekt zur Entwicklung eines kontrollierten und kontinuierlichen Zelltransfektionssystems mitgearbeitet. Dieses Zelltransfektionssystem soll unter anderem auf einer transienten Transfektion von CHO-Zellen beruhen und additiv gefertigt werden. Zur Umsetzung der Anforderungen wurden mikrofluidische, funktionelle Einheiten in ein LoC-System integriert und Anschlüsse zur direkten Verbindung an einen Bioreaktor geschaffen. Auf diese Weise soll zukünftig eine automatisierte, kontinuierliche Transfektion für die Herstellung rekombinanter Proteine realisiert werden.

A.2 Entwicklung und Etablierung von durchflusszytometrischen Methoden zur Detektion, Selektion und Rekultivierung von hochproduzierenden Zellklonen einer CHO-Zelllinie

Um eine effizientere Produktion von rekombinanten Proteinen mit beispielsweise höheren Produktausbeuten oder optimierten Prozessbedingungen bei geringeren Herstellungskosten zu ermöglichen, kommt der stetigen (Weiter)Entwicklung von Zelllinien eine wichtige Rolle zu [141,142]. Für die Analyse spezifischer Charakteristika bei der Klonauswahl eignet sich besonders die Durchflusszytometrie [143]. Diese erlaubt neben einer schnellen und semiquantitativen Analyse von Zellen bezüglich mehrerer Parameter auch die Sortierung einzelner Zellen mit definierter Charakteristik. Im Rahmen dieser Arbeit wurde eine antikörperproduzierende CHO-Zelllinie auf Zusammenhänge zwischen Zellcharakteristika und der Zellproduktivität untersucht. Die Zellkultivierung wurde dafür über die gesamte Kultivierungszeit bezüglich Lebendzellzahl, Viabilität, Glutamin-, Glutamat-, Laktat

und Glucosekonzentrationen sowie Produkttiter und der Zellgröße überwacht. Zur Detektion hochproduzierender Zellklone wurden Protokolle am Durchflusszytometer etabliert und Zellpopulationen mit ausgewählten Charakteristika sortiert und rekultiviert. In **Abbildung A-1** ist eine Übersicht über den Prozessablauf dargestellt. Eine ausführliche Beschreibung dieses Projekts ist in der Masterarbeit von Katharina Vera Meyer mit dem Titel „Analyse einer produzierenden CHO-Zelllinie mittels Durchflusszytometrie (2019)" zu finden, welche im Rahmen des Projekts angefertigt wurde.
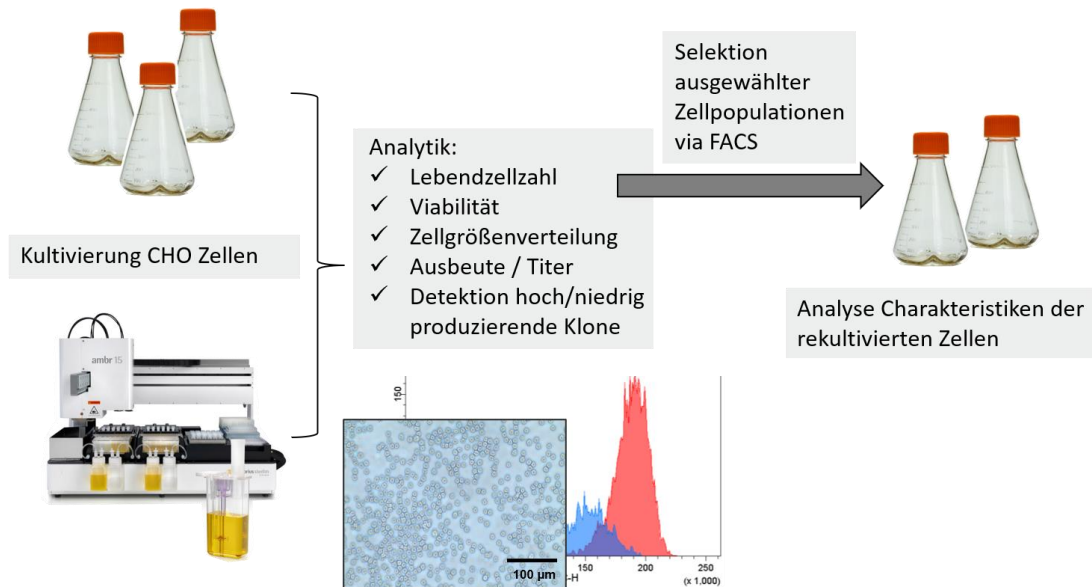

Abbildung A-1 Schematische Übersicht über den Projektablauf zur Analyse, Selektion und Rekultivierung von Zellklonen einer produzierenden CHO-Zelllinie.

Einen Teil der Ergebnisse wurde zur wissenschaftlichen Veröffentlichung eingereicht (Meyer K.V., Siller I.G., Schellenberg J., Gonzalez Salcedo A., Solle D., Matuszczyk J., Scheper T., Bahnemann J. (2020): Monitoring Cell Productivity for the Produc-tion of Recombinant Proteins by Flow Cytometry: An Effective Application using the Cold Capture Assay, Engineering in Life Science).

Betreute Abschlussarbeiten

Bachelorarbeiten

Jannick Reppin – Design und Herstellung von 3D-gedruckten mikrofluidischen Systemen für die Separation von CHO-Zellen, 2017 (geteilte Betreuung)

Phil-Oliver Thiel – Einfluss von 3D-gedruckten Materialien auf die Viabilität von CHO-Suspensionszellen, 2017

Niklas-Maximilian Epping – Transiente Transfektion von CHO-Zellen mit Cy5-markierter DNA, 2018 (geteilte Betreuung)

Laura Sophie Rösner – Untersuchungen verschiedener 3D-Druckmaterialien bezüglich Biokompatibilität für einen Einsatz in der Zellkultur, 2019

Masterarbeiten

Katharina Vera Meyer – Analyse einer produzierenden CHO-Zelllinie mittels Durchflusszytometrie, 2019

Veröffentlichungen und Konferenzbeiträge

Veröffentlichungen (antichronologisch, peer-reviewed)

Gellermann P., Grünert S., Bothe S., **Siller I.G.**, Käsehagen J., Scheper T., Pepelanova I. (2020): Production of a recombinant fibrinogen-based material in *E. coli* for use in mammalian cell culture (in Bearbeitung)

Meyer K.V., **Siller I.G.**, Schellenberg J., Gonzalez Salcedo A., Solle D., Matuszczyk J., Scheper T., Bahnemann J. (2020): Monitoring Cell Productivity for the Production of Recombinant Proteins by Flow Cytometry: An Effective Application using the Cold Capture Assay, *Engineering in Life Science*

Siller I.G., Epping N-M., Lavrentieva A., Scheper T., Bahnemann J. (2020): Customizable 3D-printed (co-)cultivation systems for *in vitro* study of angiogenesis, *MDPI Materials*

Siller I.G., Preuss J-A., Urmann K., Hoffmann M.R., Scheper T., Bahnemann J. (2020): 3D-printed compression cell for aptamer-based impedimetric detection of E. coli Crook's strain, *MDPI Sensors*

Siller I.G., Enders A., Gellermann P., Winkler S., Lavrentieva A., Scheper T., Bahnemann J. (2020): Characterization of a customized 3D-printed cell culture system using clear, translucent acrylate that enables optical online monitoring, *IOP Biomedical Materials*

Siller I.G., Enders A., Steinwedel T., Epping N-M., Kirsch M., Lavrentieva A., Scheper T., Bahnemann J. (2019): Real-Time Live-Cell Imaging Technology enables High-Throughput Screening to verify In Vitro Biocompatibility of 3D Printed Materials, *MDPI Materials*

Enders A., **Siller I.G.**, Urmann K., Hoffmann M.R., Bahnemann J. (2018): 3D printed Microfluidic Mixers – a Comparative Study on Mixing Unit Performances, *Small*

Bader A., Bintig W., Begandt D., Klett A., **Siller I.G.**, Gregor C., Schaarschmidt F., Weksler B, Romero I., Couraud P.-O., Hell S.W. and Ngezahayo A. (2017): Adenosine receptors regulate gap junction coupling of the human cerebral microvascular endothelial cells hCMEC/D3 by Ca(2+) influx through CNG channels, *Journal of Physiology*

Konferenzen und Workshops (antichronologisch)

Vorträge

Siller I.G., Enders A., Preuß J.-A., Bahnemann J. (2020): 3D-printed microfluidic systems for cell culture and biotechnological applications, 3rd International Conference on Industrial Biotechnology and Bioprocessing, Paris, France

Posterbeiträge

Winkler S., Lavrentieva A., Peplanova I., Hoffmann A., **Siller I.G.**, Bahnemann J. (2019): 3D cell cultivation in 3D-printed biocompatible microfluidic devices, EuroMBR, Braunschweig, Germany

Enders A., **Siller I.G.**, Preuß J.-A., Bahnemann J. (2019): Fabrication of microfluidic systems for use in biotechnology via 3D printing using MultiJet Printing technology, Conference of Scientific Cooperation between Lower Saxony and Israel, Hannover, Germany

Siller I.G., Preuß J.-A., Habib T., Enders A., Urmann K., Bahnemann J. (2019): Development of electrochemical and electromechanical aptasensors for bioprocess monitoring, Conference of Scientific Cooperation between Lower Saxony and Israel, Hannover, Germany

Enders A., **Siller I.G.**, Preuß J-A., Bahnemann J. (2019): Herstellung mikrofluidischer Systeme für die Biotechnologie mittels Multi Jet Modelling, DECHEMA „Chemie hilft 3D-Druck", Frankfurt, Germany

Urmann K., **Siller I.G.**, Bahnemann J., Hoffmann M. R. (2018): Electromechanical and Electrochemical Detection of Pathogens with Self-Assembled Nucleic Acid Biosensors, CEMI-Meeting at California Institute of Technology, Pasadena, USA (Im Rahmen eines fünfmonatigen Auslandsaufenthalts am California Institute of Technology)

Siller I.G., Enders A., Steinwedel T., Preuß J.-A., Bahnemann J. (2018): Biocompatibility studies of 3D-printed microfluidics, Lab-on-a-chip & Microfluidics Europe, Rotterdam, The Netherlands (Auszeichnung mit dem Posterpreis der Royal Society of Chemistry für den besten Posterbeitrag)

Enders A., **Siller I.G.**, Preuß J.-A., Bahnemann J. (2018): Comparative Study of 3D printed Microfluidic Mixers, Lab-on-a-chip & Microfluidics Europe, Rotterdam, The Netherlands

Preuß J.-A., Enders A., **Siller I.G.**, Bahnemann J. (2018): Electrostatic Induction in 3D printed Microfluidic Devices, Lab-on-a-chip & Microfluidics Europe, Rotterdam, The Netherlands

Siller I.G., Enders A., Ahamed S., Scheper T., Bahnemann J. (2017): Development of continuous microfluidic flow systems for transient transfection of CHO cells, Lab-on-a-Chip & Microfluidics World Congress, San Diego, USA

Workshops

Cellular Bioprocess Technology Short Course, Prof. Wei-Shou Hu, University of Minnesota, 2018

Lebenslauf

Persönliche Angaben

Name: Ina Gerhild Siller

Geburtsdatum und –ort: 31.12.1991 in Nordhorn

Staatsangehörigkeit: deutsch

Ausbildung

2017 - 2020   Promotionsstudium im Fach Chemie an der Leibniz Universität Hannover

2014 - 2017   Masterstudium Life Science an der Leibniz Universität Hannover

2011 - 2014   Bachelorstudium Life Science an der Leibniz Universität Hannover

2002 - 2011   Allgemeine Hochschulreife am Lise-Meitner-Gymnasium Neuenhaus

Beruflicher Werdegang

2017 - 2020   Wissenschaftliche Mitarbeiterin am Institut für Technische Chemie der Leibniz Universität Hannover

2018   Fünfmonatiger Forschungsaufenthalt am California Institute of Technology (Caltech), Pasadena, USA

2015 - 2016   Praktikum und Masterarbeit bei Emsland-Stärke GmbH in Emlichheim

2014 - 2016   Wissenschaftliche Hilfskraft am Institut für Biophysik der Leibniz Universität Hannover

2015   Forschungspraktikum am Institute of Life Science der Hebrew University Jerusalem, Israel

Danksagung

An dieser Stelle möchte ich mich bei Herrn Prof. Dr. Thomas Scheper bedanken, dass er mir die Möglichkeit gab, im Institut für Technische Chemie zu promovieren. Danke für die Bereitstellung des spannenden Themas, die angenehme Arbeitsatmosphäre und die freundliche Unterstützung während der Promotion.

Ganz herzlich bedanke ich mich bei Frau Dr. Janina Bahnemann für die hervorragende Betreuung während meiner Zeit am TCI. Vielen Dank für das immer offene Ohr, den kreativen Input und die große Freiheit bei der Ausgestaltung des Themas. Besonders bedanken möchte ich mich für die Unterstützung zur Realisierung eines Auslandsaufenthalts.

Herrn Prof. Dr. An-Ping Zeng danke ich vielmals für die Übernahme des weiteren Korreferats. Für die Übernahme des Prüfungsvorsitzes möchte ich mich herzlich bei Herrn PD Dr. Ulrich Krings bedanken.

Herrn Prof. Dr. Michael Hoffmann und Frau Dr. Katharina Urmann danke ich für die Möglichkeit einen Teil meiner Forschungsarbeiten am Caltech durchzuführen. Danke für die herzliche Betreuung und die freundliche Aufnahme in die Arbeitsgruppe.

Ein großes Dankeschön möchte ich außerdem Frau Dr. Antonina Lavrentieva für die kompetente Hilfe bei allen Fragen rund um die Zellkultur aussprechen. Danke! Bei Thorsten Strempel und Friedbert Gellermann bedanke ich mich für die großartige Unterstützung bei technischen Fragestellungen. Martina Weiß, Martin Pähler, Dr. Ivo Havlik, Dr. Michael Dors, Christiane Hellwig und Ulrike Dreschel danke ich für die Hilfe bei sämtlichen Angelegenheiten im betrieblichen Alltag.

Bei meinen Bachelor- und Masterstudenten sowie Hilfskräften bedanke ich mich an dieser Stelle ebenfalls, dass sie mich wissbegierig und mit großem wissenschaftlichem Engagement bei meiner Arbeit unterstützt haben.

Den Tierzellkultivierern, den 3D-Druck-Spezialisten und allgemein meiner Arbeitsgruppe danke ich für die Hilfe und Unterstützung, wenn sich mir beim Planen, Durchführen oder Auswerten von Experimenten Probleme ergaben.

Ein ganz besonderer Dank geht an das *junge, neue,* und *alte TCI* – ihr habt diese Zeit so besonders gemacht. Danke für die fröhlichen Stunden während und nach der Arbeit, die meine Promotion unvergesslich machen. Dem gesamten TCI danke ich für die wunderschönen Jahre in einmaliger Arbeitsatmosphäre.

Insbesondere Marline, Kimia, Elsa und Svenja möchte ich für die gegenseitige Motivation, den Zuspruch und die schönen Abende danken. Ich hoffe, dass noch viele gemeinsame Unternehmungen folgen.

Pia, Doris und Sabrina danke ich für die tiefe Freundschaft, die uns seit dem ersten Tag des Studiums verbindet – ohne euch hätte das Studium nur halb so viel Spaß gemacht und die letzten 9 Jahre sehr viel trister ausgesehen. Auf euch kann man sich immer verlassen – danke dafür. Ich bin froh, dass du, Pia, auch während der Promotion meine Sitznachbarin warst. Das war eine tolle Zeit, danke!

Zu guter Letzt möchte ich mich bei Jonas und meiner Familie bedanken. Danke, Jonas, für deinen starken Rückhalt und die bedingungslose Unterstützung, die du mir entgegenbringst. Meiner Familie möchte ich dafür danken, dass sie mir in allen Lebenslagen in jeglicher Hinsicht den Rücken gestärkt und an mich geglaubt haben. Danke für das grenzenlose Vertrauen und die immerwährende Unterstützung!